



City Research Online

City, University of London Institutional Repository

Citation: Castillo-Rivera, Salvador (2014). Advanced Modelling of Helicopter Nonlinear Dynamics and Aerodynamics. (Unpublished Doctoral thesis, City University London)

This is the accepted version of the paper.

This version of the publication may differ from the final published version.

Permanent repository link: <https://openaccess.city.ac.uk/id/eprint/13169/>

Link to published version:

Copyright: City Research Online aims to make research outputs of City, University of London available to a wider audience. Copyright and Moral Rights remain with the author(s) and/or copyright holders. URLs from City Research Online may be freely distributed and linked to.

Reuse: Copies of full items can be used for personal research or study, educational, or not-for-profit purposes without prior permission or charge. Provided that the authors, title and full bibliographic details are credited, a hyperlink and/or URL is given for the original metadata page and the content is not changed in any way.

**Advanced Modelling of Helicopter
Nonlinear
Dynamics and Aerodynamics**

Salvador Castillo-Rivera

Submitted to the City University London
for the degree of
Doctor of Philosophy

School of Engineering and Mathematical Sciences
City University London

December 2014

Contents

I	Introduction, Literature Review & VehicleSim Modelling	26
1	Introduction	27
1.1	Thesis Overview	27
1.2	Motivation and Objectives	29
1.3	Thesis Outline	30
2	Literature Review	32
2.1	Introduction	32
2.2	Simulation Approaches	33
2.3	Main Rotor	39
2.4	Tail Rotor	40
2.5	Fuselage	41
2.6	Equations	42
2.7	Stability	45
2.8	Vibrations	46
2.9	Aerodynamic Environment	48
2.10	Unmanned Aerial Vehicles (UAVs)	52

2.11 Chapter Summary	54
3 VehicleSim as Modelling Tool	56
3.1 Introduction	56
3.2 Overview of VehicleSim Lisp	56
3.2.1 VehicleSim Lisp	56
3.2.2 VehicleSim Operation	57
3.2.3 Multibody Modelling	59
3.3 VehicleSim Characteristics	62
3.3.1 State Variables	62
3.3.2 Equations of Motion	63
3.3.3 Numerical Solution	65
3.4 Building a Model	69
3.5 Chapter Summary	72
II Helicopter Models	73
4 Caliber 3 Dynamic Model	74
4.1 Introduction	74
4.2 Caliber 3 Description and Parameters Identification	75
4.3 Model Description	78
4.4 Fuselage Modelling	79
4.5 Swashplate and Main Rotor Modelling	80
4.5.1 Swashplate Modelling	80
4.5.2 Main Rotor Modelling	82

4.5.3	Controllers and Moments Definition	88
4.6	Tail Rotor Modelling	93
4.6.1	Bodies Definition	93
4.6.2	Controllers Implementation	96
4.6.3	Feather Control Definition	96
4.6.4	Flap Control Definition	97
4.7	Simulations and Results	99
4.7.1	Vibrations	99
4.7.2	Position and Rotation Control	101
4.8	Chapter Summary	103
5	Sikorsky Configuration Dynamic Model	106
5.1	Introduction	106
5.2	Model Description	112
5.3	Dynamic Model	114
5.4	Fuselage Modelling	116
5.5	Main Rotor Modelling	118
5.5.1	Bodies Definition	118
5.5.2	Controllers and Moments Definitions	122
5.6	Tail Rotor Modelling	129
5.6.1	Bodies Definition	130
5.6.2	Controllers Implementation	133
5.7	Vehicle's Longitudinal and Angular Position Control	139
5.8	Chapter Summary	141

6 External Perturbations Modelling for Sikorsky Model (Aerodynamic Model)	143
6.1 Introduction	143
6.1.1 Aerodynamic Environment	144
6.2 Earth/Ground Modelling	152
6.3 Main Rotor Tilt	153
6.4 Main Rotor Varying Angular Speed	155
6.5 Main Rotor Aerodynamic Modelling	156
6.5.1 Air Density	156
6.5.2 Induced Hover Speed	156
6.5.3 Climb, Descent and Forward Speed	157
6.5.4 Induced Climb, Descent and Forward Velocities	158
6.5.5 Blade Angle of Incidence	159
6.5.6 Lift Force	161
6.5.7 Drag Force	163
6.5.8 Thrust Coefficients	164
6.5.9 Climb Angle	166
6.6 Tail Rotor Aerodynamic Modelling	167
6.6.1 Blade Angle of Incidence for Hover, Climb, Descent and Forward Flight	167
6.6.2 Tail Rotor Lift Force	169
6.6.3 Tail Rotor Thrust Coefficient	171
6.7 Flight Control	172
6.7.1 Longitudinal Position Control	173

6.7.2	Vertical Position Control	174
6.7.3	Tail Rotor Flap Control	177
6.8	Chapter Summary	178
III	Results	180
7	Sikorsky Model in Absence of External Perturbations	181
7.1	VehicleSim Equations of Motion	181
7.1.1	Flap Dynamical Equations	182
7.1.2	Lag Dynamical Equations	184
7.1.3	Feather Equations of Motion	187
7.1.4	Coupled Equations of Flap and Lag	188
7.2	Dynamical Analysis	190
7.2.1	Flap Dynamics	190
7.2.2	Lag Dynamics	193
7.2.3	Coupled Flap and Lag Dynamics	194
7.2.4	Frequency Domain Validation	197
7.2.5	Feather	201
7.2.6	Fuselage	202
7.2.7	Tail Rotor	212
7.3	Stability and Control	217
7.3.1	Rotors' Angular Speeds	217
7.3.2	Position and Rotation Control	219
7.4	Vibrations	221

CONTENTS

7.4.1	Offset Flap Hinges' Vibrations	224
7.4.2	Lag Hinge Vibrations	232
7.4.3	Rotors Induced Fuselage's Vibrations	237
7.5	Chapter Summary	239
8	Sikorsky Model in Presence of External Perturbations	241
8.1	Earth/Ground Modelling	242
8.2	Aerodynamic Load and Flight	242
8.2.1	Aerodynamic Load Equations	243
8.2.2	Air Density	246
8.2.3	Hover Flight	247
8.2.4	Climb Flight	251
8.2.5	Descent Flight	256
8.2.6	Forward Flight	260
8.2.7	Trajectory Flight	270
8.3	Main Rotor Induced Drift	272
8.4	Vibrations	274
8.4.1	Vibration Analysis with Main Rotor Varying Angular Velocity .	275
8.4.2	Vibrations in Hover	284
8.5	Chapter Summary	286
IV	Conclusions	288
9	Conclusions and Future Work	289
9.1	Conclusions	289

CONTENTS

9.1.1	Main Findings	289
9.1.2	Contribution to the Knowledge	290
9.1.3	Scope of the Investigation	293
9.2	Future Work	294
9.2.1	Helicopter Model Improvements	294
9.2.2	Aerodynamic Modelling	294
9.2.3	Trajectory Optimization	295
9.2.4	Control Implementation	295
9.2.5	Future Contribution to the Knowledge	295
V	Appendices	297
A	Nonlinear Flap Equation using Lagrange's Method	298
B	Nonlinear Lag Equation using Lagrange's Method	301

List of Tables

4.1	<i>Caliber 3 Model parameters obtained at La Laguna University.</i>	77
5.1	<i>Sikorsky configuration model parameters [124], [142].</i>	116
7.1	<i>Obtained and predicted flap frequencies for various values of offset distance. Initial flap angle $\beta_0 = 0.0175$ rad, and rotor angular speed $\Omega = 44.4$ rad/s.</i>	191
7.2	<i>Obtained and predicted flap frequencies for various values of offset distance with a spring of constant $K_{fj} = 46772$ Nm/rad. Initial flap angle $\beta_0 = 0.0175$ rad, and rotor angular speed $\Omega = 44.4$ rad/s.</i>	192
7.3	<i>Lag frequencies. Initial conditions $\xi_0 = 0.0175$ rad without lag spring and damper, rotor angular speed $\Omega = 44.4$ rad/s.</i>	194
7.4	<i>Flap-Lag frequencies from VehicleSim obtained with initial conditions $\beta_0 = 0.0175$ rad and $\xi_0 = 0$ rad with spring in the flap ($k_{fj} = 46772$ Nm/rad) and lag hinges ($k_{lj} = 314938$ Nm/rad). The damping coefficient for the lag hinge damper is $d_{lj} = 349.58$ Nms/rad.</i>	196
7.5	<i>VehicleSim Flap/Lag ratios. Initial conditions $\beta_0 = 0.0175$ rad and $\xi_0 = 0$ rad. Springs and damper fitted.</i>	196
7.6	<i>Eigenvalues of the linearised matrix corresponding to the simulation of a helicopter model with main and tail rotor; fuselage's vertical degree of freedom is enabled. Main rotor blades have flap/lag degrees of freedom and tail rotor blades have flap degree of freedom.</i>	207

LIST OF TABLES

7.7 *Disc tilt values for the three study cases with $\tan \delta_3 = 1$. The first column shows the number of case studied and the second column corresponds to Newman's values in degrees [144].* 215

7.8 *Tail rotor collective feather. First column shows the number of cases, the second shows the numerical value of the collective feather. The third column shows the feedback gain for the collective feather.* 217

8.1 *Real values for height and air density ratio versus VehicleSim obtained values [98].* 247

List of Figures

2.1	<i>Comprehensive analyses. This figure is taken from ARC-E-DAA-TN8250, [6] and used with permission of NASA and the American Helicopter Society/The Vertical Flight Technical Society.</i>	34
2.2	<i>Representative helicopter analyses. This figure is done by the author and based on [10].</i>	35
3.1	<i>Using VehicleSim Lisp to generate C code.</i>	57
3.2	<i>Using VehicleSim Lisp to generate equations of motion.</i>	58
3.3	<i>Using VehicleSim Lisp to build DLL.</i>	59
3.4	<i>Using VehicleSim Lisp to build VehicleSim solvers for simulating multi-body systems.</i>	60
3.5	<i>Using VehicleSim Lisp to generate the state-space model in symbolic form.</i>	61
3.6	<i>Discrete samples of a state variable q and its derivative q'. This figure is drawn by the author and based on [134].</i>	66
3.7	<i>VehicleSim commands main sequence. This figure is done by the author and based on [134].</i>	70
4.1	<i>Unmanned Aerial Vehicle Caliber 3. Photography taken on June 2011, at La Laguna University (Spain). Reproduced with permission from Kyosho Corporation.</i>	76

LIST OF FIGURES

4.2	<i>Futaba radio [139]. Reproduced with permission from Kyosho Corporation.</i>	76
4.3	<i>Caliber 3 body structure diagram. The corresponding attachment points symbols are also indicated.</i>	79
4.4	<i>Configuration of the swashplate mechanism. Reproduced with permission from Kyosho Corporation.</i>	81
4.5	<i>Schematic representation of the Caliber 3 VehicleSim model.</i>	82
4.6	<i>Caliber 3 model main rotor nominal configuration.</i>	83
4.7	<i>Side graph of blade and elevators. This figure is drawn by the author and based on [141].</i>	88
4.8	<i>Spectrum of vibrations appearing on the fuselage longitudinal axis.</i>	100
4.9	<i>Spectrum of vibrations appearing on the fuselage vertical axis.</i>	101
4.10	<i>The torques from both the main/tail rotors need to be controlled in order to reach dynamical equilibrium.</i>	102
4.11	<i>Caliber 3 equilibrium position.</i>	102
4.12	<i>Caliber 3 equilibrium in rotation.</i>	103
5.1	<i>Schematic diagram of main rotor's hub and hinges system.</i>	108
5.2	<i>Side view of a flap hinge with offset eR.</i>	109
5.3	<i>Top view of a lag hinge with offset eR.</i>	110
5.4	<i>Tail rotor counteracting the torque induced by the main rotor rotation.</i>	111
5.5	<i>Rotor blade feather-flap coupling via delta three angle. This figure is drawn by the author and based on [140].</i>	112
5.6	<i>Helicopter Sikorsky configuration.</i>	113
5.7	<i>Body structure diagram of the Sikorsky model helicopter. Both main and tail rotor in this diagram contain one blade element only due to space restrictions, but the model can contain as many blades as needed.</i>	115

LIST OF FIGURES

5.8	<i>Points and distances diagram.</i>	117
5.9	<i>Main rotor configuration on nominal position.</i>	120
5.10	<i>Unit feedback system.</i>	124
5.11	<i>PID feather control.</i>	126
5.12	<i>Diagram showing the feather effect blades one and three.</i>	127
5.13	<i>Tail rotor nominal configuration.</i>	131
5.14	<i>Coning angle.</i>	133
5.15	<i>The increased cone angle.</i>	134
5.16	<i>Tail rotor blades and the collective angle.</i>	137
5.17	<i>Diagram of helicopter's longitudinal position.</i>	139
6.1	<i>Forces acting on a helicopter.</i>	144
6.2	<i>Angle of incidence is the angle between the chord line and the tip path plane.</i>	145
6.3	<i>The angle of attack is the angle between the airfoil chord line and resultant relative wind.</i>	146
6.4	<i>Main rotor disc viewed from above. This figure is plotted by the author and based on [145].</i>	147
6.5	<i>Flow conditions in vertical flight for a blade section. This figure is drawn by the author and based on [145].</i>	147
6.6	<i>Disc incidence and component velocities in forward flight. This figure is plotted by the author and based on [145].</i>	149
6.7	<i>Velocity components U_T and U_P.</i>	149
6.8	<i>Velocity components U_T, U_P and U_R.</i>	150
6.9	<i>Perturbation velocities on the blade resulting from blade flap velocity and rotor coning. This figure is plotted by the author and based on [98].</i>	151

LIST OF FIGURES

6.10	Main rotor tilt angle φ with respect to the fuselage's vertical axis.	153
6.11	Induced velocity variation as a function of climb and descent velocity. Reproduced with permission from Cambridge University Press [98].	159
6.12	Aerodynamic load representation for a main rotor blade.	161
6.13	Lift force representation for the corresponding points on the main rotor.	162
6.14	Drag force representation for a main rotor blade.	164
6.15	Sketch showing the tail rotor's configuration geometry. This figure is plotted by the author and based on [72].	176
7.1	Flap frequencies as a function of the offset without flap spring. Red 'o', represents the theoretical predicted values. Blue '*', VehicleSim obtained values.	192
7.2	Flap frequencies with the flap spring, ν_β as a function of the offset dis- tance e . Red 'o', represents the theoretical predicted values. Blue '*', VehicleSim obtained values.	193
7.3	Lag frequencies as a function of the offset for the case of no spring, no damper fitted in the lag hinge. Red 'o', represents the theoretical predicted values. Blue '*', VehicleSim obtained values.	195
7.4	Flap amplitude (in blue) and lag amplitude (in yellow) simulation results, showing free vibrations from an initial condition in which the flap angle is $\beta_0 = 0.09$ rad and lag angle is $\xi_0 = 0$ rad.	197
7.5	Uncoupled and coupled flap dynamics (red, linear flap simulation results, blue, nonlinear flap simulation results).	198
7.6	Root locus for flap and lag modes on the main rotor.	199
7.7	Flap and lag modes, being Ω the main rotor speed and μ the real part of eigenvalue or damping. Reproduced with permission from Wiley Publica- tion [142].	200

LIST OF FIGURES

7.8 *Root locus plot flap and lag modes obtained by VehicleSim with damper fitted in the flap hinge. (Note normalized in both axes).* 201

7.9 *Red '-' , collective feather of 0.01 rad for the four blades of the main rotor. Blue 'o' , the reference signal for the collective feather.* 202

7.10 *Red '-' , cyclic feather with $f_{0S} = 0.01$ and $f_{0C} = 0.01$ radians for the blades of the main rotor. Blue 'o' , the reference signal for the cyclic feather. 203*

7.11 *a) Root locus for the fuselage, the main and the tail rotors. b) Details of the root locus for two modes.* 204

7.12 *Coupled movement for the fuselage and the main rotor along the vertical axis. Solid red line, fuselage. Dotted blue line, flap.* 205

7.13 *Magnitude of the eigenvector associated to the eigenvalue $\lambda_2 = 0.0 + 50.01i$ and its influence on the state variables.* 208

7.14 *Magnitude of the eigenvector associated to eigenvalue $\lambda_3 = 0.0 + 48.86i$ when the fuselage and the rotor are coupled.* 209

7.15 *Mode 1, blue '+' , mode 2, red '•' . Influence of mass ratio on these coupled modes. Change of natural frequencies as a function of the mass ratio $mass_{blade}/mass_{fuselage}$* 210

7.16 *Sketch of main rotor and gyroscopic moments in vacuum. This figure is plotted by the author and based on [142].* 211

7.17 *In red, the displacement transmitted by the fuselage to the blades. Clearly corresponds to expression (7.43). In blue, blades' flap.* 212

7.18 *a) Fuselage's roll vibrations spectrum. Blue, represents roll vibrations without lag hinge, and red represents roll vibrations with lag hinge included in the model. b) Fuselage's pitch spectrum. Blue, represents pitch motion without lag hinge, and red represents pitch with lag hinge included in the model.* 213

7.19 *Flap frequencies for blade one on the tail rotor. In green '*' , case one. In red '△' , second case and in blue 'o' , results for the third case.* 214

LIST OF FIGURES

7.20 *First tail rotor blade flap motion. It is worked out with $a_0 = 0.078$ rad, $a_1 = 0.017$ rad and $b_1 = -0.008$ rad. Only time between 49 - 50 seconds is shown in order to clearly see the flap behaviour.* 215

7.21 *First tail rotor blade flap with $a_0 = 0.087$ rad, $a_1 = 0.043$ rad and $b_1 = -0.017$ rad. Only time between 49 - 50 seconds is shown as in the previous figure.* 216

7.22 *First tail rotor blade flap angle history. $a_0 = 0.122$ rad, $a_1 = 0.087$ rad and $b_1 = -0.034$ rad. Note the time span 49 - 50 seconds.* 217

7.23 *Angular speeds on both rotors. In blue, main rotor speed. In red, tail rotor speed. The control signals are shown on both cases, and clearly the speeds successfully follow the respective reference speeds.* 218

7.24 *Solid blue line represents angular speeds on the main rotor, dotted blue line is the control signal on the main rotor. Solid red line represents angular speeds on the tail rotor, dotted red line is the control signal on the tail rotor.* 219

7.25 *Fuselage equilibrium position around the point (0,0,0) in absence of external forces (vacuum after the action of the main an tail rotors torques). 220*

7.26 *Fuselage equilibrium around the point (0,0,0) in vacuum after the action of the main and tail rotors torques.* 221

7.27 *Rotor angular speeds. Yellow '-', the main rotor angular speed. Green '-', the tail rotor angular speed. The control signals needed to achieve them are shown on both cases. Blue '*', the reference signal for the main rotor speed. Red '*', the reference signal for the tail rotor speed.* 224

7.28 *Blade flap element velocities, relative to the main rotor axes. This figure is done by the author and based on [150].* 225

7.29 *Vertical and radial velocities. This figure is drawn by the author and based on [150].* 226

7.30 *Speed components in a rotor with hinges' offset. This figure is plotted by the author and based on [150].* 227

LIST OF FIGURES

7.31 *Blade accelerations in an offset rotor. This figure is done by the author and based on [150].* 228

7.32 *Conversion of offset hinge force to pitching and rolling moments. This figure is plotted by the author and based on [150].* 229

7.33 *Left, fuselage oscillations on the X axis for $eR = 0.01$ m. Right, spectrogram of the vibrations shows various frequencies varying between 0 - 7 Hz, 4.5 - 21 Hz and 3.5 Hz, respectively.* 229

7.34 *Left, fuselage oscillations on the Y axis for $eR = 0.01$ m. Right, spectrogram of the vibrations shows various frequencies varying between 0 - 7 Hz, 4.5 - 21 Hz and 3.5 Hz, respectively.* 230

7.35 *Left, fuselage oscillations on the X axis for $eR = 0.982$ m. Right, spectrogram of the vibrations shows various frequencies varying between 0 - 7 Hz, 4.5 - 22.5 Hz and 3.5 - 9 Hz, respectively.* 230

7.36 *Left, fuselage oscillations on the Y axis for $eR = 0.982$ m. Right, spectrogram of the vibrations shows various frequencies varying between 0 - 7 Hz, 4.5 - 21 Hz and 3.5 - 9 Hz, respectively.* 231

7.37 *a) and c) show the spectrograms for $eR = 0.01$ m cases and b) and d) show the spectrogram for $eR = 0.982$ m cases.* 232

7.38 *Sketch of the force applied on the blade with a lag hinge. This figure is drawn by the author and based on [150].* 233

7.39 *Left, fuselage oscillations on the X axis for $y_{b11} = 2.9846$ m, $y_{b12} = 2.7846$ m, $y_{b13} = 2.8846$ m, $y_{b14} = 2.6846$ m. Right, spectrogram of the vibrations shows various frequencies varying between 0 - 7 Hz, 7 - 9 Hz, respectively.* 234

7.40 *Left, fuselage oscillations on the Y axis for $y_{b11} = 2.9846$ m, $y_{b12} = 2.7846$ m, $y_{b13} = 2.8846$ m, $y_{b14} = 2.6846$ m. Right, spectrogram of the vibrations shows various frequencies varying between 0 - 7 Hz, 7 - 9 Hz, respectively.* 235

LIST OF FIGURES

7.41 *Left, fuselage oscillations on the X axis for $y_{bl1} = 3.9846$ m, $y_{bl2} = 1.7846$ m, $y_{bl3} = 3.8846$ m, $y_{bl4} = 1.6846$ m. Right, spectrogram of the vibrations shows various frequencies varying between 0 - 7 Hz and 6 - 12 Hz.* 235

7.42 *Left, fuselage oscillations on the Y axis for $y_{bl1} = 3.9846$ m, $y_{bl2} = 1.7846$ m, $y_{bl3} = 3.8846$ m, $y_{bl4} = 1.6846$ m. Right, spectrogram of the vibrations shows various frequencies varying between 0 - 7 Hz and 5 - 12 Hz.* 236

7.43 *a) and c) show the spectrograms for the first simulation when the centre of mass unbalance is given by $y_{bl1} = 2.9846$ m, $y_{bl2} = 2.7846$ m, $y_{bl3} = 2.8846$ m, $y_{bl4} = 2.6846$ m. b) and d) show the spectrograms for the second simulation when the unbalance is given by $y_{bl1} = 3.9846$ m, $y_{bl2} = 1.7846$ m, $y_{bl3} = 3.8846$ m, $y_{bl4} = 1.6846$ m.* 237

7.44 *Left, fuselage vibrations on the X axis for $m_{bl1} = 31.06$ kg, $m_{bl2} = 31.26$ kg, $m_{bl3} = 29.96$ kg and $m_{bl4} = 31.16$ kg and $m_{blt11} = 6.212$ kg and $m_{blt12} = 6.222$ kg. Right, spectrogram of the vibrations shows various frequencies at around 7 Hz and 37 Hz.* 238

7.45 *Left, fuselage vibrations on the Y axis for $m_{bl1} = 31.06$ kg, $m_{bl2} = 31.26$ kg, $m_{bl3} = 29.96$ kg and $m_{bl4} = 31.16$ kg and $m_{blt11} = 6.212$ kg and $m_{blt12} = 6.222$ kg. Right, spectrogram of the vibrations shows various frequencies varying around 7 Hz and 37 Hz.* 238

8.1 *3-D representation of the helicopter's position under the influence of ground force. Blue point represents the helicopter's position.* 242

8.2 *Variation of air density versus height calculated in VehicleSim. Red '□', represents the starting height. Red '○', final height.* 246

8.3 *Air density in hover flight.* 248

8.4 *Main rotor hover characteristics: thrust coefficient divided by solidity versus feather collective angle. This graph is plotted by the author and based on [145].* 249

LIST OF FIGURES

8.5	<i>Tail rotor hover characteristics, thrust coefficient divided by solidity versus collective angle. This graph is plotted by the author and based on [71].</i>	249
8.6	<i>3-D representation of hover flight conditions. Blue point represents the helicopter's position. Vertical axis value is 250 m. Longitudinal and lateral axes, their corresponding values are around the equilibrium point in each axis i.e., zero.</i>	250
8.7	<i>Flap amplitude for the four main rotor blades in hover flight (blue (blade 1), green (blade 2), yellow (blade 3) and red (blade 4)).</i>	251
8.8	<i>Main rotor blades' flap amplitudes in hover flight for the last two seconds of the time interval (0 - 100) s (blue (blade 1), green (blade 2), yellow (blade 3) and red (blade 4)).</i>	252
8.9	<i>Tail rotor blades' flap amplitudes in hover flight (dotted red line (blade 1), solid blue line (blade 2)).</i>	252
8.10	<i>Zoom of figure 8.9. Tail rotor blades' flap amplitudes in hover flight (dotted red line (blade 1), solid blue line (blade 2)).</i>	253
8.11	<i>Induced velocity ratio as a function of climb velocity ratio based on momentum theory (complete induced velocity curve). Reproduced with permission from Cambridge University Press [98].</i>	253
8.12	<i>Climb flight simulation. Green line shows the helicopter displacement from $h_i = 250$ m to $h_f = 744$ m. Red '□', represents the initial position. Red 'o', final position.</i>	254
8.13	<i>Variation of air density in climb flight. Red '□', represents the starting height. Red 'o', final height.</i>	255
8.14	<i>Main rotor blades' flap amplitudes during climb flight (blue (blade 1), green (blade 2), yellow (blade 3) and red (blade 4)).</i>	256
8.15	<i>Flap amplitudes (blue (blade 1), green (blade 2), yellow (blade 3) and red (blade 4)). Climb flight for the last two seconds of the time interval (0 - 100) s.</i>	257

LIST OF FIGURES

8.16 Tail rotor blades' flap amplitudes during climb flight (dotted red line (blade 1), solid blue line (blade 2)). 257

8.17 Zoom of figure 8.16. Tail rotor blades' flap amplitudes during climb flight (dotted red line (blade 1), solid blue line (blade 2)). 258

8.18 Induced velocity variation as a function of descent velocity based on momentum theory (complete induced velocity curve). Reproduced with permission from Cambridge University Press [98]. 258

8.19 Representation in three dimensions in descent flight. Green line shows the helicopter's position. Red '□', represents the initial position. Red '◦', final position. 259

8.20 Variation of air density in descent flight. Red '□', represents the starting height. Red '◦', final height. 260

8.21 Main rotor blades' flap amplitudes in descent flight (blue (blade 1), green (blade 2), yellow (blade 3) and red (blade 4)). 261

8.22 Tail rotor blades' flap amplitudes in descent flight (dotted red line (blade 1), solid blue line (blade 2)). 261

8.23 Zoom of figure 8.22. Tail rotor blades' flap amplitudes in descent flight (dotted red line (blade 1), solid blue line (blade 2)). 262

8.24 Forward flight. 262

8.25 Variation of induced velocity with forward speed. This graph is plotted by the author and based on [145]. 263

8.26 Calculated values of C_T/σ versus θ . This graph is drawn by the author and based on [145]. 264

8.27 Tail rotor feather angle versus advance ratio in forward flight. This graph is plotted by the author and based on [141]. 264

LIST OF FIGURES

8.28	<i>Vehicle's position for 50 seconds simulation in which the distance travelled is 994 m with a speed of $v_{fw} = 20$ m/s and climb rate of 110 m with a speed of 2.2 m/s. Blue '□', represents the initial position. Blue 'o', final position.</i>	265
8.29	<i>VehicleSim calculation of air density in forward flight with constant climb rate. Red '□', represents the starting height. Red 'o', final height. . . .</i>	266
8.30	<i>Main rotor blades' flap amplitudes in forward flight with constant climb rate (blue (blade 1), green line (blade 2), yellow line (blade 3) and red line (blade 4)).</i>	267
8.31	<i>Zoom of figure 8.30. Flap amplitudes in forward flight with constant climb rate (blue (blade 1), green line (blade 2), yellow line (blade 3) and red line (blade 4)).</i>	267
8.32	<i>Tail rotor blades' flap amplitudes in forward flight with constant climb rate (dotted red line (blade 1), solid blue line (blade 2)).</i>	268
8.33	<i>Zoom of figure 8.32. Tail rotor blades' flap amplitudes in forward flight with constant climb rate (dotted red line (blade 1), solid blue line (blade 2)).</i>	268
8.34	<i>Forward flight with varying tilt angle simulation. Red line shows the helicopter's position. Blue '□', represents the initial position. Blue 'o', final position.</i>	269
8.35	<i>Main rotor blades' flap amplitudes in forward flight with varying tilt angle (blue (blade 1), green (blade 2), yellow (blade 3) and red (blade 4)). . . .</i>	269
8.36	<i>Tail rotor blades' flap amplitudes in forward flight with varying tilt angle (dotted red line (blade 1), solid blue line (blade 2)).</i>	270
8.37	<i>Zoom of figure 8.36. Tail rotor blades' flap amplitudes in forward flight with varying tilt angle (dotted red line (blade 1), solid blue line (blade 2)).</i>	271
8.38	<i>Several trajectories in forward flight with constant climb rate and different rates of yaw (ryaw). Red line, represents $ryaw = 0.1$ rad/s. Green line, $ryaw = -0.1$ rad/s. Blue line, $ryaw = -0.2$ rad/s.</i>	271

LIST OF FIGURES

8.39 *Helicopter trajectory.* 272

8.40 *Schematic equilibrium of forces in a helicopter under the action of the main rotor torque and the tail rotor thrust and the resultant drift.* 273

8.41 *Helicopter's lateral displacements when the lateral controllers' action are cancelled and only the main rotor induced drift is acting.* 273

8.42 *Zoom of figure 8.41. Red line represents the distance travelled by the fuselage when main rotor tilt is 0.175 rad and blue line represents the distance travelled by the fuselage when main rotor tilt is 0.0175 rad.* . . 274

8.43 *Varying main rotor angular speed versus time. Solid blue line represents: $f_1 = 7$ Hz, $f_2 = 0.16$ Hz and $f_3 = f_1/2 = 3.5$ Hz. Dotted red line, $f_1 = 7$ Hz, $f_2 = 0.40$ Hz and $f_3 = f_1/2 = 3.5$ Hz.* 278

8.44 *Varying main rotor angular speed versus time. Solid blue line represents: $f_1 = 7$ Hz, $f_2 = 0.16$ Hz and $f_3 = f_1$. Dotted red line, $f_1 = 7$ Hz, $f_2 = 0.40$ Hz and $f_3 = f_1$.* 279

8.45 *Fuselage X position spectrogram when the varying main rotor speed is given by the frequencies: $f_1 = 7$ Hz, $f_2 = 0.16$ Hz and $f_3 = f_1/2 = 3.5$ Hz.* 280

8.46 *Fuselage Y position spectrogram when the varying main rotor speed is given by the frequencies: $f_1 = 7$ Hz, $f_2 = 0.16$ Hz and $f_3 = f_1/2 = 3.5$ Hz.* 280

8.47 *Fuselage X position spectrogram when the varying main rotor speed is given by the frequencies: $f_1 = 7$ Hz, $f_2 = 0.16$ Hz and $f_3 = f_1 = 7$ Hz.* . 281

8.48 *Fuselage Y position spectrogram when the varying main rotor speed is given by the frequencies: $f_1 = 7$ Hz, $f_2 = 0.16$ Hz and $f_3 = f_1 = 7$ Hz.* . 281

8.49 *Fuselage X rotation spectrogram when the varying main rotor speed is given by the frequencies: $f_1 = 7$ Hz, $f_2 = 0.40$ Hz and $f_3 = f_1/2 = 3.5$ Hz.* 282

8.50 *Fuselage Y rotation spectrogram when the varying main rotor speed is given by the frequencies: $f_1 = 7$ Hz, $f_2 = 0.40$ Hz and $f_3 = f_1/2 = 3.5$ Hz.* 283

8.51 *Fuselage X rotation spectrogram when the varying main rotor speed is given by the frequencies: $f_1 = 7$ Hz, $f_2 = 0.40$ Hz and $f_3 = f_1 = 7$ Hz.* . 283

LIST OF FIGURES

8.52 *Fuselage Y rotation spectrogram when the varying main rotor speed is given by the frequencies: $f_1 = 7$ Hz, $f_2 = 0.40$ Hz and $f_3 = f_1 = 7$ Hz.* 284

8.53 *Left, hover flight vibrations around the fuselage's X axis. Right, spectrogram of the simulation.* 285

8.54 *Left, hover flight vibrations around the fuselage's Y axis. Right, spectrogram of the simulation.* 285

To my mother, my sister and in memory of my father

Acknowledgements

I would like to show to my family members, my deepest gratitude because this thesis had not been completed without their unconditional support. Their endless love and confidence in me were a constant source of encouragement which provided me the strength to develop this work. I feel incredibly indebted due to their generosity, patience and respect for my work. Thanks to this, I could accomplish any challenge that I tried to do in my life. For this, I am forever grateful.

I wish to thank Dr. Maria Tomas-Rodriguez who allowed me to develop this work under her supervision. Her support and her critical thinking enabled this manuscript to take its present form. I feel very lucky because I had the opportunity to work with her which is a unique experience.

Abstract

The work presented here provides a comprehensive dynamic and aerodynamic helicopter model. The possible applications of this work are wide including, control systems applications, reference and trajectory tracking methods implementation amongst others. The model configuration corresponds to a Sikorsky helicopter; a main rotor in perpendicular combination with a tail rotor. Also, a particular model of unmanned aerial vehicle has been modelled as part of collaboration with the La Laguna University (Spain). The modelling tool is VehicleSim, a program that builds rigid body systems, solves the nonlinear equations of motion and generates the time histories of the corresponding state variables of the vehicle under study. VehicleSim is able to provide the linearised equations of motion in a Matlab file and the symbolic state-space model. This is useful when control systems are to be designed. The main rotor model accounts for flap, lag and feather motions for each blade as well as for their nonlinear dynamic coupling. The tail rotor is modelled including the flap-feather coupling via delta three angle. The main and tail rotors' angular velocities are implemented by PID controllers. Main rotor linear and nonlinear equations are derived and validated by comparison with the theory. Main rotor flap and lag degrees of freedom are validated using frequency domain approaches in the absence of external forces. Also, fuselage-main rotor interaction is studied and validated by using modal analysis and root locus methodology. Vibrations originated at the main rotor are simulated and their effects on the fuselage are examined by a Short Time Fourier transformation. The aerodynamic model uses blade element theory on the main-tail rotors. Hover, climb, descent and forward flight conditions are simulated and they allow the helicopter to follow certain trajectories. Finally, the ensuing vibrations when an external perturbation is applied to the main rotor are investigated.

Part I

Introduction, Literature Review & VehicleSim Modelling

Chapter 1

Introduction

1.1 Thesis Overview

Rotorcraft are unique vehicles with their capability of taking off, landing vertically and hover as well as performing low speed manoeuvres and conventional cruise in forward flight. These characteristics allow helicopters to perform a wide range of tasks that are not possible for other types of aircraft. These tasks include police surveillance, fire fighting, mountain and sea rescue, air ambulance, amongst others. Military roles of helicopters are extensive, for instance, troop transport, assault, etc. In rescue operations, helicopters have saved lives of thousands of people. In the year 2000 there were in excess of 40,000 helicopters flying worldwide [1], and as a consequence, there is a continuing need for advanced research and development in the area of rotorcraft dynamics.

Helicopter performance does not depend on the terrain in the area of operation as the land based vehicle does. During the recent years, the use of autonomous rotorcraft has increased. An autonomous helicopter has an advantage in manoeuvrability compared to an autonomous aeroplane. This and the ability to take off and land in limited spaces are clear advantages of autonomous helicopters.

Helicopters are highly nonlinear systems, inherently unstable by nature and they are mechanically complex vehicles composed of various bodies with several degrees of freedom and exhibit general motions in all three dimensions. The unsteady aeromechanical

environment of the main rotor is a source of enormous fuselage vibration. Helicopter's vibration has long been a problem from the earliest days of helicopter development and it has a direct impact on the production as well as the maintenance costs. Vibrations, in general, constitute a hostile environment for all kinds of equipment. Airframe vibrations are caused by several excitation sources, being the more prominent sources the main rotor hub forces and moments. For example, 90% of fuselage vibrations for the UH-60 helicopter originates from the main rotor [2]. Over the years, the helicopter development took place by the continuous struggle of the designers to solve the problems of vibrations and dynamic instabilities. The current technology allows helicopters to fly faster, and therefore, the vibration problem and its effects become more pronounced since helicopters notoriously vibrate more as the air speed is increased. As a consequence, helicopter vibration research has increased enormously during the past thirty years with the advent of new commercial and military helicopters. The activities have been developed towards sophisticated means of controlling vibration. Indeed, active control of vibrations is being vigorously pursued in helicopter industry.

Since the 1980's, scientific effort has increased to understand and solve some of the most difficult problems associated with helicopter flight, for instance, on the vehicle's structure the aerodynamic limitations are imposed by the main rotor i.e., dissymmetry of lift is differential. Due to the lift difference between advancing and retreating blades of the rotor disc, the helicopter could become uncontrollable in any flight condition other than hover [3].

The process of modelling helicopter dynamics is improving but it is not an easy task due to the complexity of the system itself. Usually, the main rotor, the fuselage and the tail rotor are considered for modelling purposes and these can display multiple configurations. Since the 1960's the modelling of helicopter's dynamics has been technically challenging. In the late 1980's, improving in the understanding due to advances in computation resources allowed this progress to accelerate. Nowadays, studies in this area are extremely wide, as they entail several approaches within various fields of engineering such as (amongst others) advanced methods in computational fluid dynamics (CFD) [4] and flexible multibody dynamics [5].

This thesis addresses the problem of dynamic and aerodynamic helicopter modelling, validation and simulation.

1.2 Motivation and Objectives

Despite the considerable amount of progress made so far in the helicopter simulation problem, the main goal to build a rotorcraft model that takes into account the nonlinear dynamics and aerodynamics, towards a full helicopter behaviour modelling is still a far fetched task. One of the primary reasons for this is the complex aerodynamic environment that surrounds a helicopter, and secondly the difficult to set up a model taking into account the full nonlinear dynamics that represents a realistic and high fidelity helicopter mechanical behaviour. The work to be carried out in this sense should be aimed at developing a robust and detailed suitable simulation program. The objective of this thesis is focused on this idea, to develop a robust and detailed helicopter simulation model by using VehicleSim so that design and testing of robust control systems for helicopter control can be carried out in future.

The main goals of this thesis can be summarized as follows:

- To propose a high fidelity helicopter dynamic model in order to provide a tool for studying the dynamics and main characteristics during helicopter flight. In addition to this, it is intended to build a dynamic model for an Unmanned Aerial Vehicle in order to simulate its dynamical behaviour.
- To obtain the linear and nonlinear equations of motion for the flap and lag degrees of freedom and flap-lag coupling on the main rotor as well as the feather degree of freedom.
- To validate the flap and lag degrees of freedom on the main rotor by using a frequency domain approach as well as to study the interaction between the fuselage and the main rotor by using modal analysis.
- To validate the flap and feather degrees of freedom on the tail rotor as well as the coupling flap-feather via delta three angle.
- To simulate the angular speeds and mechanical torques in both rotors, and to control the helicopter's position and rotation to counteract eventual instabilities introduced by those torques.

- To simulate in absence of aerodynamic forces, the ground when gravity is considered.
- To build an aerodynamic model in VehicleSim by using blade element for hover, climb, descent and forward flight on both main and tail rotors. This is accomplished with the objective of facilitating the study of trajectories and flying characteristics.
- To analyse vibrations arising mainly from the main rotor of the fuselage as a consequence of unbalance of masses. To study vibrations when an external perturbation is acting on the main rotor such as varying rotating angular speed. To analyse the aerodynamic induced vibrations.

The first step in understanding the dynamics of such a complex multibody system is the formulation of an exhaustive nonlinear set of equations that represent accurately the behaviour of both the main/tail rotors and the fuselage. The formulation of the nonlinear equations of motion for the blade's flap, lag and coupled flap/lag degrees of freedom is a fundamental step in order to achieve an improved understanding of the behaviour on these rotary-wing vehicles. On the other hand, the generation of vibrations as well as their study and analysis are carefully done in order to understand their sources. This research can thus be seen as a study to set up a dynamic and aerodynamic model of a helicopter in order to provide a comprehensive tool for studying the full set of dynamics and other characteristics during helicopter flight, as well as the vibrations induced by the rotors on the fuselage.

1.3 Thesis Outline

The thesis is organized in nine chapters as described below:

Chapter 1: *Introduction*. This chapter presents the overview, background and motivations that lead to this thesis.

Chapter 2: *Literature Review*. The chapter presents a literature review of past and recent studies and results in helicopter dynamics, aerodynamics as well as vibrations. In addition to this, Unmanned Aerial Vehicles literature review is also provided.

Chapter 3: *VehicleSim as Modelling Tool*. The purpose of this chapter is to provide an overview of VehicleSim, the main software used in this work. Operational principles of the software as well as a detailed description of the main commands are provided.

Chapter 4: *Caliber 3 Dynamic Model*. The chapter shows how a dynamic Unmanned Aerial Vehicle model is built in VehicleSim. This is a dynamical model developed under the umbrella of an academic collaboration with the La Laguna University, Spain. The results presented in this chapter, have been published in an international journal.

Chapter 5: *Sikorsky Configuration Dynamic Model*. This chapter describes how a dynamic helicopter model with Sikorsky configuration is modelled by using VehicleSim.

Chapter 6: *External Perturbations Modelling for Sikorsky Model (Aerodynamic Model)*. This chapter is an extension of the model presented in Chapter 5, gravity is taken into account and the aerodynamic model is implemented and described accordingly.

Chapter 7: *Sikorsky Model in Absence of External Perturbations*. The chapter provides the results of the simulations carried out with the model built up in Chapter 5. The results of the simulations are compared with those available in the existing literature in order to validate the presented model.

Chapter 8: *Sikorsky Model in Presence of External Perturbations*. This chapter shows the results from the model set up in Chapter 6. The results of the simulations are validated with theoretical results.

Chapter 9: *Conclusions and Future Work*. The chapter contains the conclusions of the thesis as well as guidelines for scope for future research in this field.

Chapter 2

Literature Review

2.1 Introduction

This chapter reviews the literature on several fields related to helicopter's systems as well as the simulation approaches. All of them have been reviewed in a number of places in order to provide an overview of the state of the art.

The chapter is divided into various sections in which the different helicopter aspects are dealt with, in this way the author developed the modelling process as well as the subsequent data analysis.

Over the years, immense efforts have been expanded to develop the helicopter simulation field. Nowadays, several computer packages for assisted mechanical modelling are available. These should be separated in two categories: numerical or symbolic. Numerical codes prepare and solve equations in number form and post-process the results to provide the output in graphical form or as animations. On the other hand, symbolic codes derive equations of motion using symbols instead of numbers. They require number substitution and further processing before any output can be obtained (linear analysis, time histories via numerical integration, etc). It is well known that symbolic equations are more difficult to obtain than numerical results. On the contrary, once obtained for a system they do not need to be generated again. Indeed, they are better suited for real time simulations that require fast code execution.

An example of commercially available numerical software is ADAMS, and another example of a symbolic software is VehicleSim. An advantage of VehicleSim with respect to ADAMS is that VehicleSim provides the linear and nonlinear equations of motion in analytical form, and the output is in the form of a computer language code such as C. In addition to this, the output is ready to compile and solve the equations to obtain motion time histories, or a Matlab m-file that contains the symbolic state-space matrices (A, B, C, D) for linear analysis. These characteristics of VehicleSim are advantageous and provide a good basis for multibody systems modelling purposes.

2.2 Simulation Approaches

This section describes previous work developed in the field of helicopter dynamics and aerodynamic modelling in order to introduce the context in which this work has been carried out.

Digital computer programs that simulate the aeromechanical behaviour of rotorcrafts are called comprehensive analyses. The word "comprehensive" has several different implications in rotorcraft aeromechanics [6]:

- It refers to the need for a single tool to perform all computations, for all operating conditions and all rotorcraft configurations, at all stages of the design process
- The technology is comprehensive, covering all disciplines with a high technology level
- The models are comprehensive, covering a wide range of problems, a wide range of rotorcraft configurations and rotor types, and dealing with the entire aircraft
- The software is flexible to adapt or extend the codes to new problems and new models

Comprehensive analyses have their origins in the programs developed as digital computers first became available to engineers in the 1960's. Figure 2.1 shows a summary of comprehensive analysis approaches and their evolution over the years.

2.2. SIMULATION APPROACHES

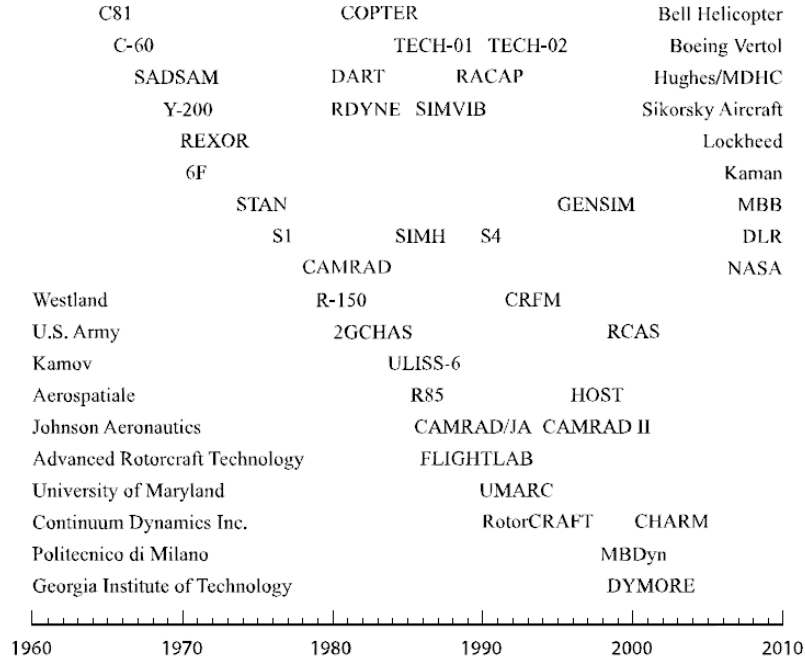


Figure 2.1: *Comprehensive analyses.* This figure is taken from *ARC-E-DAA-TN8250*, [6] and used with permission of NASA and the American Helicopter Society/The Vertical Flight Technical Society.

Of the first generation codes, C81 was an example of a comprehensive analysis. The origin was attributed to Blankenship [7] and Duhon [8]. The prerequisite was the modern digital computer, first available at Bell Helicopter in 1959. These early works describe the new experience of developing a computer program for engineering application. Key aspects of this first code were that it modelled the entire aircraft and covered both aerodynamics and structural dynamics. Aeroelastic Rotor Analysis Program (C-60) was developed by Boeing Vertol to calculate rotor structural loads in steady-state flight conditions [9]. The code G400 was developed to study a bearingless rotor stability. A number of limitations were presented in those codes as they could not deal with problems such as incomplete trim, incomplete body or rotor motion, uniform inflow or eigenanalysis capability. It was developed by United Technologies Research Center (UTRC) in 1975 ([6], [10]). Revised and Extended Rotor (REXOR) considered a four-bladed, hingeless rotor. It was developed by Lockheed in 1971, [6] and Structural Analysis by Digital Simulation of Analog Methods (SADSAM) was a finite-element structural analysis developed by MacNeal-Schwendler Corporation in 1963 [6]. These

2.2. SIMULATION APPROACHES

first generation codes were designed with very limited time and resources. In fact, they were validated only for particular helicopter types or specific technical problems. Normal Modes Aeroelastic Analysis (Y-200) was developed by Sikorsky Aircraft [11]. The flap-lag-torsion equations of motion for the rotor blade were developed by Arcidiacono [12] for an investigation of flutter, stall flutter, torsion divergence, and flap and flap-lag stability. Stability Analysis (STAN) was developed by Messerschmitt-Bolkow-Blohm (MBB) in the early 1970's. This originated with the DF55 code, which was the first complete helicopter simulation code at MBB. DF55 modelled the six aircraft degrees of freedom and the blade flap motion, simulating the Bo105 hingeless rotor blade using an equivalent offset hinge and a rigid blade [13].

On the other hand, a second generation of codes was characterized by an emphasis on the study of the coupling of components. They were developed by the US Army and the helicopter industry. The analysis was focused on the use of executive software for a flexible and unified structure (see Figure 2.2).

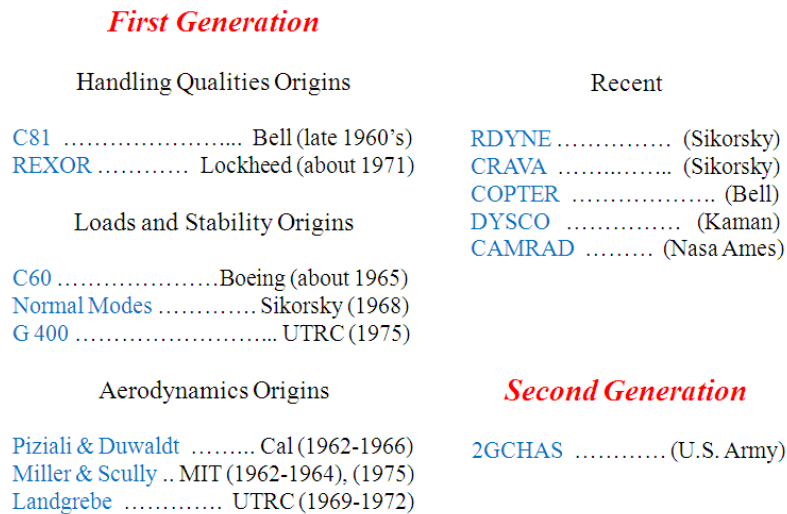


Figure 2.2: *Representative helicopter analyses. This figure is done by the author and based on [10].*

Second Generation Comprehensive Helicopter Analysis System (2GCHAS) was developed under the sponsorship of the U.S. Army [14], [15]. It was developed by a team of five manufacturing companies, three software and small business companies, and three universities [6]. Comprehensive Program for Theoretical Evaluation of Rotorcraft (COPTER) was developed by Bell Helicopter ([16]-[18]). Bell launched the COPTER

program to produce the technology needed to support Bell products. The first operational version analyzed the aeroelastic stability of hingeless and bearingless rotors by an eigenanalysis of linear equations. The equations were expanded in the uncoupled vibration modes of the blade [6]. Rotor/Airframe Comprehensive Aeroelastic Program (RCAP) was developed at McDonnell Douglas Helicopter Company [19], [20]. Rotorcraft System Dynamics Analysis (RDYNE) was developed by Sikorsky Aircraft. The blade elastic model was a new implementation of the equations of Arcidiacono [12]. Wake influence coefficients were obtained from the rotorcraft wake analysis [21]. 6F was developed at Kaman Aerospace Corporation; it modelled a servo-flap control as well as a conventional swashplate control [22], [23]. ULISS-6 was developed at Kamov, and it modelled coaxial rotors including a vortex wake with prescribed geometry [24], [25].

Additionally, the development of (1978-1980) comprehensive analytical model of rotorcraft aerodynamics and dynamics (CAMRAD) gave birth to a number of theoretical works such as the empirical dynamic stall model (1968-1969), vortex/blade interaction (1969-1970), nonuniform inflow (1968-1970), rotor/wing dynamic stability (1972-1975) and dynamic stability in free flight (1975-1976). From these works, the stability research provided linearised equations of motion for the rotor [10]. S4 (4th generation rotor Simulation program) was a high-resolution rotor simulation tool developed by the German Aerospace Center (DLR) for investigations of rotor dynamics, vibration and noise reduction, dynamic stall, blade airloads, and performance [26]. FLIGHTLAB was developed as a real-time blade-element helicopter simulation by Advanced Rotorcraft Technology, Inc. ([27]-[29]). This is a software development environment to support the modelling of dynamic systems from a predefined library of physically based modelling components. Computation of Rotor Aerodynamics in Forward Flight (RotorCRAFT) was developed by Continuum Dynamics, Inc. [30]. The University of Maryland Advanced Rotorcraft Code (UMARC) was developed at the University of Maryland [31], [32]. These codes were applied to a wide range of configurations including articulated, hingeless, and bearingless rotors, servo-flap control, and tiltrotor aircraft. The Coupled Rotor Fuselage Model (CRFM) was developed by Westland Helicopters in cooperation with the Royal Aircraft Establishment [33], [34]. The objective was to predict the rotor performance and loads and fuselage vibration in all flight conditions, both level and manoeuvring flight, using a model of the coupled dynamics of the rotor and fuselage. This required extending the model to multiple blades, taking into account coupling between

the rotor and fuselage, and flying three-dimensional manoeuvres. GENSIM was Eurocopter's in-house helicopter simulation tool for global steady and unsteady performance, flight mechanics, and loads calculations [35]. The blade aerodynamic model was based on blade element/momentum theory with simple analytical downwash models and rigid blades. Helicopter Overall Simulation Tool (HOST) was developed initially by Aerospatiale [36]. It tackled the trim conditions problem. For trim, harmonic representation of the motion was used with a Newton method to simulate the flight condition. DYMORE was developed in the late 1990's at the Georgia Institute of Technology [37], [38]. It was a finite-element-based tool for analysis of nonlinear, flexible multibody systems, providing a general and flexible modelling approach that was modular and expandable. The multibody dynamics approach was needed to deal with complex mechanisms of arbitrary topology. Comprehensive Hierarchical Aeromechanics Rotorcraft Model (CHARM) was developed by Continuum Dynamics, Inc. It was a comprehensive analysis applicable to a wide range of rotorcraft problems including wake/surface interaction, vibratory air-loading, and noise generation. The aerodynamic model covered multiple rotors, wakes, and bodies, in free air and in an enclosure (including ground effect or a wind tunnel). Rotorcraft Comprehensive Analysis (RCAS) system was developed for the U.S. Army by Advanced Rotorcraft Technology, Inc. [39]. MultiBody Dynamics (MBDyn) was a multibody, multidisciplinary code that provided a framework for integrated simulation of complex multiphysics problems; it was developed at Politecnico di Milano [40], [41]. On the other hand, several of the existing mathematical modelling approaches to date have been based on linearised models [42], [43]. Moreover, there exist some nonlinear descriptions of helicopter dynamics but only for reduced order models [44] or without taking into consideration the interaction of the main rotor with the fuselage [45]. [46] discussed a multibody system simulation architecture capable of generating the dynamical equations of a multibody system symbolically, automatically create the computer code to simulate the equations numerically, run the simulation and graphically display the results. In this work, the equations were described in a theoretical manner but analytical form of them was not provided. The Modelica-Dymola environment has been also used previously to address the problem of modelling helicopter dynamics ([47]-[49]), where parametric and reconfigurable helicopter dynamic models were presented but the dynamical equations of the main rotor were not presented. Some other authors (see [50] as an example) have used MAPLE to formulate the complete set of nonlinear equations of motion for a coupled rotor and fuselage system. This symbolic software automati-

cally converted the equations of motion into C, Fortran or Matlab. The compiled source code can be accessed and numerically integrated by the dynamic simulation software Simulink. It was then used to generate the time history of the blade's and fuselage's motion. In order to obtain the nonlinear equations of motion, a combination of several codes was needed, which complicated the process in great manner and increased the execution time.

There exist several other mathematical modelling approaches to study helicopter dynamics; they comprise nonlinear equations of motion derived by Lagrangian methods, but they lack of an automated modelling tool in order to expand the equations and incorporate a control system/simulation environment such as Matlab, Maple or Simulink, see ([51]-[53]) as examples. Some other approaches used within the context of helicopter dynamics do not address directly the modelling aspects of it, but focus on stability analysis instead. In these cases, some sort of modelling methodology is needed, being based in most cases on linearised models, reduced order models [54] and more rarely on nonlinear models for which the integration process was tedious, computationally expensive and state space representation of the system or dynamical equations of motion are not presented to the user [38], [55], [56]. In addition to this, an early work using ADAMS was done by Bertogalli [57], this work shows the results of a study aiming at the design of an ADAMS based simulation program for the dynamics and aerodynamics of the main rotor of the Agusta A109c helicopter. The complexity of the system under investigation (rotor blade flexibility, unsteady aerodynamic loading, non-uniform and time-varying wake) required use of ADAMS's features as user-written subroutines and linear systems simulation and the development of subroutine (CONSUB) for simulation management and control [57]. On the other hand, Bianchi dealt with ADAMS and the helicopter tail rotor analysis, they presented some major results obtained from the dynamic simulation of a partially flexible tail rotor model of an Agusta helicopter, being the aim to investigate the features of ADAMS as a mechanical system simulation tool through an application to a case of interest for Agusta. The results obtained from the simulations performed were satisfactory, but the authors admitted that much work was still needed to be carried out in some areas [58]. Brown developed a computational tool, Vortex Transport Model (VTM) that allows to analyse aerodynamic and dynamic performance on several rotor helicopter configurations under both steady and manoeuvring flight conditions. The aerodynamical module uses a computational solution of the Navier-Stokes equations. It is expressed in vorticity velocity form in

order to simulate the evolution of the wake of a helicopter rotor ([59]-[62]). Some of the more challenging aspects of modelling the mechanical dynamics of rotorcraft systems are addressed in this work and the corresponding dynamics are analysed. The modelling tool is VehicleSim, [63], a multibody systems software package that derives a realistic nonlinear model of the fundamental dynamics of an articulated rigid-bladed rotorcraft. One of the advantages of using VehicleSim is that compared to hand derived equations (usually prone to errors), the automated equations give an accurate representation of the complex system's dynamics. Also, due to its software engineering features, it uses a reduced execution time. VehicleSim uses an advanced form of Kane's equations and applies extensive algebraic and programming optimization methods to achieve high efficiency. Within the context of automatic modelling of system's dynamics, [64] provides a method for representing rigid multibody systems in symbolic form by means of AutoSim (previous version of VehicleSim).

2.3 Main Rotor

The main system of a helicopter is the rotor as it allows the helicopter to fly. The main rotor has two different parts: the rotor and the blades linked to it. The rotor has an influence on the blade's displacement. It is known that blades have three degrees of freedom: flap, lag and feather influenced by the main rotor.

Flap, lag and feather are studied as independent degrees of freedom. In fact, Majhi and Ganguli [65] derived the general equation describing the blade's flap dynamics for a large flap angle and large induced inflow angle of attack. Numerical simulations were carried out solving the nonlinear flap ordinary differential equations for steady state conditions and the validity of the small angle approximations was examined. A semi-empirical dynamic stall aerodynamics model was used. The results showed that a small flap angle assumption, and to a lesser extent, the small induced angle of attack assumption could lead to inaccurate predictions of blade flap response under certain flight conditions for some rotors when nonlinear aerodynamics were considered [65]. The coupling between blade flap and lag motions was tackled in the work by Pavel [66]. They studied the Micon 1500/600 lead-lag instability on high wind speed runs when the blades were operating in the stall region. This work derives the coupled flap-lag equations of motion for rigid blades and axial wind at the rotor hub with hinge offsets and spring restraints.

The equation of motion was extended and blade flexibility was introduced in the model. In addition to this, the variation of the coupled flap and lag eigenvalues with the feather angle were presented in the complex plane for various wind speeds. The study concluded that coupling between blade flap and lag motions would occur when the wind turbine was operating in the stall area [66].

Ormiston and Bousman [67] used the AH-56A Cheyenne helicopter to determine fundamental stability characteristics of the hingeless rotor when considering the flap and lead-lag degrees of freedom of a single blade. This work was carried out in the absence of available experimental data, a model rotor was designed and tested to validate the theoretical analysis instead. As a result of these investigations, various applied approaches were suggested for hingeless rotor blades inherent stability improvement.

Eigenvalues and eigenvectors analysis have an extensive use in rotorcraft data analysis. Al-jawi and Mohamad [68] studied the stability of a rotorcraft with five degrees of body freedom. The study focused on linear formulations of the system. Eigenvalues were used to obtain the system's stability boundaries, while the eigenvectors determined the blade's behaviour. This work proved that in the case of identical blades, the blade's complex eigenvectors are orthogonal to each other.

Although many previous analyses were carried out, Du Val presented an extensive study dealing with the inertial dynamics of a fully articulated stiff rotor blade. The model used in this derivation included a hinge offset and a six degrees of freedom rotor shaft. The main objective was to facilitate an organized program for simulation applications. The results were compared to the flap and lead-lag equations used in the Rotor Systems Research Aircraft (RSRA) simulation model [69]. In order to understand the rotorcraft flight dynamics, the work presented by Hohenemser [70] was reviewed in here, the author dealt with the basic rotor design parameters that affect the flight dynamics, analytical modelling techniques as well as mathematical analysis techniques (nonlinear modelling).

2.4 Tail Rotor

The tail rotor plays a fundamental role in a Sikorsky configuration helicopter. In order to model and simulate the tail rotor in VehicleSim, several contributions were reviewed. A complete report on the tail and its design was presented by Wiesner and Kohler [71].

This work is a general guideline for a preliminary design of tail rotors operating at low speed and hover flight. The directional control problems of single rotor helicopters under certain conditions such as altitude, wind speed and direction amongst others, were studied. The database used to carry out this work was wind tunnel tests of a tail rotor helicopter model. The tests were run in and out of ground effect, in various wind speeds up to 35 knots and with varying wind azimuths. In addition to this, parameters that affect flying qualities and structural loads were studied together with feather-flap coupling, tail rotor shaft sweep, pedal control rate limiting, etc.

An early work on helicopter directional stability and control at low speed flight was presented by Amer and Gessow. In here, the tail rotor collective feather was studied using charts, these were based on equations for the collective feather of a tail rotor at low forward speeds in terms of its forward speed, tip speed, thrust coefficient, solidity and yawing speed of the helicopter. As a consequence of this, tail rotor design studies of directional trim and control response at low forward speed could be carried out. The charts were used to study the main rotor stability derivatives of thrust with respect to the collective feather and angle of attack at low forward speeds [72].

Pereira et al. analysed the influence of the positive pitch-flap coupling on the flap response of an articulated tail rotor blade. The geometric parameters were similar to those of the AS355 Twin-Engine Squirrel helicopter. Mathematical models were presented for hovering flight and forward flight conditions. These allowed to model the tail rotor implemented in this thesis [73].

Stanislawski presented a simulation method for calculating tail rotor loads and blades' deflections in a directional manoeuvre. Additionally, aerodynamic forces acting on a blade segment at a given azimuth position on the tail rotor disc were obtained using blade element theory. Simulations calculations concerning the work of tail rotor at direction manoeuvre of helicopter in hover and level flight condition were performed [74].

2.5 Fuselage

The fuselage is an essential part of the helicopter and it plays an important object of study in this thesis. The fuselage has been studied and analyzed as a fundamental part

of the helicopter as shown in Guo-cai's work. In here, the authors derived nonlinear differential equations and integrated them in the time domain to yield responses of rotor blade flap, lead-lag and fuselage motions. The objective of this work was to accurately predict the dynamic instabilities of a helicopter coupled rotor-fuselage system. Fast Fourier Transform (FFT) was used to estimate the modal frequencies, and Fourier series based moving-block analysis was employed in the predictions of the modal damping in terms of the response time history. Time-domain methods and eigenanalyses were applied to predict dynamic instabilities and compared to wind tunnel test data of reference. The results showed excellent agreement between analytical and experimental data in the ground resonance cases. Thus, it could be applied to the dynamic stability analysis of rotor-fuselage coupled systems together with nonlinear and unsteady aerodynamic models as well as nonlinear blade lag dampers [75].

Coupling mechanics have an important role to play in helicopter's behaviour. Keller examined the off-axis response problem using an analytical model, with the goal of understanding the coupling mechanics. The effects of a wake distortion created by the pitch rate were included by an induced velocity model. The inclusion of these effects results in a significant change in the lateral flap response to a steady pitch rate. The results showed that the inclusion of an induced velocity variation due to the shaft rate improved the correlation in the pitch response to lateral cyclic inputs. The proposed inflow model was coupled to the full rotor-body dynamics model and comparisons were carried out between the existing model and flight test data for a UH-60 in hover [76].

Simulation models as well as their development and validation processes play a main role; Manimala et al. described the development and validation of a high fidelity simulation model of the Bell-412 in the FLIGHTLAB environment for handling qualities and flight control investigations. The following main steps were carried out, rotor hub design, modelling of the hub and blade retention, blade aerodynamics description, rotor inflow, tail rotor and fuselage modelling, and finally model validation [77].

2.6 Equations

An extensive body of literature exists on the equations that govern helicopter's rotors. Early work was published by Zbrozek, the mathematical expression for describing the

2.6. EQUATIONS

moment due to blade's angular acceleration in flap motion and the moment due to centrifugal force were presented. The blade's angular velocity and acceleration were expressed as functions of the angles of tilt when the tip-path plane was tilted with respect to the shaft in the plane of oscillation and in the plane perpendicular to it. Also, the blade inertia was treated through the values of blade inertia number, and its influence over the acceleration when the blades were heavy. The mathematical analysis of the dynamic blade flap during a simple harmonic motion of the helicopter provided the existence of angular velocity and acceleration derivatives. The effect of the angular acceleration derivative on the helicopter's dynamic stability was small, as a result, the usual values of blade inertia number were neglected. The effect of the frequency ratio $\bar{\nu} = \nu/\Omega$ (ν is the frequency of shaft oscillation and Ω is the rotor's rotational velocity) on the values of the rotor's derivatives was also small, due to the fact that for all helicopter models built to dynamic and aerodynamic scale, the value of $\bar{\nu}$ was likely to be much less than 0.1. It was for the case of helicopters with heavy blades i.e., $\gamma < 8$ (where γ is the blade inertia number), that the effects of the acceleration term and the frequency ratio need to be taken into account [78].

Stewart performed a large study of blade's flap motion. It treated the flap angle as harmonics and derived a mathematical expression for flap and pitch. At high tip speed ratio and blade's collective pitch large values, where blade stalling can occur on the outer sections of the blade, the amplitude of some of the flap harmonics may be increased considerably [79].

The work by Lewis obtained the transient solution of the helicopter's rotor blade flap motion as well as the effective damping of the motion determined for high tip speed ratios. The equation for flap motion was presented for an untwisted blade with constant chord and did not bend or twist. The flap hinge was assumed to be on the axis of rotation and perpendicular to the spanwise axis of the blade i.e., $\delta_3 = 0$. Furthermore, regions of reverse flow over the retreating blade were not taken into account. The solution of the flap equation of motion led directly to the parameter which measures the stability of the motion using the method proposed by the author [80].

Wilde et al. solved the blade flap equation taking into account the reversed flow region but neglecting stall. The effects of springs, dampers, offset and δ_3 hinges were also considered. The flap behaviour of articulated rotors was studied for high tip speed ratio values. It was shown that flap motion became unstable about $\mu = 2.25$ (μ is tip speed

ratio), and it slightly depended on the Lock's inertia number. The flap amplitude in response to a change of disc incidence was larger as μ increases. Furthermore, an offset hinge had little effect on the blade flap amplitude. The effect of a δ_3 hinge on a fully articulated blade was approximately the half of the flap, over the whole range of μ , when δ_3 angle was 30 degrees. Finally, viscous dampers were effective in restraining blade flap and it appeared that little was gained by using springs [81].

The unsteadiness of aerodynamic, inertial and gravitational forces generates vibratory loads and stresses which act on the rotor [82]. In this work, blade forces were studied together with aerodynamic, inertial and gravity forces. The aerodynamic loads were generated by the unsteady nonuniform wind environment. Inertial blade loads included centrifugal tension due to rotation as well as lead-lag and flap loads due to Coriolis forces arising from blade oscillations, and gyroscopic forces due to precession of the rotor shaft to maintain alignment with the wind velocity vector.

When the flap and lag are studied independently from each other, the Coriolis force can be neglected and the centrifugal force must be considered on each case. Stafford and Giurgiutiu studied these uncoupled equations for the case of the Timoshenko beams. Solutions were obtained using the Frobenius power series method. The principal advantage of this approach was the exact representation of the centrifugal force [83].

Later on, this work was extended and coupled flap/lag, together with pitch degrees of freedom were included in the equations [84].

Vyas derived the equations of motion of a blade mounted on a disc rotating with variable angular velocity. The acceleration of the disc was constant. In addition to this, the calculus of variations method was used to obtain the equation that governs the subsequent free vibrations [85].

Chen did a complete work on the flap-lag nonlinear dynamical equations of motion. Three hinges sequences were used in order to obtain the equations: lag-feather-flap, flap-feather-lag, flap-lag-feather. The Lagrange method was used to work out the coupled flap-lag equations of motions [86].

2.7 Stability

The stability is a fundamental aspect that should be taken into account when modelling any type of vehicle. Several contributions were reviewed in this sense. An early work was done by Gessow and Amer where static stability with angle of attack, speeds and damping due to a pitching or rolling velocity were studied. In hovering flight conditions, the helicopter has neutral static stability with respect to attitude changes. On the other hand, the helicopter showed positive static stability with respect to changes in translational velocity. The resulting motion of the helicopter oscillated if disturbed from hovering conditions. The period of oscillation depended on two factors, the moments appearing due to changes in speed and the moments due to the helicopter's angular velocity. In forward flight, static stability with attitude changes and static stability depending on speed changes were considered as well. This work concluded that the helicopter's rotor is statically stable with speed and statically unstable with angle of attack. The static stability is unaffected by centre of gravity shifts if the moments are not contributed by components other than the rotor. If there exist other moments contributions such as a fixed tail surface, the static stability is as well affected [87].

Reeder and Gustafson [88] studied the impact of the angle of attack in forward flight on stability as well as the control sensitivity in hovering and the control forces following control actions for manoeuvring. Rotor instability appeared as a result of flap and increased in severity with increasing speed.

Root locus techniques were used to study the stability and the various modes of motion. Curtiss considered some aspects of the prediction of flap and lag instabilities on hingeless rotor blades whilst hover flight. The dependence of the characteristic modes on blade's pitch angle was examined for various analytical models using root locus techniques. Prediction of flap-lag stability using a single bending mode for each degree of freedom was examined. As a result of this study, prediction of flap-lag stability was very sensitive to the model used in modelling the rotor blades aerodynamic and elastic characteristics. Furthermore, the equivalent lumped spring constants for either the parallel or series spring model can be determined from the results of an elastic analysis of a rotor blade [89].

Ormiston and Hodges examined the linear stability characteristics of rotor blade flap-lag oscillations in hover flight. The study focused on the effects of pre-cone, variable elastic coupling, pitch-lag coupling and, the aerodynamics of the induced inflow. The effects of kinematic pitch-lag coupling on flap-lag stability are highly dependent on the elastic coupling for stiff in-plane rotor blades, but not for soft in-plane ones. This work showed that the flap phase response for pitch excitations was significantly altered by elastic coupling. This implied that coupled rotor-fuselage dynamic equations should include the rotor blade's in plane degree of freedom [90].

Antequera et al. designed a UAV controller based in the eigenvalues assignment technique. The system (which was initially unstable) was satisfactory stabilized. In addition to this, the flexibility of the eigenstructure assignment improved the system's response by applying a recurrent algorithm for selecting new eigenvalues and/or eigenvectors for decoupling purposes [91].

2.8 Vibrations

Vibrations constitute the major source of unwanted oscillations in helicopter systems and one of the main areas of active research. During years, efforts have been devoted to the detection, characterization, analysis and suppressions of unwanted vibrations. The existing literature covers most of the aspects already mentioned.

In this section, some of the most relevant contributions in this field are revised. Bazov states the existence of many sources of exciting forces which cause forced vibrations in helicopter. Such sources include the main and tail rotors, power system, transmission gearboxes and shafts. Each of these sources creates exciting forces with a definite frequency. The lowest exciting force frequency is that of the main rotor. It may be found from the formula $n_{mr} = n_s k$ where n_{mr} is the main rotor exciting frequency; n_s is the main rotor rps and k is the number of main rotor blades. The frequency of the main rotor exciting forces varies in the range of 8 – 16 Hz. The tail rotor excites forces with a frequency of 10 – 60 Hz. The transmission shafts and gearboxes create a higher frequency of the exciting forces: from 50 to several hundred vibrations per second. The power plant yields a broad spectrum of exciting forces with frequencies of 600 – 1000 Hz. The primary forced vibration source is the main rotor with hinged blade support.

Blade oscillations relative to the hinges are also the source of several vibrations [92].

Chen et al. analyzed blade's nonlinear vibrations with varying rotating speed. Thin-walled beams were considered in this study because they have been used in a broad range of fields including aerospace and mechanical industry. The model of rotating thin-walled beams could be employed in the designs of turbine blades, helicopter blades, etc. On the other hand, the vibration analysis plays a central role in reliability of rotating blades. Therefore, a comprehensive understanding of their vibration characteristics, especially nonlinear behaviour is of importance to predict their dynamic response to external excitations. As a consequence, they proposed an analytical expression for the varying angular velocity case [93].

The work made in Santos et al. presented a theoretical and experimental contribution to the problem of rotor and blades dynamic interaction. A simple test rig, built by a mass and spring system attached to four flexible rotating blades was used to validate the mathematical models. Only lateral displacement of the rotor in the horizontal direction was taken into account. Gyroscopic effects due to angular vibrations of the rotor were eliminated in the test rig by attaching the rigid rotor to a flexible foundation. The blades were modelled as Euler and Bernoulli beams. Indeed, the linear model could correctly estimate parametric vibrations in a short range of low rotational speed, where the stiffening effect was of minor importance. Superharmonic vibration associated to the movement of the flexible rotating parts, with large amplitude, could only be detected with the help of the fully nonlinear model [94].

Keysan showed that the harmonics from a rotor slotting machine can be utilized for control or diagnostic purposes. In the existing literature, rotor slot harmonics are mostly utilized for condition monitoring. The study illustrates a new approach to the identification of rotor slot harmonics which consumed very little computation time [95].

Tuma studied the rotor vibration's stability. The rotor was considered to be under the influence of a perturbation caused by external forces. The perturbation force was assumed to be rotating at the angular velocity ω , which was considered to be independent from the rotor angular velocity Ω . The rotor was perturbed by the non-synchronous force with respect to the rotor angular frequency. The equation of motion contained complex variables as a function of time. The work showed how to solve such equation using Simulink [96].

Schulz studied possible isolation methods for a helicopter. The compensation of vibrations generated by the rotor of a helicopter and transmitted to the cabin is of great importance for rotorcraft design. These vibrations occur at discrete frequencies i.e., rotor blade harmonic frequencies. For the compensation of vibrations, a control law was derived, which isolated the cabin from the rotor/gear-box unit at the disturbance frequency, by use of electro-hydraulic actuators [97].

In the area of vibrations control of helicopters there are several contributions that up to now investigate different methods ranging from IBC (Individual Blade Control) to HBC (Harmonic Blade Control) among many others. The problem of vibration's control is not within the scope of this thesis.

2.9 Aerodynamic Environment

The aerodynamic forces around the helicopter system are the ultimate reason for its flight. Therefore, studying the nature of these forces, obtaining a good mathematical representation and good understanding of them becomes a necessary task before approaching further issues on helicopter research.

Helicopter aerodynamics have been studied since the first concept of these vehicles was conceived and therefore it counts with an endless amount of existing relevant literature.

Aerodynamic force modelling has a great impact in the helicopter simulation research field. The following review is done in order to understand the main aspects of the helicopter flight by using blade element theory as well as the parameters that this method involves.

Blade element theory is commonly used in helicopter flight simulation models. The theory consists on dividing a blade into various blade elements orientated in the chord wise direction; each element is aerodynamically independent from the neighbouring elements. This allows the use of 2D aerofoil characteristics in order to determine the forces and moments produced on the blade [98].

An early work in the literature that used blade element analysis was carried out by Castles Jr. and New. A set of blade element equations were derived by giving the relation between the thrust and flight path velocity components and the equilibrium

blade angles, torque and in-plane forces. The inflow angle and blade angle of the blade elements were taken into account for small angles [99].

Myers provided basic data on helicopter rotor blade motion; photographic records of the behaviour of a blade in flight were obtained with a conventional single rotor helicopter. In addition to this, some fundamental mathematical expression and values such as inflow ratio, solidity, tip-loss factor amongst others, were also provided [100].

Majhi and Ganguli examined the small flap angle approximations for steady state flight conditions and solved the nonlinear flap ordinary differential equation using numerical simulations. This work, showed how the blade element analysis allows to develop an aerodynamic model that deals with rotor blade flap motion considering nonlinear aerodynamics [101].

Vilchis et al. studied the aerodynamic forces and provided its algebraic expressions as well as the torques used to deduce the generalized external forces acting on the helicopter, this work presented the development of a nonlinear control strategy for a VARIO scale model helicopter [102].

In Dingeldein and Schaefer, some fundamental aerodynamic aspects were studied in order to analyze the aerodynamic characteristics of a single rotor helicopter in forward flight [103].

Mikhailov et al. analyzed blade motion stability in forward flight, as for a helicopter, the unstable coupled flap, torsional and lag oscillation that occurs due to the interaction of inertial, aerodynamic and elastic forces of main rotor blades may be detrimental towards stability. The equations of a coupled blade motion were obtained using blade element theory [104].

Salazar developed a helicopter mathematical model with main and tail rotors, the model consisted of six nonlinear equations. Some simulations were carried out under specific flight conditions and each induced velocities were also used according to these. Perturbations such as wind crossing or vibration engine were considered in order to build up a robust model. Simulations of lateral and ascend flight could be found using the mathematical model. This approach was suitable to simulate and to control a helicopter, as a result the model could be used to control autonomous radio helicopter or automatic helicopter pilot as well as to build a flying computer training program [105].

Siva et al. studied the effect of uncertainties on performance predictions of a helicopter. They considered uncertain variables, the main rotor angular velocity, main rotor radius, air density, blade chord and blade profile drag coefficient. The propagation of these uncertainties in the performance parameters such as thrust coefficient, induced velocity amongst others, were studied. In the formulation of this work different flight regimes were dealt as well as the aerodynamic environment involved in these regimes [106].

Rotor wake modelling was extensively covered by [59]. The author developed a computational helicopter rotor wake model, based on the numerical solution of the unsteady fluid dynamic equations that governs the generation and the convection of vorticity in the helicopter rotor environment. The model predicted the wake structure for cases such as hover and forward flight. On the other hand, Griffiths and Leishman [107] developed a free-vortex wake model in order to examine the rotor's problems on rotor interference as well as rotors operating in ground effect. Rotor performance for dual rotor systems under various combinations of gap and stagger was studied and the predicted results were compared to experimental measurements. For a dual rotor system the free-vortex model results provided a beneficial aerodynamic interference effect in hover flight for a limited range of stagger spacings. Furthermore, a new momentum theory for the performance of overlapping dual rotors with gap was obtained. This was used as a reference solution and compared to the free-vortex results and experimental data for larger overlap ratios. The free-vortex results confirmed that ground effect on rotor power depends on both the rotor height off the ground as well as flight speed. Results for hover and forward flight were found to be in good agreement with limited experimental measurements. The authors indicated that additional validation of the approach was essential to improve the confidence in the method.

Leishman et al. [108] reviewed the theoretical basis and numerical implementation of one class of free-vortex filament methods, which proved to be robust and flexible numerical methods that should be taken into account to the prediction and analysis of helicopter rotor wakes. Various examples of the application of free-vortex filament methods to helicopter rotor problems were provided, including the wake structure and performance of single and multirotor configurations, the flight in ground effect, the effects on the wake dynamics during manoeuvring flight conditions, and the descending flight through the vortex ring state. The author indicated that free-vortex filament models considered for helicopter rotor wake analyses got predictive capability, further algorithmic improve-

ments and better validation of the methods were required. In particular, research was required to integrate rigorously the blade wake and tip vortex models and viscous effects, for example turbulent diffusion of vorticity, into vortex filament methods. In [109] the helicopter rotor wake is also studied. In here, Bhagwat and Leishman studied the helicopter rotor wake stability in hover and axial flight by using eigenvalue analysis. The rotor wake was shown to be unstable, with the tip vortices exhibiting various possible unstable deformation modes.

Analytical helicopter rotor aerodynamics were studied by [110]. The authors presented a method for predicting the onset of the vortex ring state in terms of a model for the propagation and growth of disturbances within the rotor flow. Numerical simulations of the onset of the vortex ring state provided that the transition into the vortex ring state was increasingly gradual as the acceleration of the rotor was increased. The combination of high forward speed and vertical acceleration, the vortex ring state could be replaced by a qualitatively different, highly transient state where the collapse of the wake into the toroidal form that was usually associated with the onset of this flow condition was suppressed. The absence of an abrupt and universal transition marking the onset of the vortex ring state under accelerated flight conditions complicated the application of simple analytical models. This generated that the specific details of the time-dependent dynamics of the rotor wake as well as its interaction with the rotor could not be ignored.

Aerodynamic simulation was as well tackled by Phillips and Brown for brownout problem analysis [60]. In this work, Brown's Vorticity Transport Model (VTM) was used to simulate the development of the dust cloud that could form around a helicopter when operated in dusty or desert conditions. In addition to this, the flow field around a tandem rotor configuration was simulated for the final stages of landing. VTM simulations provided that for a tandem rotor helicopter the sudden growth of the dust cloud that was responsible for the onset of brownout was due to a change in mode within the flow field surrounding the aircraft. At higher advance ratios the flow was dominated by a strong ground vortex that was created by the tail rotor.

Computational Fluids Dynamic (CFD), is an extensive method of research. An early work in this field applied to helicopter research was carried out by Caradonna. In this work, the author indicated that the performance of rotary wing aircraft was limited by a host of aerodynamic problems. The ability to design rotorcrafts with confidence required a new order of aerodynamic predictive technology that was both true to the

basic flow physics and readily usable by industry. CFD approaches can solve issues such as rotor wake prediction, compressible aerodynamics, interaction problems, etc [111]. In [112], the rotor interactions with vortices were studied as these are common problems, especially in descent or manoeuvre and the Blade/Vortex Interaction (BVI) is the predominant noise source. The ability to predict the wake was the basic problem in BVI aeroacoustics and the problem was considered from a CFD point of view. It was suggested that new approaches to CFD should be taken into account as methods in which vortex cores were not resolved.

2.10 Unmanned Aerial Vehicles (UAVs)

UAVs have been in the past years object of several studies from many different points of view. Industry and government institutions all over the world have invested great amount of money in investigation and developing these types of systems. Research conducted in the field of UAV ranges from dynamical modelling, mechanical and technical improvements, control of trajectories, control of groups of these vehicles, communication systems, etc. UAV modelling has been also explored in this work.

UAV modelling and simulation was analyzed by Velez et al. They presented a Rapid Software Prototyping Environment (RSPE) for the design, simulation, and real time implementation of a control system for an autonomous mini-helicopter. The software prototyping environment consisted of diverse modules such as mini-helicopter simulation model, controllers, ground control station, a navigation filter and linearization and parameter identification tools [113].

Johnson and DeBitett developed a simulation capability to support the design, development, and test of the navigation, control, guidance, and vision processing subsystems, as well as human machine interfaces and procedures for Unmanned Vehicle Systems [114].

Vilchis et al. presented the development a nonlinear model and a nonlinear control strategy for a VARIO scale model helicopter. The contribution focused on the particular case of a reduced order model i.e., three degrees of freedom where a scale model helicopter mounted on an experimental platform was represented. The theoretical development was illustrated using numerical results and experiments. Additionally to this,

the robustness with respect to parameter uncertainties was also studied [102].

Main rotor loads and tail rotor force fluctuations are in the majority of cases the primary source of unwanted vibrations in these type of vehicles.

The work done by Cai et al. presented a comprehensive design methodology for constructing small-scale UAV helicopters. The systematic design procedure, which included hardware component selection, design and integration, as well as experimental evaluation, was utilized to construct a fully functional UAV helicopter. In this work, the author studied the vibration sources in UAV helicopters and three sources were identified: rotation of the main rotor (30.8 Hz), rotation of tail rotor (143.4 Hz) and engine as vibration source (260.5 Hz). These frequencies are estimated based on a governed motor speed at 1850 rpm (revolution per minute) [115].

Dunbabin et al. carried out the design and construction of an integrated isolated vision and sensor platform and landing gear for the CSIRO autonomous X-Cell helicopter. In this work, the authors studied various vibration sources. These can be mechanical, aerodynamic and from normal flight motion with a broad amplitude and frequency spectrum. A range of vibrations for autonomous helicopter was given as: main rotor speed 25 Hz, tail rotor speed 113 Hz and engine speed 160 Hz [116].

A fundamental aspect in UAV helicopter modelling is the gyroscopic system that is used to stabilize the system under the action of different flight conditions. Affanni described the design, development and dynamic characterization of a high performance MEMS-based gyroscopic control system for the yaw channel of Unmanned Aerial Vehicles for aerobatic manoeuvres. The yaw channel was composed by a servomotor and the tail blades. A transfer function between the normalized servomotor position and the yaw angular rate was provided. A new asymmetrical controller was implemented to compensate the torque of the main rotor. The yaw rate characterization demonstrated a high and constant pirouette speed. Indeed, aerobatic tests demonstrated high accuracy entry into the manoeuvres [117].

Kim and Tilbury presented a mathematical model for a UAV helicopter robot, focusing on the dynamics of the flybar. The work demonstrated how the flybar's flap increases the helicopter's stability robot as well as assists on its actuation. In addition to this, the equations of motion for a six degrees of freedom model with a flybar degree of freedom were derived, system identification experiments and results were presented to verify the

mathematical model structure and to identify model parameters [118].

Cunha and Silvestre studied Bell-Hiller stabilizing bar dynamics. They presented a helicopter dynamic model, it was parameterized as a Vario X-Treme acrobatic helicopter. The simulation model included a rigid body, main rotor flap and the stabilizing bar dynamics. Solutions for a set of trimming trajectories were identified and discussed. The Bell-Hiller stabilizing bar is a mechanical blade pitch control system that generates helicopter stability. It is a standard component of model-scale helicopters. Stabilizing bars provide roll and pitch rates' dynamic feedback. In fact, the system consists of a flybar, a teetering rotor placed at a 90 degrees rotation interval from the main rotor blades and tipped on both ends by aerodynamic paddles. The stabilizing bars and its impact on the overall helicopter dynamics were analyzed [119].

Lau et al. presented a new method based on the fact that when the angular momentum of the spinning rotor was disturbed by the incremental lift along the main blades due to the varying cyclic pitch angle controlled by the servo mechanisms, the off-axis moments were induced to counteract the changes of the angular momentum according to the gyroscope principle. This work did not explain the responses by which the hingeless helicopters behave, it just quantifies a set of coupled auxiliary responses. The authors simulated the derived analytical forms and validated in experiments using the instrumented hingeless helicopter. It is concluded that using the proposed treatment, the unintuitive off-axis responses can be predicted and the on-axis responses can also be quantified [120].

These are, of course just a short number of contributions existing in the field of UAV literature. At the present, the existing amount of articles and works in this field is vast and will continue to increase in the near future. The references here mentioned are just a short selection of them in order to illustrate the main lines of research being carried out in the area of UAV research.

2.11 Chapter Summary

In this chapter existing relevant literature in various helicopter's topics has been revised. The first part was devoted to review the state of the art of several existing simulation approaches. In this work, it will be shown how symbolic software is advantageous with

respect to previous numerical software approaches such as ADAMS.

On the other hand, topics such as main and tail rotors, fuselage, dynamic equations, stability, vibrations, UAVs and aerodynamic environment modelling were also reviewed. In particular, for the aerodynamic literature review, blade element theory was thoroughly revised as this is the theoretical approach taken in this work for the aerodynamic modelling still, other aerodynamic approaches were revised such as CFD and VTM.

In conclusion, the chapter reviewed the state of the art in helicopter field modelling aspects and the existing simulation approaches revision showed that VehicleSim can provide multiple benefits when used as a simulation tool.

In fact, this is the first (to the author's knowledge) work existing in rotorcraft dynamics and aerodynamics made using VehicleSim as the only modelling tool.

Chapter 3

VehicleSim as Modelling Tool

3.1 Introduction

This chapter presents an overview and background of VehicleSim as the modelling software used in this work. VehicleSim is one of a number of multibody modelling systems currently in common use [63]. It consists on a set of Lisp macros, enabling the description of mechanical multibody systems with possible addition of non-mechanical subsystems [121]. The system has been used over a wide range of mechanical dynamic problems, mainly in connection with vehicle dynamics; in fact the previous version AutoSim was used by: [64], ([122]-[127]) and it has provided the basis for the commercial simulation codes TruckSim, CarSim and BikeSim (see reference [121]). VehicleSim has been also used, see references: ([128]-[131]).

3.2 Overview of VehicleSim Lisp

3.2.1 VehicleSim Lisp

VehicleSim Lisp is a computer program that allows to model, simulate as well as to derive symbolic equations of motion for mechanical systems composed of multiple rigid bodies. The VehicleSim code is used to generate a C simulation program, capable of computing general motions corresponding to specified cases with initial conditions and

3.2. OVERVIEW OF VEHICLESIM LISP

external forcing inputs.

The geometric and inertial properties of the rigid bodies that will conform the model are provided as inputs. Forces and torques between the various model's component can be added acting on the corresponding bodies.

VehicleSim solvers on Windows are compiled as dynamically linked library (DLL) files with a standard VehicleSim application program interface (API) that works with several possible simulation environments, including the VehicleSim browser and Matlab. The source code generated by VehicleSim Lisp is accessible by the user.

3.2.2 VehicleSim Operation

VehicleSim Lisp generates the equations of motion for a multibody system in symbolic form. Then a C source code is generated such that this program will solve the equations numerically to simulate the behaviour of the system represented by the model.

The information needed to generate the source code in C for the VehicleSim solver is assembled in VehicleSim Lisp as it processes the model description that the user provides (see Figure 3.1).

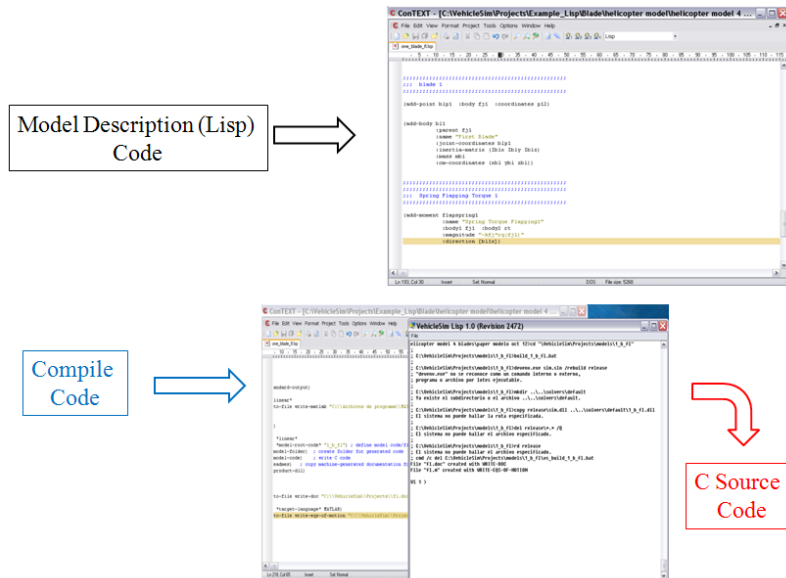


Figure 3.1: Using VehicleSim Lisp to generate C code.

3.2. OVERVIEW OF VEHICLESIM LISP

The symbolic equations generated by VehicleSim Lisp can be viewed and used with other software packages such as Word or Matlab (see Figure 3.2). VehicleSim Lisp is not a complete simulation system as it can generate equations but it does not solve them. Therefore, a C compiler is needed to compile the source code generated for a VehicleSim solver program (Microsoft Visual Studio C/C++ compiler is used), and the DLL solvers are built up as Figure 3.3 shows [132].

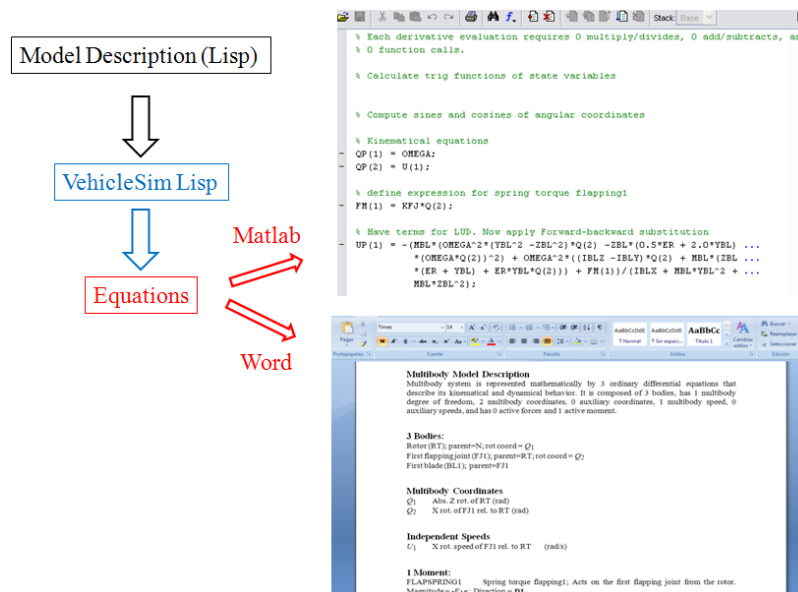


Figure 3.2: Using VehicleSim Lisp to generate equations of motion.

New solvers can be made with the same architecture and behaviour as those in packages. These are compatible with VehicleSim browser and associated tools such as the animator and plotter (see Figure 3.4).

The main purpose of each VehicleSim solver is to calculate time histories of the system's variables, this is, the positions, speeds and accelerations of the bodies conforming the system and all user-created variables. These time histories are stored in a binary data file with the extension BIN. The data in a BIN file are organized by variable name and sample number. A companion file, with extension ERD, documents the layout of the BIN file. The ERD header file also contains labelling information for each variable.

Data processing programs for ERD and BIN files obtain the information needed from the ERD file. For example, the high level of automation in the animator and plotter is possible because both are designed to extract the information from ERD files [133].

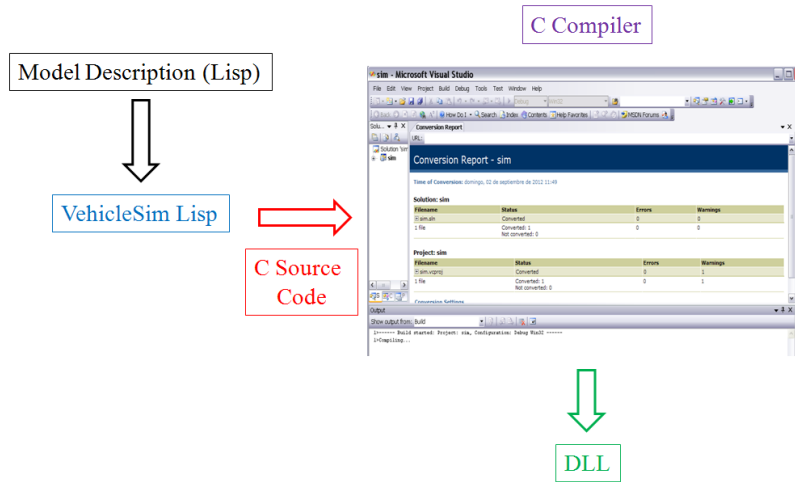


Figure 3.3: Using *VehicleSim Lisp* to build DLL.

On the other hand, *VehicleSim* generates the model’s linearised and nonlinearised equations of motion in form of differential equations (see Figure 3.2). In addition to this, *VehicleSim* also provides in form of a Matlab file the linearised state-space model in symbolic form, as Figure 3.5 shows.

3.2.3 Multibody Modelling

Most of the *VehicleSim* Lisp input descriptions are geometric and are based on vector notation because the major geometric elements used in describing the model are points, vectors, and bodies.

A point is an object that identifies a position in space. The point may represent a physical spot on a fixed mechanical object; it may represent a spot on a mechanical object that can move; or it may represent a position in space that is not part of any physical component of the system, but which is of interest when describing the multibody system.

For *VehicleSim*, a vector means a mathematical entity with a direction and length. The units assigned to its length determine the physical meaning of a vector such as length on time (velocity), force, length times force (moment), etc. A vector with a dimensionless length of one is called a unit vector and is used solely to define a direction.

3.2. OVERVIEW OF VEHICLESIM LISP

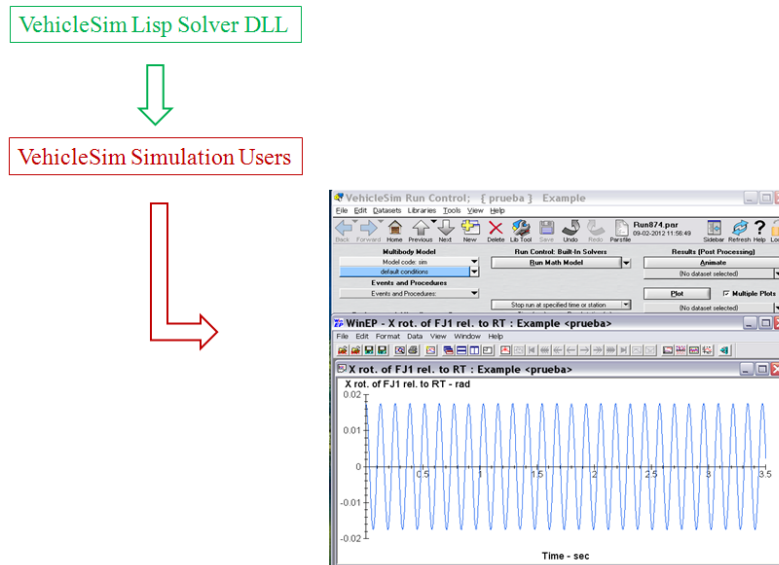


Figure 3.4: *Using VehicleSim Lisp to build VehicleSim solvers for simulating multibody systems.*

It is known that a reference frame is a geometric environment in which points remain fixed with respect to each other at all times. Although the reference frame might move and rotate, the spatial relationships between objects fixed in the reference frame do not change relative to each other. In VehicleSim, each reference frame has a rectangular 3D coordinate system that associates a unique ordered trio of numbers to each point fixed in that reference frame.

In concept, a physical rigid body is a mechanical object with inertial properties. The location and orientation of the object are tied to a geometric reference frame. In VehicleSim Lisp, both the reference frame and the physical rigid body are represented by a body data structure. Bodies are added to the model with the `add-body` command. Each body in the VehicleSim Lisp environment can be used to represent a physical part in the multibody model.

VehicleSim Lisp automatically keeps track of the angular orientation of all rigid bodies in the model. When describing model details, the effects of orientation are typically handled with the VehicleSim Lisp functions `dot`, `cross`, and `angle`. To support these functions, VehicleSim Lisp maintains a directional cosine matrix for each body, linking its orientation to that of its parent [134], [135].

3.2. OVERVIEW OF VEHICLESIM LISP

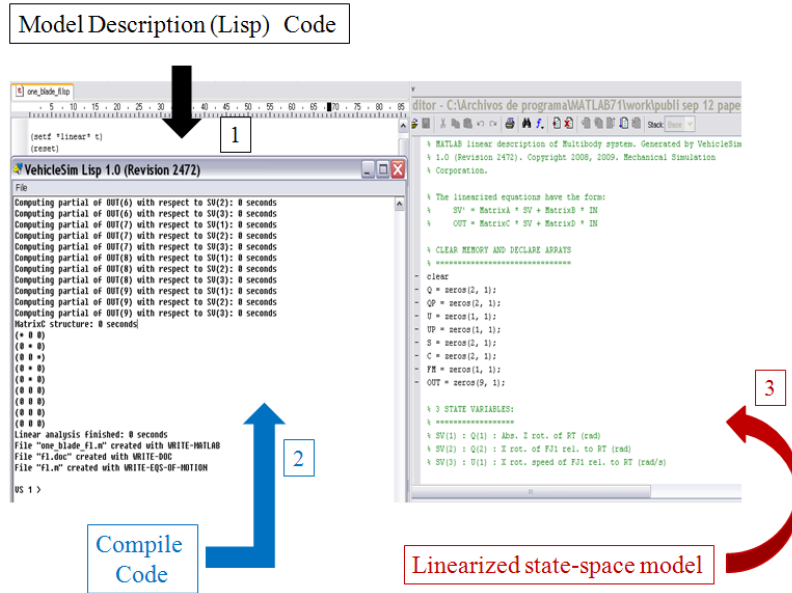


Figure 3.5: Using VehicleSim Lisp to generate the state-space model in symbolic form.

In a general case with body B with unit-vectors \mathbf{b}_x , \mathbf{b}_y , and \mathbf{b}_z , and parent body A with unit vectors \mathbf{a}_x , \mathbf{a}_y , and \mathbf{a}_z , the directional cosine matrix C is defined as:

$$\mathbf{C} = \begin{pmatrix} \mathbf{b}_x \cdot \mathbf{a}_x & \mathbf{b}_x \cdot \mathbf{a}_y & \mathbf{b}_x \cdot \mathbf{a}_z \\ \mathbf{b}_y \cdot \mathbf{a}_x & \mathbf{b}_y \cdot \mathbf{a}_y & \mathbf{b}_y \cdot \mathbf{a}_z \\ \mathbf{b}_z \cdot \mathbf{a}_x & \mathbf{b}_z \cdot \mathbf{a}_y & \mathbf{b}_z \cdot \mathbf{a}_z \end{pmatrix} \quad (3.1)$$

VehicleSim Lisp generates this matrix based on the rotational variables that were introduced for the body. VehicleSim Lisp uses the direction cosine matrix to handle vector expressions involving the unit vectors from the new body.

The next fundamental concepts have an important role in the modelling process: the translation and rotation information provided in the `add-body` command define how the new body moves relative to the parent body. The number of independent motions allowed between the new body and the parent is known as the number of body degrees of freedom. A body can have up to three rotational degrees of freedom, and up to three translational degrees of freedom. A force is represented mathematically as a vector and a point. The magnitude of the vector has units of force. The point (fixed on the body to which the force is applied to) and the direction of the vector defines the line of action of the force.

Other fundamental concept used in VehicleSim is the moment; it is always defined relative to a point, such that the distance vector in the moment expression is the position vector connecting the reference point for the moment with any point lying on the line of action of the force [134], [135].

3.3 VehicleSim Characteristics

The purpose of the VehicleSim solver is to solve the dynamical equations of motion to calculate the time histories of the variables contained in the mathematical model that represent the system's variables.

3.3.1 State Variables

VehicleSim Lisp introduces the state variables needed to describe the moving reference frames, and uses them as needed to develop mathematical expressions of variables that represent the equations of motion of the system under study. The state variables for a VehicleSim multibody system are divided into two sets: generalized coordinates and generalized speeds.

The generalized coordinates are the variables involving angular and translational displacements. The set of generalized coordinates is defined such that it is possible to reconstruct the position of any point in any part in the system. VehicleSim Lisp can derive expressions for the absolute coordinates of any point located on any mechanical part using the generalized coordinates and dimensional parameters. On the other hand, a set of generalized speeds complements the set of generalized coordinates, by adding the capability for VehicleSim Lisp to determine the velocity vector of any point located on any part in the multibody system.

From the user point of view, the set of state variables also includes variables that are not defined by differential equations, but whose values are, nevertheless, required to fully define the current state of the model. However, in VehicleSim environment, the term "state variables" usually refers only to variables that are defined by differential equations.

The `add-variables` command is used to include one or more variables in the coded program and to declare that they are not constant during a run [134].

Controlling the Definition of the State Variables

State variables are introduced automatically when the command `add-body` is used to define a body that can move relative to its parent. One generalized coordinate is introduced for each degree of freedom of the new body relative to its parent, and the coordinates are the amplitudes of the permitted movements. The equations of motion for a system involve a minimum number of coordinates and a speed variable is introduced automatically with each coordinate. The speed variable is defined as the derivative of the coordinate, except for the following three cases [134]:

- A body with three rotational degrees of freedom relative to its parent has three rotational speed variables defined as scalar measures of the absolute rotational velocity of the body.
- A body with three translational degrees of freedom relative to its parent has three translational speed variables defined as scalar measures of the absolute velocity of the body mass center.
- A body restricted to planar motions, with two translational degrees of freedom has the translational speeds defined as scalar measures of the absolute velocity of the body mass center.

3.3.2 Equations of Motion

VehicleSim can provide pure kinematical analyses and simulation in quasi-static equilibrium conditions. In these cases, values of the state variables are obtained as functions of time. The majority of equations produced by VehicleSim Lisp are arithmetic statements that define the output variables and the derivatives of the state variables [134].

Dynamic System Simulation

The form of simulation generated by VehicleSim Lisp is one in which the system responds dynamically to specified inputs. The number of degrees of freedom of the multibody system model is the minimal number of independent generalized speeds needed to define the absolute velocity vector of any point on any body in the system.

During the simulation the generalized coordinates are computed by numerical integration of a set of ordinary differential equations of the form:

$$\dot{q} = s \quad (3.2)$$

where q is an array of the derivatives of the generalized coordinates, and s is an array of speeds defined in terms of the current values of the state variables and known functions of time. The equation (3.2) defines the geometric relationships between the generalized coordinates and generalized speeds.

$$\dot{u} = f \quad (3.3)$$

u is an array of the derivatives of the generalized speeds, and f is an array whose elements are computed from the current values of the state variables and time.

The equations (3.3) are developed by VehicleSim Lisp such that they: a) are independent and b) satisfy Newton's second law and Euler's equations. In vector form, Newton's second law for a rigid body is:

$$\sum f = \frac{dp}{dt} = ma \quad (3.4)$$

where $\sum f$ is the vector sum of all forces acting on the body, p is the vector momentum of the body, m is the body mass, and a is the vector acceleration of the mass centre of the body. The vector form of Euler's equations for a rigid body is:

$$\sum t = \frac{dh}{dt} = I \cdot \alpha + \omega \times I \cdot \omega \quad (3.5)$$

where $\sum t$ is the vector sum of all torques and moments acting on the body about its mass centre, h is the vector angular momentum of the body about its mass centre, I is the inertia dyadic of the body relative to its mass centre, α is the vector angular acceleration of the body, and ω is the vector angular velocity of the body.

A dynamical simulation program computes the state variables (generalized coordinates and generalized speeds) by numerically integrating equations (3.2) and (3.3).

The mathematical model might use numerical methods to solve a set of nonlinear algebraic equations that implicitly define some variables that are similar to generalized coordinates because they define locations or orientations of rigid bodies in the system. In addition to this, coordinate variables that are calculated directly are called computed coordinates. They are calculated by applying simple arithmetic statements, if it is required. They are computed numerically by using the Newton-Raphson iteration method [134].

Kinematics

A kinematical model has no dynamical degree of freedom, and therefore, no generalized speeds. In most cases, a kinematical simulation does not involve differential equations. Generalized coordinates used to describe positions of points are all either explicit functions of time or dependent computed coordinates that are computed on the basis of algebraic equations [134].

3.3.3 Numerical Solution

The purpose of the solver program produced by VehicleSim Lisp (VehicleSim-Browser) is to compute the output variables at intervals of time as the simulation is being carried out. The output variables are defined by solving the dynamical equations of motion containing the state variables.

There are four classes of computation methods that might be used by in a VehicleSim solver program.

- Simple arithmetic statements.
- Numerical integration of a set of ordinary differential equations.
- Solution of a set of simultaneous linear algebraic equations.
- Solution of a set of simultaneous nonlinear algebraic equations.

Numerical Integration

The equations of motion derived by VehicleSim Lisp for a multibody system are in the form of a set of first-order, ordinary differential equations. In theory, each state variable is a continuous function of time. However, in a simulation run, calculations are made at discrete intervals of time. Figure 3.6 shows the history for a generalized coordinate $q(t)$ at discrete values of time separated by a constant step ΔT . At each step, identified by i , there is a corresponding value for each state-variable q_i and its derivative (generalized speed), indicated as q'_i .

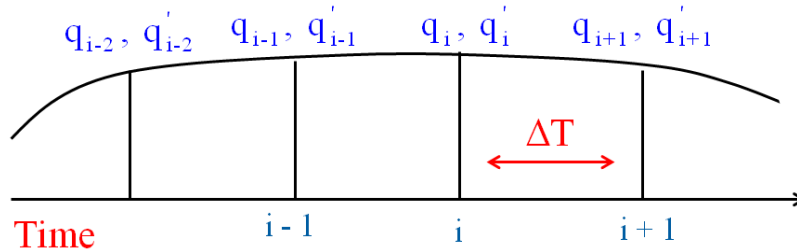


Figure 3.6: *Discrete samples of a state variable q and its derivative q' . This figure is drawn by the author and based on [134].*

The solver program computes the values of each output variable in the mathematical model at each time interval, using current values of the generalized coordinates (q) and speeds (\dot{q}) and possibly their derivatives. The state variables are in turn calculated using numerical integration.

If the time t and value of q are known at interval i ($time = T_i$, $q = q_i$), then ordinary differential equations in the mathematical model can be used to calculate the corresponding value of the derivative q' .

The correct value of the state variable at the following interval ($i + 1$) is:

$$q_{i+1} = q(T_i + \Delta T) = q_i + \int_{T_i}^{T_i + \Delta T} q'(t) dt \quad (3.6)$$

where $q'(t)$ is a function of q and possibly other variables that might vary over the interval ΔT . An exact solution for equation (3.6) is usually not possible, so the general solution method is to calculate the new value of q_{i+1} via numerical integration.

Euler integration methodology does not account for any change in the derivatives over the time interval and is not accurate unless ΔT is small and changes in the derivative are negligible over the step [134].

Solution of Simultaneous Algebraic Equations

It is assumed that there is a set of n equations for independent variables x_1, x_2, \dots, x_n in column vector x with the form:

$$\begin{aligned} g_1(x_1, x_2, \dots, x_n) &= 0 \\ g_2(x_1, x_2, \dots, x_n) &= 0 \\ &\dots \\ g_n(x_1, x_2, \dots, x_n) &= 0 \end{aligned} \tag{3.7}$$

These equations are written in vector form as:

$$g(x, t) = 0 \tag{3.8}$$

where t is the time.

If the equations are independent, then there might be enough information to solve for the variables x if the number of equations equals the number of variables. There are two solution methods used in VehicleSim solver programs, depending on whether the equations are linear or nonlinear.

Linear Algebraic Equations

Linear equations are given in the form:

$$Ax = b \tag{3.9}$$

where A is an $n \times n$ matrix and b is a column vector of length n . The elements of A and b can be complicated to calculate, and can include nonlinear functions. Nevertheless, if they do not involve any of the elements of x , then the equations are linear in x . The solution in this linear case is of the form:

$$x = A^{-1}b \quad (3.10)$$

A more efficient solution is the Lower-Upper triangular Decomposition (LUD). The matrix A is written as a product of two matrices, L and U , such that L has a lower-triangular form, and U has an upper-triangular form. The equation set can then be written in the form:

$$Ax = (LU)x = L(Ux) = b \quad (3.11)$$

and equation (3.11) can be written as two equation sets:

$$Ly = b \quad (3.12)$$

$$Ux = y \quad (3.13)$$

The advantage of the above form is that triangular sets of equations can be solved by sequential substitution. Solution of linear equations by LUD methodology involves two steps: a) the original A matrix is decomposed into $L - U$ form. This is normally done such that the values of L and U matrices occupy the computer storage space originally used to hold the elements of the A matrix. (Values that are defined as always being zero or one are not stored). Equations (3.12) and (3.13) are solved in the second step by forward and backward substitution.

Most multibody mathematical models will include sets of simultaneous linear algebraic equations. In most cases, VehicleSim Lisp solves those sets of equations by applying the LUD method symbolically [134].

Nonlinear Algebraic Equations

Nonlinear algebraic equations can be expressed as:

$$g(x, t) = 0 \quad (3.14)$$

They can be solved iteratively if: a) a solution exists, b) an initial guess is provided for x that is reasonably close to the right solution. Newton-Raphson method is used when needed in VehicleSim solver programs. This method is based in a sequence of steps as follows:

- provided guesses values for $[x_1, x_2, \dots, x_n]^T = x(i)$, where the index i is the iteration number.
- compute $-g_i$ i.e., iteration. If all $|g_j| < \epsilon$ with $j = 1, \dots, n$ (j is the subscript iteration) and ϵ is an error threshold, then stop. The solution is x_i . Otherwise, continue.
- Compute the Jacobian matrix J_i , where each element is defined as:

$$(J_{j,k})_i = \left(\frac{\partial g_j}{\partial x_k} \right)_i \quad (3.15)$$

- Solve for Δx_i using the LUD method and equation set: $J_i \Delta x_i = -g_i$
- Update the best guess of solution: $x_{i+1} \leftarrow x_i + \Delta x_i$
- Increment i ($i \leftarrow i + 1$), then go to second step.

When the Newton-Raphson iteration is used in a VehicleSim solver, the VehicleSim Lisp derives the elements of the Jacobian matrix symbolically and writes a C function that calculates the matrix based on the current values of the state variables [134].

3.4 Building a Model

When writing up the code for building a VehicleSim model certain order in which the commands appear is usually followed. In general, at the head of a VehicleSim program there are certain commands that are used to reset the system, define the gravitational field, select the unit system to be used, the possible linearization of equations of motion, etc. When the analyst does not exercise choice overtly in these matters, default settings come from a configuration file that the analyst is free to access.

VehicleSim Lisp in general follows the modelling sequence as shown in Figure 3.7. VehicleSim commands are used to describe the components of a multibody system in a parent-child relationship according to their physical constraints and joints. As it can be seen in Figure 3.7, the commands incorporate and describe in sequential manner the

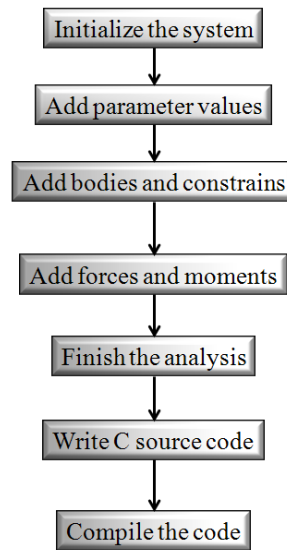


Figure 3.7: *VehicleSim* commands main sequence. This figure is done by the author and based on [134].

rigid bodies that conform the system, the corresponding physical values such as name, mass, inertia, the rotations amongst others, are also included.

A *VehicleSim* program begins with an inertial reference frame \mathbf{n} , with fixed origin, \mathbf{n}_o , and fixed directions $[\mathbf{n}_x]$, $[\mathbf{n}_y]$ and $[\mathbf{n}_z]$ already defined. As new bodies are added to the system, having freedoms relative to \mathbf{n} , local origins and axes are defined.

The code can transform from local coordinates to global ones and vice versa. Points specified globally are conveniently used to define points in bodies. The body fixed points coincide with the corresponding global points, fixed in \mathbf{n} , when the system is on its nominal configuration. Most points are fixed in bodies but a point may be defined as moving with its location in a body determined by its specified coordinates. This is especially useful for describing time varying contact points between two bodies.

The main commands used to build a multibody model are briefly described as follows:

- **add-gravity**

This command defines a uniform gravitational field, its direction. If not specified with the keyword `:direction`, it is set to `nz` as in *VehicleSim* the direction along the Z axis positive in down direction. `nz` is the unit vector in \mathbf{n} . As it was mentioned before, \mathbf{n} is the inertial reference frame.

- **add-point**

This command defines a point that can later be used for describing forces, etc. The required argument `symbol` is used to identify the point at a later stage.

- **add-body**

This command defines a rigid body, its coordinate system, its mass properties, and the kinematics of a joint connecting it to another body that is already in the model. The existing body used as a reference for the new body is called the parent of the new body, which is recalled as the child.

The `add-body` command has one required argument, `symbol`, used to identify the new body in all future references and to generate symbols for parameters and points associated with this new body.

- **add-line-force**

This command defines a force in the system that passes through a given point and whose line of action has a specified direction. The required argument, `symbol`, is a "symbol" used later to identify the force.

- **add-moment**

This command introduces a moment between two bodies. The required argument is a symbol used to identify the moment. Note that at least one of the optional arguments `body1` or `body2` must be included in order for the moment to act.

- **add-speed-constraint**

It is an algebraic expression that is identically zero when the constraint is satisfied. The optional argument `u` is a generalized speed that is eliminated by the constraint. If `u` is not provided, then `add-speed-constraint` uses some programmed criteria to select one automatically [134], [135].

3.5 Chapter Summary

In this chapter the main characteristics, properties and commands of VehicleSim Lisp that will be used in this work have been introduced and briefly described.

The general properties and operation conditions of VehicleSim were presented in section 3.2.1 and 3.2.2. Section 3.2.3 explains in detail the fundamental characteristics of VehicleSim Lisp as multibody software. Section 3.3 has been provided an overview of the numerical methods that VehicleSim uses. Finally, section 3.4 contains and describes the main sequence of VehicleSim commands that are used in the modelling process in this work.

In the following chapters, a specific type of helicopter will be modelled following the general program structure described in here. It will be shown how by using VehicleSim, systems conformed of rigid bodies can be modelled and the convenience of this approach with respect to other modelling tools in terms of reduced complexity of the program, reduced computing time and possibility of modifying the model without the need of building it again.

Part II

Helicopter Models

Chapter 4

Caliber 3 Dynamic Model

4.1 Introduction

Unmanned Aerial Vehicles have existed for many decades; in fact, various type of drones have been used since World War I. In the previous decade, the development, procurement and deployment of UAVs for military applications rapidly expanded. These days, the use of Unmanned Aerial Vehicle (UAV) is growing in the private and civil sectors, due to their ability for forest fire fighting, emergency mountain rescue, climate monitoring, aerial photography, mapping and surveying, etc. A wide range of UAVs are used by the police and civil security for law enforcement as well as border security and coastguard surveillance. These machines are designed to perform surveillance tasks, typically carrying cameras and other type of sensors.

Small unmanned aerial rotorcrafts have two main features that make them very useful. First, small UAVs are designed to be carried by either a single man, or transported with a vehicle, without the need of dedicated loading equipment. Second, unmanned rotorcrafts have a vertical take off, landing and hovering capabilities. They do not require a runway, a launching device or a dedicated recovery system and can easily hold their position when required [136].

The purpose of this chapter is to model a particular type of Unmanned Aerial Vehicle by using VehicleSim, showing as other subsystems are as well implemented, the elevators

and the swashplate. The modelling process is similar to the one will describe in the following chapter, whereas the dimensions, the physical parameters such as fuselage's mass, blades' masses amongst others, do differ from the following case. First, a general overview of the UAV prototype under study (Caliber 3) is given. This is followed by modelling the details and a description of the multibody model in VehicleSim and, finally some results from the simulations carried out are shown.

The work carried out in this chapter was performed under the umbrella of a joint project between The City University London and the La Laguna University, Spain: "DPI2010-20751-C02-02. Diseño de estrategias inteligentes de control y diagnóstico basadas en el análisis de vibraciones: Aplicación a helicópteros no tripulados UAV's" granted by the Innovation and Science Ministry (Spain).

At City University the model was implemented in VehicleSim, vibrations were generated on the main rotor in order to detect their impact on the fuselage. After that, the La Laguna University team developed strategies of control based in artificial intelligence methods in order to reduce the effects of these vibrations on the fuselage, and potentially improve in this way the quality of images obtained by the UAV's onboard vision system. As a result of this work, a journal paper was published ([128]).

4.2 Caliber 3 Description and Parameters Identification

The physical prototype of the model under study is shown in Figure 4.1. It is a radio controlled engine helicopter, Caliber 3 [139].

The engine is a KYOSHO GX36H for helicopter and it has a radio for engine-powered R/C helicopter (see Figure 4.2).

As it can be seen in Figure 4.1, the helicopter consists in three main subsystems: main rotor, fuselage and tail rotor, the fuselage in this case contains a fuel tank.

The initial design of the VehicleSim model of the Caliber 3 was approached from a dynamics-only perspective. The physical properties such as weight, fuselage's mass, blades' masses amongst others, were measured at La Laguna University. Other impor-

4.2. CALIBER 3 DESCRIPTION AND PARAMETERS IDENTIFICATION



Figure 4.1: *Unmanned Aerial Vehicle Caliber 3. Photography taken on June 2011, at La Laguna University (Spain). Reproduced with permission from Kyosho Corporation.*

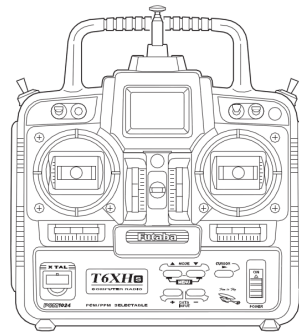


Figure 4.2: *Futaba radio [139]. Reproduced with permission from Kyosho Corporation.*

tant data such as the rotor's and blade's inertias amongst others, were obtained by using Autodesk Inventor program [137]. It is a 3-dimensional modelling package that allows to select a wide range of options in order to create and design mechanically sound and competent models. It allows to create life like 3D models and then use certain features in order to create an overall assembly. Autodesk Inventor works as a Windows interface [137], [138].

The physical parameters were obtained by a collaborative work with La Laguna University staff. This was made in several phases, firstly, the shape and configuration of the various subsystems were analyzed on the Caliber 3. After that, the reference system was defined on the system according to the standard procedure used in VehicleSim. This was a fundamental step as La Laguna University team used a different reference system. When both reference systems were fixed, the flux of information between both

4.2. CALIBER 3 DESCRIPTION AND PARAMETERS IDENTIFICATION

groups was coherent between VehicleSim and Autodesk Inventor. Secondly, the physical dimensions of the system such the blades' masses, distance between the tail rotor and the fuselage, the offset distance on the main and tail rotors blades amongst others, were directly measured in the laboratory, this was a difficult task as the configuration, the shape, as well as the small dimensions of the model did not allow to easily obtain the measurements in an easy manner. Thirdly, according to VehicleSim requirements, other parameters such as centre of mass, blades moment of inertia amongst others, were obtained, these parameters were calculated using Autodesk Inventor. Finally, the helicopter's model implementation in VehicleSim took place.

The Caliber 3 parameters are given in Table 4.1.

Parameters	Symbol	Magnitude
Fuselage mass	m_f	2.428 (kg)
Main rotor blade mass	m_{bl}	0.121 (kg)
Elevator mass	m_{elev}	0.041 (kg)
Tail rotor blade mass	m_{btll}	0.00441 (kg)
Fuselage-main rotor vertical distance	h	0.105 (m)
Fuselage-swashplate vertical distance	h_{sw}	0.01 (m)
Fuselage-elevators vertical distance	h_{elev}	0.09 (m)
Fuselage-tail rotor vertical distance	h_{tl}	0.07 (m)
Fuselage-tail rotor longitudinal distance	x_t	0.625 (m)
Fuselage-tail rotor cross distance	y_t	0.05 (m)
Main rotor blade length	l	0.55 (m)
Tail rotor blade length	l_{tl}	0.08 (m)
Main rotor flap hinge spring stiffness	k_{fj}	1 (Nm/rad)
Main rotor lag hinge spring stiffness	k_{lj}	57 (Nm/rad)
Tail rotor flap hinge spring stiffness	k_{fjtl}	45 (Nm/rad)
Delta three angle	$delta3_{tl}$	0.785 (rad)
Main rotor angular speed	ω	177.93 (rad/s)
Tail rotor gearing	k_{rttl}	5

Table 4.1: *Caliber 3 Model parameters obtained at La Laguna University.*

4.3 Model Description

Multibody systems can be modelled in various ways, one of them is the combination of several interacting subsystems. The main aim of this section is to implement a model of an UAV as a multibody system with several subsystems as well as several constraints between the different degrees of freedom. VehicleSim allows to develop other technical considerations in the modelling process, for example, the elevators can be modelled by imposing restrictions. The general considerations taken into account for the modelling process are described in the following lines:

- The helicopter is on Sikorsky configuration: this is, the main rotor is perpendicular to the tail rotor. The axis of rotation of the tail rotor is transverse to the axis of rotation of the main rotor. Both subsystems are mounted on the fuselage.
- The main rotor consists of two equally spaced blades as well as two elevators pinned to a central hub. The blades have free motion in the plane of the disc and this is allowed by the blade's hinges.
- The tail rotor consists of two equally spaced blades joined to a secondary hub.
- The blades are rigid in both rotors.
- The angular speeds are implemented as constant parameters in both rotors and there exists a proportional ratio between them.
- The main rotor's hinges have three degrees of freedom: feather, lag and flap.
- The tail rotor hinges have two degrees of freedom: feather and flap.
- Feather-flap coupling effects are considered in the case of the tail rotor.
- The fuselage has six degrees of freedom: three translations along the corresponding (X , Y , Z) axes and three rotations (φ , ϕ , ζ) around the same axes.

The arrangement of the bodies and connecting linkages are shown in Figure 4.3. These points are then used to divide the Caliber 3 into its constituent bodies for the purpose of building the model. The bodies are arranged in a parent-child relationship as shown in Figure 4.3 with respect to the inertial body n . The VehicleSim command `add-body` specifies the details of the new body and its relationship to the previous body, as it will be detailed in the following Chapter 5.

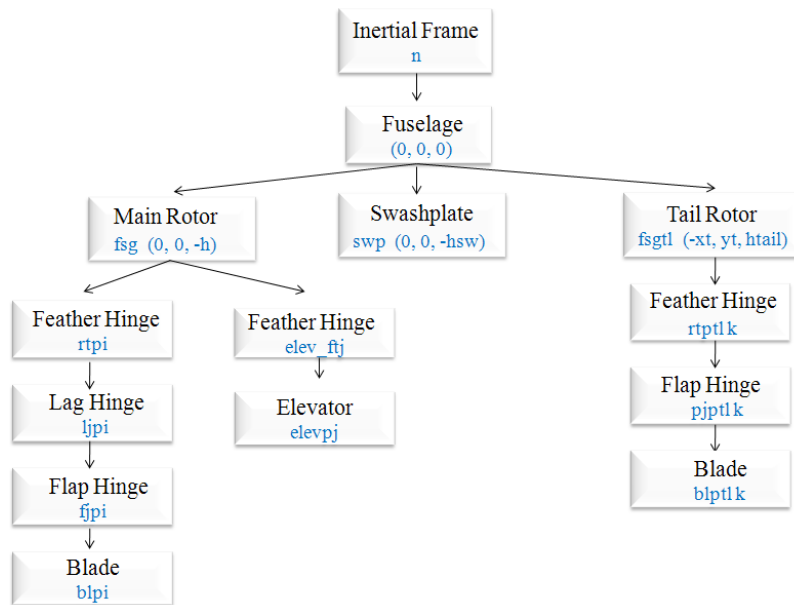


Figure 4.3: *Caliber 3 body structure diagram. The corresponding attachment points symbols are also indicated.*

4.4 Fuselage Modelling

The fuselage is defined and added to the program as body, it is implemented as the child of the nominal reference frame n and it is the parent of three bodies: the swashplate, and the main/tail rotors.

```

(add-body fuselage
  :name "Fuselage"
  :parent n
  :mass mf
  :joint-coordinates (0 0 0)

```

```
:translate (x y z)
:body-rotation-axes (z y x)
:parent-rotation-axis z
:reference-axis x
:inertia-matrix (Ifx Ify Ifz)
:cm-coordinates (xcmf ycmf zcmf))
```

The fuselage is added as a body with mass, moments of inertia as well as centre of mass. It has translational degrees of freedom along the x , y and z directions of \mathbf{n} , as \mathbf{n} is its parent. The yaw, pitch and roll rotational degrees of freedom around the axes z , y and x are respectively considered in order to describe the full rotation of the helicopter in the space.

As mentioned before, the helicopter structure is complex, the fuselage has a fuel tank, besides the fuselage itself, the tail rotor is assembled with a mechanical connection as well as the swashplate and the main rotor, being this structure a mesh of mechanical connections.

4.5 Swashplate and Main Rotor Modelling

The modelling process of the Caliber 3 is similar to the helicopter model build up in the following chapter. The main differences between both models are that the swashplate is modelled here as new body and the elevators are now included and implemented on the main rotor.

4.5.1 Swashplate Modelling

The blade feather angles can be mathematically described as a Fourier series. Blade feather is mechanically induced from two sources:

- The helicopter control system uses a swashplate, the orientation of which is controlled by the pilot. The control inputs produced by the swashplate consist of the collective and cyclic feather angles. The collective feather controls the average blade feather angle, therefore, the blade lift and the average total thrust. On the

4.5. SWASHPLATE AND MAIN ROTOR MODELLING

other hand, the cyclic feather controls the orientation or tilt of the rotor disc and so the direction of the rotor thrust vector, see Figure 4.4.



Figure 4.4: *Configuration of the swashplate mechanism. Reproduced with permission from Kyosho Corporation.*

- Blade elastic deformation and control system, also play a role in the blade's feather angle, [98] nevertheless, in this thesis only rigid blades are considered where no elastic effect is taken into account.

The swashplate is implemented in VehicleSim using a parent-child structure. The swashplate is the "child" of the fuselage, and it will be the "parent" of the next subsystem. The swashplate is connected to the fuselage at the point `swp` (see Figure 4.5).

The swashplate is implemented as body with a rotating degree of freedom around the helicopter's vertical shaft.

```
(add-point swp :body fuselage :coordinates (0 0 -hsw))
```

The commands defining the swashplate:

```
(add-body sw
  :name "Swashplate"
  :parent fuselage
  :mass msw)
```

```

:joint-coordinates swp
:body-rotation-axes z
:parent-rotation-axis z
:reference-axis x
(inertia-matrix (Iswx Iswy Iswz))
:cm-coordinates (xsw ysw zsw))

```

The swashplate is added as a body with mass, moments of inertia and centre of mass. The swashplate angular speed is given in the form of a constrain that forces it to rotate at the same angular speed "omega" as the main rotor:

```
(add-speed-constraint "ru(sw)-(omega)" :u "ru(sw)")
```

where omega is the angular speed.

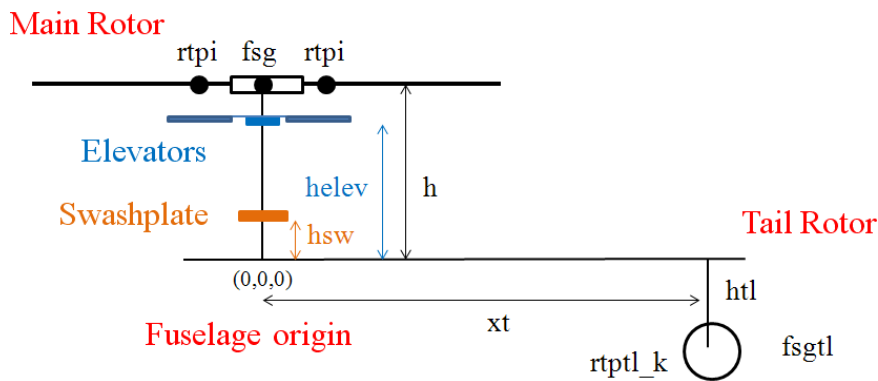


Figure 4.5: Schematic representation of the Caliber 3 VehicleSim model.

4.5.2 Main Rotor Modelling

The main rotor has two blades that are modelled similarly to that in the following chapter, and two elevators. The relative blades' positions and the elevators with respect to the main rotor axes origin must be considered in order to define the joint locations. The separation angle between the blades and the elevators and the main rotor axis is defined with the variable α_i with $i = 2, 4$ for the number of blades and α_j with $j = 1, 3$ for the number of elevators. These notations are used because the blades and the elevators have alternate locations on the main rotor, as Figure 4.6 shows. These angles will define the local axis for each blade and each elevator.

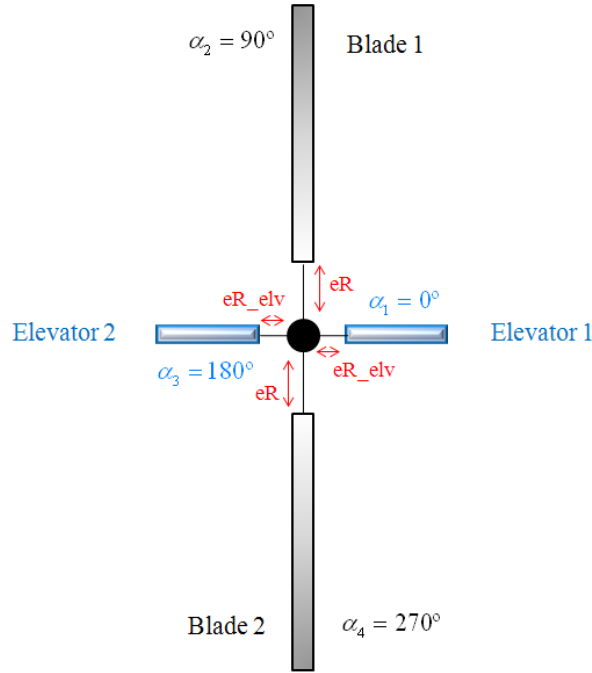


Figure 4.6: *Caliber 3 model main rotor nominal configuration.*

The azimuth angle for the i^{th} -blade is given by the next expressions:

```
(setsym alphai "360*((nblades-bladenumberi)/(nblades))")
(setsym argi "2*pi*(@alphai/360)")
```

where `nblades` is the parameter representing the total number of blades and the elevators in the main rotor i.e., a constant value of four and `bladenumberi` is the corresponding blade being modelled.

The azimuth angle for the j^{th} -elevator with ($j = 1, 3$) is given by the next expression:

```
(setsym alphaj "360*((nblades-bladenumberj)/(nblades))")
(setsym argj "2*pi*(@alphaj/360)")
```

`nblades` was defined previously and `bladenumberj` is the corresponding elevator being modelled.

The blade hinges have been located at an offset distance `eR` from the main rotor centre point. The elevators hinges have been placed at an offset distance `eR_elv` from the main rotor centre point. The hinges are added in a sequential manner such that each of them

is the child of the previous one and the parent of the following hinge.

The blades' offset positions are defined as two variables `xi`, `yi`:

```
(setsym xi "eR*sin(@argi)")
(setsym yi "eR*cos(@argi)")
```

The angles `argi` are used to define the local axis for each blade as `biaxesx`, `biaxesy` and `biaxesz`. The blades' local axes are defined in terms of the inertial reference axes.

The position of each blade with respect to the main rotor is determined as:

```
(setsym biaxesx "-sin(@argi)*[rty]+cos(@argi)*[rtx]")
(setsym biaxesy "sin(@argi)*[rtx]+cos(@argi)*[rty]")
(setsym biaxesz "[rtz]")
```

The locations of the elevators offset are represented by the variables `xj`, `yj`:

```
(setsym xj "eR_elv*sin(@argj)")
(setsym yj "eR_elv*cos(@argj)")
```

The angles `argj` are used to define the local axis for each elevator as `bjaxesx`, `bjaxesy` and `bjaxesz`. Therefore, the local axes for the elevators are implemented in terms of the inertial reference axes. The position of each elevator with respect to the main rotor is given as:

```
(setsym bjaxesx "-sin(@argj)*[rty]+cos(@argj)*[rtx]")
(setsym bjaxesy "sin(@argj)*[rtx]+cos(@argj)*[rty]")
(setsym bjaxesz "[rtz]")
```

The rotor is connected to the fuselage at the point `fsg` (see Figure 4.5) using a similar parent-children structure:

```
(add-point fsg :body fuselage :coordinates (0 0 -h))

(add-body rt
  :name "Rotor"
  :parent fuselage
  :mass mrt
  :joint-coordinates fsg
  :body-rotation-axes z
```

```

:parent-rotation-axis z
:reference-axis x
(inertia-matrix (Irtx Irty Irtz)
:cm-coordinates (xcmrt ycmrt zcmrt))

```

The rotor is set up as a body with mass, moments of inertia as well as centre of mass. The rotational degree of freedom around the axes Z is allowed.

The different degrees of freedom are added on the blades in a sequential manner where each of them is the child of the previous one. The hinges are connected to the main rotor, at the points rt_{pi} , where $i = 2, 4$. (Figure 4.5).

The blades hinges are also connected to the main rotor, at the point rt_{pi} with $i = 2, 4$. Various points in the helicopter nominal configuration within the coordinate system of body n need to be defined because the feather will be connected as a subsequent degree of freedom as well as the lag and flap. The blades will be connected to the last of these points.

Thus, the main rotor nominal configuration is built in a sequential manner:

```
(add-point p_nblabes_i :body n :coordinates ("@xi" "@yi" -h))
```

the variables $@xi$ and $@yi$ were previously defined.

```
(add-point rt_{pi} :body rt :coordinates p_nblabes_i)
```

The feather hinge is connected to the main rotor at the point rt_{pi} :

```

(add-body p_{ji}
  :name "i-th Feather Joint"
  :parent rt
  :joint-coordinates rt_{pi}
  :body-rotation-axes y
  :parent-rotation-axis "@biaxesy"
  :reference-axis "@biaxesz"
  :inertia-matrix 0
  :mass 0)

```

4.5. SWASHPLATE AND MAIN ROTOR MODELLING

Once the feather hinge is defined, the lag hinge is connected to the feather hinge at the point `ljpi` as a child of the feather hinge:

```
(add-point ljpi :body pji :coordinates p_nblabes_i)

(add-body lji
  :name "i-th Lag Joint"
  :parent pji
  :joint-coordinates ljpi
  :body-rotation-axes z
  :parent-rotation-axis z
  :reference-axis "@biaxesx"
  :inertia-matrix 0
  :mass 0)
```

The flap hinge is added as the child of the lag hinge at the point `fjpi` being the parent of the blade:

```
(add-point fjpi :body lji :coordinates p_nblabes_i)

(add-body fji
  :name "i-th Flap Joint"
  :parent lji
  :joint-coordinates fjpi
  :body-rotation-axes x
  :parent-rotation-axis "@biaxesx"
  :reference-axis "@biaxesy"
  :inertia-matrix 0
  :mass 0)
```

Now, the blade is added as the child of the flap hinge:

```
(add-point blpi :body fji :coordinates p_nblabes_i)

(add-body bli
  :name "i-th Blade"
  :parent fji
  :mass mbli)
```

```

:joint-coordinates blpi
(inertia-matrix (Iblxi Iblyi Iblzi)
:cm-coordinates (xbli ybli zbli))

```

The elevators hinges are connected to the main rotor, at the points `p_elev_j`, where $j = 1, 3$. (See Figure 4.5). Various points in the helicopter nominal configuration within the coordinate system of body `n` as the feather and the elevators will be added to the model to these points.

```

(add-point p_elev_j :body n :coordinates ("@xj" "@yj" -helev))

(add-point elev_ftj :body rt :coordinates p_elev_j)

```

On the other hand, the elevator is connected to the main rotor at the point `elevftj`.

```

(add-body pj_j
  :name "j-th Feather Joint"
  :parent rt
  :joint-coordinates elev_ftj
  :body-rotation-axes y
  :parent-rotation-axis "@bjaxesy"
  :reference-axis "@bjaxesz"
  :inertia-matrix 0
  :mass 0)

```

The elevator is similarly added as:

```

(add-point elevpj :body pj_j :coordinates p_elev_j)

(add-body elevj
  :name "j-th Elevator Joint"
  :parent pj_j
  :mass melevj
  :joint-coordinates elevpj
  :inertia-matrix (Ielevxj Ielevyj Ielevzj)
  :cm-coordinates (xblelevj yblelevj zblelevj))

```

4.5.3 Controllers and Moments Definition

Once the code has been set up and the corresponding points have been implemented, the moments and the controllers need to be included in the model.

Elevator Feather Control Definition

It is known that aircraft require frequent corrections and this is a tedious task to perform for extended periods of time. Stabilisation devices in common use fall into two categories:

- a mechanical/gyro device which is an integral part of the rotor system.
- automatic flight control systems that use feedback control laws based on signals obtained from sensors.

The elevators action on the main rotor can be considered as mechanical/gyro devices i.e., simple stabilising system. It is basically a bar pivoted to the main rotor shaft that behaves as a gyroscope (see Figure 4.7) [141].

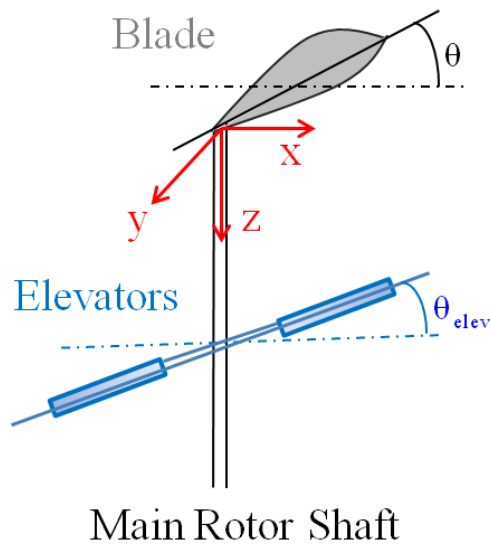


Figure 4.7: Side graph of blade and elevators. This figure is drawn by the author and based on [141].

The elevator is linked to the blade in such a manner that a tilt of the elevator relative to the shaft introduces a change in the blades' feather angle. As the elevator can pivot relative to the shaft, its equation of motion on the same form as that of the blade under the excitation of gyroscopic and inertia moments.

Let c_l be the linkage ratio such that:

$$\theta = c_l \theta_{elev} \quad (4.1)$$

θ_{elev} is the elevator's angular displacement.

If c_l is equal to one, one degree elevator tilt introduces one degree of blade feather. Since the elevator does not affect the collective feather, equation (4.1) can be written in the form [141]:

$$c_l \theta_{elev} = -A_1 \sin \psi - B_1 \cos \psi \quad (4.2)$$

where the cyclic pitch amplitudes A_1 and B_1 are functions of time and are given as:

$$B_1 = c_l \left(\frac{q}{\Omega} \right) \psi + cte \quad (4.3)$$

$\psi = \Omega t$, q is the rate of pitch and cte is an integration constant. A similar relationship exists between the lateral cyclic pitch A_1 and the rate of roll p .

$$A_1 = c_l \left(\frac{p}{\Omega} \right) \psi + cte \quad (4.4)$$

In order to model the elevator's feather angle, a PID controller needs to be defined. It uses the variable `@fhterror_j`, that it is defined as the input variable, and the output is the moment applied to the feather hinge so that certain cyclic control is achieved.

Several variables need to be defined as well:

```
(setsym fhtpj_j "rq(pjj)")
```

where $j = 1, 3$ and `rq(pjj)` specifies the angular position of the feather hinge with respect to the main rotor.

The second variable, `@afth_j` is the cyclic feather coefficient implemented as dictated by equation (4.3):

```
(setsym afth_j "c1*(rq(fuselage,2)/omega)*omega*t+k1_inte")
```

`c1` and `k1_inte` are constant values, `omega` is the main rotor angular speed (see Table 4.1) and `rq(fuselage,2)` is the fuselage's pitch rate of change.

The third introduced variable `@bfth_j`, is the second feather coefficient (see equation (4.4)):

```
(setsym bfth_j "c1*(rq(fuselage,3)/omega)*omega*t+k2_inte")
```

`k2_inte` is a constant a value and `rq(fuselage,3)` is the fuselage's roll rate of change.

Finally, the elevator's cyclic feather `@fht_ref_j`, can be written as:

```
(setsym fht_ref_j "-@afth_j*cos(omega*t)-@bfth_j*sin(omega*t)")
```

where the coefficients `afth_j` and `bfth_j` previously described as variables, are used.

Now, the PID can be modelled:

```
(setsym fhterror_j "@fhtiref_j-@fhtpj_j")
(add-state-variable ftq_j ftqp_j "F*L")
(set-aux-state-deriv ftqp_j "kifht_j*@fhterror_j")
```

The command `add-state-variable` introduces a state variable for the moment expression that it is used to implement the elevator's feather control. The integral part of the moment control is defined by the `set-aux-state-deriv` command and uses the value of the `@fhterror_j` which is the tracking error.

This moment is applied between the fuselage and the elevator's feather hinge.

```
(add-moment fhc_j
  :name "pjctrl_j"
  :direction -[pjy]
  :body1 fuselage
  :body2 pjy
  :magnitude "ftq_j+kfht_j*(@fhterror_j)+kdfht_j*dxdt(@fhterror_j)")
```

This controller uses the variable `@fhterror_j` as the input, and the output is the moment applied to the elevator feather hinge so that cyclic control is achieved. The parameters `kifht_j`, `kfht_j` and `kdfht_j` are the gains of the controller.

The elevators rotate with opposite direction around of their local reference axes [pjjx, pjyy, pjyz]. As a consequence of this, another moment needs to be considered on the implementation of the second elevator.

Blade Feather Angle Control Implementation

The feather angle controller for each blade is defined in a similar way to the elevators control. The variable @fht_pj_i is defined:

```
(setsym fht_pj_i "rq(pj_i)")
```

where $i = 2, 4$ and $rq(pj_i)$ is the blades' feather angular position with respect to the main rotor.

The variable @fht_ref is implemented as:

```
(setsym fht_ref "fo-@afth_j*cos(omega*t)-@bfth_j*sin(omega*t)")
```

the coefficient fo describes the blades' collective feather angle and the coefficients afth_j and bfth_j describe the blades cyclic feather, keeping a ratio to the cyclic elevator coefficients. The choice of these coefficients is dictated by the desired flight conditions. fht_ref is the Fourier series representation for the blade's feather angle.

Now, some variables need to be defined before implemented a PID controller.

```
(setsym fht_error_i "@fht_ref-@fht_pj_i")
(add-state-variable ft_tq_i ft_tqp_i "F*L")
(set-aux-state-deriv ft_tqp_i "kifht_i*@fht_error_i")
```

The add-state-variable command introduces a state variable for the moment expression that it is used to implement the elevator's feather control. The integral part of the moment control is defined by the command set-aux-state-deriv and uses the value of the variable @fhterror_i defined above, being the tracking error.

This moment is applied between the swashplate and the blade feather.

```
(add-moment fht_c_i
  :name "pj_ctrl_i"
  :direction -[pj_iy]
  :body1 sw
  :body2 pj_i
  :magnitude "ft_tq_i+kfht_i*(@fht_error_i)+kdfht_i*dxdt(@fht_error_i)")
```

This controller uses the variable `@fhterror_i` as the input, and the output is the moment applied to the blade feather hinge so that collective and cyclic controls are adequately implemented. The parameters `kifht_i`, `kfht_i` and `kdfht_i` are the gains of the controller.

The blades rotate with opposite direction around of their local reference axes [`pjix`, `pjiy`, `pjiz`]. As a consequence of this, another similar but opposite in sign moment needs to be defined for the second blade.

Once that the fuselage, swashplate and the main rotor as well the elevators and blades feather control have been modelled, the main rotor angular speed control also needs to be implemented, being this task similar to the described in the following chapter, so its process of implementation it is not included in here in order to avoid redundancy.

Moments Definition

The moments appearing on the main rotor (lag and flap moments respectively) are here described: the lag hinges have a spring that introduces a force acting between the lag hinge and the feather hinge, the spring stiffness is represented by the parameter `klj`. The magnitude is given by Hooke's Law:

```
(add-moment lagspringi
  :name "i-th Lag Spring"
  :body1 lji
  :body2 pji
  :magnitude "-klj*rq(lji)"
  :direction [bliz])
```

and `rq(lji)` represents the angular displacement of the lag hinge.

The flap hinges have a flap spring that introduces a spring force acting between the lag hinge and the correspondent flap hinge (`fji`), the spring stiffness is represented by the parameter `kfj`.

```
(add-moment flapspringi
  :name "i-th Flap Spring"
  :body1 fji
  :body2 lji
  :magnitude "-kfj*rq(fji)"
  :direction [blix])
```

`rq(fji)` represents the angular displacement of the flap hinge. The magnitudes of the flap and lag springs are indicated in Table 4.1.

4.6 Tail Rotor Modelling

The tail rotor modelling is implemented once the main rotor has been modelled. There exist two main differences between the modelling of the main and tail rotors; there is no modelled lag degree of freedom in the later case as there is no lag hinge on the Caliber 3 tail rotor. On the contrary, there is feather-flap coupling via delta three angle mechanism.

4.6.1 Bodies Definition

The tail rotor is built using a parent-child structure. First, the tail rotor is implemented as the child of the fuselage, and then it is defined as the parent of the following components. The tail rotor is connected to the fuselage at the point `fsgtl`:

```
(add-point fsgtl :body fuselage :coordinates (-xt yt htail))

(add-body tailrt
  :name "Tail Rotor"
  :parent fuselage
  :mass mtailrt
  :joint-coordinates fsgtl)
```

```
:body-rotation-axes y
:parent-rotation-axis y
:reference-axis z
:inertia-matrix (Irtlx Irtly Irtlz)
:cm-coordinates (xcmtl ycmtl zcmtl))
```

The tail rotor is set up as a body with mass, moments of inertia and centre of mass. The rotational degree of freedom around the Y axes is considered. Note at this point that the tail rotor rotation axes is perpendicular to the main rotor's one. The coordinates of the joint between the tail rotor and the fuselage are given by the command `:joint-coordinates`, its numerical value is defined by the point `fsgt1`. Finally, its moments of inertia are added in the last part of the modelling script.

The tail rotor has two blades, the relative blades' positions with respect to the tail rotor axes origin must be considered in order to define the joint locations. The separation angle between the blades and the tail rotor axis is defined by the variable, `@alphaltk`, being $k = 1, \dots, n$ (n is the maximum number of blades).

The azimuth angle for each k -blade is given by:

```
(setsym alphaltk "360*((nblades_t1-blade_numberk_t1)/(nblades_t1))")
(setsym argk_t1 "2*pi*(@alphaltk/360)")
```

where `nblades_t1` is a parameter representing the total number of blades in the tail rotor and, `blade_numberk_t1` is the corresponding blade being modelled.

All the blade hinges have been located at the same offset distance `eRt1` from the tail rotor centre point.

The distance for each blade offset is defined as:

```
(setsym xk_t1 "eRt1*sin(@argk_t1)")
(setsym zk_t1 "eRt1*cos(@argk_t1)")
```

The angles `@argk_t1` will be used to define the local axis for each blade (`baxesxt1_k`, `baxesyt1_k`, `baxeszt1_k`) are defined in terms of the inertial reference axes. Therefore, it can be determined by using the blade's position with respect to the tail rotor.

4.6. TAIL ROTOR MODELLING

A new set of local axes system is defined for each blade and its position with respect to the tail rotor's local axes (`[tail_rtx]`, `[tail_rty]`, `[tail_rtz]`):

```
(setsym baxesxtl_k "cos(@argk_tl)*[tail_rtx]+sin(@argk_tl)*[tail_rtz]")
(setsym baxesytl_k "[tail_rty]")
(setsym baxesztl_k "-sin(@argk_tl)*[tail_rtx]+cos(@argk_tl)*[tail_rtz]")
```

A point in the helicopter nominal configuration within the coordinate system of body `n` is defined because the feather hinge will be connected to it as well as a flap hinge. The blade will be attached to this point.

The feather hinge is connected to the tail rotor at the point `rtptl_k` where `k = 1, 2`. The tail rotor nominal configuration can now be implemented:

```
(add-point ptl_k1 :body n :coordinates ("-xt-@xk_tl" yt "htail+@zk_tl"))
(add-point rtptl_k :body tailrt :coordinates ptl_k1)
```

Each feather hinge is now included in the model with the following lines:

```
(add-body pjtl_k
      :name "k-th Feather Joint Tail"
      :parent tailrt
      :joint-coordinates rtptl_k
      :body-rotation-axes z
      :parent-rotation-axis "@baxesztl_k"
      :reference-axis "@baxesxtl_k"
      :inertia-matrix 0
      :mass 0)
```

It is a child of the tail rotor. Its mass is zero as well as the moment of inertia.

The flap hinge is connected to the feather hinge at the point `pjptl_k` and it is the parent of the blade and the child of the feather hinge:

```
(add-point ptl_k2 :body n :coordinates ("-xt-@xk_tl" yt "htail+@zk_tl"))
(add-point pjptl_k :body pjtl_k :coordinates ptl_k2)
```

```
(add-body fjtl_k
      :name "k-th Flap Joint Tail"
      :parent pjtl_k
      :joint-coordinates pjptl_k
      :body-rotation-axes x
      :parent-rotation-axis "@baxesxtl_k"
      :reference-axis "@baxesytl_k"
      :inertia-matrix 0
      :mass 0)
```

Finally, the tail rotor blades are added as flap hinges' children:

```
(add-body bltl_k
      :name "k-th Blade Tail"
      :parent fjtl_k
      :mass mbltl_k
      :joint-coordinates blptl_k
      :inertia-matrix (Iblxtl Iblytl Iblztl)
      :cm-coordinates (xbltl ybltl zbltl))
```

The blades are added as bodies with mass, moments of inertia and centre of mass.

4.6.2 Controllers Implementation

In this section, the blades' feather and flap dynamics are implemented under the action of PID controllers. Details on how the implementation was carried out in VehicleSim are provided in here.

4.6.3 Feather Control Definition

The tail rotor blades feather and delta three angle are modelled by using a PID controller. This constrains the blades' angular displacement with respect to the tail feather axis ([tail_rtz]).

The first line specifies the variable @ptlpj_k as the first blade feather angular speed as $rq(pjtl_k)$. Then, the variable @ptlref_k is defined as the reference value for the

collective feather angle, `fotl`, under the influence of the delta three angle on the blade's flap angle `fjtl_k`.

```
(setsym ptlpj_k "rq(pjtl_k)")
(setsym ptlref_k "fotl-tan(delta3tl)*rq(fjtl_k)")
```

Next, a state variable is introduced for the torque that is used to control the blade's feather angle. The integral part of the torque is defined by the `set-aux-state-deriv` and uses the error variable `ptlerror_k`:

```
(setsym ptlerror_k "@ptlref_k-@ptlpj_k")
(add-state-variable pltq_k tptqp_k "F*L")
(set-aux-state-deriv tptqp_k "kiptl_k*@ptlerror_k")
```

The torque is applied between the tail rotor and the first blade's feather hinge. This controller uses the variable `@ptlerror_k` as the input, and the output is the moment applied to the first feather hinge so that satisfactory collective control is achieved. The parameters `kiptl_k`, `kpptl_k` and `kdptl_k` are the corresponding controller gains:

```
(add-moment ptlm_k
  :name "pjctl_k"
  :direction -[pjtlkz]
  :body1 tailrt
  :body2 pjtl_k
  :magnitude "pltq_k+kpptl_k*(@ptlerror_k)+kdptl_k*dxdt(@ptlerror_k)")
```

The tail rotor mechanism forces the second blade to rotate around the Z axis in opposite direction to the first tail blade, therefore, a second moment is considered on the tail rotor and it is implemented in the similar manner to the previous one.

4.6.4 Flap Control Definition

In order to implement the tail rotor flap dynamics, a PID controller is designed; its function is to maintain the flap angle since it is coupled to the feather angle by the delta three angle:

```
(setsym fltl_k "rq(fjttl_k)")
(setsym wvr "(cos(aic)/cos(a0))*(krttl*omega)")
(setsym fltlref_k "a0-a1*cos(@wvr*t)-b1*sin(@wvr*t)")
```

`krttl` is the tail rotor gearing, its numerical value is given in Table 4.1 and `aic` is the initial cone angle. The meaning of the variables and parameters above will be introduced in the following chapter.

The third line, defines the blade's angular speed at the increased cone angle and the steady-state flap motion. The parameter `aic` is the initial value of the flap angle.

```
(setsym fltlerror_k "@fltlref_k-@fltl_k")
(add-state-variable fltl_tq_k fltl_tqp_k "F*L")
(set-aux-state-deriv fltl_tqp_k "kifl_tl*@fltlerror_k")
```

The command `add-state-variable` introduces a state variable for the torque expression that it is used to control the flap. The integral part of the torque is defined by the `set-aux-state-deriv` and uses the value of the `@fltlerror_k` defined above.

The expression to model this control is as follows:

```
(add-moment fltm_k
  :name "fjcttl_k"
  :direction [fjttl_kx]
  :body1 fjttl_k
  :body2 tailrt
  :magnitude "fltl_tq_k+kpfl_tl*(@fltlerror_k)+kdfl_tl*dxdt(@fltlerror_k)")
```

These controllers use the variable `@fltlerror_k` as the inputs, and the outputs are the moments applied to the flap hinge. The variables `kifl_tl`, `kpfl_tl` and `kdfl_tl` are the gains of the controllers.

The position and angular controls are implemented similarly to the control developed in the following chapter. The description of this is omitted in here.

4.7 Simulations and Results

The purpose of this section is to study the dynamics of the Caliber 3 helicopter in vacuum and without gravity. Several tests were carried out in order to shed light on the stability as well as the vibrations appearing on the helicopter due to the rotor action when external forces are not considered. This work will also allow to obtain information on the structural dynamics of the system.

4.7.1 Vibrations

The present study on vibrations is compared to that in [115] and [116] as it studies the most common range of vibrations appearing in UAV helicopters.

[115] analyzed the main vibration sources in UAV helicopters. This work started that there are typically three main sources: main rotor rotation (30.8 Hz); tail rotor rotation (143.4 Hz) and engine (260.5 Hz). These frequencies that appear in the fuselage are estimated based on a governed motor speed at 1850 rpm (revolution per minute).

[116] characterized the range of vibrations appearing in autonomous helicopters in terms of their sources such as the main rotor speed (about 25 Hz) tail rotor speed (113 Hz) and engine (160 Hz). The vibration sources can be mechanical, aerodynamic and from standard flight motion, with a broad range of amplitudes and frequencies spectrum.

In order to study the range of vibrations appearing on the Caliber 3 and to compare to those predicted, the following test is carried out: vibrations are generated by inducing a mass imbalance on the rotors, by doing this, the case for which vibrations on the main rotor may appear is simulated, and then be transferred to the fuselage.

It is assumed that the engine regime is 1700 rpm. The fuselage has six degrees of freedom: longitudinal, lateral and vertical along the axes X , Y , Z respectively and the corresponding rotations about these same axes. The purpose in here is to analyse the forces and accelerations that appear in the fuselage as a result of interactions and couplings between the various UAV components.

In order to study the characteristics of the vibrations appearing in the fuselage due to the main rotor only, a simulation is carried out where the main rotor has an angular

4.7. SIMULATIONS AND RESULTS

speed of $\Omega = 177.9$ rad/s (see Table 4.1) and the tail rotor angular speed is $\Omega_{tl} = 0$ rad/s. As the main objective at this stage is vibration generation, a mass imbalance can be introduced artificially in order to produce vibrations, i.e. the mass of the second blade (main rotor) is set to be the double of the other blade's mass $m_{bl2} = 0.282$ kg. The vibrations that appear are transmitted to the fuselage.

The vibrations appearing along the fuselage's X and Z axis are taken from the VehicleSim time history of vertical and longitudinal motions for a simulation of 5 seconds. The output of the simulation (time history of the position, velocities and accelerations on the fuselage) is stored in the workspace and analysed using a FFT (Fast Fourier Transform) Matlab algorithm. It was found that the main frequency component of the spectrum of vibrations appearing on the fuselage X axis is of a frequency of $f = 28.32$ Hz or (177.93 rad/s) (see Figure 4.8).

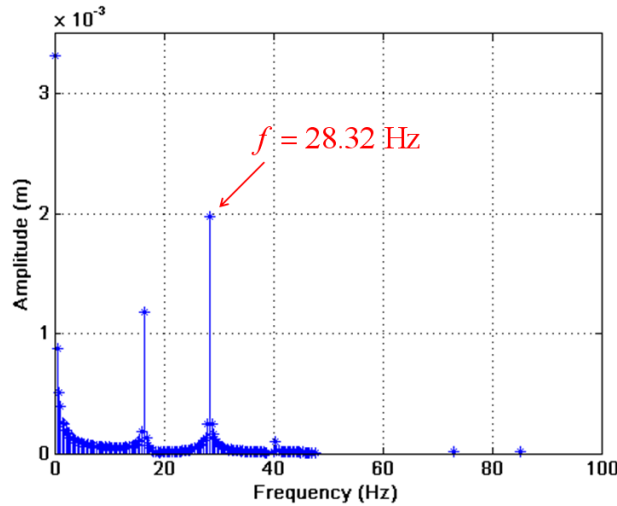


Figure 4.8: *Spectrum of vibrations appearing on the fuselage longitudinal axis.*

The main peak of frequencies is around 28.32 Hz. This is due to the main rotors blade mass imbalance introduced. These results follow the theoretical predictions in [115] and [116].

In the same way, if the spectrum of vibrations appearing on the fuselage's vertical direction (Z axis) is analysed, frequencies of 16.36 Hz or (102.79 rad/s) and 28.32 Hz or (177.93 rad/s) appear as major contributors of the spectrum (see Figure 4.9).

Two peaks of frequencies appear and their amplitudes are of similar ranges. The source of the vibration characterised by the dominant frequency is the steady load of the system i.e., the tail rotor and the fuselage shapes and configurations. The secondary peak in this case, is caused by the main rotor and its mass imbalance, as it was in the case of the longitudinal vibrations (see Figure 4.8).

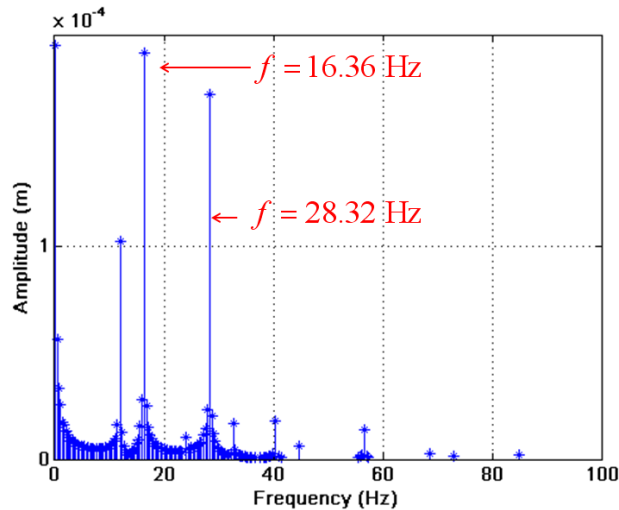


Figure 4.9: *Spectrum of vibrations appearing on the fuselage vertical axis.*

The ranges of peak frequencies detected in these simulations were used in order to design an intelligent control algorithm that isolated a vision system from these unwanted disturbances at the indicated frequencies, as indicated on the introduction of this chapter leading to publication [128].

4.7.2 Position and Rotation Control

Position Control

The purpose of this section is to show how the position of the Caliber 3 is controlled as a consequence of the torques applied from the main and tail rotors. The rotors create an imbalance of forces on the helicopter's fuselage. Therefore, equilibrium should be reached. This is carried out by the action of various PID controllers (as will explain in the following chapter).

Several controllers must be considered on the longitudinal, lateral and vertical directions, respectively. As mentioned before, the model has six degrees of freedom (three translations and three rotations). The effects of these controllers are shown in Figure 4.11.

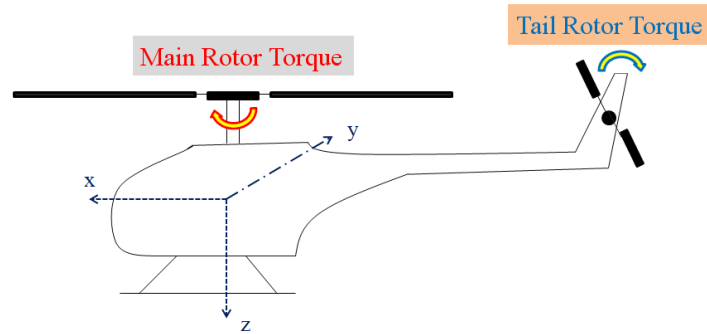


Figure 4.10: *The torques from both the main/tail rotors need to be controlled in order to reach dynamical equilibrium.*

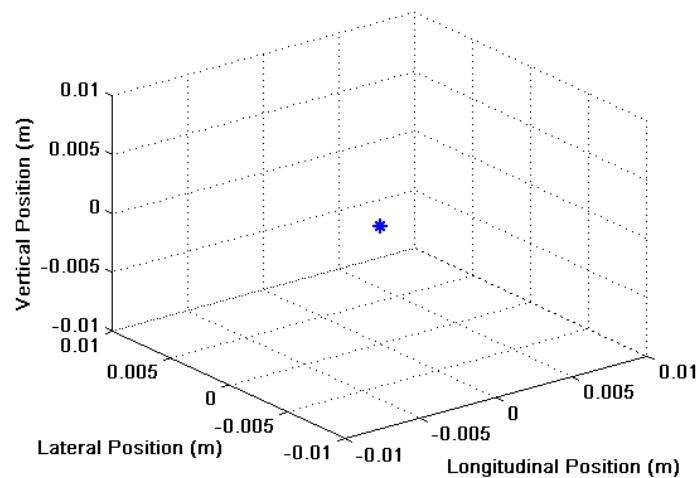


Figure 4.11: *Caliber 3 equilibrium position.*

If a simulation is carried out for 50 s, both rotors are rotating under the action of the PID controllers. As it can be seen in Figure 4.11, the Caliber 3 remains on the equilibrium position $(0, 0, 0)$ under the torques' action on the system, which are the outputs of the designed PID controllers.

Rotation Control

In this section, three controllers were introduced on the roll, pitch and yaw, respectively, in order to achieve rotational control of the helicopter. These will be presented in Chapter 5 and details of their implementation will be provided. The action of these controller is shown in Figure 4.12.

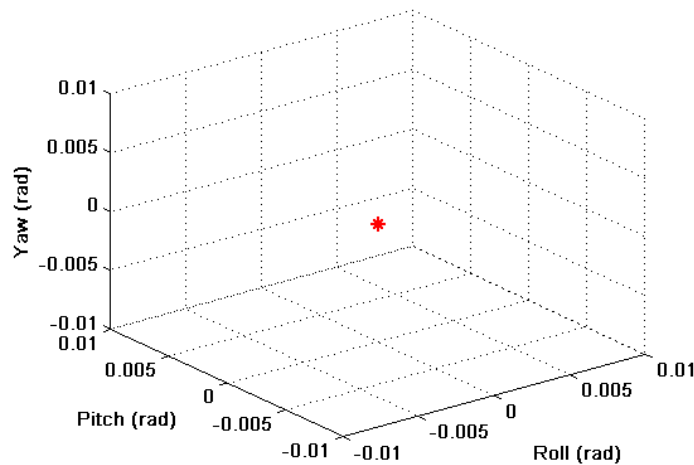


Figure 4.12: *Caliber 3 equilibrium in rotation.*

The equilibrium in rotation around the point $(0, 0, 0)$ for the case of the Caliber 3 is clearly achieved as a result of the PID controllers being implemented in the three rotational degrees of freedom.

4.8 Chapter Summary

This chapter contains the modelling details for a Caliber 3 (UAV) by using the VehicleSim. The model has been developed without the influence of any external force i.e., the system can be considered to be in vacuum and no aerodynamic loads were taken into account. The main contribution of this chapter with respect to the following one is that now the swashplate is implemented as a new body and the elevators are carefully described in order to show their behaviour on the system. Clearly, this is a more complex model than the one shown in the following chapter.

This work was carried out in collaboration with La Laguna University (Spain), during a four months Erasmus research visit. The main task was to measure the physical parameters such as fuselage weight, blade lengths, etc. The helicopter configuration was as well analyzed in order to implement it in VehicleSim as a multibody system. After that, some additional parameters were obtained by using Autodesk Inventor, however the results from this software were not of enough accuracy for the VehicleSim parameters requirement. For example, the centre of mass was not generated by Inventor. On the contrary, centres of gravity were provided. Nevertheless, the obtained data were enough to build up an initial Caliber 3 model in VehicleSim.

A physical description of the model was provided, the bodies, their degrees of freedom as well as their linkages were identified. As it has been shown, the fuselage, the swashplate, the main rotor and tail rotor have been modelled by using a parent-child relation in VehicleSim. In addition to this, the connections between the several bodies have been established and the degrees of freedom for each body have been included.

The main rotor has been described as a body composed of several hinges as well as several degrees of freedom, these being the feather, lag and flap. The blades were added as bodies with mass and inertial properties. Two elevators are also modelled on the main rotor with mass and inertial properties. The swashplate was defined as a body on the fuselage, being the parent of the main rotor; its action on the blades has been included by using PID controllers. The elevator feather cyclic angle was designed and modelled, showing the connection to the cyclic blade feather. The delta three angle and its effects on the tail rotor have been modelled as well.

In addition to all these, this Caliber 3 model has been used to analyze the vibrations appearing on the fuselage, as a consequence of mass imbalance on the main rotor. They were used by the La Laguna University to develop robust control methodology for an onboard vision system. The conditions to generate these vibrations were imposed by them in order to get the vibrations with the correct characteristics to achieve their control. The vibrations were provided in two axes because they requested only this information. On the other hand, the vibrations obtained agreed with the experimental values proposed by various authors [115], [116], validating in the case the provided model.

Once the vibrations were generated, two torques were implemented in both rotors in order to simulate the engine action. Whereas, this action produces that the system loses the initial equilibrium around the point $(0, 0, 0)$. Therefore, various PID controllers were implemented and included in the model so that the initial equilibrium could be restored.

Chapter 5

Sikorsky Configuration Dynamic Model

5.1 Introduction

The aim of this chapter is to present the modelling techniques developed to build the VehicleSim code for a helicopter in Sikorsky configuration. The multibody structure and the main modelling commands are presented in here. First of all, a general overview of the helicopter model is given. This is followed by programming details and a description of the multibody model program in VehicleSim. The procedure is focused on the fuselage, the main and tail rotors. The engine and the swashplate models are not presented, but their actions are modelled and introduced in the program.

Helicopters are complex systems, composed by several bodies as well as several degrees of freedoms, motions are allowed in three dimensions. The modelling of helicopter dynamics is necessary in order to study the interactions between the different parts of the helicopter and the instabilities on the system under various flight conditions.

There exists several studies carried out in this field but, the majority of existing models have been built under linearised conditions [5], [42]. There are also some nonlinear works on helicopter dynamics but mainly these are for reduced order models [44]. Therefore, the modelling of the rotorcraft system by considering the nonlinear dynamics is an

interesting and much needed task. A full model of a helicopter is developed by using VehicleSim in order to capture the nonlinear behaviour of the system. This allows to develop a comprehensive understanding of the interaction between the several parts of the helicopter and their dynamics, whilst the linear analysis does not explain these behaviours completely.

A helicopter can be defined as an aircraft that uses rotating wings to provide lift, propulsion and control. It is made up as the combination of several subsystems such as main rotor, fuselage, tail rotor and engine. In this chapter, the model under study is known as Sikorsky configuration, it consists of one main rotor, fuselage and one tail rotor mounted in perpendicular to the main rotor. The main rotor subsystem model in here is based on a previous work [124]. It was built by using Autosim software (previous version of VehicleSim).

The fuselage is the rotorcraft's main body section that holds crew and passengers or cargo. Its degrees of freedom are the lateral and longitudinal translation in the horizontal plane $X - Y$ axis, vertical translation in the Z axis and rotation about these same axes corresponding to yaw, pitch and roll. The rotors of a helicopter, due to its rotating nature, are prone to introducing vibrations on the fuselage that may affect the aircraft's performance, the passengers' comfort and the accuracy of on board measurement devices, for example, vision systems.

The role of the main rotor is to support the aircraft's weight, as it generates the lift force. It allows to keep the helicopter suspended in the air and provides the control that allows to follow a prescribed trajectory in the various spatial directions by changing altitude and executing turns. It transfers prevalingly aerodynamic forces and moments from the rotating blades to the non-rotating frame (fuselage); a conventional rotor consists of two or more identical equally spaced blades attached to a central hub. The blades are kept in uniform rotational motion (rotational speed Ω), by a shaft torque from the engine.

A common design solution adopted in the development of the helicopter is to use hinges at the blades roots that allow blade free motion and in the plane of the disc, see Figure 5.1.

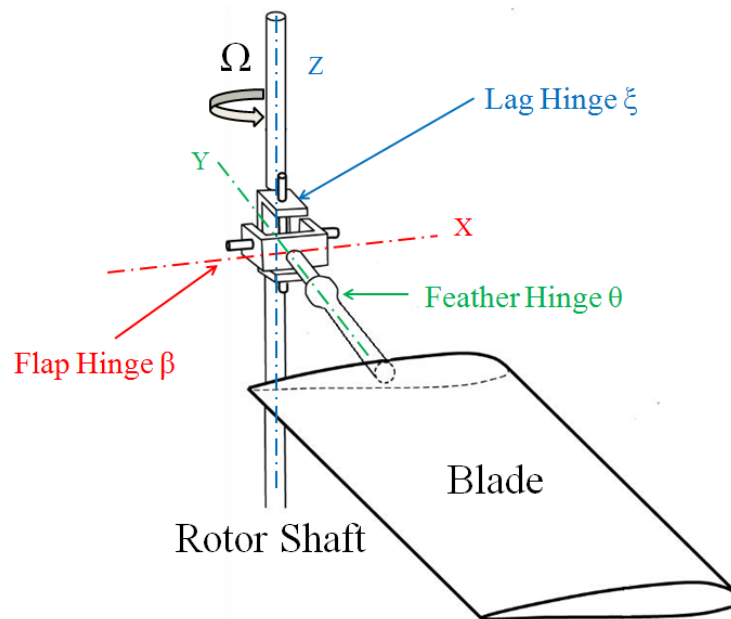


Figure 5.1: *Schematic diagram of main rotor's hub and hinges system.*

The most common of these hinges is the flap hinge which allows the blade to flap, this is, to move in a plane containing the blade and the shaft, of the disc plane, about either the actual flap hinge or in some other cases, the flap hinge is substituted by a region of structural flexibility at the blade's root. The flap angle is commonly represented by β and considered to be positive for upward blade motion. The flap hinge is more frequently designed to be a short distance from the centre line. This is termed as "offset" flap hinge, and it offers the designer a number of important advantages. The flap motion is the result of the constantly changing balance between lift, centrifugal, and inertial forces. The flap hinge together with the natural flexibility found in most blades, allows the blade to drop when the rotor is not turning and the helicopter is at rest. During flight, the necessary rigidity is provided by the centrifugal force which results from the blades' rotation; this force pulls outward from the tip, stiffening in this way the blade and, in fact, it is the only factor which prevents it from folding up. In Figure 5.2, an articulated rotor with a flap hinge offset from the centre of rotation by a distance eR is considered. Such an arrangement is usually mechanically simpler than one with no offset, and in addition, it has a favourable influence on the helicopter handling qualities [140], [141].

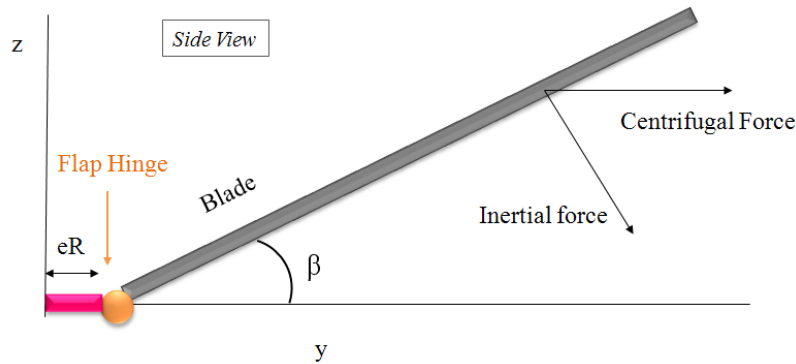


Figure 5.2: Side view of a flap hinge with offset eR .

A blade which is free to flap, experiences large Coriolis moments in the plane of rotation and a further hinge (called lag) is provided to relieve these moments. This degree of freedom produces blade motion on the same plane as the disc. The lag angle is represented by ξ and it is considered to be positive when opposite to the direction of rotation of the rotor, as produced by the blade drag forces (see Figure 5.3) [98].

Additionally to these, a blade can also feather around an axis parallel to the blade span. Blade feather motions are necessary to control the aerodynamic lift developed and, in forward motion of the helicopter, to allow the advancing blade to have a lower angle of incidence than the retreating blade and thereby to balance the lift across the craft. The feather angle θ , is considered to be positive for nose-up blade's rotations. In order to be able to climb up, the feather angle needs to be increased. On the other hand, in order to descend, the blade's feather angle is decreased. Because all blades are acting simultaneously in this case, or collectively, this is known as collective feather and allows the rotorcraft to rise/fall vertically. Additionally to this control, for achieving forward, backward and sideways flight, a different additional change of feather is required. The feather on each individual blade is increased at the same selected point on its circular pathway. This is known as cyclic feather or cyclic control. Blade feather control is achieved by linking the blade to a swashplate, the pilot having control of the height (collective) and angle (cyclic) of the plate through a joy-stick.

In the Sikorsky configuration, the tail rotor of the helicopter is mounted on the perpendicular to the main rotor. It counteracts the torque and the yaw motion that the

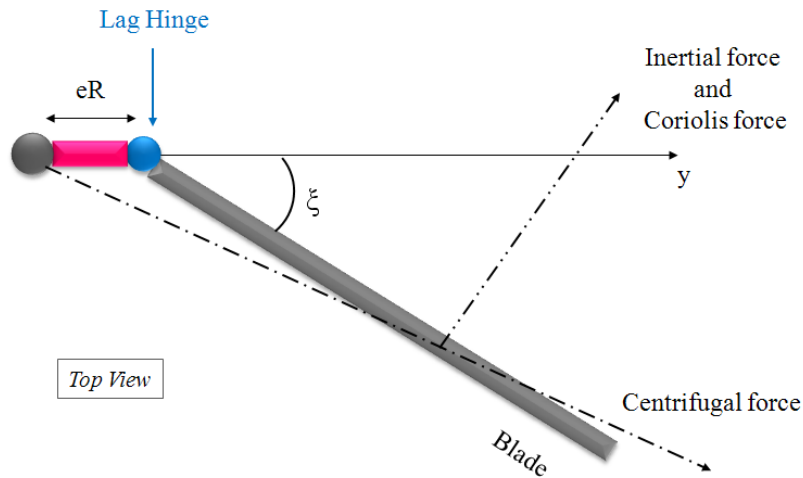


Figure 5.3: *Top view of a lag hinge with offset eR .*

main rotor disc naturally produces. In accordance to Newton's third law of action and reaction, the fuselage tends to rotate on the opposite direction to the main rotor's blades as a reaction of the torque that appears. This torque must be counteracted and/or controlled before any type of flight is possible. Two anti-torque pedals allow the pilot to compensate for torque variance by providing a means of changing pitch (angle of attack) of the tail rotor blades. This provides heading and directional control in hover and at low airspeeds. Driven by the main rotor at a constant ratio, the tail rotor produces thrust in a horizontal plane opposite to torque reaction developed by the main rotor. Since the torque magnitude varies during flight when power changes are made, it is necessary to accordingly modify the tail rotor's thrust. A significant part of the engine power is required to drive the tail rotor, especially during operations when maximum power is used. Any change in engine power output produces a change in the torque. Furthermore, power varies with the flight manoeuvre and results in a variable torque effect that must be continually corrected, by the tail rotor (see Figure 5.4), ([140]- [143]).

The tail rotor has no need for the disc attitude to be controlled and so does not require cyclic feather. In order to obtain lightest a tail rotor design, a lag hinge is usually not included in the tail rotor with the proviso that any flap caused by disturbances is kept to an absolute minimum if not totally avoided. The blade flap can be triggered by the effects of forward flight or by aerodynamic disturbances and means of minimising this are included in a tail rotor control system, known as "delta-three" configuration.

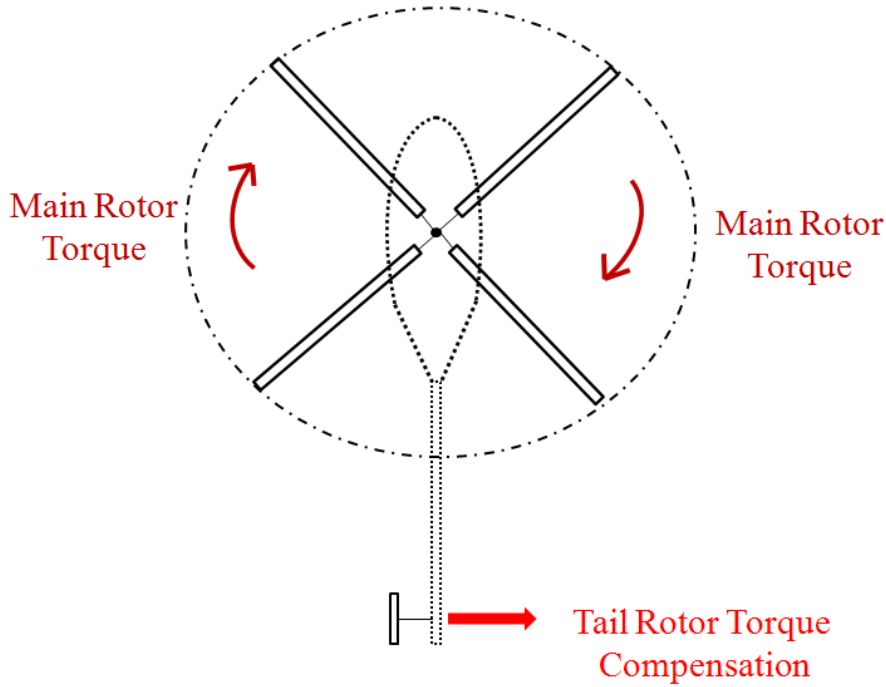


Figure 5.4: Tail rotor counteracting the torque induced by the main rotor rotation.

In addition to this, this coupling is designed to reduce transient flap angles and blade stresses [142], [144]. The feather-flap coupling is a kinematic feedback of the flap angular displacement to the blade feather motion that can be algebraically described as:

$$\Delta\theta = -k\beta \quad (5.1)$$

where θ is the feather angle and k is the feather-flap coupling coefficient. This acts as an aerodynamic spring for the flap mode because the lower feather means less lift. The feather-flap coupling plays an important role in flight stability and the handling qualities of the vehicle as well as aeroelastic blade's stability. The simplest approach is to skew the flap hinge by an angle ("delta-three") so that it is not longer perpendicular to the blade radial axis. Then a rotation about the hinge with a flap angle β must also produce a feather change of $-\beta\tan\delta_3$. The feedback gain for this arrangement is therefore $k = \tan\delta_3$. Feather-flap coupling is defined in terms of the delta three angle (see Figure 5.5) [140].

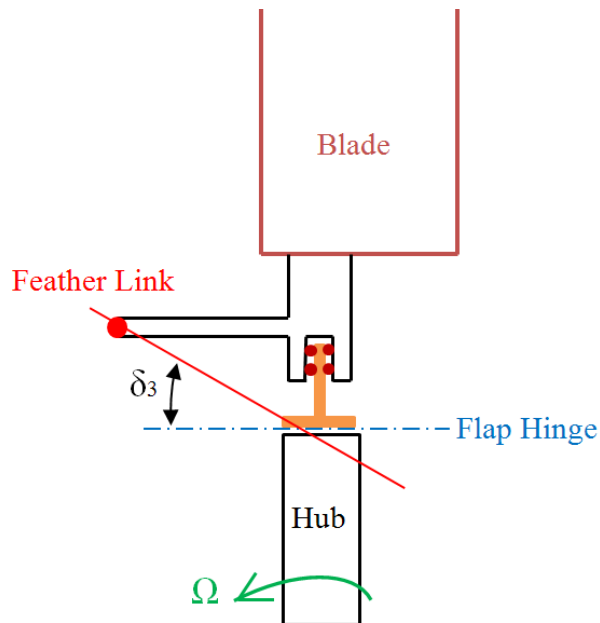


Figure 5.5: Rotor blade feather-flap coupling via delta three angle. This figure is drawn by the author and based on [140].

5.2 Model Description

A helicopter can be modelled in different ways; one of them is the combination of several interacting subsystems. For the purposes of this work, a full dynamic model of the helicopter is considered as multibody system with several subsystems as well as several constraints between the different degrees of freedom. VehicleSim allows to develop other technical considerations in the modelling process, for example, the coupling between the flap-feather on the tail rotor by using the various restrictions and constraints that the software allows to implement. The general considerations of the model are described in the following lines. The aerodynamic model is not yet included in here and will be presented in the next chapters.

VehicleSim derives a realistic nonlinear model of the fundamental dynamics of an articulated rigid-bladed rotorcraft. One of the advantages of using this approach is that compared with hand derived equations (usually prone to errors), the automated equations give an accurate representation of the complex system's dynamics. Also, due to its software engineering features it uses a reduced execution time. The general structure of the helicopter is represented in Figure 5.6.

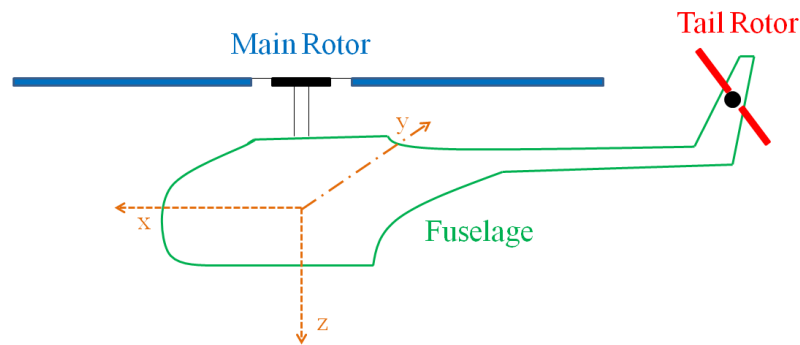


Figure 5.6: *Helicopter Sikorsky configuration.*

The following considerations are made regarding the physical structure of the helicopter.

- The helicopter has the Sikorsky configuration i.e., main rotor in combination with a tail rotor. Both systems are mounted on the fuselage.
- The main rotor consists of four equally spaced blades joined to a central hub. The blades have free motion in and out of the plane of the disc; this is allowed by the inclusion of hinges.
- The tail rotor consists of two equally spaced blades joined to a secondary hub.
- The blades are rigid in both rotors. (The case of flexible blades is a natural extension of the work here presented and the author is currently working on it).
- The rotor's angular speeds are constant, and a proportional ratio exists between them. The axis of rotation of the tail rotor is transverse to the main rotor's axis.
- The main rotor hinges allow for three degrees of freedom: flap, lag and feather motions.
- The tail rotor hinges allow for two degrees of freedom: flap and feather.
- Feather-flap coupling is considered in the tail rotor analysis.
- The helicopter's main body has six degrees of freedom. Three translations along the (X, Y, Z) axes and three rotations around the same axes.

5.3 Dynamic Model

VehicleSim (Version 1.0, August 2008) Lisp is used to develop the multibody system code that represents the helicopter system as described in section 5.2 (see Figure 5.6). The multibody system is subdivided into its constituent bodies for the purpose of writing the VehicleSim code. The bodies are arranged as a parent-child relationship as shown in Figure 5.7. In VehicleSim, each reference frame has a rectangular 3D coordinate system that associates a unique ordered trio of numbers to each point fixed in that reference frame. \mathbf{n} is the inertial reference frame. As new bodies are added to the system, having freedoms relative to \mathbf{n} , local origins and axes are defined. All VehicleSim coordinate systems are right-handed Cartesian systems defined, by (i) a reference frame in which the coordinate system is fixed, (ii) an origin point, and (iii) three mutually orthogonal directions that define the axes. By "right handed", it means that if two of the directions are X and Y , then the third direction $\mathbf{z} = \mathbf{x} \times \mathbf{y}$. The body-fixed points coincide with the corresponding global points, fixed in \mathbf{n} , when the system is on its nominal configuration. Most points are fixed in bodies but a point may be defined as mobile with its location in a body determined from its specified coordinates. This is useful for describing time varying points of contact between one body and another one. The code starts with an inertial reference frame \mathbf{n} , with fixed origin, \mathbf{n}_0 , and fixed directions $[\mathbf{nx}]$, $[\mathbf{ny}]$ and $[\mathbf{nz}]$ already defined [134]. The first body included in the code is the fuselage, it is implemented as the child of the nominal reference frame. The fuselage is located at the origin of the inertial coordinates system and it is the parent of both the main and tail rotors. The main rotor rotates around its vertical axis, Z axis. The main rotor is the parent of the flap hinges that rotates around the corresponding X axis, each lag hinge is the child of the corresponding flap hinge. The lag hinges rotate around the Z axis. The feather hinges are the child of the lag hinges. Each feather hinge rotates around the Y axis. Finally, a blade is added to the program structure as the child of each feather hinge. The tail rotor is built up following this same parent-child structure.

```
(reset)
(si)
(add-gravity)
(setf *linear* t) ; or (nil if nonlinear simulation is needed)
```

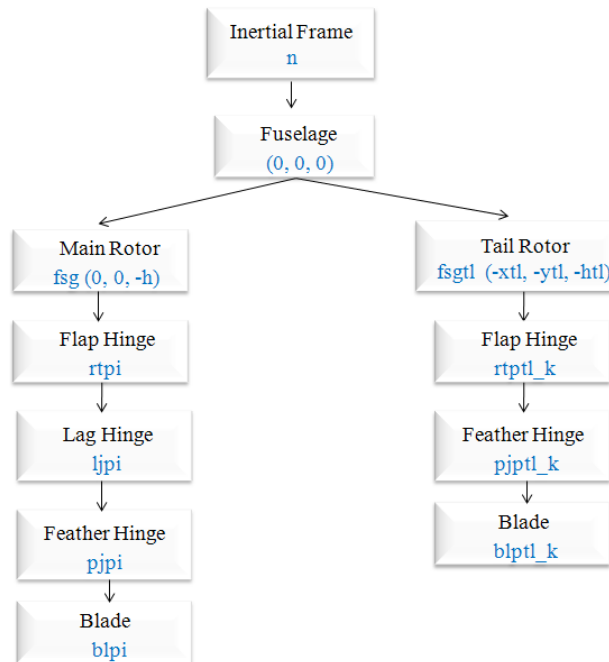


Figure 5.7: *Body structure diagram of the Sikorsky model helicopter. Both main and tail rotor in this diagram contain one blade element only due to space restrictions, but the model can contain as many blades as needed.*

The first lines of the code include the commands that are used to reset (clear description of multibody system and initialize) the system, select the unit system to be employed SI (install SI unit system. No scale factors are needed for internal dynamical equations. Angles are radian), gravity (declare presence of gravity field and its direction).

Linear and nonlinear models can be obtained; they are generated using various commands. The option `*linear*` is set to be `true` or `false` the linear and nonlinear parts of the code are separated and chosen accordingly to the option made by the boolean variable `*linear*`. The nonlinear part of the VehicleSim code is used to generate the C file that solves the nonlinear equations of motion. The linear part is used to generate the symbolic representation of the linearised system matrices. The different parts of the code are described in the following sections.

The remaining commands in the program describe in a sequential manner the set of rigid bodies that conform the dynamical system to be modelled. This also includes data parameters such as masses, inertia values, positions of gravity centres and the allowed

rotations and translations of each body. At this point, it is convenient to remind the reader that the system to be modelled in here consists of three subsystems: fuselage, main rotor and tail rotor.

Parameters	Symbol	Value
Helicopter mass	m_h	2200 (kg)
Main rotor blade mass	m_{bl}	31.06 (kg)
Tail rotor blade mass	m_{btl}	6.212 (kg)
Fuselage-main rotor vertical distance	h	1.48 (m)
Fuselage-tail rotor longitudinal distance	x_t	6 (m)
Fuselage-tail rotor vertical distance	h_{tl}	1.72 (m)
Main rotor blade length	l	4.91 (m)
Tail rotor blade length	l_{tl}	0.982 (m)
Main rotor flap hinge spring stiffness	k_{fj}	46772 (Nm/rad)
Main rotor lag hinge spring stiffness	k_{lj}	314938 (Nm/rad)
Main rotor lag hinge damping coefficient	d_{lj}	349.58 (Nms/rad)
Delta three angle	δ_{3tl}	-0.785 (rad)
Main rotor angular speed	ω	44.4 (rad/s)
Tail rotor gearing	k_{rttl}	5.25

Table 5.1: Sikorsky configuration model parameters [124], [142].

5.4 Fuselage Modelling

The first body to be defined in the program script is the **fuselage**. It is implemented on the nominal reference frame **n**. The fuselage is the parent of both main and tail rotors. These new bodies will be added to the system, having freedoms relative to **n**, their local origins and axes will also be defined. The fuselage is built using VehicleSim commands as follows:

```
(add-body fuselage
  :name "Fuselage"
  :parent n
  :mass mf)
```

5.4. FUSELAGE MODELLING

```

:joint-coordinates (0 0 0)
:translate (x y z)
:body-rotation-axes (z y x)
:parent-rotation-axis z
:reference-axis x
:inertia-matrix ((Ifxx 0 Ifxz)
                 (0 Ifyy 0)
                 (0 0 Ifzz))
:cm-coordinates (xfs yfs zfs))

```

The "fuselage" is set up as a body with mass, moments of inertia as well as centre of mass and it is the child of body *n*. Located on the inertial reference system of coordinates. Furthermore, it has translational degrees of freedom along the *x*, *y* and *z* directions of *n*, because *n* is its parent. The yaw, pitch and roll rotational degree of freedom around the axes *z*, *y* and *x* respectively are also considered, to allow the full rotation of the helicopter in space.

Figure 5.8 shows a diagram of the points and the distance that define the helicopter's system geometry.

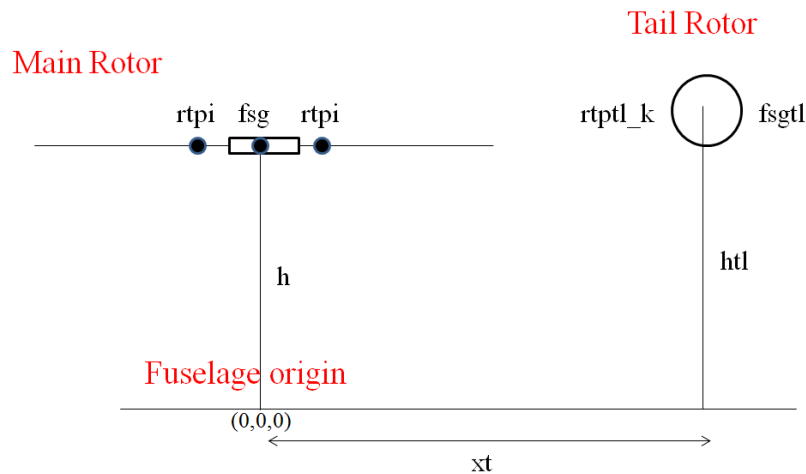


Figure 5.8: *Points and distances diagram.*

5.5 Main Rotor Modelling

5.5.1 Bodies Definition

The main rotor is built on a similar parent-child structure. First, the main rotor is implemented as a child of the fuselage, and it will be the parent of the corresponding subsystems. The rotor is connected to the fuselage at the point `fsg` (see Figure 5.8) which needs to be defined prior to the main rotor definition.

```
(add-point fsg :body fuselage :coordinates (0 0 -h))
```

The point `fsg` is located at a vertical distance `-h` from the origin of the inertial axes system. Note that the negative sign of the vertical distance `h`, is due to VehicleSim sign convention of considering the positive vertical direction to be downwards.

The main rotor is introduced into the model:

```
(add-body rt
  :name "Rotor"
  :parent fuselage
  :mass 0
  :joint-coordinates fsg
  :body-rotation-axes z
  :parent-rotation-axis z
  :reference-axis x
  :inertia-matrix(0 0 Irtz))
```

The "rotor" is set up as a massless body. The rotational degree of freedom around the axes Z is considered. The coordinates of the joint between the main rotor and the fuselage is given by the command `:joint-coordinates`, (its numerical value was previously defined by the point `fsg`). Finally, its moments of inertia are also provided.

The main rotor has four blades equally spaced, this can be generalized to any number of blades that may be required. The relative position of each of the blades with respect to the main rotor axes origin is important in order to define the joining points to which the hinges will be attached. The separation angle between each of the blades on the main rotor disc can be defined as `alphai`, with $i = (1, \dots, j)$, being j the total number of

blades in the main rotor. These angles help to define a local axes system for each blade in terms of the rotor axial position. The angular displacement of each blade i with respect to the main rotor axes, is represented by the variable `argi`.

The angle is defined by using the command `setsym`, its nomenclature is given as: `setsym (symbol values)`. The argument of this command (`symbol values`) can work as global variable or external symbols and it can be a string, symbol, number or list. If `symbol` is a VehicleSim lisp global variable, the type of data expected is checked with the type provided. Any other type of data causes an error message. If `symbol` is not a VehicleSim Lisp global variable, then a string provided as a value is passed as an f-string. The variables defined by this command, such as `alphai` are called with the symbol `@`.

The azimuth angle for each i -blade is given by:

```
(setsym alphai "360*((nblades-bladenumberi)/(nblades))")
(setsym argi "2*@pi*(@alphai/360)")
```

`nblades` is a parameter representing the total number of blades in the main rotor and, `bladenumberi` is the corresponding blade being modelled.

On the other hand, the command `set-defaults`, is used to assign different values to parameters and initial conditions. It is also used to specify the numerical values of universal constants associated to the units system. These values are provided at the beginning (or end lines) of the script and can be changed for each simulation from an external file without the need of modifying the Lisp script.

All the blade hinges have been located at the same offset distance `eR` from the main rotor centre point, being possible to define different offset distances for each one. The offset is the distance existing between the rotor hub and the blade hinges. `R` is the blade's radius, and `e` is a factor used to define the total offset distance, `eR`. The hinges are added in a sequential manner such that each of them is the child of the previous one and the parent of the following hinge.

The distance for each blades' offset is defined as:

```
(setsym xi "eR*sin(@argi)")
(setsym yi "eR*cos(@argi)")
```

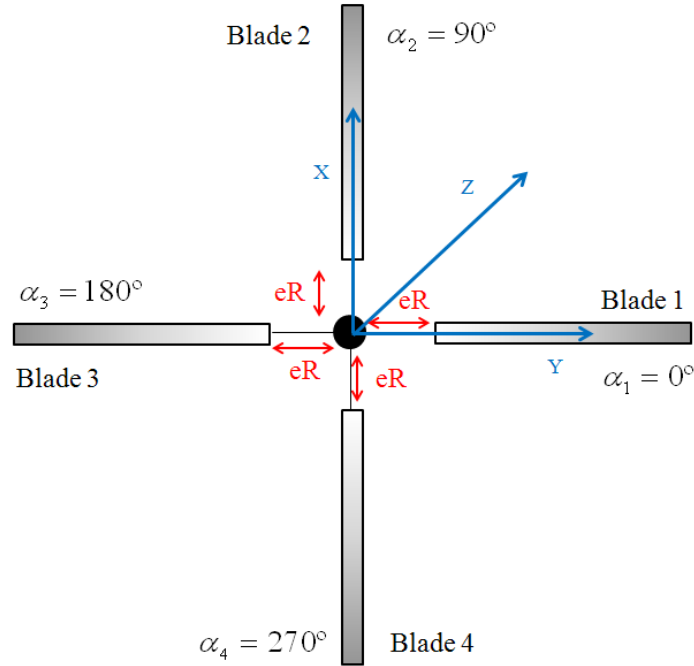


Figure 5.9: Main rotor configuration on nominal position.

The previously defined angles arg_i will be used to define the local axis for each particular blade (biaxesx , biaxesy , biaxesz) are defined in terms of the inertial reference axes. As a consequence, the blade's position respect to the main rotor is determined.

Now, a new set of local axes system is defined for each blade (blade_i) and its position with respect to the main rotor's local axes ($[\text{rtx}]$, $[\text{rty}]$, $[\text{rtz}]$):

```
(setsym biaxesx "-sin(@argi)*[rty]+cos(@argi)*[rtx]")
(setsym biaxesy "sin(@argi)*[rtx]+cos(@argi)*[rty]")
(setsym biaxesz "[rtz]")
```

The different degrees of freedom flap, lag and feather are added to the blades sequentially, being each of them the child of the previous degree of freedom and the parent of the following one. Figure 5.1 shows a diagram of this sequence.

Each flap hinge is connected to the main rotor, at the point rtpi , where $i = 1, \dots, j$. (See Figure 5.8).

```
(add-point p_nblabes_i :body n :coordinates ("@xi" "@yi" -h))
```

```
(add-point rtpi :body rt :coordinates p_nblabes_i)
```

The flap is added as:

```
(add-body fji
  :name "i-th Flap Joint"
  :parent rt
  :joint-coordinates rtpi
  :body-rotation-axes x
  :parent-rotation-axis "@biaxesx"
  :reference-axis "@biaxesy"
  :inertia-matrix 0
  :mass 0)
```

Each flap hinge, `fji` is a child of the main rotor. Its mass is zero as well as its moment of inertia.

Once the lag hinge is defined, the lag hinge is connected to the flap hinge at the point `ljpi` as a child.

```
(add-point ljpi :body fji :coordinates p_nblabes_i)
```

```
(add-body lji
  :name "i-th Lag Joint"
  :parent fji
  :joint-coordinates ljpi
  :body-rotation-axes z
  :parent-rotation-axis z
  :reference-axis "@biaxesx"
  :inertia-matrix 0
  :mass 0)
```

The mass is zero as well as the moment of inertia.

The feather hinge is connected to the lag hinge at the point `pjpi` being the parent of the blade and the child of the lag hinge. The point `pjpi` is added at the corresponding coordinates `p_nblabes_i`.

```
(add-point pjpi :body lji :coordinates p_nblabes_i)
```

```
(add-body pji
  :name "i-th Feather Joint"
  :parent lji
  :joint-coordinates pjpi
  :body-rotation-axes y
  :parent-rotation-axis "@biaxesy"
  :reference-axis "@biaxesz"
  :inertia-matrix 0
  :mass 0)
```

Finally, the blade is added at the end of each hinge sequence at the point `blpi` with coordinates `p_nblabes_i`.

```
(add-point blpi :body pji :coordinates p_nblabes_i)
```

```
(add-body bli
  :name "i-th Blade"
  :parent pji
  :mass mbli
  :joint-coordinates blpi
  :inertia-matrix (Iblx Ibly Iblz)
  :cm-coordinates (xbl ybl zbl))
```

The blade is added as a body with mass, moments of inertia and centre of mass. Furthermore, it inherits its parent's degrees of freedom as a consequence of the parent-child relationship. The physical parameters of the blade such as mass, `mbli`, inertias, (`Iblx Ibly Iblz`) and centre of mass position, (`xbl ybl zbl`), are values provided at the beginning of the code and can be changed for each simulation from an external file without the need of modifying the Lisp script.

5.5.2 Controllers and Moments Definitions

Once the code has been built up to accommodate the parent-child dependence structure, and the corresponding points have been defined, moments, forces and controllers need

to be included.

Feather Control Definition

In order to control the feather mode as the swashplate normally does in a rotor system, various PID controllers needed to be included in the system and therefore, modelled in the script. They will be used to constrain the blades' positions around the feather axis `pj_npy` and provide in this manner, a suitable and accurate cyclic and collective feather control.

The PID controller is a feedback controller which purpose is to reduce the stationary error, between a given reference signal and the output of the system under control. Ideally, the objective is that the difference should asymptotically converge to zero.

Usually PID controllers are capable to solve the control problem for many applications. Especially when a dynamic process allows it (in general processes can be described by first and second order dynamical system) and the system requirements are limited to the stationary error, as well as when a fast response when the signal reference changes is required.

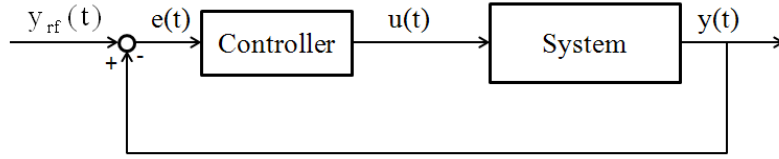
The feedback mechanism can be mathematically described as: $e(t) = y(t)_{rf} - y(t)$, this is the difference between the desired input value $y(t)_{rf}$ and the actual output $y(t)$. It is called the "tracking error", $e(t)$ is the input to the PID controller, and the controller computes both the derivative and the integral of this error signal.

A general PID control law has the form:

$$u(t) = K_p e(t) + \frac{K_i}{T_i} \int_0^t e(t) dt + K_d T_d \frac{de(t)}{dt} \quad (5.2)$$

where $u(t)$ is the control variable and $e(t)$ is the error. The control variable is the sum of three terms: the term proportional to the error, the term proportional to the integral error, and the term proportional to the differentiate error. The controller parameters are the proportional gains K_p , K_i and K_d as well as the integral time T_i and differentiate time T_d .

The controller provides the signal to control the overall system's behaviour. This signal $u(t)$ will be sent to the system, and the new output $y(t)$ will be obtained. This new

Figure 5.10: *Unit feedback system.*

output $y(t)$ will be feedback to find the new error signal $e(t)$. The controller takes this new error signal and computes its derivative and its integral (see Figure 5.10).

The proportional part of the controller will have the effect of reducing the rise time T_r and will reduce, but never eliminate, the steady-state error $ess(t)$. The integral control has the capability of eliminating the steady-state error, but it may make the transient response worse. The derivative control will have the effect of increasing the stability of the system, reducing the overshoot, and improving the transient response.

A PID controller will be used in the various parts of the helicopter model because it is the easier control that it can be developed, and it is strong to get the required objectives. The PID controllers in this work are modelled in VehicleSim, being not necessary to use any external code.

The procedure to build a PID controller in VehicleSim is given the following commands. Two variables need to be defined, the first one is:

```
(setsym fhtpj_np "rq(pj_np)")
```

where $np = 1, 2$ and $rq(pj_np)$ specifies the rotational position of the feather with respect to the main rotor.

The second variable is named as `@fht_ref`, it is the desired feather reference signal, $y_{rf}(t)$, and it is defined as a Fourier series.

```
(setsym fht_ref "fo+foc*cos(omega*t)+fos*sin(omega*t)")
```

ω is the main rotor angular speed (see Table 5.1). The variable `@fht_ref` is defined by the coefficient `fo` for the collective feather angle and the coefficients `fos` and `foc` for the cyclic feather. The choice of these coefficients is dictated by the desired flight conditions. `@fht_ref` is the Fourier series representation for the blade feather.

The Fourier series representation for the blade feather motion is:

$$\theta = \theta_0 + \theta_{1C}\cos\psi + \theta_{1S}\sin\psi + \dots \quad (5.3)$$

where $\psi = \Omega t$ being Ω the constant rotational speed of the main rotor.

The control inputs consist of just the mean and first harmonics: $\theta_0 + \theta_{1C}\cos\psi + \theta_{1S}\sin\psi$. The mean angle θ_0 is called the collective feather, and the harmonics θ_{1C} and θ_{1S} are called the cyclic feather angles. The collective feather controls the average blade force, and hence the rotor thrust magnitude. Additionally, the cyclic feather controls the tip-path-plane tilt and hence the thrust vector orientation (θ_{1C} controls the lateral orientation, while θ_{1S} controls the longitudinal orientation) [140].

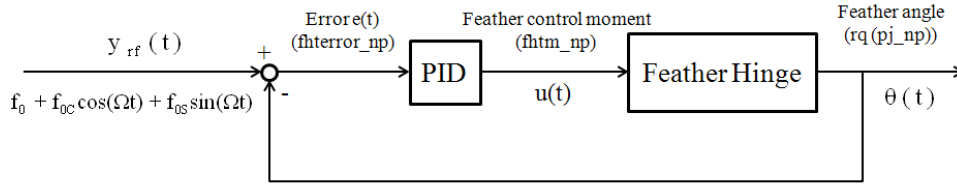
```
(setsym fhterror_np "@fht_ref-@fhtpj_np")
(add-state-variable fttq_np fttqp_np "F*L")
(set-aux-state-deriv fttqp_np "kifht*@fhterror_np")
```

The `add-state-variable` introduces a state variable for the torque expression that it is used to implement the feather control. The integral part of the torque control is defined by `set-aux-state-deriv` and uses the value of the `@fhterror_np` defined above, being this the tracking error.

The expression for the PID feather controller on the feather is therefore implemented in VehicleSim as:

```
(add-moment fhtm_np
  :name "pjctrl_np"
  :direction -[pj_npy]
  :body1 fuselage
  :body2 pj_np
  :magnitude "fttq_np+kfht*(@fhterror_np)+kdfht*dxdt(@fhterror_np)")
```

This moment is applied between the fuselage and the feather hinges. It represents the swashplate action on the feather hinges. The controller uses the variable `@fhterror_np` as input, and the outputs are the moments applied to the feather hinges so that cyclic/collective control for blades one and two are achieved. Figure 5.11 shows a diagram of the PID feather controller. The parameters: `kifht`, `kfht` and `kdfht` are the gains of the controllers and their values are tuned and indicated at the beginning of the program script together with the rest of model's parameters.

Figure 5.11: *PID feather control.*

Blades one and two rotate around the `pj_npy` axis with an opposite direction to blades three and four as the swashplate action would do, being these rotations around the local reference axis for each blade `[blx bly blz]`. Figure 5.12 shows this for blades one and three being the same behaviour for the blades two and four. As a consequence of this, other PID controllers need to be considered on this system and are built in a similar manner as before. The feather control for blades three and four is given by:

```
(setsym fhtpj_no "rq(pj_no)")
```

where `no = 3, 4` and `rq(pj_no)` specifies the feather's rotational speed.

```
(setsym fhterror_no "@fhhref-@fhftpj_no")
(add-state-variable fttq_no fttqp_no "F*L")
(set-aux-state-deriv fttqp_no "kifht_no*@fhterror_no")

(add-moment fhfm_no
  :name "pjctrl_no"
  :direction [pj_noy]
  :body1 fuselage
  :body2 pj_no
  :magnitude "fttq_no+kpfht_no*(@fhterror_no)+
    kdfht_no*dxdt(@fhterror_no)")
```

This moment is applied between the fuselage and the corresponding feather hinges. The controller uses the variable `@fhterror_no` as input, and the output are the moments applied to the feather hinge so that cyclic/collective control for the blades three and four is delivered. The parameters `kifht_no`, `kpfht_no` and `kdfht_no` are the gains of the controllers.

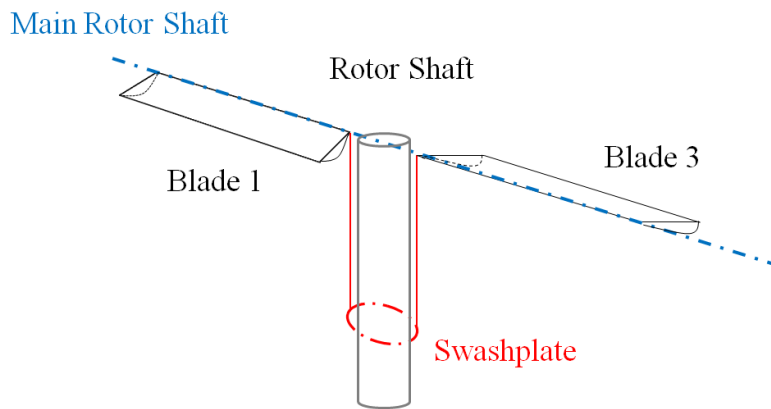


Figure 5.12: Diagram showing the feather effect blades one and three.

Main Rotor Speed Control Modelling

The main rotor rotational speed Ω is taken as constant, it can be introduced in the model as a constraint by using the VehicleSim command `ru(rt,1)` that specifies the first rotational speed for the main rotor:

```
(add-speed-constraint "ru(rt)-omega" :u "ru(rt)")
```

`omega` is the main rotor angular speed (Table 5.1). The main rotor rotational speed could also be modelled in a more realistic manner by designing a PID controller that aims to control the rotor speed so that it follows a desired prescribed rotational speed; it is introduced in the form of a torque applied between the fuselage and the main rotor. It is representative of the engine action on the main rotor.

```
(setsym wrotor "ru(rt,1)")
```

```
(setsym wref "omega")
```

Two variables are defined, the first one, `@wrotor`, is the actual rotational speed of the main rotor around its Z axis and the second variable, `@wref`, is the reference value of the main rotor angular speed `omega`, its numerical value should be defined by the user at the beginning of the program.

```
(setsym werror "@wref-@wrotor")
```

```
(add-state-variable wrttq wrttqp "F*L")
```

```
(set-aux-state-deriv wrttqp "ki*@werror")
```

The `add-state-variable` introduces a new state variable; this is needed for the torque expression that leads the main rotor speed. The integral part of the torque is defined by the command `set-aux-state-deriv` and uses the variable `@werror` defined above.

```
(add-moment rtcon
  :name "Rotor Torque"
  :direction [rtz]
  :body1 fuselage
  :body2 rt
  :magnitude "wrqtt+kp*(@werror)+kd*dxdt(@werror)")
```

This controller uses the variable `@werror` as the input, and the output is the moment applied to the main rotor so that the desired rotational speed is reached and sustained. The parameters `ki`, `kp` and `kd` are the corresponding controller gains that can be adjusted without the need of new program compilation and are indicated at the beginning of the program script.

Moments Definition

The flap hinges have a flap spring that introduces a spring moment between the rotor (`rt`) and the correspondent flap hinge (`fji`), the spring stiffness is represented by the parameter (`kfj`) which value can be changed for different simulation cases and it is assumed to be equal for each flap hinge in this model. The magnitude is given at each time by the well known Hooke's Law:

```
(add-moment flapspringi
  :name "i-th Flap Spring"
  :body1 fji
  :body2 rt
  :magnitude "-kfj*rq(fji)"
  :direction [blix])
```

In here, `rq(fji)` represents the angular displacement of the flap hinge, β measured in radians.

On the other hand, the lag hinges have a damper of damping coefficient `dlj` that introduces a moment between the lag hinge and the flap hinge. The magnitude of this

moment is given by the product of the damper and the angular speed of the corresponding lag hinge:

```
(add-moment Lagdamperi
  :name "i-th Lag Damper"
  :body1 lji
  :body2 fji
  :magnitude "-dlj*ru(lji)"
  :direction [bliz])
```

In here, $ru(lji)$ represents the rotational velocity of the lag hinge. The directions of both the flap and lag moments are indicated in terms of the local axes of each blade since not always will the blade axis coincide with the rotor axis.

Also, the lag hinges have a lag spring that introduces a spring moment between the lag hinge and the flap hinge, the spring stiffness is represented by the parameter klj .

```
(add-moment lagspringi
  :name "i-th Lag Spring"
  :body1 lji
  :body2 fji
  :magnitude "-klj*rq(lji)"
  :direction [bliz])
```

where $rq(lji)$ represents the angular displacement of the lag hinge, ξ measured in radians. The numerical values for the flap and lag springs and lag damper are given in Table 5.1.

5.6 Tail Rotor Modelling

In this section, the tail rotor modelling process is described once that the main rotor has been implemented. There are significant differences compared to the main rotor structure: the tail rotor has not offset, the lag degree of freedom is neglected (as often in these type of rotors) and the existence of a coupling feather-flap via delta three angle.

5.6.1 Bodies Definition

The tail rotor is built using similar parent-child structure to the previous sections. First, the tail rotor is added as the child of the fuselage, and then it is defined as the parent of the next subsystems. The tail rotor is connected to the fuselage at the point `fsgt1` (see Figure 5.8):

```
(add-point fsgt1 :body fuselage :coordinates (-xt -yt -ht))

(add-body tailrt
  :name "Tail Rotor"
  :parent fuselage
  :mass 0
  :joint-coordinates fsgt1
  :body-rotation-axes y
  :parent-rotation-axis y
  :reference-axis z
  :inertia-matrix (0 Irtly 0))
```

The tail rotor itself is a massless body. The rotational degree of freedom around the local axes Y is allowed. The coordinates of the joint between the tail rotor and the fuselage are given by the command `:joint-coordinates`, its numerical value is defined by the point `fsgt1`. Finally, its moments of inertia are also provided.

The tail rotor in this model has two blades, the relative blades' positions with respect to the tail rotor axes origin must be considered in order to properly define the joint locations. The tail rotor blades' angular displacement on the disc plane is defined as a variable `@alpha_tl_k`, being k the number of existing tail rotor blades.

```
(setsym alpha_tl_k "360*((nblades_tl-blade_number_tl_k)/(nblades_tl))")
(setsym arg_tl_k "2*@pi*(@alfa_tl_k/360)")
```

and $k = 1, 2$.

These angles will define the local axis for each blade. Thus, the local axes are defined in terms of the inertial reference axes `[tail_rtx]`, `[tail_rty]`, `[tail_rtz]`. Therefore, the blade's position with respect to the tail rotor is determined in this way.

5.6. TAIL ROTOR MODELLING

```
(setsym baxesxtl_k "cos(@arg_tl_k)*[tail_rtx]+sin(@arg_tl_k)*[tail_rtz]")
(setsym baxesytl_k "[tail_rty]")
(setsym baxesztl_k "-sin(@arg_tl_k)*[tail_rtx]+cos(@arg_tl_k)*[tail_rtz]")
```

The hinges are added in a sequential manner such that each of them is the child of the previous one and the parent of the following hinge.

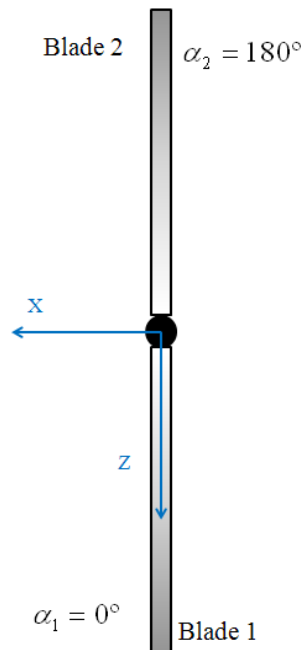


Figure 5.13: *Tail rotor nominal configuration.*

The flap hinge is connected to the main rotor at the point `rtptl_k` where $k = 1, 2$ (see Figure 5.8).

```
(add-point ptl_kr :body n :coordinates (-xt -yt -ht))
(add-point rtptl_k :body tailrt :coordinates ptl_kr)
```

The tail rotor flap hinge is added now as a child of the tail rotor, with zero mass and inertia values:

```
(add-body fjtl_k
  :name "k-th Flap Joint Tail"
  :parent tailrt
  :joint-coordinates rtptl_k)
```

```

:body-rotation-axes x
:parent-rotation-axis "@baxesxtl.k"
:reference-axis "@baxesytl.k"
(inertia-matrix 0
:mass 0)

```

The feather hinge is connected to the flap hinge at the point `pjptl.k` being the parent of the blade and the child of the flap hinge:

```
(add-point pjptl.k :body fjtl.k :coordinates ptl.kr)
```

```
(add-body pjtl.k
```

```

:name "k-th Feather Joint Tail"
:parent fjtl.k
:joint-coordinates pjptl.k
:body-rotation-axes z
:parent-rotation-axis "@baxesztl.k"
:reference-axis "@baxesxtl.k"
(inertia-matrix 0
:mass 0)

```

Finally, the tail rotor blade is added at the point `blptl.k`:

```
(add-point blptl.k :body pjtl.k :coordinates ptl.kr)
```

```
(add-body bltl.k
```

```

:name "k-th Blade Tail"
:parent pjtl.k
:mass mbltl.k
:joint-coordinates blptl.k
(inertia-matrix (Ibltlx Ibltly Ibltlz)
:cm-coordinates (xbltl ybltl zbltl))

```

The tail rotor blades are added as a body with mass, moments of inertia and centre of mass.

5.6.2 Controllers Implementation

Flap Control Definition

In order to simulate the flap mode in the tail rotor, a PID controller is designed, it keeps the flap under control by its coupling with the feather motion by using the delta three angle geometry. The feather-flap coupling by using a delta three configuration reduces the flap amplitude and increases the flap frequency. This is a feature pertinent to the tail rotor only.

On the other hand, it is known that the coning angle is the angle between a blade and a plane passing through the rotor hub, see Figure 5.14.

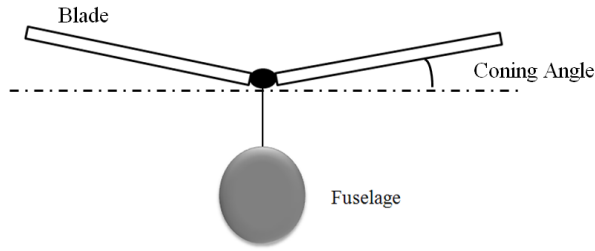


Figure 5.14: *Coning angle.*

The kinetic energy in a helicopter's rotor does not change, on the contrary, the coning angle changes. The kinetic energy on the rotor is given by:

$$T_{rot} = \frac{1}{2} I \Omega^2 \quad (5.4)$$

where I is the angular moment of inertia and Ω is the angular speed of the rotor. The following notation will be adopted: subscript i denotes the initial values, it is associated to no cone or smaller cone. Subscript f corresponds to the final values, it is associated to a larger cone. On the tail rotor the cone angle is the existing angle between the blade and the vertical axis of this rotor, see Figure 5.15, and it is different to the flap angle, as it will explained in the following lines.

As the kinetic energy is constant:

$$\frac{1}{2} I_i \Omega_i^2 = \frac{1}{2} I_f \Omega_f^2 \quad (5.5)$$

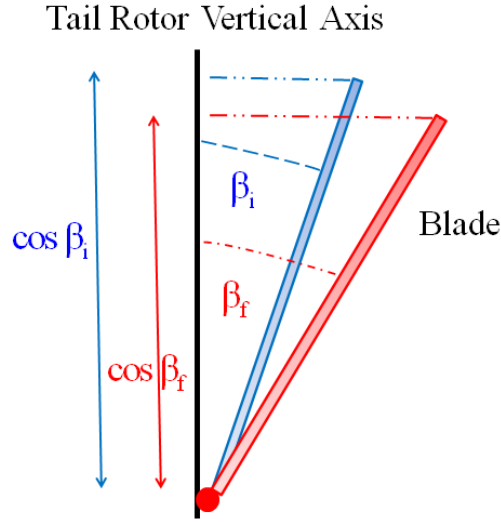


Figure 5.15: *The increased cone angle.*

The angular moments of inertia are equal to: $I = mr^2$, m is the blade's mass and r is the distance of the centre of mass from the rotor hub. Therefore, equation (5.4) can be written:

$$m_i r_i^2 \Omega_i^2 = m_f r_f^2 \Omega_f^2 \quad (5.6)$$

As the mass does not change, equation (5.6) is:

$$r_i^2 \Omega_i^2 = r_f^2 \Omega_f^2 \quad (5.7)$$

and rearranging:

$$\Omega_f^2 = (r_i^2 / r_f^2) \Omega_i^2 \quad (5.8)$$

On the other hand, the variation in the radius is the difference existing between the initial and final blades vertical projection.

$$r_i^2 / r_f^2 = (\cos \beta_i^2 / \cos \beta_f^2) \quad (5.9)$$

Therefore:

$$\Omega_f^2 = (\cos \beta_i^2 / \cos \beta_f^2) \Omega_i^2 \quad (5.10)$$

The blade angular speed can be obtained as a function of the blade's increased cone angle. In order to implement the blade flap motion on the tail rotor, the blade flap can

be defined as Fourier series [144]:

$$\beta = a_0 - a_1 \cos \psi_f - b_1 \sin \psi_f \quad (5.11)$$

where $\psi_f = \Omega_f t$, being Ω_f the blade angular speed obtained as a function of the blade's cone angle (see equation (5.10)) and a_0, a_1, b_1 are the corresponding Fourier coefficients.

```
(setsym fltl_k "rq(fjtl_k)")
(setsym wvr "(cos(aic)/cos(a0))*(krttl*omega)")
(setsym fltlref_k "a0-a1*cos(@wvr*t)-b1*sin(@wvr*t)")
```

The first line provides the flap angle of the tail rotor blades. The second line defines the blades' rotational speed at the increased cone angle according to equation (5.10) where the parameter `krttl` represents the tail rotor gearing, its numerical value is given in Table 5.1 and `aic` is the initial cone angle. The third line, defines the flap angle on the tail rotor as a Fourier series.

Once the flap reference signal has been defined, the PID controller can be implemented by first defining the error variable:

```
(setsym fltlerror_k "@fltlref_k-@fltl_k")
(add-state-variable fltl_tq_k fltl_tqp_k "F*L")
(set-aux-state-deriv fltl_tqp_k "kifl_tl*@fltlerror_k")
```

The `add-state-variable` command introduces a state variable for the moment expression. The integral part of the moment control is defined by `set-aux-state-deriv` command and uses the value of the variable `@fltlerror_k` defined above.

```
(add-moment ftlm_k
  :name "fjcttl_k"
  :direction [fjtl_kx]
  :body1 fjtl_k
  :body2 tailrt
  :magnitude "fltl_tq_k+kpfl_tl*(@fltlerror_k)+kdfl_tl*dxdt(@fltlerror_k)")
```

The controller uses the variable `@fltlerror_k` as the input, and the output is the moment applied to the blade flap hinges so that blade flap control is achieved. The parameters `kifl_tl`, `kpfl_tl` and `kdfl_tl` are the integral, proportional and derivative gains of the controller respectively.

Feather Control Definition

Take blade one on the tail rotor, the feather angle control, the delta three angle structure can be implemented by using a PID controller that constrains the blades' position around the tail rotor feather axis (Z). The feather control in this case is modelled as follows:

```
(setsym ptlpj1 "rq(pj1t1)")
(setsym ptlref1 "fotl-tan(delta3t1)*rq(fj1t1)")
```

The first line creates a variable representing the first blade feather as `rq(pj1t1)`. Then, the variable `@ptlref1` is defined, being the desired collective feather reference signal `fotl`. The feather angle reduces its value by `tan(delta3t1)*rq(fj1t1)`, as the consequence of introducing the delta three angle.

```
(setsym ptlerror1 "@ptlref1-@ptlpj1")
(add-state-variable pl1tq tp1tqp "F*L")
(set-aux-state-deriv tp1tqp "kipt1*@ptlerror1")
```

`add-state-variable` introduces a state variable for the torque expression used to control the feather. The integral part of the torque is defined by `set-aux-state-deriv` and uses the value of the `@ptlerror1` defined above.

The expression to model this control moment is as follows:

```
(add-moment ptlm1
  :name "pj1ctt1"
  :direction -[pj1t1z]
  :body1 tailrt
  :body2 pj1t1
  :magnitude "pl1tq+kppt1*(@ptlerror1)+kdpt1*dxdt(@ptlerror1)")
```

The torque is applied between the tail rotor and the first feather hinge. This controller uses the variable `@ptlerror1` as the input, and the output is the moment applied to the first feather hinge so that collective control is achieved. `kipt1`, `kppt1` and `kdpt1` are the integral, proportional and derivative gains of the controller respectively.

This was shown in here for the case of the tail rotor blade one; in the case of the blade two, a similar moment was modelled and implemented in equal manner but in this case, the direction of rotation around its local reference axis is just opposite (see Figure 5.16).

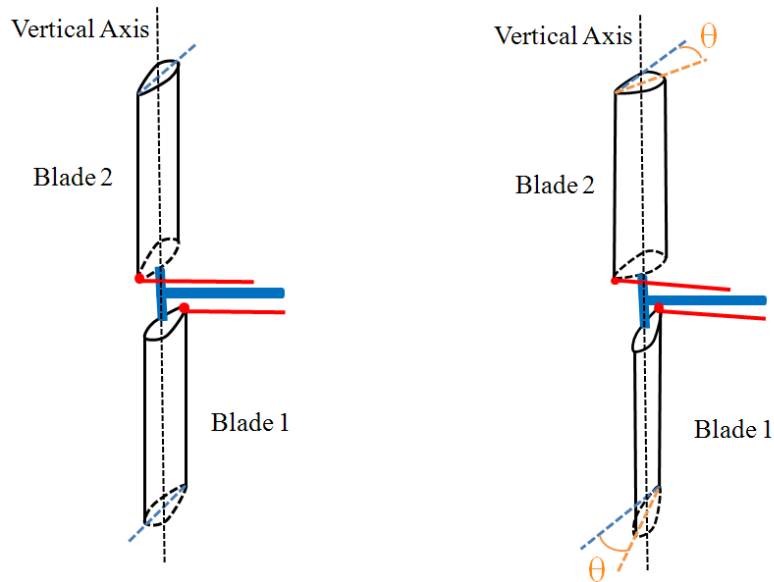


Figure 5.16: Tail rotor blades and the collective angle.

Tail Rotor Speed Control Modelling

As mentioned before, the tail rotor angular speed is proportional to the main rotor angular speed [142]. Being this proportion the value of the tail rotor gearing `krttl` (see Table 5.1).

The tail rotor rotational speed can be modelled as a constraint by using the VehicleSim command `ru(tailrt,1)` which specifies the first rotational speed for the tail rotor:

```
(add-speed-constraint "ru(tailrt)-krttl*omega" :u "ru(tailrt)")
```

the value of the parameter `krttl` is defined at the beginning of the code.

On the other hand, the tail rotor speed can also be implemented by using a PID controller in order to maintain a constant angular speed. In this case, the engine action on the tail rotor can be modelled as a torque applied between the fuselage and the tail rotor:

```
(setsym wrotortl "ru(tailrt,1)")
(setsym wreftl "krttl*omega")
```

Two variables are defined, the first one, `@wrotortl` is the rotational speed of the tail rotor around its Y axis and the second variable, `@wreftl` is the desired reference tail rotor angular speed value.

```
(setsym werrortl "@wreftl-@wrotortl")
```

`@werrortl` is a variable that defines the existing error between the desired input angular speed value `@wreftl` and the actual output angular speed, `@wrotortl`.

```
(add-state-variable wrttltq wrttltqp "F*L")
(set-aux-state-deriv wrttltqp "kirttl*@werrortl")
```

The `add-state-variable` introduces a new state variable. The integral part of the controller is defined by `set-aux-state-deriv` and uses the value of the `@werrortl` defined previously.

The expression of the moment applied in order to control the tail rotor speed is:

```
(add-moment tlcon
  :name "Tail Torque"
  :direction [tailrty]
  :body1 fuselage
  :body2 tailrt
  :magnitude "wrttltq+kprttl*(@werrortl)+kdrttl*
  dxdt(@werrortl)")
```

This controller uses the variable `@werrortl` as the input, and the output is the moment applied to the tail rotor so that a desired rotational speed control is reached and sustained. The variables `kirttl`, `kprttl` and `kdrttl` are the integral, proportional and derivative gains of the controller respectively.

5.7 Vehicle's Longitudinal and Angular Position Control

As a consequence of the actuation torques from the main and tail rotors on the fuselage, the helicopter's equilibrium can be compromised. Therefore, various controllers on the rotational and translational degrees of freedom must be added. The helicopter's translational position control will be restored as well as the angular position. This process is a fundamental step in the model's full development.

Longitudinal Position Control

In order to control the position of the helicopter along the X axis, a new controller needs to be implemented. The longitudinal position of the helicopter is defined as:

```
(setsym xlong "dir(cross([fuselagey],[nz]))")
(setsym xheli "dot(pos(fuselage0,n0),@xlong)")
```

The first line, defines the fuselage's longitudinal direction. The last line finds the fuselage's longitudinal position i.e., the position x component.

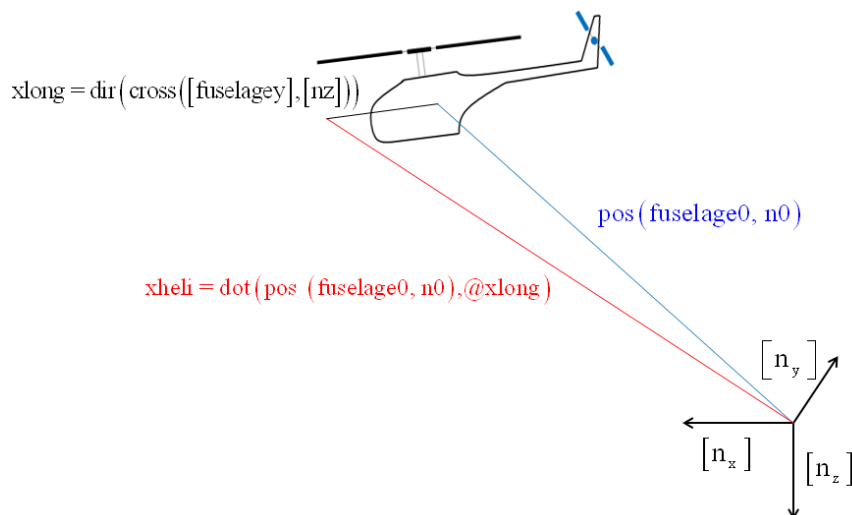


Figure 5.17: Diagram of helicopter's longitudinal position.

```
(setsym xref "x_ref")
```

The variable `@xref` is added, as the reference value for the fuselage's longitudinal position. It is defined as a numerical value in this case zero because the equilibrium position (point (0,0,0)) should remain. In the next chapters, this variable will be an equation to allow for longitudinal trajectory prescription.

```
(setsym xerror "@xref-@xheli")
(add-state-variable xfutq xfutqp "F")
(set-aux-state-deriv xfutqp "kix*@xerror")
```

The `add-state-variable` introduces a state variable for the force expression used to control the helicopter's longitudinal position. The integral part of the force is defined with the `set-aux-state-deriv` and uses the value of the `@xerror` defined as the difference between the actual and desired helicopter longitudinal position.

```
(add-line-force xcon
  :name "xctrl"
  :direction [fuselagex]
  :point1 fuselage0
  :point2 n0
  :magnitude "xfutq+kpx*(@xerror)+kdx*dxdt(@xerror)")
```

The force is applied between the fuselage (fuselage's centre `fuselage0`) and the inertial frame. The controller uses the variable `@xerror` as the input variable and the output is the force applied to the fuselage, so a desired longitudinal position control is achieved. The parameters `kix`, `kpx` and `kdx` are the gains of the controller.

The lateral and vertical position controls are modelled similarly to the longitudinal position control and therefore are not included in this report.

Fuselage's Yaw Control

In order to control the helicopter's yaw (rotation around the Z axis), a new controller is added. The yaw is calculated as:

```
(setsym phifusez "rq(fuselage,1)")
```

where `rq(fuselage,1)` specifies the fuselage's first rotational coordinate.

```
(setsym phirefz "fuszref")
```

The variable `@phirefz` is defined as the reference value for the fuselage's yaw. It is defined as a zero because the equilibrium position should be restored. Its numerical value is defined at the beginning of the program. In the following chapters, this variable will be an equation that allows to describe a yaw helicopter trajectory in the space.

```
(setsym phierrorz "@phirefz-@phifusez")
(add-state-variable fuseztq fuseztqp "F*L")
(set-aux-state-deriv fuseztqp "kifsz*@phierrorz")
```

The `add-state-variable` introduces a state variable for the torque expression that it is used to control the helicopter yaw. The integral part of the torque is defined with the `set-aux-state-deriv` and uses the value of the `phierrorz` defined above. `@phierrorz` is the difference between the actual and desired fuselage's yaw.

```
(add-moment fszphi
  :name "phictrlz"
  :direction -[fuselagez]
  :body1 fuselage
  :body2 n
  :magnitude "fuseztq+kpfsz*(@phierrorz)+kdfsz*dxdt(@phierrorz)")
```

The torque is applied between the fuselage and the inertial frame. The controller uses the variable `@phierrorz` as the input variable and the output is the torque applied to the fuselage adequate yaw control is achieved. The parameters `kifsz`, `kpfsz` and `kdfsz` are the gains of the controller.

The pitch and roll control are modelled similarly to the yaw control.

5.8 Chapter Summary

The aim of this chapter was to provide a model of a helicopter by using the multibody modelling code `VehicleSim`. The derived model has been developed without the influence of external forces i.e., the system is considered to be in vacuum. As it has been shown,

the fuselage, the main rotor and tail rotor have been built by using the parent-child structure dictated by VehicleSim. In addition to this, the connections between the several bodies have been represented and the degrees of freedom for each body have been modelled.

The procedure for modelling the main rotor consisted of defining a body composed by several hinges as well as flap, lag and feather degrees of freedom. The blades are added as bodies with mass and inertial properties, and they are rigid. The actions of the washplate on the blades were simulated implementing various PID controllers, so the blades' motions on the disc plane can be simulated together with the flap and lag hinges. The collective and cyclic feather control has been designed and modelled.

Additionally, the speed ratio between the main and the tail rotors has been set up, as well as the effects the engine has on the fuselage. The delta three angle and its effects on the tail rotor has been modelled. It is worthy of note that the coupling existing between the flap and the feather degree of freedom on the tail rotor has been explained carefully in order to understand this complex effect. This allowed the next stage in the modelling process as the feather collective was designed and modelled according to the delta three implementation.

Various PID controllers are included to achieve position and rotation equilibrium. The modelling for longitudinal position control as well as yaw control were carefully described. Taking into account the previous considerations, the control of the helicopter around the equilibrium point $(0, 0, 0)$ is obtained, getting the desired equilibrium when both main and tail torques operate on the system.

Overall, this model here presented captures nonlinear dynamics and couplings existing in a complex mechanical system such as a helicopter.

The following chapters will explore further the nature of these couplings, their mathematical representations, their implications on the vehicle's behaviour and their physical impact on the blade's and fuselage's degrees of freedom in the absence of an aerodynamic environment. In the last chapters of this thesis, the problem of adding aerodynamic forces on this model is also treated.

Chapter 6

External Perturbations

Modelling for Sikorsky Model (Aerodynamic Model)

6.1 Introduction

The main aim of this chapter is to describe the modelling developed for analyzing the external perturbations on the helicopter dynamics model described in Chapter 5. First, gravity is added to the system, so the equilibrium on the vehicle under the action of this force should be restored. The ground is also simulated on the helicopter. After that, the inclination on the main rotor is considered in order to build up a helicopter model close to a real model as well as to study the impact this inclination has on the system when the aerodynamic forces are included. On the other hand, the model is enhanced by modelling varying rotating speed on the main rotor. Finally, an aerodynamic model is presented for both main and tail rotors, the fuselage's aerodynamic effects are not considered, this task will be developed in the near future by the author, the aerodynamic modelling is focused on both rotors using blade element theory.

6.1.1 Aerodynamic Environment

A helicopter rotor experiences a complex aerodynamic phenomenon that does not occur in fixed-wing airplanes. The rotor blades produce lift by rotating and induce their own airspeed over the airfoils. Once a helicopter leaves the ground (take off), it is acted upon by four forces; thrust, drag, lift and weight. Understanding how these forces act and how to equilibrate them using flight controls is essential to flight (see Figure 6.1). The lift is the upward force created by the airflow as it passes around an airfoil. The weight opposes the lift force and is caused by the gravity. The thrust is the force that propels the helicopter through the air. Opposing lift and thrust is drag, which is a retarding force created by the development of lift and the movement of an object through the air [3].

The lift generated by an airfoil depends on various factors: airflow speed, air density, total area of the segment or airfoil and angle of attack between the air and the airfoil. The angle of attack is the angle at which the airfoil meets the oncoming airflow or vice versa. In the case of a helicopter, the object is the rotor blade (airfoil) and the fluid is the air. Lift is produced when a mass of air is deflected, and it always acts perpendicular to the resultant relative wind. A symmetric airfoil must have a positive angle of attack to generate positive lift. At a zero angle of attack, no lift is produced. At a negative angle of attack, negative lift is generated [3].

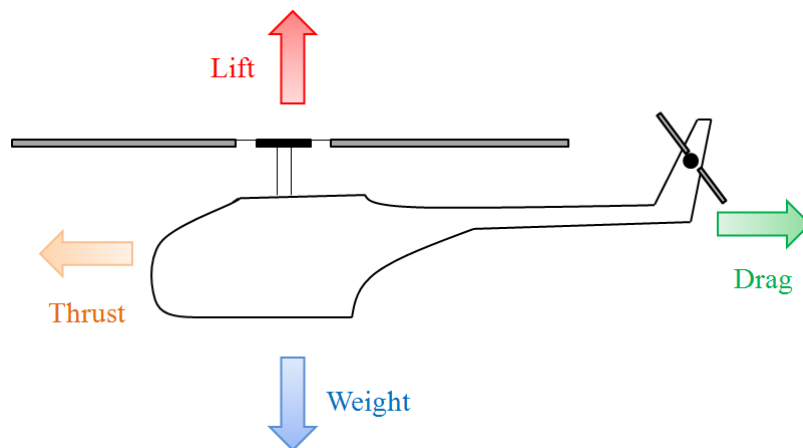


Figure 6.1: *Forces acting on a helicopter.*

Rotor Blade Angles

There are two angles that allow a rotor system to produce the lift required to fly, these are the angle of incidence and the angle of attack.

a) Angle of incidence

The angle of incidence is the angle between the chord line of a main or tail rotor blade and the rotor hub. In fact, it is a mechanical angle and it is sometimes referred as blade feather angle (figure 6.2) [3].

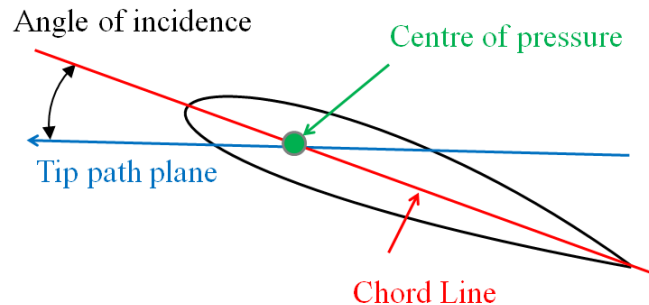


Figure 6.2: *Angle of incidence is the angle between the chord line and the tip path plane.*

b) Angle of attack

The angle of attack is the angle between the airfoil chord line and the resultant relative wind. It is an aerodynamic angle (see Figure 6.3). If the angle of attack is increased, the lift increases its value until the critical angle of attack is reached. After that, any increase in the angle of attack beyond this point generates a stall and a rapid decrease in the lift force [3].

In the absence of induced flow, angle of attack and angle of incidence are equal [3]. Several factors may change the rotor blade angle of attack. The pilots have small direct control the over the angle of attack except for indirectly the flight control input. Collective and cyclic feather help to generate these changes. Collective feather changes the angle of incidence equally on rotor blades, simultaneously. This action changes the angle of attack, which changes the lift coefficient, and also affects the overall lift of the rotor system. Most of the changes in the angle of attack come from changes in airspeed and rate of climb or descent. Pilots adjust the angle of attack through mechanical control manipulation of the feather angle of the blades. If the feather angle is increased,

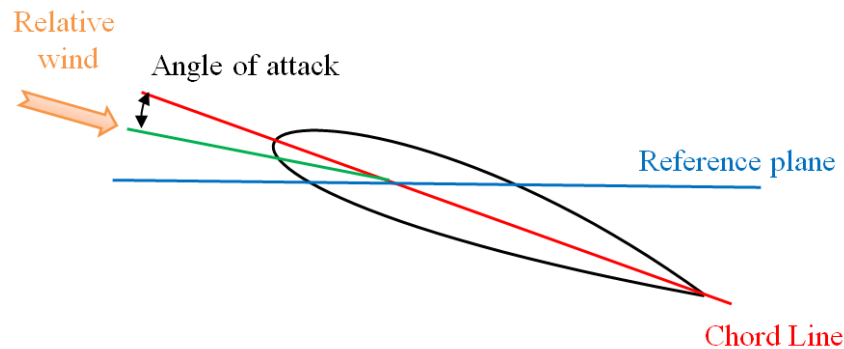


Figure 6.3: *The angle of attack is the angle between the airfoil chord line and resultant relative wind.*

the angle of attack raises; if the feather angle is reduced, the angle of attack is also reduced [3].

Centre of Pressure

The loading on the airfoil can be replaced only by normal and axial (chord) forces acting at this point, which is called the centre of pressure. The centre of pressure moves to different locations on the chord with changes in angle of attack. The centre of pressure may be found on an airfoil using the normal force and pitching moment about the 1/4 chord (see Figure 6.2) [98].

Blade Element Analysis in Hover and Axial Flight

Blade element theory forms the basis of most modern analyses of helicopter rotor aerodynamics as it estimates the radial and azimuthal distributions of blade aerodynamic forces (and moments). In addition to this, the rotor performance can be obtained by integrating the sectional airloads at each blade's elements over the length of the blade and averaging the result over a rotor revolution [98].

Figure 6.4 is a plan view of the rotor disc, viewed from above. The blade radius is R and the tip speed is given by ΩR . An elementary blade section is considered at radius y , of chord length c and spanwise width dy .

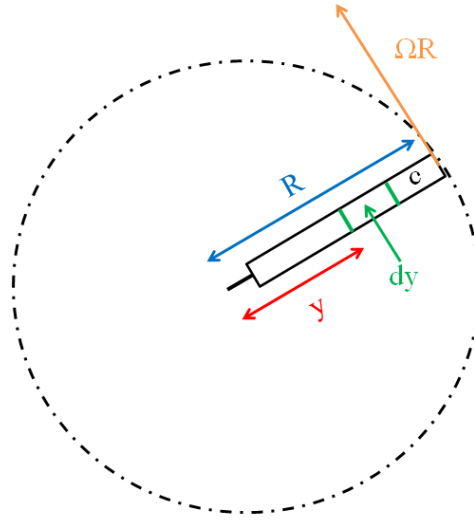


Figure 6.4: Main rotor disc viewed from above. This figure is plotted by the author and based on [145].

The forces on the blade's section are shown in Figure 6.5. The flow seen by the section has velocity components Ωy in the disc plane and $(v_i + V_c)$ (v_i is the induced velocity and V_c is the upward velocity) perpendicular to it [145].

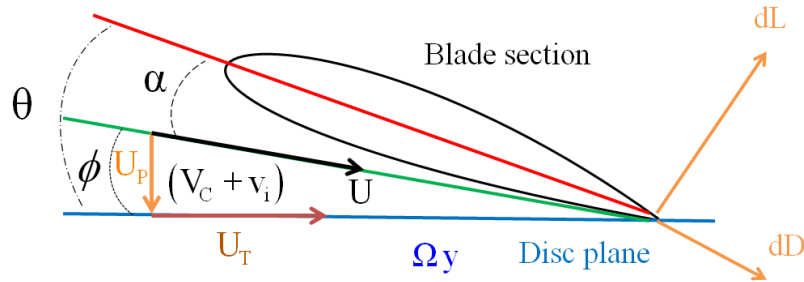


Figure 6.5: Flow conditions in vertical flight for a blade section. This figure is drawn by the author and based on [145].

The resultant local flow velocity at any blade element at a radial distance y from the rotational axis has an out of plane component $U_P = (v_i + V_c)$ normal to the rotor plane as a result of climb and induced inflow and an in plane component $U_T = \Omega y$ parallel to the rotor due to the blade rotation, relative to the disc plane. The resultant velocity at the blade element is therefore the composition of both [98]:

$$U = \sqrt{U_T^2 + U_P^2} = \left[(v_i + V_c)^2 + (\Omega y)^2 \right]^{1/2} \quad (6.1)$$

The blade feather angle θ , is imposed by the pilot's collective control input. The angle between the flow direction and the plane of rotation, known as the inflow angle ϕ , is therefore [145]:

$$\tan\phi = \frac{(V_c + v_i)}{\Omega y} \quad (6.2)$$

If the feather angle at the blade element is θ , then the aerodynamic or effective angle of attack is:

$$\alpha = \theta - \phi \quad (6.3)$$

The resultant incremental lift, dL , and drag dD per unit span on a blade element are:

$$dL = \frac{1}{2}\rho U^2 c C_l dy \quad (6.4)$$

$$dD = \frac{1}{2}\rho U^2 c C_d dy \quad (6.5)$$

where ρ is the air density, C_l and C_d are the lift and drag coefficients, c is the local blade chord. The lift dL and drag dD act perpendicular and parallel respectively to the resultant flow velocity.

Blade Element Analysis in Forward Flight

In forward flight, a similar approach to that used in hover conditions can be used, taking into account some extra complexities involved in forward flight. There exist additional factors which play a role into forward flight conditions. Figure 6.6 shows a side view of the rotor disc.

Forward motion is assumed to the left and horizontal, i.e., without a climb component. The plane containing the edge of the disc (the tip path plane) forms an angle α_r with the oncoming stream direction. α_r is positive downwards since that is the natural direction of tilt needed to obtain a forward component of the thrust. The flight velocity V has components $V\cos\alpha_r$ and $V\sin\alpha_r$ along and the normal to the tip path plane. The advance ratio is the ratio of the forward velocity and the rotor speed [140], [145]:

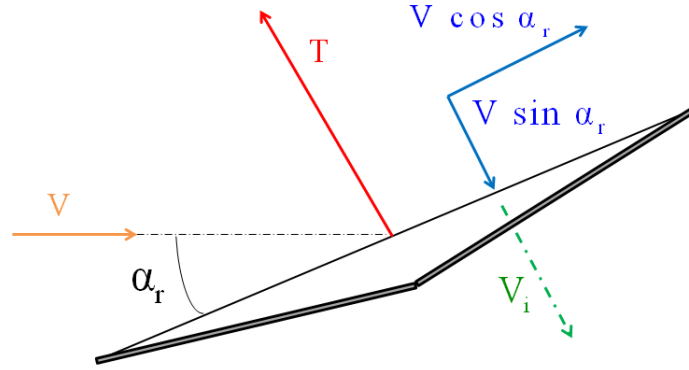


Figure 6.6: *Disc incidence and component velocities in forward flight. This figure is plotted by the author and based on [145].*

$$\mu = \frac{V \cos \alpha_r}{\Omega R} \approx \frac{V}{\Omega R} \quad (6.6)$$

The total inflow through the rotor is the sum of $V \sin \alpha_r$ and v_i the thrust related induced velocity.

Referring to figure 6.7, the resultant velocity U for a blade section is a function of the rotor rotation, the forward speed, the induced velocity and the blade flap motion [145].

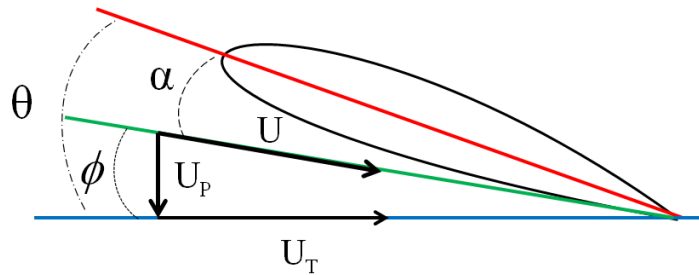
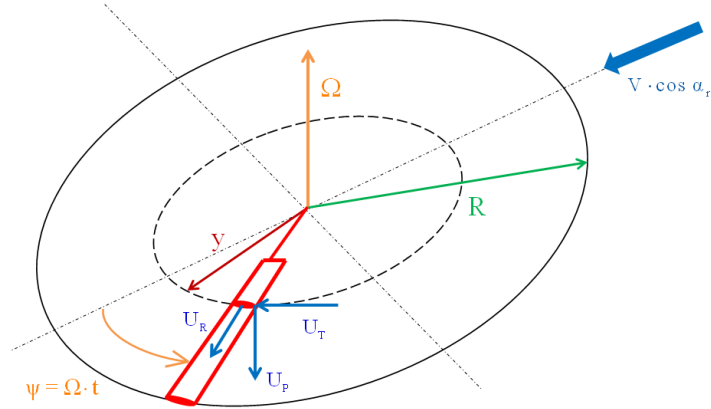


Figure 6.7: *Velocity components U_T and U_P .*

The components of U are U_T and U_P , additionally to these, due to the forward speed factor there is also a spanwise component U_R as shown in Figure 6.8.

In forward flight, the blade elements velocity components are periodic at the rotor's rotational frequency. There is an in plane velocity component due to the blade rotation

Figure 6.8: Velocity components U_T , U_P and U_R .

about the rotor shaft [98]:

$$U_T = \Omega y + V \sin \psi = \Omega y + \mu \Omega R \sin \psi \quad (6.7)$$

The out of plane component consists of three terms: the first is a term containing the inflow velocity. The other two terms result from perturbations in the velocity at the blade element and they are produced by the blade motion. With reference to figures 6.8 and 6.9, a perturbation in velocity, $y\dot{\beta}$, is generated as a consequence of the blade flap velocity about a hinge, with another perturbation $\mu\Omega R\beta\cos\psi$ appearing due to the blade flap angular motion (coning). Therefore, the perpendicular component of the velocity can be written:

$$U_P = \lambda\Omega R + y\dot{\beta} + \mu\Omega R\beta\cos\psi \quad (6.8)$$

ψ is blade azimuth angle for a constant rotational speed, $\psi = \Omega t$.

As mentioned before, there exists as well a radial velocity component parallel to the span axis of the blade [98] and this is:

$$U_R = \mu\Omega R\cos\psi \quad (6.9)$$

The inflow ratio λ is the ratio of the total inflow velocity to the rotor tip speed [140]:

$$\lambda = \frac{V \sin \alpha_r + v_i}{\Omega R} = \mu \alpha_r + \lambda_i \quad (6.10)$$

where v_i is the induced velocity.

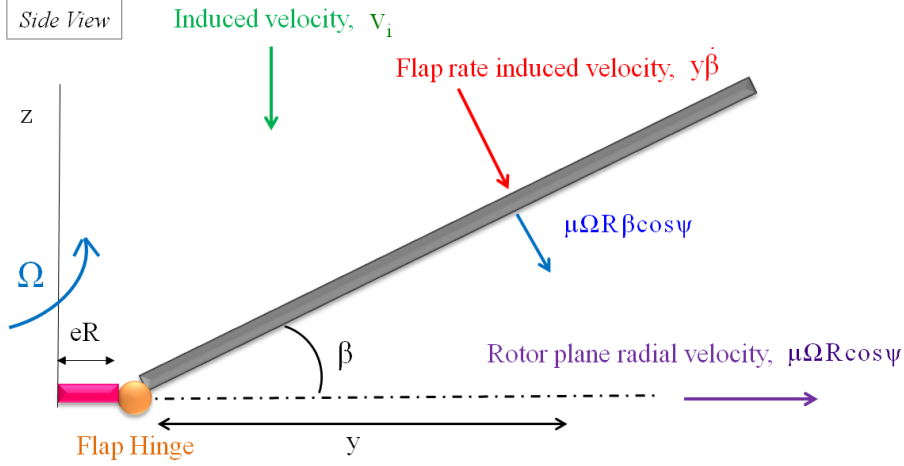


Figure 6.9: Perturbation velocities on the blade resulting from blade flap velocity and rotor coning. This figure is plotted by the author and based on [98].

For helicopter rotors the following assumptions can be made:

- The out of plane velocity U_P is smaller than the in plane velocity U_T , so that $U = \sqrt{U_T^2 + U_P^2} \approx U_T$. This is a valid approximation except near the blade root, but the aerodynamic forces are small here anyway.
- The induced angle ϕ , is small, so that $\phi = U_P/U_T$ [98].

As a result of these approximations, the blade angle of incidence may now be written as:

$$\alpha = \theta - \phi = \theta - \frac{U_P}{U_T} \quad (6.11)$$

The resultant incremental lift dL per unit span on the blade element is now:

$$dL = \frac{1}{2}\rho U^2 c C_l dy \quad (6.12)$$

and similarly the incremental drag is:

$$dD = \frac{1}{2}\rho U^2 c C_d dy \quad (6.13)$$

which act perpendicular and parallel to the resultant flow velocity at the blade section.

6.2 Earth/Ground Modelling

The first external force that it is included on the model script derived in this work is the gravity force. The helicopter simulation model is subjected to an unbalance of forces that should be taken into account in order to restore the equilibrium.

First, gravity is added by the command:

```
(add-gravity)
```

Taking into account third Newton's law on the fuselage i.e., the gravity force acts in the vertical downwards direction whereas the earth/ground exerts a force with opposite direction (reaction) an equal magnitude. As a result, a vertical force should be introduced in the model:

```
(setsym z_long "dir(cross([fuselagex],[ny]))")  
(setsym hheli "dot(pos(fuselage0,n0),@z_long)")
```

The first line, defines the vertical direction of the fuselage. The second line finds the exact fuselage vertical position i.e., the z position component.

The magnitude of the ground reaction is modelled as follows:

```
(setsym Fzm "kgrsp*(rg-@hheli)+kgrd*dxdt(rg-@hheli)")
```

where `kgrsp` and `kgrd` are constant values defined at the beginning of the program. They are the values of a spring and damper modelled to help to simulate the ground reaction to gravity. The ground force on the helicopter is modelled under the action of a spring and damper to allow changes in the force when the helicopter's mass changes. For example, if an additional load is needed (cargo, etc) the new helicopter's weight and ground force are calibrated by changing the spring constant and damping coefficient. Finally, `rg` is the reference value for the ground i.e., zero.

The command `add-line-force` introduces a normal force on the fuselage with a magnitude defined by the variable `@Fzm` in opposite direction to the gravity force.

```
(add-line-force f_gr
  :name "Ground Force"
  :direction -[nz]
  :point1 fuselage0
  :point2 n0
  :magnitude "@Fzm")
```

The force is applied between centre of the fuselage and the inertial frame origin.

In this way, the fuselage remains in the equilibrium position ($Z = 0$) under the gravity force action.

6.3 Main Rotor Tilt

The main rotor can rotate around the Y fuselage axis producing an inclination of the overall main rotor known as "tilt". The main rotor experiments an inclination with respect to the fuselage vertical axis, being this value a structural parameter that it has a constant value (see Figure 6.10).

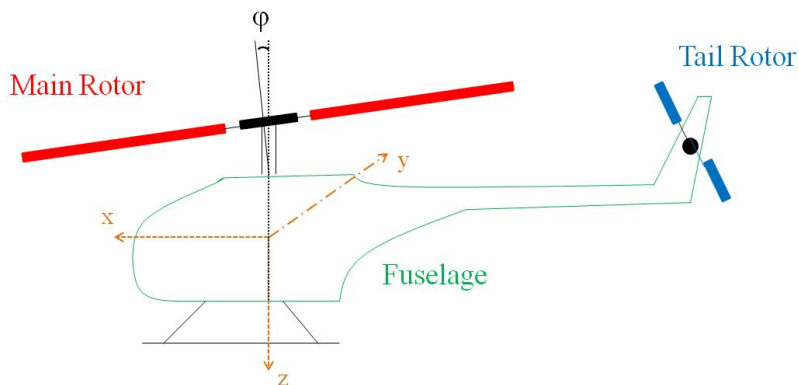


Figure 6.10: *Main rotor tilt angle φ with respect to the fuselage's vertical axis.*

In order to model the existence of an main rotor tilt, a new set of local axes is defined for the main rotor with respect to the fuselage's local axes (`[fuselage x]`, `[fuselage y]`, `[fuselage z]`):

6.3. MAIN ROTOR TILT

```
(setsym rt_inclx "cos(ang)*[fuselagex]+sin(ang)*[fuselagez] ")
(setsym rt_incly "[fuselagey] ")
(setsym rt_inclz "-sin(ang)*[fuselagex]+cos(ang)*[fuselagez] ")
```

`ang` is the tilt angle, its value is constant and it is defined at the beginning of the program.

A point in the helicopter nominal configuration within the coordinate system of body `n` needs to be defined to connect the rotor to the fuselage at the point `fsg`.

```
(add-point fsgp :body n :coordinates (0 0 -h))
(add-point fsg :body fuselage :coordinates fsgp)
```

The point `fsg` is located at a vertical distance `-h` from the origin of the inertial axes system.

The main rotor is introduced in the model as follows:

```
(add-body rt
      :name "Rotor"
      :parent fuselage
      :mass 0
      :joint-coordinates fsg
      :body-rotation-axes z
      :parent-rotation-axis "@rt_inclz"
      :reference-axis "@rt_inclx"
      :inertia-matrix (0 0 Irt.z))
```

The rotor has the fuselage as parent. It is set up as a massless body. The rotational degree of freedom around the rotor's Z axes is considered and takes into account the new axes defined as tilted with respect to the fuselage (see "`@rt_inclz`" defined as the parent-rotation-axis). The coordinates of the joint between the main rotor and the fuselage are given by the command: `joint-coordinates`, its numerical value is defined by the point `fsg`. Finally, its moments of inertia are provided.

6.4 Main Rotor Varying Angular Speed

The main rotor angular speed in this model, makes use of a PID controller in order to change the angular speed according to some specific demand. This is dictated by the expression: $\Omega(t) = 2\pi f_1 + 2\pi f_2 \cos(2\pi f_3 t)$ where f_1 , f_2 and f_3 are frequencies expressed in Hz [93]. A torque between the fuselage and the main rotor will be introduced as means to change the angular speed.

```
(setsym wrotor "ru(rt,1)")  
(setsym wref "(2*@pi*f1)+(2*@pi*f2)*cos(2*@pi*f3*t)+acce*t")
```

Two variables are defined, the first one, `@wrotor` is the angular speed of the main rotor around the Z axis and the second variable, `@wref`, is the reference value of the angular speed of the main rotor. As it can be seen, three parameters need to be defined, `f1`, `f2`, `f3`, the corresponding frequency values. The first one represents the main rotor angular speed, the second and third introduce a variation on the main rotor angular speed. Their numerical values are defined at the beginning of the program. Also, an acceleration value, `acce`, is introduced so the targeted main rotor angular speed can be reached gradually in a realistic manner, as `acce*t` appears on the variable `@wref`.

`add-state-variable` introduces a state variable for the torque expression that will dictate the main rotor speed. The integral part of the torque is defined by the `set-aux-state-deriv` command and uses the value of `@werror`.

```
(setsym werror "@wref-@wrotor")  
(add-state-variable wrttq wrttqp "F*L")  
(set-aux-state-deriv wrttqp "ki*@werror")  
  
(add-moment rtcon  
  :name "Rotor Torque"  
  :direction [rtz]  
  :body1 fuselage  
  :body2 rt  
  :magnitude "wrttq+kp*(@werror)+kd*dxdt(@werror)")
```

This controller uses the variable `@werror` as the input and the output is the moment applied to the main rotor so that main rotor angular speed control is achieved. The

variables k_i , k_p and k_d are the gains of the controller that can be adjusted without the need of new compilation.

6.5 Main Rotor Aerodynamic Modelling

In order to model the aerodynamic environment, in this section, fundamental concepts such as air density, induced speeds, lift and drag forces, thrust coefficients are introduced.

6.5.1 Air Density

In every flight condition, the air density changes with the height (h), for the lower atmosphere where helicopters fly below 6000 m, the standard value of air density can be approximated as [98]:

$$\rho = \rho_0 e^{-0.0296h/304.8} \quad (6.14)$$

where h is expressed in meters and $\rho_0 = 1.225 \text{ kg/m}^3$.

The previous expression is implemented in VehicleSim as:

```
(setsym ro.air "rho*(exp((-0.0296*abs(tq(fuselage,3)))/304.8))")
```

the height is given by the fuselage's vertical position `tq(fuselage,3)`. This expression provides the air density value for all the height range reached by the helicopter.

6.5.2 Induced Hover Speed

In hovering flight, the induced velocity can be obtained according to the expression $v_i = v_{i0}$, v_{i0} is the hover induced velocity, which can be considered constant in hover, the traction force, T , becomes equal to the disc loading (weight of the helicopter) [98]:

$$v_{i0} = \sqrt{\frac{T}{2\rho\pi R^2}} \quad (6.15)$$

The induced hover velocity is implemented in VehicleSim as follows:

```
(setsym vih "sqrt(((mf+mb11+mb12+mb13+mb14+mb1_t11+mb1_t12)*g)/  
(2*@ro_air*@pi*Rt**2)))")
```

the traction force, magnitude T , is equal to weight of the helicopter, where `mf` is the fuselage mass, `mb11`, `mb12`, `mb13`, `mb14` are the main rotor blades' masses. `mb1_t11`, `mb1_t12` are the tail rotor blades' masses. `@ro_air` is the air density and `Rt` is the main rotor radius.

6.5.3 Climb, Descent and Forward Speed

Climb Velocity

The climb velocity can be modelled as a function of the induced velocity in hover:

```
(setsym vc "cteclimb*(Kclimb*@vih)")
```

where `cteclimb` is a boolean parameter that will allow to choose one from the different options of flight such as hover, climb, descent and forward flight, all of them are modelled in the same code. In order to simulate this, one of the boolean parameters takes the value one for the corresponding flight condition and the rest of them remain null. The parameter `Kclimb` is the ratio between the climb velocity and the induced hover velocity, it will be defined by using several theoretical considerations. Finally, `@vih` is the variable representing the induced hover velocity.

Descent Velocity

The descent velocity is implemented as:

```
(setsym vdes "ctevid*(ctdesc*@vih)")
```

`ctevid` is the corresponding boolean parameter. The value `ctdesc` is the ratio between the descent velocity and the induced hover velocity. It is obtained by taking into account the theoretical approach and `@vih` is the variable represented the induced hover velocity.

Forward Velocity

The forward velocity expression is given by:

$$V = \frac{\mu\Omega R}{\cos(\alpha_r)} \quad (6.16)$$

μ is the advance ratio, Ω is the rotor angular speed, R is the rotor radius and α_r is assumed positive downwards since that is the natural direction of the tilt needed to obtain a forward component of the thrust.

According to this, the forward velocity can be modelled as:

```
(setsym vveli "(mu*Rt*@wrotor)/cos((ktray1*gamma)+(ktray2*@phi_fusey))")
```

μ is the advance ratio, its value is defined at the beginning of the program. Rt is the main rotor radius. $@wrotor$ is the main rotor angular speed. Two boolean variables are defined, $ktray1$ and $ktray2$, they allow to consider the natural direction of tilt. For a constant tilt, γ is indicated, its numerical value is defined at the beginning of the program. On the other hand, for a variable tilt $@phi_fusey$, indicates the fuselage's pitch.

6.5.4 Induced Climb, Descent and Forward Velocities

Induced Climb Velocity

The induced climb velocity is proportional to the induced hover speed, as Figure 6.11 shows [98]. The induced climb velocity in vertical flight is then implemented as:

```
(setsym viclmb "ctecli*(cteviclmb*(@vih))")
```

$ctecli$ is a boolean parameter, $cteviclmb$ is the parameter that provides the proportional value between both speeds. The variable $@vih$ is the induced hover velocity.

Induced Descent Velocity

In vertical descent, the air flow through the rotor undergoes significant changes. The stream velocity, V_c , is now negative whilst the induced velocity remains positive as the rotor maintains the lift.

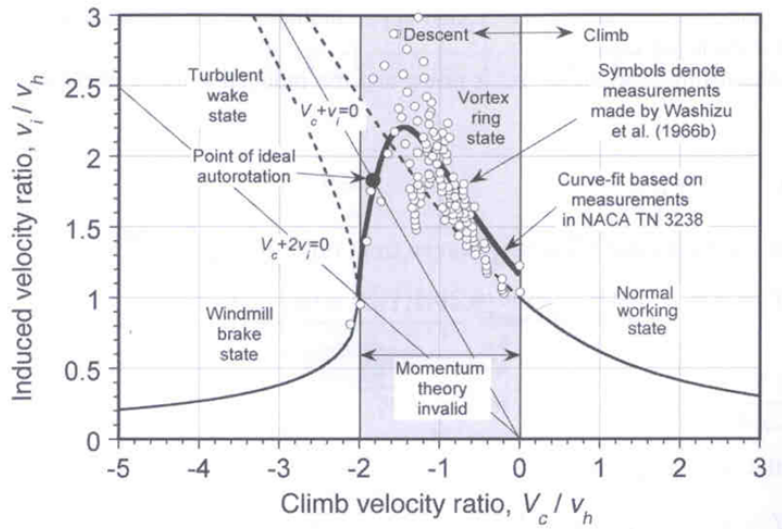


Figure 6.11: *Induced velocity variation as a function of climb and descent velocity. Reproduced with permission from Cambridge University Press [98].*

```
(setsym vides "ctevid*(kdes*@vih)")
```

`ctevid` is a boolean parameter. The variable `@vih` is the induced hover velocity and `kdes` is a constant defined at the beginning of the program and its numerical value depends on the theoretical approach considered.

Induced Forward Velocity

The induced forward velocity can be implemented as:

```
(setsym vifw "Kfw*@vih")
```

The variable `@vih` is the induced hover velocity and `Kfw` is a constant value defined at the beginning of the program and it depends on the theoretical approach considered.

6.5.5 Blade Angle of Incidence

The definition of the blades' angle of incidence makes use of the blade element theory (see equation (6.3)). The blade angle of incidence for various flight conditions is defined as:

Hover:

$$\alpha = \theta - \arctan\left(\frac{v_{ih}}{\Omega y}\right) \quad (6.17)$$

Climbing flight:

$$\alpha = \theta - \arctan\left(\frac{V_c + v_{ic}}{\Omega y}\right) \quad (6.18)$$

Descent flight:

$$\alpha = \theta - \arctan\left(\frac{V_{des} + v_{id}}{\Omega y}\right) \quad (6.19)$$

Forward flight:

$$\alpha = \theta - \left(\frac{U_P}{U_T}\right) \quad (6.20)$$

In VehicleSim, the angle of incidence for forward flight is implemented by using equation (6.7). U_T is modelled as:

$$(\text{setsym ut_i } "(\omega*(y_i+eR))+(\omega*Rt*\mu*\sin(@wrotor*t))")$$

for $i = 1, \dots, 3$. i is the corresponding point on the blade where the aerodynamic load is applied to.

By using equation (6.8), U_P is:

$$(\text{setsym up_j_i } "(@wrotor*Rt*@lambda)+(@wrotor*Rt*\mu*\cos(@wrotor*t)*\text{rq}(fj_j))+((y_i+eR)*\text{dxdt}(\text{rq}(fj_j))))")$$

where $j = 1, \dots, 4$ (j is number of blades) and $i = 1, \dots, 3$.

Taking into account equations (6.11) and (6.17 - 6.19) the total angle of incidence for hover, climb and descent/forward flight can be implemented as:

$$(\text{setsym alpha_j_i } "\text{rq}(pj_j)-\text{atan}(((\text{ctec1}*(\text{vc}+\text{viclmb}))/(\omega*(y_i+eR)))+((\text{ctvids}*(\text{vdes}+\text{vides}))/(\omega*(y_i+eR)))+((\text{ctehv}*\text{vih}))/(\omega*(y_i+eR))))+(\text{ctefw}*\text{up_j_i})/\text{ut_i}")$$

where $\text{rq}(pj_j)$ is the feather angle of each blade. ctec1 , ctvids , ctehv and ctefw are boolean variables, they allow to choose the corresponding flight condition on each case by setting one of them to 1 and letting the rest of them as 0. y_i is the distance along the blade's Y axis where the angle of incidence is measured (see Figure 6.12). In order to solve the error that VehicleSim provides when the variable $@wrotor$ is used as

denominator, ω is used. In the expression above, ω is used in the denominator instead of the variable ω_{rotor} , as this latest variable may reach near to zero values for very short time, and division by zero is not allowed in VehicleSim. On the contrary, if ω is used, the problem is avoided due to its constant value different from zero during of the simulation time.

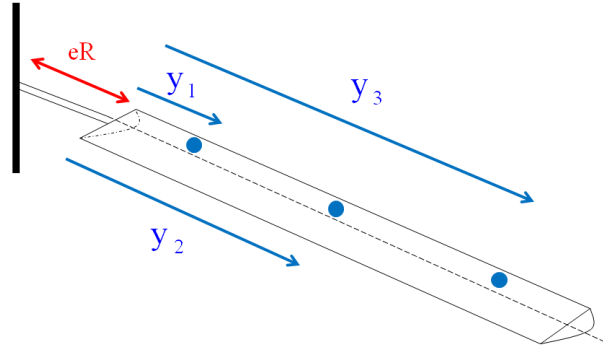


Figure 6.12: Aerodynamic load representation for a main rotor blade.

6.5.6 Lift Force

The lift coefficient C_l is proportional to the angle of attack α [140], [146].

$$C_l = a\alpha \quad (6.21)$$

where "a" is the lift slope and it is equal to 2π when the angle α is measured in radians [146].

The lift coefficient can be implemented in VehicleSim as a variable:

```
(setsym cl_j_i "2*@pi*@alpha_j_i")
```

j indicates the blade number and i is the corresponding point on the blade where the aerodynamic load is applied and $2*\pi$ is the coefficient of proportionality or lift curve slope.

Taking into account equations (6.4) and (6.12), the lift force is implemented in VehicleSim as:

```
(setsym lift_j_i "cte*@ro_air*((ctecl*@cl_j_i*(@wrotor*(y_i+eR))**2)+
(ctvids*@cl_j_i*(@wrotor*(y_i+eR))**2)+(ctehv*@cl_j_i*(@wrotor*
(y_i+eR))**2)+(ctefw*@cl_j_i*(@ut_i)**2))*chord*dy_i")
```

cte is equal to $1/2$, @ro_air is the air density, @wrotor is the main rotor angular speed, chord is the chord of the blade and y_i are the different points on the main rotor blades where the lift forces are applied (see Figure 6.13). Finally, dy_i are the differential length intervals in which the differential lift forces are divided. Various points on the helicopter nominal configuration within the coordinate system of body n need to be defined as the lift and drag forces will be applied on them:

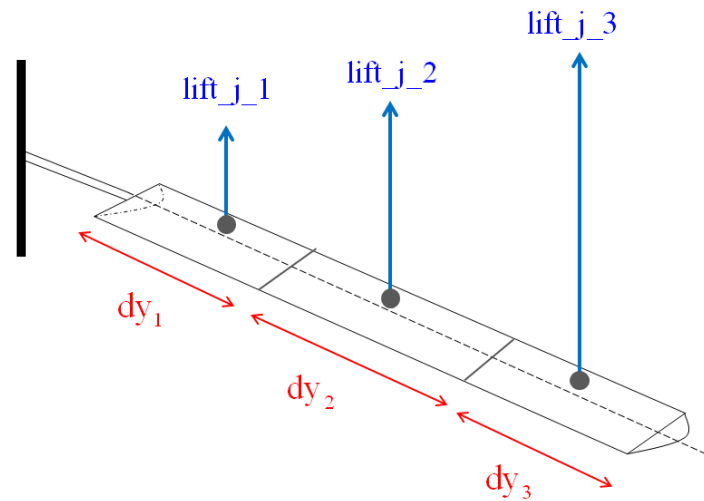


Figure 6.13: Lift force representation for the corresponding points on the main rotor.

```
(add-point co_j_i :body n :coordinates ("± @x_j ± x_i" "@y_j ± y_i"
"-h ± x_i*sin(ang)"))
```

for odd blades $j = 1, 3$ and $i = 1, \dots, 3$.

```
(add-point co_j_i :body n :coordinates ("(@x_j ± y_i)*cos(ang)"
"∓ (@y_j+x_i)* cos(ang)" "-h ± (eR+y_i)*sin(ang)"))
```

for even blades $j = 2, 4$ and $i = 1, \dots, 3$.

The points cmp_j_i define the centre of pressure.

```
(add-point cmp_j_i :body bl_j :coordinates co_j_i)
```

The lift forces are applied to the blades at the points `cmp_j_i`. The command `add-line-force` introduces the lift forces in the model:

```
(add-line-force f_lift_j_i
  :name "lift_j_i"
  :point1 cmp_j_i
  :direction -[bl_jz]
  :magnitude "@lift_j_i")
```

6.5.7 Drag Force

The drag coefficient C_d is proportional to the angle of attack α [98], [140], [141]:

$$C_d = d_0 + d_1\alpha + d_2\alpha^2 \quad (6.22)$$

where $d_0 = 0.087$, $d_1 = -0.021$ and $d_2 = 0.400$ as in [140].

The drag coefficient is modelled in `VehicleSim` as:

```
(setsym cd_j_i "delta0+delta1*@alpha_j_i+delta2*@alpha_j_i**2")
```

and the numerical parameters `delta0`, `delta1` and `delta2` are defined at the beginning of the program with the above mentioned values.

Taking into account equation (6.5) and (6.13), the drag force magnitude can be expressed in `VehicleSim`:

```
(setsym drag_j_i "cte*@ro_air*((ctecl*(@wrotor*(y_i+eR))**2)+
(ctvids*(@wrotor*(y_i+eR))**2)+(ctehv*(@wrotor*(y_i+eR))**2)+
(ctefw*@ut_i**2))*chord*@cd_j_i*dy_i")
```

where `cte`, `@ro_air`, `@wrotor`, `chord`, are defined as in the previous section. `y_i` represent the different points on the main rotor blades where the drag forces are applied to (see Figure 6.14) and `dy_i` are the differential length intervals in which the differential drag forces are split (see Figure 6.14).

The command `add-line-force` introduces the drag forces on the main rotor blades.

```
(add-line-force f_drag-j_i
  :name "drag-j_i"
  :point1 cmp-j_i
  :direction [bl-jx]
  :magnitude "@drag-j_i")
```

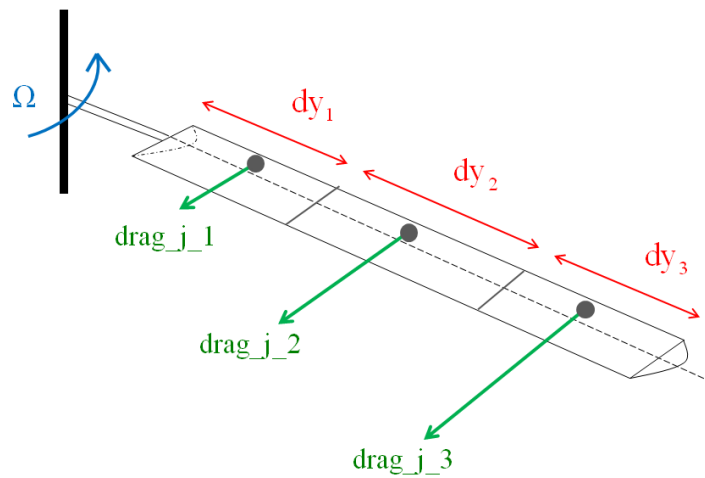


Figure 6.14: Drag force representation for a main rotor blade.

6.5.8 Thrust Coefficients

In this section, thrust coefficients in hover and forward flight are modelled. They provide aerodynamic information used to calculate other relevant parameters such as the feather angle, etc.

Hover Flight

The thrust coefficient approximation for hover flight can be written as [145]:

$$C_T = \frac{1}{2} \sigma a \left[\frac{1}{3} \theta - \frac{1}{2} \lambda \right] \quad (6.23)$$

θ is the feather angle, a is the lift slope, $\lambda = v_{ih}/\Omega R$, v_{ih} is the induced hover velocity, R is the rotor radius and σ is the solidity factor which for a constant blade chord is given by:

$$\sigma = \frac{Nc}{\pi R} \quad (6.24)$$

N is the number of main rotor blades and c is the blade chord.

The solidity factor, σ , is implemented in VehicleSim as a variable:

```
(setsym solifc "(nblades*chord)/(@pi*Rt)")
```

`nblades` is the number of blades and the rest of variables have been defined before.

The thrust coefficient is now modelled as:

```
(setsym Ct_j "cte*@solifc*2*@pi*(((1/3)*rq(pj-j))-cte*(@vih/
(omega*Rt34))))")
```

`Rt34` is the rotor radius calculated as $0.75 \cdot Rt$ i.e., at three quarters of the radius value. This distance is usually used as reference, because modern blades have a negative degree of twist, decreasing the feather angle towards the tip [145]. The rest of variables have been defined previously.

Forward Flight Conditions

The thrust coefficient in forward flight is given by [145]:

$$C_T = \frac{1}{2} \sigma a \left[\frac{1}{3} \theta_0 \left(1 + \frac{3\mu^2}{2} \right) - \frac{1}{2} \lambda \right] \quad (6.25)$$

This is the simplest expression for the lift coefficient of a rotor in forward level flight. This equation is valid if the value of θ is taken to be that at three quarters of the radius.

The variables involved in this equation are calculated at three quarters of the radius. By using blade element theory in forward flight, the variables involved in the thrust coefficient can be modelled.

Taking into account equations (6.7), (6.8) and (6.10) at $0.75Rt$, the inflow factor can now be calculated at three quarters of the radius:

```
(setsym lambda34 "mu*sin(gamma)+@ld_ifw34")
```

where the variable @ld_ifw34 is given as:

```
(setsym ld_ifw34 "(Kfw*@vih)/(omega*Rt34)")
```

U_T and U_P are implemented as the variables @ut34 and @up34 respectively:

```
(setsym ut34 "(omega*Rt34)+(omega*Rt34*mu*sin(@wrotor*t))")
(setsym up34 "@wrotor*Rt34*@lambda34+(@wrotor*Rt34*mu*cos(@wrotor*t)*
rq(fj-j))+(Rt34*dxdt(rq(fj-j)))")
```

The angle of attack is given by (6.11) and is modelled as the variable @alp34:

```
(setsym alp34 "rq(pj_j)-(@up34/@ut34)")
```

Therefore, taking into account equation (6.25), the thrust coefficient in forward flight is:

```
(setsym Ctfw "cte*@solifc*2*pi*((1/3)*fo*(1+((3*mu**2)/2))-
(cte*@lambda34))")
```

fo is the collective feather angle and mu is the advance ratio. The rest of variables have already been defined.

6.5.9 Climb Angle

Blade element theory can be used to estimate the collective feather increase required for climb [140].

$$\Delta\theta = \frac{3}{2} \frac{V + v - v_h}{\Omega R} \quad (6.26)$$

V is the climb speed, v is the induced climb speed and v_h in the hover speed.

The climb angle is modelled in VehicleSim as:

```
(setsym dthetacl "(3/2)*((@vc+@viclmb-@vih)/(omega*Rt))")
```

6.6 Tail Rotor Aerodynamic Modelling

6.6.1 Blade Angle of Incidence for Hover, Climb, Descent and Forward Flight

The aerodynamic forces acting on a blade segment at a given azimuth position on the tail rotor disc are calculated using blade element theory. The local angle of attack α , depends on the instantaneous conditions of blade profiles' airflow along the rotor radius [74]:

$$\alpha = \theta - \arctan\left(\frac{V_{out}}{V_{in}}\right) \quad (6.27)$$

θ is the tail rotor blade feather angle, V_{out} and V_{in} are the components of the blade profile airflow: out of plane and in plane of tail rotor disc, respectively.

Hover Flight Conditions

The induced velocity on the tail rotor in hovering flight is given by [73]:

$$V_{i0} = \sqrt{\frac{F}{2\rho S}} \quad (6.28)$$

F is the tail rotor lift force in hovering, S is the tail rotor disc area and ρ is the air density in the flight level.

The angle of incidence is given by:

$$\alpha = \theta - \arctan\left(\frac{V_{i0}}{\Omega r}\right) \quad (6.29)$$

θ is the blade feather angle, Ω is the tail rotor angular speed and r is the corresponding length on the tail rotor where the aerodynamic load is applied.

Taking into account the previous equations, the angle of incidence on the tail for hover conditions is implemented. First, the induced velocity in hovering flight is modelled as in equation (6.28):

```
(setsym vih.tl "sqrt(((mf+mb11+mb12+mb13+mb14+mb1.tl1+mb1.tl2)*g)/
(2*@ro_air*@pi*R.tl**2)))")
```

where R_{tl} is the tail rotor radius, the rest of variables have been defined before.

Then, using equation (6.29), the angle of incidence is implemented as:

```
(setsym alphas1_p_i "rq(pj_tl_p)-arctg(@vih_tl/((k_rt_tl*omega)*zt_i))")
```

where $p = 1, 2$ and $i = 1, \dots, 3$, $rq(pj_tl_p)$ is the blade feather angle and zt_i is the distance along the Z axis of the tail rotor blade.

Climb Flight Conditions

Similarly, by using blade element theory, the angle of incidence in climb can be modelled.

In this case, the velocity in climb flight is:

```
(setsym vc_tl "cteclimb*(Kclimb*@vih_tl)")
```

where $cteclimb$ is a boolean variable, its function was explained previously. $Kclimb$ is a constant value that will be defined by the climb velocity. Finally, $@vih_tl$ is the induced hover velocity mentioned before.

The angle of incidence in climb conditions is modelled in VehicleSim as:

```
(setsym alptlc_p_i "rq(pj_tl_j)-arctg(@vc_tl/((k_rt_tl*omega)*zt_i))")
```

Descent Flight Conditions

The velocity in descent flight can be implemented as:

```
(setsym vides_tl "ctevid*(kdes*@vih_tl)")
```

where $ctevid$ is a boolean variable. $kdes$ is a constant value that will be defined by the descent velocity. Finally, $@vih_tl$ is the induced hover velocity was explained previously.

The angle of incidence in descent flight is given by:

```
(setsym alptld_p_i "rq(pj_tl_j)-arctg(@vides_tl/((k_rt_tl*omega)*zt_i))")
```

Forward Flight Conditions

In forward flight, the velocity components on the blade element are periodic, vary with the azimuth position of the blade, ψ . Taking into account [73], the air speed's tangential component U_T , is written as:

$$U_T = \Omega r + V_0 \sin \psi \quad (6.30)$$

r is the length of the tail rotor blade where the aerodynamic force is considered, V_0 is the helicopter velocity with respect to the air. Considering [73], the air speed's perpendicular component U_P is given by:

$$U_P = (r - e) \dot{\beta} + (V_0 \cos \psi) \beta + V_i \quad (6.31)$$

V_i is the induced velocity in forward flight.

The angle of incidence can be obtained as:

$$\alpha = \theta - \frac{U_P}{U_T} \quad (6.32)$$

As in equation (6.30), U_T is modelled as:

```
(setsym ut_tl_p_i "((k_rt_tl*omega)*zt_i)+(omega*Rt*mu*sin((k_rt_tl*
@wrotor)*t))")
```

and U_P is:

```
(setsym up_tl_p_i "@vifw+(@wrotor*Rt*mu*cos((k_rt_tl*@wrotor)*t)*
rq(fj_tl_p))+zt_i*dxdt(rq(fj_tl_p))")
```

Finally, the angle of incidence is modelled as:

```
(setsym alptlfw_p_i "rq(pj_tl_p)-(@up_tl_p_i/@ut_tl_i)")
```

6.6.2 Tail Rotor Lift Force

The lift coefficient in hover, climb, descent and forward flight can be written respectively as:

```
(setsym cltl_p_i "2*@pi*@alphaltl_p_i")
```

```
(setsym cltlc_p_i "2*@pi*@alptlc_p_i")
```

```
(setsym cltld_p_i "2*@pi*@alptld_p_i")
```

```
(setsym cltlfw_p_i "2*@pi*@alptlfw_p_i")
```

The resultant lift force per unit span on the tail blade element in forward flight is [144]:

$$L = \frac{1}{2} U_T^2 c C_l \left(\theta - \frac{U_P}{U_T} \right) dr \quad (6.33)$$

being the expressions for hover, climb and descent analogous to the expression used in the main rotor. As a result, the lift force on the tail rotor can be modelled as:

```
(setsym lf_tl_p_i "cte*@ro_air*((ctecl*((k_rt_tl*@wrotor*zt_i)**2)*
@cltlc_p_i)+(ctvids*((k_rt_tl*@wrotor*zt_i)**2)*@cltld_p_i)+
(ctehv*((k_rt_tl*@wrotor*zt_i)**2)*@cltl_p_i)+
(ctefw*(@ut_tl_p**2)*@cltlfw_p_i))*chordt*dz_i")
```

where `chordt` is the chord of the tail rotor blade and `zt_i` are the different points on the tail rotor blades where the lift forces are applied to. Finally, `dz_i` are the differential length intervals in which the differential lift forces are divided.

Various points in the helicopter's nominal configuration are defined to allow the modelling of the lift force, these are defined on the body `n`:

```
(add-point cmptl_p_i :body n :coordinates ("-xt ± xt_i" -yt "-ht ± zt_i"))
```

where `p = 1, 2` (tail rotor number of blades) and `i = 1, ..., 3` (points on the tail rotor blades where the aerodynamic load are applied).

The points `cmt_p_i` define the centre of pressure which are points on the tail rotor blades.

```
(add-point cmt_p_i :body bl_tl_p :coordinates cmptl_p_i)
```

The command `add-line-force` introduces the lift forces in the model:

```
(add-line-force f_lift_tl_p_i
:name "lift_tl_p_i")
```

```

:point1 cmt_p_i
:direction [bl_tl_py]
:magnitude "@lf_tl_p_i")

```

6.6.3 Tail Rotor Thrust Coefficient

The tail rotor thrust coefficient is calculated once some previous coefficients are introduced and calculated:

$$s = \frac{bc}{\pi R} \quad (6.34)$$

being s the solidity, b the tail rotor number of blade, c is the chord of the tail rotor blade and R is the tail rotor radius. In addition to this, the thrust coefficient can be written as:

$$t_{cD} = \frac{a}{4} \left[\frac{2}{3} \theta_0 \frac{1 - \mu^2 + 9\mu^4/4}{1 + 3\mu^2/2} + \lambda_D \frac{1 - \mu^2/2}{1 + 3\mu^2/2} \right] \quad (6.35)$$

The H-force coefficient can also be written as:

$$h_{cD} = \frac{1}{4} \mu \delta + \frac{a\mu\lambda_D}{4} \left[\frac{(\theta_0/3)(1 - 9\mu^2)}{1 + 3\mu^2/2} + \frac{\lambda_D}{1 + 3\mu^2/2} \right] \quad (6.36)$$

The torque coefficient is:

$$q_c = \frac{\delta(1 + 3\mu^2)}{8} - \lambda_D t_{cD} - \mu h_{cD} \quad (6.37)$$

So, the rotor torque is calculated as:

$$Q = q_c \rho s A \Omega^2 R^3 \quad (6.38)$$

The tail rotor thrust is [141]:

$$T_t = \frac{Q}{l_t R} \quad (6.39)$$

where $l_t R$ is the distance from the tail rotor to the helicopter's centre of gravity.

Finally, the thrust coefficient based on disc area is [72]:

$$C_t = \frac{T}{\pi R^2 \rho (\Omega R)^2} \quad (6.40)$$

Taking into account the previous expressions, the tail rotor thrust coefficient can be modelled in VehicleSim as:

```
(setsym lambda_D "mu*sin(gamma)-@lbda_ifw")

(setsym solif_tl "(nblades_tl*chordt)/(@pi*R_tl)")

(setsym tcd "((2*@pi)/4)*((2/3)*fo*((1-(mu**2)+(9*mu**4))/4)/
(1+(3*(mu**2))/2))+@lambda_D*((1-(mu**2)/2)/(1+(3*(mu**2))/2)))")
```

μ is the advance ratio.

```
(setsym hcd "((1/4)*mu*@cd_34fw+((2*@pi*@lambda_D)/4)*(((fo/3)*
(1-(9*(mu**2))/2))/(1+(3*(mu**2))/2))+(@lambda_D/(1+(3*mu**2)/2))))")
```

$@cd_34fw$ is the drag coefficient calculated at $0.75 * R_{tl}$ and it is given by:

```
(setsym cd_34fw "delta0+delta1*@alp34+delta2*@alp34**2")
```

and $@alp34$ is the tail rotor blade's angle of incidence, and it is implemented as:

```
(setsym alp34 "rq(pj_j)-atan(@up34/@ut34)")

(setsym qc "(@cd_34fw*(1+(3*(mu**2))))/8)-(@lambda_D*@tcd)-(mu*@hcd)")

(setsym Q "@qc*@ro_air*@solifc*(@pi*(Rt**2))*(@wrotor**2)*(Rt**3)")
```

```
(setsym Tt "@Q/(xt+xf_s)")
```

$xt+xf_s$ is the tail rotor's distance from the helicopter's centre of mass:

```
(setsym Cttail "@Tt/((@pi*(R_tl**2))*@ro_air*((k_rt_tl*omega)*R_tl)**2)")
```

$@Cttail$ is the VehicleSim variable implemented to model the tail rotor thrust coefficient.

6.7 Flight Control

As a consequence of the aerodynamic load action on the helicopter, various controllers on the rotational and the translational degrees of freedom must be implemented. So that at all the times a stable trajectory can be achieved. Aerodynamic forces and loads

do have an impact on the vehicle's trajectory and therefore there exist a clear need for paying special attention to the flight control aspects. This is a fundamental step in the aerodynamic model here presented.

6.7.1 Longitudinal Position Control

In order to control the helicopter's position and displacement on the X axis, some means of control need to be implemented. The longitudinal position of the helicopter is implemented by first defining the following variables:

```
(setsym x_long "dir(cross([fuselagey],[nz]))")
(setsym xheli "dot(pos(fuselage0,n0),@x_long)")
```

The first line, defines the longitudinal direction of the fuselage. The second line finds the fuselage longitudinal position in the direction of `@x_long`.

The helicopter speed in forward flight is implemented as:

```
(setsym v_heli "(mu*Rt*@wrotor)/cos((ktray1*gamma)+(ktray2*@phi_fusey))")
```

where `mu` is the advance ratio and the rest of variables have been defined before.

```
(setsym xref "x_ref+@v_heli*t")
```

The variable `xref` is added to represent the longitudinal trajectory prescription for the fuselage's longitudinal position. It provides the reference value for the longitudinal position; it allows to describe the trajectory in the space. `gamma` is the flight path angle and its numerical value is defined at the beginning of the program.

```
(setsym xerror "@xref-@xheli")
(add-state-variable xfutq xfutqp "F")
(set-aux-state-deriv xfutqp "kix*@xerror")
```

The command `add-state-variable` introduces a state variable for the force expressions used to control the helicopter's longitudinal position. The integral part of the force is defined by the command `set-aux-state-deriv` and it uses the value of the variable `@xerror` defined as the difference between the actual and prescribed longitudinal positions.

```
(add-line-force xcon
  :name "xctrl"
  :direction [fuselagex]
  :point1 fuselage0
  :point2 n0
  :magnitude "xfutq+kpx*(@xerror)+kdx*dxdt(@xerror)")
```

The force is applied between the fuselage (centre of the fuselage `fuselage0`) and the inertial frame. The controller uses the variable `@xerror` as the input variable and the output is the force applied to the fuselage so a desired longitudinal position control is achieved. The parameters `kix`, `kpx` and `kdx` are the gains of the controller that is of PID type.

The lateral position control is modelled similarly to the controller explained in Chapter 5 and therefore it is not included in this report.

6.7.2 Vertical Position Control

In order to control the position of the helicopter on the Z axis, a new controller needs to be implemented. In a similar way to the longitudinal position control defined before, the vertical position of the helicopter is calculated after defining two necessary variables:

```
(setsym z_long "dir(cross([fuselagex],[ny]))")
(setsym hheli "dot(pos(fuselage0,n0),@z_long)")
```

The first line, defines the vertical direction of the fuselage, `@z_long`. The last one finds the fuselage's vertical position, `@hheli`, this is, the height.

The helicopter's velocities in climb and descent flight are modelled as:

```
(setsym vcc "(ctecl*@vc)+(ctvids*@vdes)")
```

where `ctecl`, `ctvids` are boolean variables defining the helicopter's ascending `@vc` or descending `@vdes` velocities, respectively.

```
(setsym href "-height-@vcc*t")
```

The variable `@href` is added as the helicopter's vertical trajectory prescribed for the vertical position.

```
(setsym herror "@href-@hheli")
(add-state-variable hfu_tq hfu_tqp "F")
(set-aux-state-deriv hfu_tqp "kih*@herror")
```

The command `add-state-variable` introduces a state variable, for the force expression is used to control the vertical position. The integral part of the force is defined by the `set-aux-state-deriv` command and uses the value of the `@herror` defined before.

```
(add-line-force hcon
      :name "hctrl"
      :direction -[fuselagez]
      :point1 fuselage0
      :point2 n0
      :magnitude "hfu_tq+kph*(@herror)+kdh*dxdt(@herror)")
```

The force is applied between the fuselage and the inertia frame. The controller uses the variable `@herror` as the input variable and the output is the force applied to the fuselage so the desired vertical position is achieved. The parameters `kih`, `kph` and `kdh` are the controller's gains.

Fuselage's Yaw Control

In order to control the helicopter's yaw, a new controller needs to be added. The yaw angle is obtained as the first rotational coordinate of the fuselage:

```
(setsym phi_fusez "rq(fuselage,1)")
```

The sideslip angle in forward flight is [72]:

$$\eta_t = \tan^{-1} \left(\tan\eta - \frac{rl_t}{V\cos\eta} \right) \quad (6.41)$$

where η is the sideslip angle (angle between plane of symmetry and flight path). V is forward velocity, r is the yaw speed and l_t is the distance of the tail rotor from the centre of the fuselage (see Figure 6.15).

The variable `@phi_refz` is defined as the fuselage's yaw reference value. This is an equation that allows to describe a yaw helicopter trajectory in the space. It is implemented in `VehicleSim` as:

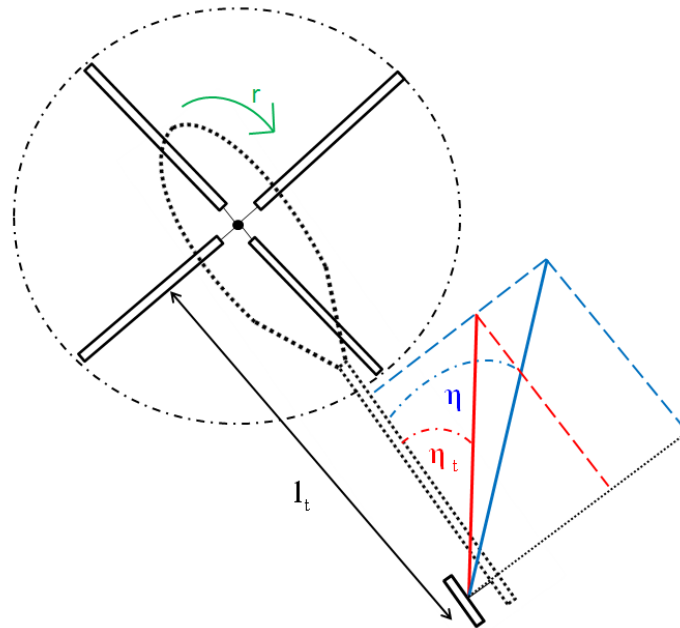


Figure 6.15: Sketch showing the tail rotor's configuration geometry. This figure is plotted by the author and based on [72].

```
(setsym phi_refz "(ctehv*fusz_ref)+(ctecl*fusz_ref)+(ctvids*fusz_ref)+
(ctefw*(atan(tan(fusz_ref)-((ryaw*xt)/(@vtail*cos(fusz_ref))))))")
```

the parameter `fusz_ref` is the fuselage yaw reference for hover, climb and descent. Its numerical value is defined at the beginning of the program. `ctehv`, `ctecl`, `ctvids` and `ctefw` are boolean variables for allowing the user to choose between hover, climb, descent and forward flight conditions, respectively. As it can be seen, forward flight yaw control is modelled using equation (6.41), being `ryaw` the fuselage's yaw speed in this flight condition. In addition to this, the variable `@vtail` needs to be modelled:

```
(setsym vtail "(mu*Rt*omega)/cos((ktray1*gamma)+(ktray2*@phi_fusey))")
```

A variable `@phi_refz` will be defined as the reference value for the fuselage's yaw. This variable allows to describe the helicopter's yaw trajectory in the space.

```
(setsym phi_errorz "@phi_refz-@phi_fusez")
(add-state-variable fusez_tq fusez_tqp "F*L")
(set-aux-state-deriv fusez_tqp "kifsz*@phi_errorz")
```

The `add-state-variable` command introduces a state variable for the torque expression that it is used to control the helicopter's yaw. The integral part of the torque is defined with the `set-aux-state-deriv` command and uses the value of the `@phi_errorz` defined above. The variable `@phi_errorz` is the difference between the fuselage's actual and desired yaw position.

```
(add-moment fsz_phi
  :name "phi_ctrlz"
  :direction -[fuselagez]
  :body1 fuselage
  :body2 n
  :magnitude "fusez_tq+kpfsz*(@phi_errorz)+kdfsz*dxdt(@phi_errorz)")
```

The moment is applied between the fuselage and the inertia frame. The controller uses the variable `@phierrorz` as the input variable, and the output is the moment applied to the fuselage, so satisfactory yaw control is achieved. The parameters `kifsz`, `kpfsz` and `kdfsz` are the controller's gains.

6.7.3 Tail Rotor Flap Control

In order to control the tail rotor blade's flap under the effect of the delta three angle, some previous considerations should be considered.

The coning angle is reduced for a given collective feather angle as indicated in [144]:

$$a_0 = \frac{\Gamma (\theta_0 - \frac{4}{3}\lambda)}{8 + \Gamma \tan \delta_3} \quad (6.42)$$

In addition to this, the flap coefficients a_1 and b_1 can be written as indicated in [147]:

$$a_1 = \frac{q}{\Omega} \frac{(\frac{16}{\Gamma} - K)}{1 + K^2} \quad (6.43)$$

$$b_1 = -\frac{q(1 + K\frac{16}{\Gamma})}{\Omega(1 + K^2)} \quad (6.44)$$

where $K = \tan \delta_3$, q is the component of the rotor axis tilt rate in the feather plane of the rotor, and Γ is given by:

$$\Gamma = \frac{c\rho a R^4}{I_f} \quad (6.45)$$

being the mass (inertia) constant of the blade to zero flap hinge offset.

Taking into account the previous considerations about the delta three angle, the tail rotor blade's flap motion can be modelled now:

```
(setsym gamma_tl "(@rho_air*(2*pi)*chordt**(R_tl**4))/Iblx_tl")
```

where `Iblx_tl` is the moment of inertia about the flap axis.

The flap harmonics can be modelled using the previous equations:

```
(setsym a0 "(@gamma_tl*(fo_tl-((4/3)*@lbdairfw)))/(8+@gamma_tl*
tan(delta3_tl))")
```

```
(setsym a1 "(alpha_tp/(k_rt_tl*omega))*(((16/@gamma_tl)-tan(delta3_tl))/
(1+((tan(delta3_tl)**2))))")
```

```
(setsym b1 "-(alpha_tp*(1+tan(delta3_tl)*(16/@gamma_tl)))/
((k_rt_tl*omega)*(1+((tan(delta3_tl)**2))))")
```

`fo_tl` is the tail rotor collective feather and `alpha_tp` is the tail plane incidence setting its numerical values at the beginning of the program.

6.8 Chapter Summary

This chapter provides a description of the modelling process when there exist external forces on the helicopter model described in Chapter 5. The first step taken, was to consider the aerodynamic environment. In here, the forces acting on a helicopter were described as well as the rotor blades angles i.e., angle of incidence and angle of attack. In addition to this, blade element theory in hover, axial and forward flight was applied.

Gravity and its effect was the first external force to be included in the model. Implementation of the ground on the fuselage in absence of aerodynamic loads has been considered. Once the gravity force was added to the existing model, the main rotor tilt was modelled as well. A main rotor local axis was defined in terms of the inertial

reference axes with respect to the fuselage.

Other external perturbation was as well modelled in absence of aerodynamic load; a change on the main rotor's angular speed following some specific demand. As a result, three frequencies were defined and an acceleration was also provided. A PID controller was implemented in order to change the main rotor angular speed.

The aerodynamic modelling process has been described in detail, first on the main rotor and after that on the tail rotor. The air density has an influence on the aerodynamic equations, it was modelled by taking into account the entire height range reached by helicopters during flight. The induced hover speed was described and implemented, as a consequence of this, climb, descent and forward speeds were also obtained. Additionally, induced climb, descent and forward speed were provided using the induced hover speed.

Once the speeds and the induced speeds were modelled, the blade's angle of incidence was modelled in hover, climb, descent and forward flight separately. This allowed to obtain the lift and the drag forces on the main rotor blades. The thrust coefficients in hover and forward flight were also included in the model. On the other hand, the collective feather increase required in climb was calculated.

The tail rotor aerodynamic model was implemented too, the blade's incidence angles for hover, climb, descent and forward flight were modelled. Given that, the lift force on the tail could then be modelled. The tail rotor thrust coefficient was analyzed and also included in the model.

The flight control methodology was described, this a fundamental task in order to achieve prescribed trajectories. Longitudinal, vertical positions control and fuselage yaw control were implemented using PID controllers. Finally, the tail rotor flap control was modelled.

As it can be seen, this chapter contains a comprehensive and details model of the aerodynamical load and its effects on the helicopter system.

For the modelling process, previous existing theoretical approaches have been considered and adequately referenced along the chapter.

Part III

Results

Chapter 7

Sikorsky Model in Absence of External Perturbations

This chapter is aimed at furthering the understanding of the dynamic behaviour of a helicopter in vacuum and without gravity. The effect of each property is individually analyzed by assuming that the nominal helicopter configuration is the one described in Chapter 5. The analysis is done purely through simulations and validated by comparing the results with existing theory. The equations of motion are obtained for flap, lag, flap-lag coupled and feather dynamics. A blade dynamic analysis is carried out, the fuselage and its interaction with the main rotor as well as the tail rotor are also studied. After that, main and tail rotors' angular speeds are introduced/implemented by using the torques on the rotors. The six degrees of freedom of the helicopter and their stability are studied. Finally, the vibrations appearing on the fuselage are studied; structural unbalances are generated on the main and tail rotors respectively for this purpose.

7.1 VehicleSim Equations of Motion

Once the model has been built, the symbolic multibody software VehicleSim derives the linear and nonlinear equations of motion for the dynamics involved in the system as well as the time series representing the nonlinear behaviour. In order to validate the model, the results here presented will be compared to those predicted by the theory and

experimental tests. Initially, the results for the case of uncoupled flap and lag degrees of freedom are presented. After that, both of them will be studied simultaneously and their coupling will be analysed and compared to existing theoretical knowledge. Finally, feather equations are also provided and analysed. It is convenient to remind at this point that the case under study is for rigid blades, being flexibility and torsion two properties not considered at present in this work.

7.1.1 Flap Dynamical Equations

Flap is the first degree of freedom of the blade under consideration. In order to model the flap mode, a spring is included in the flap hinge, it creates a restoring moment on the blade. If the spring stiffness is zero, the flap natural frequency is equal to the angular frequency of the main rotor. The flap offset is the distance existing between the rotor hub and the flap hinge. It is provided as a percentage $e\%$ of the radius R of the blade. Once the blade (flap) model is built, simulations are carried out with VehicleSim in order to generate the linear and nonlinear equations. This same program script can then be used to study the behaviour of the system under several conditions as external forces.

One of the most comprehensive surveys on rotor dynamics is proposed by [141], here the flap motion is represented by a second order differential equation of the form:

$$B\ddot{\beta} + \Omega^2 (B\cos\beta + M_b e x_g R^2) \sin\beta = M_A \quad (7.1)$$

B is the moment of the inertia around the flap axis, M_A is the aerodynamic moment and M_b is the blade mass. In this reference, the position vector of the blade c.g (centre of gravity) is $r_g = x_g R$. In our system, the c.g of the blade is considered to lie on the longitudinal axis, so it can be written as $r_g = y_g$. The equations are obtained by using the term eR instead of eR^2 . Approximations for small angles, $\cos\beta \cong 1$ and $\sin\beta \cong \beta$ can be applied to equation (7.1). Thus, it can be written as:

$$B\ddot{\beta} + \Omega^2 (B + M_b e x_g R^2) \beta = M_A \quad (7.2)$$

VehicleSim Linear Flap Equation

The flap dynamics linear equation is obtained by using the appropriate Lisp code commands in VehicleSim, the application of such a linearization provides the equation:

$$\ddot{\beta} (I_{blx} + m_{bl}y_{bl}^2) = -m_{bl}\Omega^2 y_{bl} (eR + y_{bl}) \beta - \Omega^2 (I_{blz} - I_{bly}) \beta \quad (7.3)$$

A simple comparison between equations (7.2) and (7.3) can be done. Similarities between both equations are found. The moment of inertia around the blade's flap axis, is given by $I_{blx} + m_{bl}y_{bl}^2$. If a plane figure is considered, then, $I_z = I_x + I_y$ and equation (7.3) can be now written as:

$$\ddot{\beta} (I_{blx} + m_{bl}y_{bl}^2) = -\Omega^2 (I_{blx} + m_{bl}y_{bl}^2 + m_{bl}eRy_{bl}) \beta \quad (7.4)$$

It is clear to see that both equations (7.2) and (7.4) are similar except for the presence of aerodynamical moments as in this section they are not considered.

When the model has a spring fitted in the flap hinge it generates a restoring moment on the blade. VehicleSim equation obtained in this case yield the following expression which contains the restoring moment:

$$\ddot{\beta} (I_{blx} + m_{bl}y_{bl}^2) = -m_{bl}\Omega^2 y_{bl} (eR + y_{bl}) \beta - \Omega^2 (I_{blz} - I_{bly}) \beta - k_{fj} \beta \quad (7.5)$$

being k_{fj} the spring stiffness coefficient.

From equation (7.5), the blade's flap frequency can be obtained as:

$$\nu = \sqrt{\frac{\Omega^2 [eRm_{bl}y_{bl} + m_{bl}y_{bl}^2 + (I_{blz} - I_{bly})] + k_{fj}}{(I_{blx} + m_{bl}y_{bl}^2)}} \quad (7.6)$$

which is $\nu = 48.856$ rad/s if the parameters involved in this expression, Ω , eR , m_{bl} , y_{bl} amongst others, are substituted by the corresponding numerical values of a real Sikorsky model.

If a simulation is carried out for a blade with pure flap degree of freedom for 50 s with an initial flap angle, $\beta_0 = 0.0175$ rad, the VehicleSim obtained flap mode frequency is 7.78 Hz or (48.88 rad/s), this value was calculated using a FFT (Fast Fourier Transform) Matlab algorithm. This frequency is near to the angular frequency of the rotor, as it was expected following theoretical predictions [148]. The value of the frequency is now

slightly higher as the offset and the spring stiffness increase it. These effects will be analysed in the next sections.

VehicleSim NonLinear Flap Equation

In the nonlinear case, VehicleSim can also derive the equations of motion. The nonlinear equation for the flap dynamics is generated by stating the corresponding Lisp code commands. Two cases are presented in here, with and without spring in the flap hinge.

- NonLinear Flap Equation without Spring Stiffness

$$\ddot{\beta} (I_{blx} + m_{bl}y_{bl}^2) = -eRm_{bl}y_{bl}\Omega^2 \sin\beta - m_{bl}y_{bl}^2\Omega^2 \cos\beta \sin\beta - (I_{blz} - I_{bly}) \Omega^2 \cos\beta \sin\beta \quad (7.7)$$

If a comparison between equations (7.1) and (7.7) is made, similarities between them are observed. Taking into account the previous considerations about the centre of gravity, plane blade amongst others, equation (7.7) now is:

$$\ddot{\beta} (I_{blx} + m_{bl}y_{bl}^2) = -\Omega^2 ((I_{blx} + m_{bl}y_{bl}^2) \cos\beta + m_{bl}eRy_{bl}) \sin\beta \quad (7.8)$$

It is seen that equation (7.1) and equation (7.8) are equal if $M_A = 0$.

- NonLinear Flap Equation with Spring Stiffness

VehicleSim provides the following equation that contains the term corresponding to the spring force.

$$\ddot{\beta} (I_{blx} + m_{bl}y_{bl}^2) = -eRm_{bl}y_{bl}\Omega^2 \sin\beta - m_{bl}y_{bl}^2\Omega^2 \cos\beta \sin\beta - (I_{blz} - I_{bly}) \Omega^2 \cos\beta \sin\beta - k_{fj}\beta \quad (7.9)$$

The nonlinear equation (7.9) has been validated by using a Lagrangian approach and this derivation is included in Appendix A.

7.1.2 Lag Dynamical Equations

In this section, the author analyzes pure lag motion and validates the obtained results. This is, the lag equations of motion in the absence of a flap hinge are obtained by using

VehicleSim Lisp and compared to those available in the literature. In order to validate the equations obtained by VehicleSim, the following accepted expression for pure lag motion is taken into consideration [141]:

$$C\ddot{\xi} + M_b e x_g \Omega^2 R^2 \sin \xi = N \quad (7.10)$$

where C is the moment of the inertia about the lag axis, N is the aerodynamic lag moment and M_b is the blade mass. Now, if small angles approximation is taken, then equation (7.10) can be simplified to:

$$\ddot{\xi} + \Omega^2 \epsilon \xi = N/C \quad (7.11)$$

where ϵ is $M_b e x_g R^2 / C$ and eR is the corresponding lag hinge offset distance.

VehicleSim Linear Lag Equation

The linear equation for the lag is generated by using corresponding commands in Lisp code. The application yields the following expression:

$$\ddot{\xi} (I_{blz} + m_{bl} y_{bl}^2) + e R m_{bl} \Omega^2 y_{bl} \xi = 0 \quad (7.12)$$

Now, equation (7.11) is compared to equation (7.12). The previous considerations about the c.g and the null value for the aerodynamic lag moment and the moment of the inertia around the lag axis (C) being equal to $I_{blz} + m_{bl} y_{bl}^2$ need to be taken into account. It is clear to see that equations (7.11) and (7.12) are equivalent.

By now, equation (7.12) does not have any spring stiffness or damping coefficient included. In the total moment calculation, a spring is included in order to get the equilibrium moment about the lag hinge [140]. Moreover, a damper is also used in the lag hinge, because when the aerodynamic forces are considered, their damping is usually not enough to allow the lag motion and the blade can be under the effect of unwanted stress forces [144].

- Linear Lag Equation with Spring Stiffness and Damping Coefficient

If these are included in the system, the VehicleSim equation of motion is as follows:

$$\ddot{\xi} (I_{blz} + m_{bl}y_{bl}^2) = -eRm_{bl}\Omega^2y_{bl}\xi - d_{lj}\dot{\xi} - k_{lj}\xi \quad (7.13)$$

From the above expression, the blade's lag mode frequency is obtained:

$$\nu = \sqrt{\frac{eRm_{bl}y_{bl}\Omega^2 + k_{lj}}{(I_{blz} + m_{bl}y_{bl}^2)}} \quad (7.14)$$

By substituting the parameters' values involved in equation (7.14) from the Sikorsky model, it is shown that the lag mode frequency is 5.63 Hz or (35.38 rad/s).

VehicleSim NonLinear Lag Equation

For the nonlinear lag case, the equations can be obtained by using VehicleSim:

- NonLinear Lag Equation without Spring Stiffness and without Damping Coefficient

$$\ddot{\xi} (I_{blz} + m_{bl}y_{bl}^2) + eRm_{bl}\Omega^2y_{bl}\sin\xi = 0 \quad (7.15)$$

A comparison between equation (7.10) (theoretical prediction) and equation (7.15) is performed. Taking into account the previous considerations for the c.g, the aerodynamic lag moment and the moment of the inertia around the lag axis, it is seen how this two expressions are equivalent. Equation (7.15) is validated in this way.

- NonLinear Lag Equation with Spring Stiffness and with Damping Coefficient

If now both a spring and a damper are included in the model, the VehicleSim nonlinear equation of motion is given by:

$$\ddot{\xi} (I_{blz} + m_{bl}y_{bl}^2) = -eRm_{bl}\Omega^2y_{bl}\sin\xi - d_{lj}\dot{\xi} - k_{lj}\xi \quad (7.16)$$

where d_{lj} and k_{lj} are the damping coefficient and spring stiffness respectively.

The nonlinear equation (7.16) can be validated by using the Lagrangian Mechanic approach (see Appendix B for the mathematical derivation).

7.1.3 Feather Equations of Motion

The feather is the third degree of freedom allowed on the blade's motion. The feather motion can be described by the following equation [141]:

$$A\ddot{\theta} + A\Omega^2 \sin\theta \cos\theta = L \quad (7.17)$$

where θ is the feather angle, A is the moment of inertia on the longitudinal blade axis and L is the moment on the feather axis. In many cases, feather motion takes place only for small angles, so this can be simplified as:

$$\ddot{\theta} + \Omega^2\theta = L/A \quad (7.18)$$

VehicleSim Linear Feather Equation

Using VehicleSim to obtain the feather motion linear equation yields:

$$\ddot{\theta} (I_{bly} + m_{bl}x_{bl}^2) = ((I_{blx} - I_{blz}) - m_{bl}x_{bl}^2) \Omega^2\theta \quad (7.19)$$

Analogies between the equations (7.18) and (7.19) can be found. Taking into account that for a plane figure, the ratio $I_z = I_x + I_y$ is satisfied and that the moment about the feather axis is zero, equation (7.19) can be written as:

$$\ddot{\theta} (I_{bly} + m_{bl}x_{bl}^2) + (I_{bly} + m_{bl}x_{bl}^2) \Omega^2\theta = 0 \quad (7.20)$$

Equations (7.18) and (7.20) are similar with $A = (I_{bly} + m_{bl}x_{bl}^2)$.

VehicleSim NonLinear Feather Equation

The nonlinear equation for feather motion can be obtained with VehicleSim. This equation matches that proposed by [141] (see equation (7.17)):

$$\ddot{\theta} (I_{bly} + m_{bl}x_{bl}^2) = -m_{bl}\Omega^2 x_{bl}^2 \cos\theta \sin\theta + \Omega^2 (I_{blx} - I_{blz}) \cos\theta \sin\theta \quad (7.21)$$

Grouping terms and taking into account $I_{bly} = I_{blx} - I_{blz}$, the above equation becomes:

$$(I_{bly} + m_{bl}x_{bl}^2) \ddot{\theta} + (I_{bly} + m_{bl}x_{bl}^2) \Omega^2 \cos\theta \sin\theta = 0 \quad (7.22)$$

Equations (7.17) and (7.22) are shown to be similar, showing in this way the validity of the blade nonlinear model under study.

7.1.4 Coupled Equations of Flap and Lag

In most cases for articulated rotors, flap and lag hinges are mounted simultaneously on the rotor structure. These two degrees of freedom are coupled due to the existing Coriolis forces and the mathematical expression representing the respective motions can become quite complex and prone to errors if they were to be hand derived. The reader is reminded at this point that the aerodynamic forces are not considered in this work as the author wants to focus this study in the coupled dynamics in absence of gravity and air influence. It will be shown how the Coriolis effect introduces a coupling term between the blade flap (out of plane motion) and the lag motion (in plane). In a rotating frame of reference, inertial forces become relevant and cannot be neglected. On a rotor, Coriolis forces will appear whenever there exists a radial lengthening or shortening of the blade about the rotational axis, which is a result of the blade flap motion [98].

In a dynamic model, the forces acting on the blade for the flap motion are supported by the inertia acceleration, its expression is given by $\ddot{\beta}$. The centrifugal force is supported by the term $my\Omega^2$ and the Coriolis force appearing at the flap hinge corresponds to the term $2m\Omega\dot{\xi}$. Additionally, in the case of the lag motion, the forces are supported by the inertia acceleration as $\ddot{\xi}$. The centrifugal force, is given by the expression $my\Omega^2$ [98]. Finally, Coriolis inertia forces are represented by the term $2B\Omega\dot{\beta}\sin\beta$, where B is the moment of the inertia [141].

Small Order Equations for Flap/Lag Coupled Motion

The small order equations obtained in VehicleSim for the case when both flap and lag hinges are included in the blade's model are as follows:

Flap equation of motion:

$$\begin{aligned} \ddot{\beta} \left(I_{bly}\xi^2 + I_{blx} (1 - (1/2)\xi^2)^2 + m_{bl}y_{bl}^2 (1 - \xi^2) \right) &= -\Omega^2\beta (I_{blz} - I_{bly}) + \Omega\beta\dot{\xi} \\ (I_{bly} - I_{blz}) - (1 - (1/2)\xi^2) k_{fj}\beta - m_{bl}\Omega^2 y_{bl}\beta (eR + y_{bl}) - m_{bl}\Omega\beta y_{bl}^2 \dot{\xi} & \end{aligned} \quad (7.23)$$

Lag equation of motion:

$$\begin{aligned} \ddot{\xi} \left(I_{blz} + m_{bl}y_{bl}^2 / (I_{blx} + m_{bl}y_{bl}^2)^3 \right) &= I_{blz}\Omega\beta\dot{\beta} - m_{bl}\Omega^2 eR y_{bl}\xi + m_{bl}\Omega\dot{\beta} y_{bl}^2 \beta \\ -d_{lj}\dot{\xi} - k_{lj}\xi & \end{aligned} \quad (7.24)$$

It is clearly seen now how these equations are coupled, as the flap degree of freedom (β) and lag degree of freedom (ξ) depend on each other.

Non Small Order Equations for Flap/Lag Coupled Motion

Using the corresponding nonlinear set up of VehicleSim more complex expressions of both flap and lag degrees of freedom are obtained. The modelling capabilities of VehicleSim start becoming evident now, as obtaining these equations by hand could be a cumbersome process:

Flap equation of motion

$$\begin{aligned} \ddot{\beta} (I_{blx} \cos^2 \xi + I_{bly} \sin^2 \xi + m_{bl} y_{bl}^2 \cos^2 \xi) - 2m_{bl} \sin \xi y_{bl}^2 \cos \xi \dot{\beta} \dot{\xi} = & -k_{fj} \cos \xi + \Omega \cos^2 \xi \sin \beta \\ (I_{bly} - I_{blz}) (\dot{\xi} + \Omega \cos \beta) - \dot{\beta} \cos \xi \sin \xi (I_{bly} - I_{blz}) (\dot{\xi} + \Omega \cos \beta) - I_{blx} \cos^2 \xi \Omega \dot{\xi} \sin \beta + & \\ I_{blx} \cos \xi \dot{\beta} \sin \xi (\dot{\xi} + \Omega \cos \beta) + \Omega \sin \beta \sin^2 \xi (I_{blx} - I_{blz}) (\dot{\xi} + \Omega \cos \beta) + \dot{\beta} \cos \xi \sin \xi & \\ (I_{blx} - I_{blz}) (\dot{\xi} + \Omega \cos \beta) + I_{bly} \sin \xi \Omega \dot{\beta} \cos \beta \cos \xi - I_{bly} \dot{\xi} \sin \xi \dot{\beta} \cos \xi - I_{bly} \dot{\xi} \sin \xi \Omega \sin \beta \sin \xi & \\ - m_{bl} \cos \xi y_{bl} e R \Omega^2 \sin \beta - m_{bl} \cos \beta \Omega^2 \cos^2 \xi y_{bl}^2 \sin \beta - 2m_{bl} \sin \beta \Omega \dot{\xi} y_{bl}^2 \cos^2 \xi & \end{aligned} \quad (7.25)$$

Lag equation of motion

$$\begin{aligned} \ddot{\xi} (I_{blz} + m_{bl} y_{bl}^2) + m_{bl} \sin \xi \cos \xi y_{bl}^2 \dot{\beta}^2 = & -k_{lj} \xi - d_{lj} \dot{\xi} + I_{blx} \Omega \dot{\beta} \cos^2 \xi \sin \beta - (I_{bly} - I_{blx}) \\ \sin \xi \cos \xi \Omega^2 \sin^2 \beta + \Omega \dot{\beta} (I_{blz} - I_{bly} \cos^2 \xi) \sin \beta - \dot{\beta} \sin \xi (I_{blx} - I_{bly}) (\dot{\beta} \cos \xi + \Omega \sin \beta \sin \xi) & \\ + m_{bl} \sin \xi \cos \xi y_{bl}^2 \Omega^2 \sin^2 \beta - m_{bl} y_{bl} \sin \xi e R \Omega^2 \cos \beta & \\ + \underbrace{m_{bl} \Omega \sin \beta y_{bl}^2 \dot{\beta} - m_{bl} \Omega \dot{\beta} \sin \beta y_{bl}^2 \cos^2 \xi + m_{bl} \Omega \dot{\beta} \sin \beta y_{bl}^2 \sin^2 \xi}_{(*)} & \end{aligned} \quad (7.26)$$

The last three terms in equation (7.26), (*), can be rearranged taking into account that $\sin \xi = \sqrt{1 - \cos^2 \xi}$ and this yields:

$$\begin{aligned} m_{bl} \Omega \sin \beta y_{bl}^2 \dot{\beta} - m_{bl} \Omega \dot{\beta} \sin \beta y_{bl}^2 \cos^2 \xi + m_{bl} \Omega \dot{\beta} \sin \beta y_{bl}^2 \sin^2 \xi = & \\ m_{bl} \Omega \sin \beta y_{bl}^2 \dot{\beta} (1 - \cos^2 \xi) + m_{bl} \Omega \dot{\beta} \sin \beta y_{bl}^2 \sin^2 \xi & \end{aligned} \quad (7.27)$$

And this is:

$$m_{bl} \Omega \sin \beta y_{bl}^2 \dot{\beta} (1 - \cos^2 \xi) + m_{bl} \Omega \dot{\beta} \sin \beta y_{bl}^2 \sin^2 \xi = 2m_{bl} \Omega \dot{\beta} \sin \beta y_{bl}^2 \sin^2 \xi \quad (7.28)$$

which is the corresponding Coriolis term expected to appear in the lag motion equation.

In this section, the inertia accelerations, centrifugal force and Coriolis terms have been obtained for flap and lag coupled motions as equations (7.25), (7.26) and (7.27) show. The equations for flap and lag have been shown to contain the terms that the theory predicts for this coupling effect, probing in this way, the correct and adequate modelling of the blade motion by using VehicleSim.

7.2 Dynamical Analysis

Once the main rotor's blade dynamical model has been built and validated, the next stage is to show the results of the simulations performed and to carry out a dynamical analysis. The dynamical impact of both spring and damper will be considered on the flap and lag degrees of freedom. Feather behaviour will also be studied. Moreover, dynamical interaction between the fuselage and the main rotor will be shown to occur and studied due to its potential impact in the helicopter's overall behaviour; very often vibrations appear in the fuselage due to the main rotor, this usually represents a hazard for the vehicle's stability or for successful duty achievement (see references [128], [129] as example). The results here presented will be validated as well with previous existing knowledge.

7.2.1 Flap Dynamics

Well known rotor theory ([98], [140] amongst others), states the existence of a direct relationship between the flap frequency, ν_β , and the offset distance existing between the flap hinge and the rotor origin, e , in absence of a flap spring:

$$\nu_\beta = \sqrt{1 + \frac{3e}{2(1-e)}} \approx \sqrt{1 + \frac{3}{2}e} \quad (7.29)$$

Various simulations were carried out in this sense to investigate this relationship in the rotor system modelled in this work, the lag is not considered in order to study pure flap hinge behaviour. Different values for the flap frequencies under different offset values are obtained and shown to coincide with the theoretical predictions.

Blade Behaviour in Absence of Flap Spring

In here, different simulations are run for same conditions when various values of the offset distance are considered. As mentioned before, gravity effects are not taken into account, therefore there is a need to introduce a small flap initial angle in order to simulate this system. The initial flap angle is set to be $\beta_0 = 0.0175$ rad. The obtained system's states and velocities data were exported to Matlab and stored in the workspace and analysed using a FFT (Fast Fourier Transform) Matlab algorithm, in this way, the corresponding frequencies were obtained for different offset cases. The results are shown in Table 7.1. It can be seen that when the offset values are increased, the flap frequencies increase following the theoretical predictions indicated in equation (7.29). It is to note that the flap frequency coincides with the rotor rotational frequency in the absence of offset ($e = 0\%$).

Offset eR(m)	VehicleSim Flap Frequency (Hz)	Nondimensional VehicleSim Flap Frequency	Nondimensional Theoretical Flap Frequency
0	7.064	0.99	1.00
0.491	7.538	1.06	1.07
0.982	7.980	1.13	1.14

Table 7.1: *Obtained and predicted flap frequencies for various values of offset distance. Initial flap angle $\beta_0 = 0.0175$ rad, and rotor angular speed $\Omega = 44.4$ rad/s.*

Blade Behaviour in Presence of Flap Spring

Following the dynamical equations of motion obtained in the previous section, the flap frequency is expected to increase when a flap spring is included in the system as indicated in the equation (7.30):

$$\nu = \sqrt{\frac{\Omega^2 [eRm_{bl}y_{bl} + m_{bl}y_{bl}^2 + (I_{blz} - I_{bly})] + k_{fj}}{(I_{blx} + m_{bl}y_{bl}^2)}} \quad (7.30)$$

Therefore, a spring of stiffness $K_{fj} = 46772$ Nm/rad is included in the derived VehicleSim model, and several simulations are carried out for various values of offset distance, eR . The initial flap angle is $\beta_0 = 0.0175$ rad. The obtained frequency values are shown

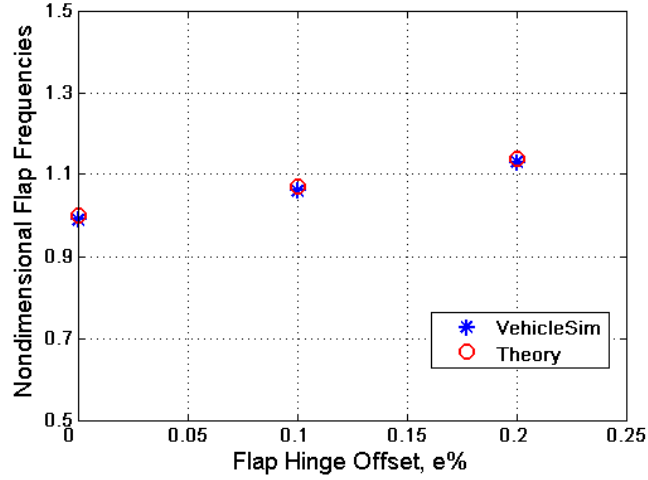


Figure 7.1: Flap frequencies as a function of the offset without flap spring. Red 'o', represents the theoretical predicted values. Blue '*', VehicleSim obtained values.

(see Table 7.2), two things need to be observed, first of all, the obtained frequencies are slightly higher than in the previous case (no spring) and secondly, the good match of the obtained results with those predicted by the theory, which validates the flap hinge model built in VehicleSim.

Offset eR(m)	VehicleSim Flap Frequency (Hz)	Nondimensional VehicleSim Flap Frequency	Nondimensional Theoretical Flap Frequency
0	7.324	1.03	1.01
0.491	7.782	1.10	1.09
0.982	8.209	1.16	1.18

Table 7.2: Obtained and predicted flap frequencies for various values of offset distance with a spring of constant $K_{fj} = 46772 \text{ Nm/rad}$. Initial flap angle $\beta_0 = 0.0175 \text{ rad}$, and rotor angular speed $\Omega = 44.4 \text{ rad/s}$.

The theoretical nondimensional flap frequencies in Table 7.2 are calculated as [77], [140]:

$$\nu_{\beta}^2 - 1 = \frac{e_{\beta}}{I_{\beta}} M_{\beta} + \frac{K_{\beta}}{I_{\beta} \Omega^2} \quad (7.31)$$

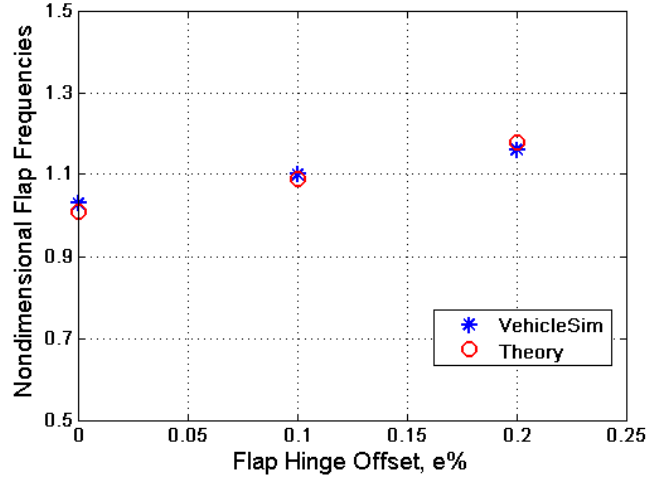


Figure 7.2: Flap frequencies with the flap spring, ν_β as a function of the offset distance e . Red 'o', represents the theoretical predicted values. Blue '*', VehicleSim obtained values.

where

$$I_\beta = \int_{e_\beta}^l m (r - e_\beta)^2 dr \quad (7.32)$$

being the equation (7.32) the flap moment of inertia with respect to the flap hinge, M_β is the first mass moment with respect to the flap hinge offset, e_β is the flap hinge offset, K_β is the flap hinge spring stiffness, l is the length of the blade and Ω is the main rotor angular speed.

$$M_\beta = \int_{e_\beta}^l m (r - e_\beta) dr \quad (7.33)$$

The simulation has shown that the obtained flap frequency results coincide with the theory in the case of including a spring k_{fj} in the flap hinge.

7.2.2 Lag Dynamics

It is well known that in the absence of lag hinge spring, the offset should not be zero or there would be no other means to deliver torque to the rotor. The lag frequency, ν_ξ , is directly related to the offset distance ([98], [140]) by the following expression:

$$\nu_\xi = \sqrt{\frac{3}{2} \left(\frac{eR}{R - eR} \right)} \approx \sqrt{\frac{3}{2}} e \quad (7.34)$$

The blade's lag natural frequency, is about one-third to one-fourth of the rotor's angular speed [148]. Therefore, first, simulations are carried out without offset distance, without spring and without damper in the lag hinge with the objective of validating the obtained results. Secondly, simulations will be carried out with offset distance, with lag spring, lag damper and results will be compared to those predicted in the theory.

Pure Lag Motion with no Spring-Damper

For simulation purposes, the initial lag angle is set up to be $\xi_0 = 0.0175$ rad. The simulations were carried out for different values of offset distance, e , the obtained VehicleSim time histories of the lag angle were analysed with Matlab, and the corresponding obtained lag frequencies, ν_ξ , are shown in Table 7.3.

Offset eR (m)	VehicleSim Lag Frequency (Hz)	Nondimensional VehicleSim Lag Frequency	Nondimensional Theoretical Lag Frequency
0	0.000	0.000	0.000
0.491	2.609	0.369	0.387
0.982	3.707	0.524	0.547

Table 7.3: *Lag frequencies. Initial conditions $\xi_0 = 0.0175$ rad without lag spring and damper, rotor angular speed $\Omega = 44.4$ rad/s.*

As it can be seen, Table 7.3 shows that when the offset is increased, the lag frequency increases as proposed in [98].

7.2.3 Coupled Flap and Lag Dynamics

As discussed in section 7.2.2, the lag hinge must have an offset or spring in order to obtain nonzero lag frequency this is in order to have lag motion. The centrifugal force always acts a spring on the flap mode. Furthermore, the lag motion depends on the hinge offset to obtain a centrifugal spring [140]. In addition to these, it is important

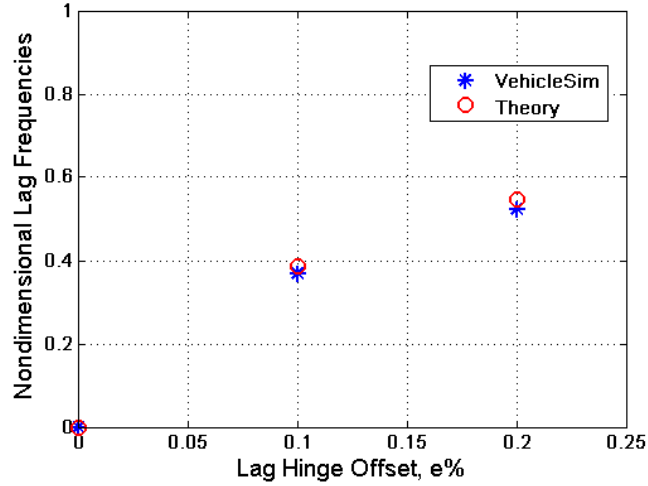


Figure 7.3: Lag frequencies as a function of the offset for the case of no spring, no damper fitted in the lag hinge. Red 'o', represents the theoretical predicted values. Blue '*', VehicleSim obtained values.

to note that whilst blade flap motion is essentially a resonant phenomenon; lag motion has a natural frequency well below the rotational speed for lag hinge offset. The lag motion natural frequency wherein spring forces are always in equilibrium with mass forces, depends on the inertia moment and centrifugal moment, which is different from that for flap [148]. In order to validate this, VehicleSim simulations are carried out with a spring on the flap and lag hinges as well as a damper in the lag hinge. Similarly to the previous sections, the simulation is carried out for an initial flap angle of $\beta_0 = 0.0175$ rad, and the lag initial angle is $\xi_0 = 0$ rad.

The theory predicts a lag frequency double those of the flap frequency [125]. Simulations were carried out using VehicleSim for different values of the offset. The results of the simulations are given in tables 7.4 and 7.5.

It can be seen in Table 7.5 how the ratio 2 : 1 the blade's between lag and flap frequencies is satisfied for the different offsets. It is clear to see how the results agree with the theoretical predictions.

Analyzing the simulation results relating flap and lag angles, the coupling between flap and lag arising from the nonlinear terms in equations (7.25) and (7.26) can be observed in the decay of both signals amplitudes over time (see Figure 7.4). The simulation was

7.2. DYNAMICAL ANALYSIS

Offset eR (m)	VehicleSim Flap Frequency (Hz)	VehicleSim Lag Frequency (Hz)	β (rad/s)	ξ (rad/s)
0	7.324	14.648	46.018	92.036
0.491	7.782	15.548	48.895	97.690
0.982	8.209	16.403	51.578	103.063

Table 7.4: Flap-Lag frequencies from VehicleSim obtained with initial conditions $\beta_0 = 0.0175$ rad and $\xi_0 = 0$ rad with spring in the flap ($k_{fj} = 46772$ Nm/rad) and lag hinges ($k_{lj} = 314938$ Nm/rad). The damping coefficient for the lag hinge damper is $d_{lj} = 349.58$ Nms/rad.

Offset eR (m)	VehicleSim Normalised Flap Frequency	VehicleSim Normalised Lag Frequency	VehicleSim Ratio Lag-Flap
0	1.03	2.07	2.00
0.491	1.10	2.20	2.00
0.982	1.16	2.32	2.00

Table 7.5: VehicleSim Flap/Lag ratios. Initial conditions $\beta_0 = 0.0175$ rad and $\xi_0 = 0$ rad. Springs and damper fitted.

carried out for a initial flap angle of $\beta_0 = 0.09$ rad and the lag angle is $\xi_0 = 0$ rad in order to observe the decay of the flap angle amplitude due to the presence of damping in the lag hinge, without this, there would be no energy dissipation in the system and no decay of the flap amplitude would take place.

It is expected that the two degrees of freedom become independent from each other if the coupling did not exist. Figure 7.5 shows the uncoupled equations of motion results independent from the lag motion as they are not influenced by the presence of the lag damper. The flap amplitude therefore, remains constant in the absence of external forces/moments and does not show any decay on its behaviour over the entire simulation interval.

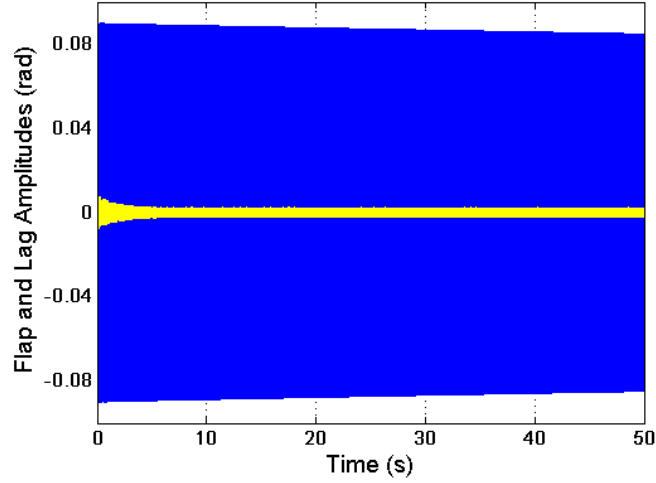


Figure 7.4: Flap amplitude (in blue) and lag amplitude (in yellow) simulation results, showing free vibrations from an initial condition in which the flap angle is $\beta_0 = 0.09$ rad and lag angle is $\xi_0 = 0$ rad.

7.2.4 Frequency Domain Validation

The results here presented are relevant in order to study the dynamic behaviour of small amplitude perturbations about the equilibrium. With this purpose, the dynamic equations of motion are considered and a frequency domain analysis can be performed by using an approach involving the eigenvalues/eigenvectors of the system.

VehicleSim generates the linearised model that contains the symbolic state-space A, B, C, D matrices for linear analysis. In addition to this, the nonlinear equations of motion on each case are obtained in C code, and this is used to generate states' time histories. In order to obtain the eigenvalues/eigenvectors, the state's time histories are imported from the nonlinear model into the symbolic linearised model matrices.

The flap linear state equation is obtained in VehicleSim as:

$$\ddot{\beta} (I_{blx} + m_{bl}y_{bl}^2) = -m_{bl}\Omega^2 y_{bl} (eR + y_{bl}) \beta - \Omega^2 (I_{blz} - I_{bly}) \beta - k_{fj} \beta \quad (7.35)$$

This can be written in matrix form:

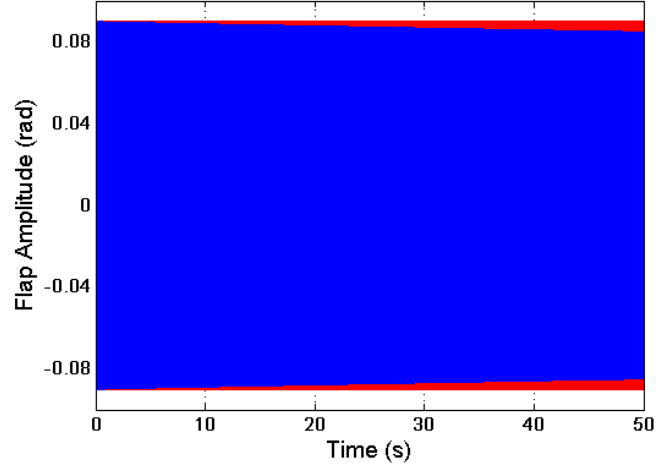


Figure 7.5: *Uncoupled and coupled flap dynamics (red, linear flap simulation results, blue, nonlinear flap simulation results).*

$$\begin{pmatrix} \dot{x}_1 \\ \dot{x}_2 \end{pmatrix} = \begin{bmatrix} 0 & 1 \\ F & 0 \end{bmatrix} \begin{Bmatrix} x_1 \\ x_2 \end{Bmatrix}$$

where $x_1 = \beta$, $x_2 = \dot{\beta}$ and F is equal to:

$$[-k_{fj} - m_{bl}y_{bl}^2\Omega^2 - \Omega^2 eRm_{bl}y_{bl} + \Omega^2 (I_{bly} - I_{blz})] / (I_{blx} + m_{bl}y_{bl}^2) \quad (7.36)$$

By feeding the matrix with the corresponding physical parameters, the eigenvalues are: $\lambda_{1,2} = 0 \pm 48.8564i$ where the complex part of $\lambda_{1,2}$ is the flap natural frequency, 48.8564 rad/s slightly above the main rotor's angular speed as this simulation corresponds to the case where there is a flap spring k_{fj} , and offset $eR \neq 0$.

In similar manner, the linear lag equation of motion yields can be written as a first order system:

$$\begin{pmatrix} \dot{y}_1 \\ \dot{y}_2 \end{pmatrix} = \begin{bmatrix} 0 & 1 \\ H & G \end{bmatrix} \begin{Bmatrix} y_1 \\ y_2 \end{Bmatrix}$$

where $y_1 = \xi$, $y_2 = \dot{\xi}$ and:

$$H = -(k_{fj} + eRm_{bl}\Omega^2 y_{bl}) / (I_{blz} + m_{bl}y_{bl}^2) \quad (7.37)$$

and

$$G = -d_{lj} / (I_{blz} + m_{bl}y_{bl}^2) \quad (7.38)$$

In this case, the eigenvalues of the matrix are: $\lambda_{1,2} = -0.5448 \pm 35.3776i$. The natural lag frequency is 35.3776 rad/s and the system's damping is provided by the real part of $\lambda_{1,2}$.

Root Locus

The linear approximation allows to shed some insight on the complex motion of the blade. The linear natural modes of the blade are analysed from the stability point of view.

A layout of the uncoupled flap and lag modes is represented on the complex eigenvalues plane in Figure 7.6. The stability conditions are studied in the equilibrium by using the root locus.

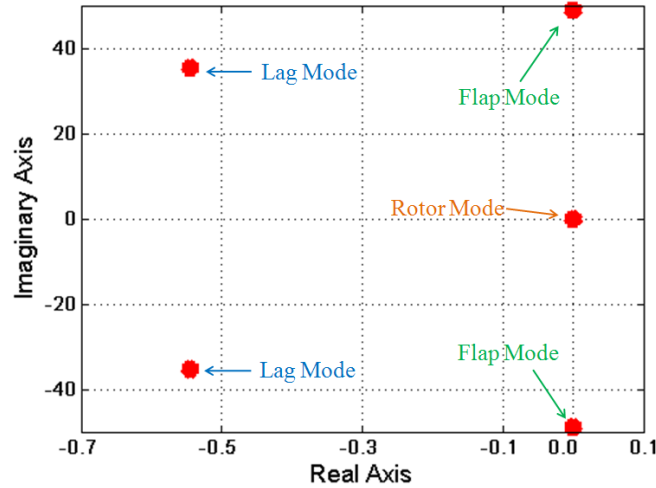


Figure 7.6: *Root locus for flap and lag modes on the main rotor.*

As it can be seen in Figure 7.6, the lag mode is well damped ($d_{lj} = 349.58$ Nms/rad) and located into the left hand side of the plane. The flap mode in this case does not have a damper, therefore its mode it is located on the imaginary axis.

A typical layout of the uncoupled flap and lag modes is shown on the complex plane in Figure 7.7. It shows how the flap modes are well damped and located far into the left hand side of the plane. In contrast, the lag modes are often weakly damped, even in the presence of mechanical dampers, and are more susceptible to being driven unstable [142].

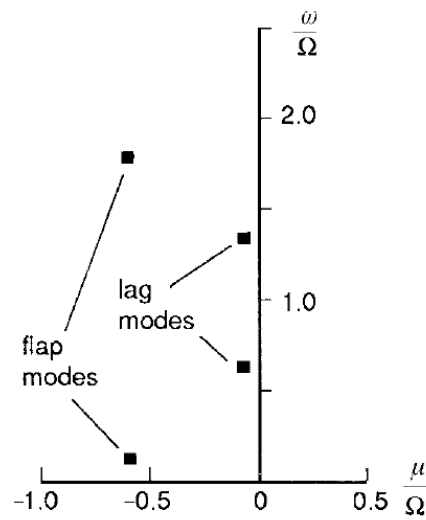


Figure 7.7: *Flap and lag modes, being Ω the main rotor speed and μ the real part of eigenvalue or damping. Reproduced with permission from Wiley Publication [142].*

In Figure 7.6, the modes flap and lag as obtained by VehicleSim were shown. In this case, the flap hinge did not have a damper, and therefore, the marginal stability of this mode.

If now a damper of 500 Nms/rad on the flap hinge is included new simulations carried out the root locus is given in Figure 7.8. A comparison can be done between figure 7.7 and 7.8, in both graphs the imaginary axes are normalized. The frequencies of the modes are slightly different due to the fact that in Figure 7.7, the aerodynamic load was considered in the model. The aerodynamic load helps to increase the frequency.

Nevertheless, parameter differences aside, Figure 7.8 clearly shows an agreement with the expected behaviour (Figure 7.7) [142].

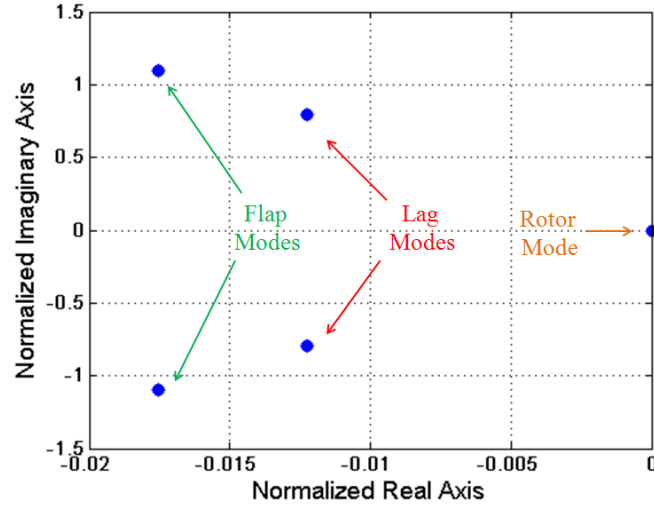


Figure 7.8: Root locus plot flap and lag modes obtained by *VehicleSim* with damper fitted in the flap hinge. (Note normalized in both axes).

7.2.5 Feather

The rotor has mechanical means of producing the required collective and cyclic changes on the rotor blades feather angles. The swashplate is a mechanical actuator that transmits the pilot's control motion in the nonrotating frame to the blade cyclic feather motion in the rotating frame. The blade feather angle, obeys the commanded input from the helicopter's control system.

The feather angle was modelled by introducing a PID controller in the rotor model such that provides the desired angle θ .

$$\theta = f_0 + f_{0S}\sin(\Omega t) + f_{0C}\cos(\Omega t) \quad (7.39)$$

Ω is the rotor angular speed, f_0 defines the collective feather and f_{0S} and f_{0C} define the cyclic feather. The selection of these coefficients is dictated by the desired state of flight.

If the collective feather is to be controlled, f_0 takes a constant value and f_{0S} , f_{0C} should be set to null.

Figure 7.9, shows a collective feather of 0.01 radians achieved after the adequate control acted on the blade. There is a short peak transient that quickly drops to the desired

feather value.

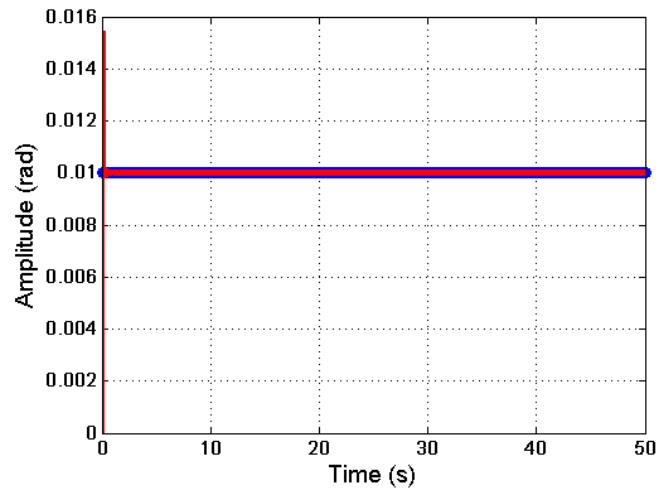


Figure 7.9: Red '-', collective feather of 0.01 rad for the four blades of the main rotor. Blue 'o', the reference signal for the collective feather.

If the cyclic feather is to be controlled, the parameters f_{0S} , f_{0C} should have constant values and f_0 remains set to zero.

In Figure 7.10, it can be seen how the feather cyclic angle of the rotor blades follow the prescribed cyclic angle when the values are $f_{0S} = 0.01$ and $f_{0C} = 0.01$ radians. An interval of time of 1 second is shown in order to see the behaviour clearly, although the simulation was carried out for 50 seconds. The reference signal is also shown.

It has been shown how both satisfactory cyclic and collective feather controls are achieved by implemented a PID controller, replicating in this way the pilot's input.

7.2.6 Fuselage

In this section, various simulations are carried out in order to shed light onto the fuselage's behaviour and its interaction with the main rotor and viceversa.

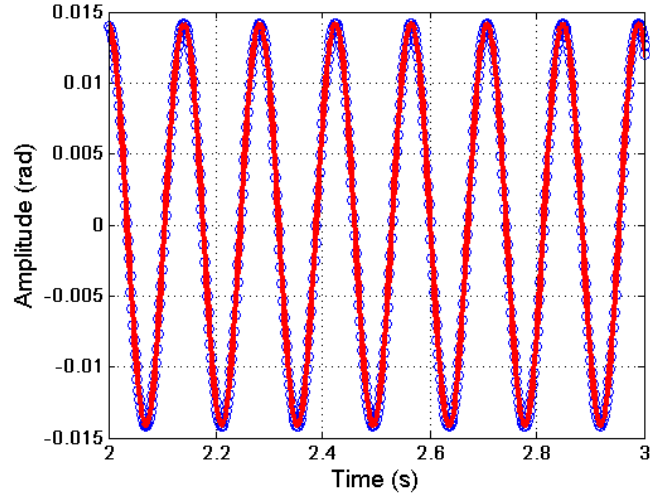


Figure 7.10: Red 'x', cyclic feather with $f_{0S} = 0.01$ and $f_{0C} = 0.01$ radians for the blades of the main rotor. Blue 'o', the reference signal for the cyclic feather.

Fuselage Motion and Blade Flap Coupling

The study of the fuselage's motion and blade flap coupling is given in this section. If the blade flap hinge spring stiffness is zero, the rotor disc remains aligned to the original position, as there is no other mechanism to generate a turning moment on the blade. With a spring added to the flap hinge, the blade will develop a persistent oscillation about the shaft orientation with an inertial moment appearing due to out of the plane flap and the centrifugal moment continually in balance [142]. It is assumed that the fuselage is allowed to perform vertical motions, the rest of degrees of freedom are not considered in this case, and the rotor blades are mounted with flap and lag hinges. The rotor's angular speeds are given in the form of a constraint, torques are not considered in this case. The stability of this case is studied by using the root locus when equilibrium conditions are simulated. The results are shown in Figure 7.11.

The oscillatory behaviour between the fuselage and the blades' flap motion on the main rotor are simulated by using the next conditions: the four blades have initial flap angle $\beta_0 = 0.0175$ rad, gravity is not taken into account. The system shows the behaviour in Figure 7.12: vertical oscillations appear on the fuselage as a consequence of the dynamic coupling with the blades flap motion. The frequency of these oscillations coincides with the blades' flap frequency and the movement direction is the opposite.

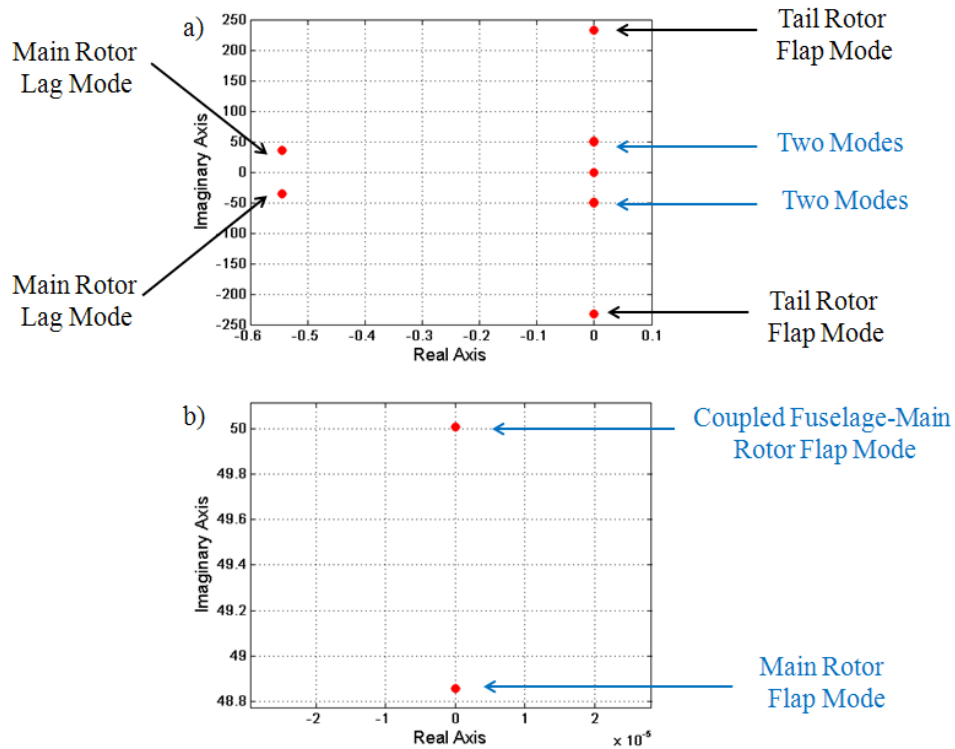


Figure 7.11: a) Root locus for the fuselage, the main and the tail rotors. b) Details of the root locus for two modes.

- Modal Analysis

A theoretical modal analysis approach is used as it allows to study complex phenomenon on the dynamic structures with simple methods such as the natural shape modes. In order to understand the coupling between the fuselage vertical motion and the blades' vertical displacement, several simulations were carried out.

The eigenvalues of the system are the square of the natural frequencies at which the system oscillates and the eigenvectors represent the mode shapes as well as the relative amplitude between the masses conforming the system when it oscillates at one or the other frequencies. In other words, the eigenvectors represent how the various parts of the system oscillate with respect to each other.

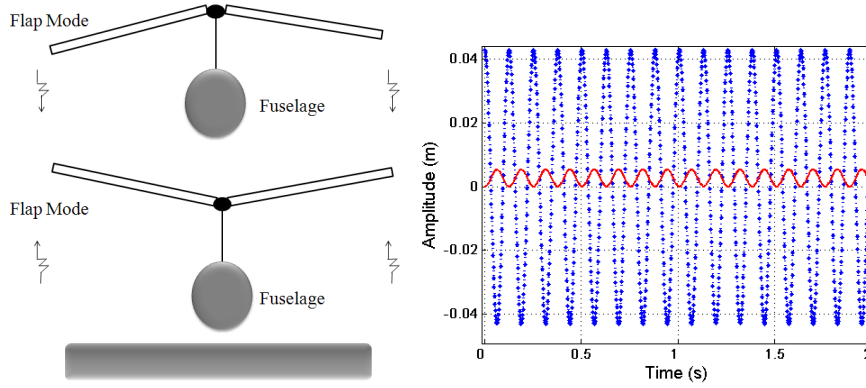


Figure 7.12: *Coupled movement for the fuselage and the main rotor along the vertical axis. Solid red line, fuselage. Dotted blue line, flap.*

This section is based on the mathematical analysis of the linearised model. In general, it is well known that the eigenvalues, λ , of a matrix A satisfy the equation:

$$(A - \lambda I) \phi = 0 \quad (7.40)$$

being ϕ an eigenvector.

The solution of the algebraic equation (7.40) is:

$$\det(A - \lambda I) = 0 \quad (7.41)$$

The corresponding eigenvectors, are obtained for any eigenvalue λ_i by:

$$A\phi_i = \lambda_i\phi_i \quad (7.42)$$

The elements of the eigenvectors give a measure of the relative activity of the state variables when a particular mode is excited. In other words, the i -th element of the eigenvector ϕ_i measures the activity of the state variable x_i in the i -th eigenvalue [142], [149].

The mathematical model of the system under study has twenty four state variables, $q(t) = \{x_1, x_2, x_3, \dots, x_{24}\}^T$ where the first variable x_1 describes the fuselage's vertical translation, x_2 describes the main rotor rotation, x_3, x_5, x_7 and x_9 describe the flap angle for the first, second, third and fourth blades on the main rotor, respectively. x_4, x_6, x_8 and x_{10} describe the lag angle for the first second, third and fourth blade on the main rotor, respectively. x_{11} describes the angular displacement of the tail rotor, x_{12}

and x_{13} describe the flap angle for the first, second blade on the tail rotor, respectively. x_{14} describes the vertical speed of the fuselage. x_{15} , x_{17} , x_{19} and x_{21} describe the flaps rotational speeds for the first, second, third and fourth blade on the main rotor. x_{16} , x_{18} , x_{20} and x_{22} describe the lag's angular speed for the first, second, third and fourth blade on the main rotor. Finally, x_{23} and x_{24} describe the flap angle for the first and second tail rotor blades.

A simulation is performed in order to study the eigenvalues of the linearised model that are associated to the equilibrium points. In this case, the linearisation was taken about the main and tail rotors angular speeds, the rest of the values remain near to zero (the initial flap and lag angles on the main rotor as well as the initial flap angle on the tail rotor are zero. The feather angles on the main and tail rotors are also zero). The linearised model is imported into Matlab (m-file) as a symbolic state-space representation (A, B, C, D matrices) for linear analysis. The study requires time histories from the nonlinear model and the symbolic linearised equations of motion generated by the linear VehicleSim code. The obtained eigenvalues are shown in Table 7.6. Their complex conjugates values can be neglected, because they do not provide any additional information.

The eigenvectors matrix is also found using Matlab. Each eigenvalue can be associated to its corresponding eigenvector in order to identify the various modes of oscillations. According to [142] the i -th element of the eigenvector ϕ_2 measures the activity of the state variable x_i in the eigenvalue λ_2 .

An analysis is carried out to study how the fuselage, flap and lag modes vibrate with respect to each other. The natural frequency for the eigenvalue: $\lambda_2 = 0.0000 + 50.01i$ is 5.00 rad/s, it calculated as the eigenvalue root square. If the magnitude of the eigenvector associated to this eigenvalue is represented (see Figure 7.13), it can be seen that the state variables associated to the translational speed of the fuselage, x_{14} and the rotational speed for the flap degree of freedom (x_{15} , x_{17} , x_{19} , x_{21}) in the main rotor provided show an influence as the magnitude of the mentioned eigenvectors show activity and the rest of the magnitudes remain null, as Figure 7.13 shows.

The natural frequency of the eigenvalue $\lambda_3 = 0.0000 + 48.86i$ is 4.94 rad/s. The magnitude of the eigenvector associated to this eigenvalue is represented in Figure 7.14, the state variables associated to the rotational speed of flap of the second blade on the main

Name	Eigenvalues
λ_1	0.00
λ_2	$0.00 + 50.01i$
λ_3	$0.00 + 48.86i$
λ_4	$0.00 + 48.86i$
λ_5	$0.00 + 48.86i$
λ_6	$0.00 + 232.97i$
λ_7	$0.00 + 232.97i$
λ_8	$-0.54 + 35.38i$
λ_9	$-0.54 + 35.38i$
λ_{10}	$-0.54 + 35.38i$
λ_{11}	$-0.54 + 35.38i$
λ_{12}	0.00

Table 7.6: *Eigenvalues of the linearised matrix corresponding to the simulation of a helicopter model with main and tail rotor; fuselage's vertical degree of freedom is enabled. Main rotor blades have flap/lag degrees of freedom and tail rotor blades have flap degree of freedom.*

rotor is larger than the rest of blades. The fuselage does not show any influence in this mode nor does the lag mode. The flap is the main contributor to this mode.

The natural frequencies of the eigenvalues: λ_4 , λ_5 are the flap frequencies of the main rotor without any influence of the fuselage on them.

The natural frequency of the eigenvalues: λ_6 , λ_7 with values $0.0000 + 232.97i$ is 10.79 rad/s and these are associated to the tail rotor blades' flap without any influence of the fuselage on them.

The eigenvalues λ_8 , λ_9 , λ_{10} and λ_{11} with values $-0.54 + 35.38i$ are associated to the lag mode. The natural frequency of these eigenvalues is 4.17 rad/s.

It should be noted that the first mode associated to the eigenvector ϕ_2 shows coupled motions between the fuselage and the main rotor flap angle, while the rest of the modes are associated to the blade's motion only.

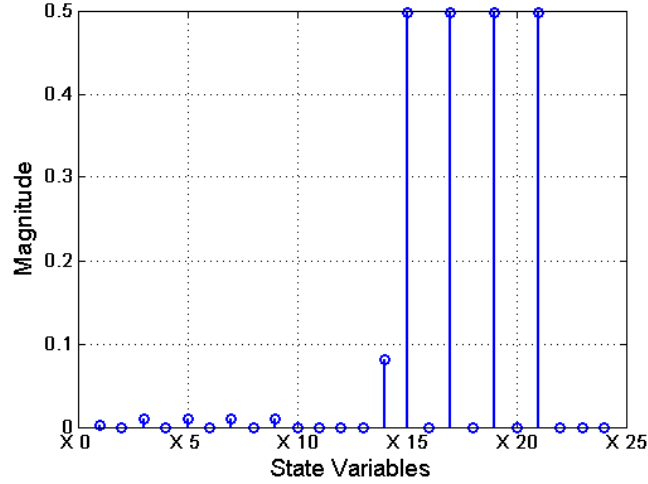


Figure 7.13: *Magnitude of the eigenvector associated to the eigenvalue $\lambda_2 = 0.0 + 50.01i$ and its influence on the state variables.*

If a comparison between the natural frequencies related to mode 1 (coupled fuselage-flap ϕ_2) and mode 2 associated to eigenvector ϕ_3 is done, it is found that their values are similar. As a consequence of this, a coupling between these two modes when the natural frequencies change as a function of the mass ratio is expected. The next part in this section will focus on validating this expectation.

The influence of the mass ratio on the coupled modes is given as $\text{mass}_{blade}/\text{mass}_{fuselage}$. If the blade's mass is 31.06 kg and the fuselage's mass is 2063.336 kg, the mass ratio is 0.015. As it can be seen in Figure 7.15, the difference between the frequencies associated to mode 1 and mode 2 is small in this case. However, the mass ratio increases the difference between the natural frequencies associated to mode 1 and mode 2. The fuselage's mass decreases from 2063.336 kg to 863.336 kg and the blades' masses increase from 31.06 kg to 34.06 kg, respectively. In Figure 7.15, the behaviour shows the influence of mass ratio on these coupled modes through the change of natural frequencies as a function of the mass ratio.

As the mass ratio is increased, the coupling between the fuselage and flap becomes larger. Conversely, if the mass ratio decreases, the coupling is reduced.

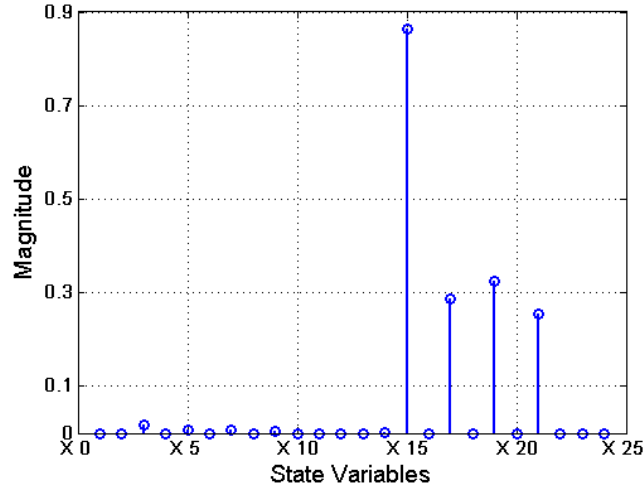


Figure 7.14: *Magnitude of the eigenvector associated to eigenvalue $\lambda_3 = 0.0 + 48.86i$ when the fuselage and the rotor are coupled.*

Fuselage Influence on the Flap Mode

It is worthy to investigate the case when the main rotor shaft is rotated in pitch and roll. In this cases, the rotor blades experience additional gyroscopic accelerations caused by mutually perpendicular angular velocities ω_p , ω_r and Ω (see Figure 7.16). The flap dynamics on the steady state:

$$\beta = \beta_{1C} \cos(\Omega t) + \beta_{1S} \sin(\Omega t) \quad (7.43)$$

where

$$\beta_{1C} = \frac{2}{\Omega (\lambda_\beta^2 - 1)} \omega_p \quad (7.44)$$

$$\beta_{1S} = \frac{-2}{\Omega (\lambda_\beta^2 - 1)} \omega_r \quad (7.45)$$

These solutions represent the gyroscopic motions experienced when a rotating mass is rotated out of plane. β_{1C} is the longitudinal disc tilt in response to roll rate and β_{1S} the lateral tilt in response to pitch rate [142].

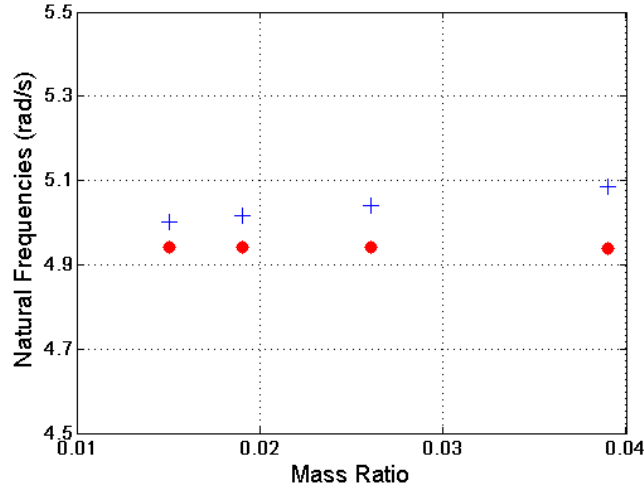


Figure 7.15: *Mode 1, blue '+' , mode 2, red '•' . Influence of mass ratio on these coupled modes. Change of natural frequencies as a function of the mass ratio $mass_{blade}/mass_{fuselage}$.*

Based on the previous considerations, if now a torque is introduced around the Y axis on the fuselage producing a pitch rotation and the initial flap angles on the blades are zero, this will be transmitted through the shaft to the flap hinges on each blade. The torque is included in the VehicleSim model as a step function, its magnitude being 1750 N·m. In here, flap hinges are included in the model to allow for the flap degree of freedom, but neither lag hinges nor tail rotor have been included in the model because this section is focused in the analysis of the interaction between the fuselage and the flap only. The main rotor rotational speed is described in VehicleSim as a constraint.

The impact of the fuselage's pitch and roll on the flap dynamics are calculated by using the expression (7.43) where $\lambda_\beta^2 = 1.2$ is a standard value applicable to this model [142]. It is expected that the flap on the four blades behaves accordingly to the fuselage's displacement. Figure 7.17 shows the blade flap angle, in blue. In red, the expected flap angle is shown.

It has been shown how an induced flap motion can be introduced by the fuselage's roll/pitch rate, as it was expected from the theory.

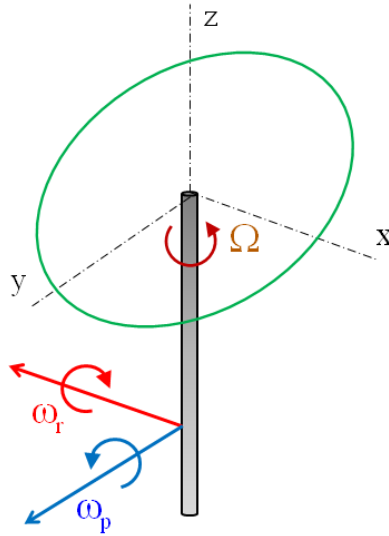


Figure 7.16: *Sketch of main rotor and gyroscopic moments in vacuum. This figure is plotted by the author and based on [142].*

Lag Mode Influence on the Fuselage

In order to establish new a test for model's validation purposes, the interaction between the flap and fuselage motion and the lag is studied. Due to the roll and pitch of the fuselage, the associated acceleration of the hub contributes with inertial terms to the lag equations. However, blade flap takes place in this case, and the corresponding Coriolis inertia terms must be also included. The inertia of the blades' lag causes further pitching and rolling moments on the helicopter [141].

The previous assumptions suggest the following validation test: if two torques around the fuselage's X and Y axes are considered, the fuselage will experience roll and pitch motions. The effects of these will be transmitted through the rotor shaft onto the blades. In order to test this behaviour in the VehicleSim model, the corresponding torques are included as pulse functions, their magnitudes are 500 N·m from $t = 0$ to $t = 1$ s. The main rotor rotational speed is given in the form of a constraint. In Figure 7.18, the spectrums for the roll and pitch motions appearing in the fuselage as a consequence of the impulses are shown. In blue, both cases are shown when the lag motion is not considered. In red, the pitch and the roll of the fuselage when the lag is taken into account in the model.

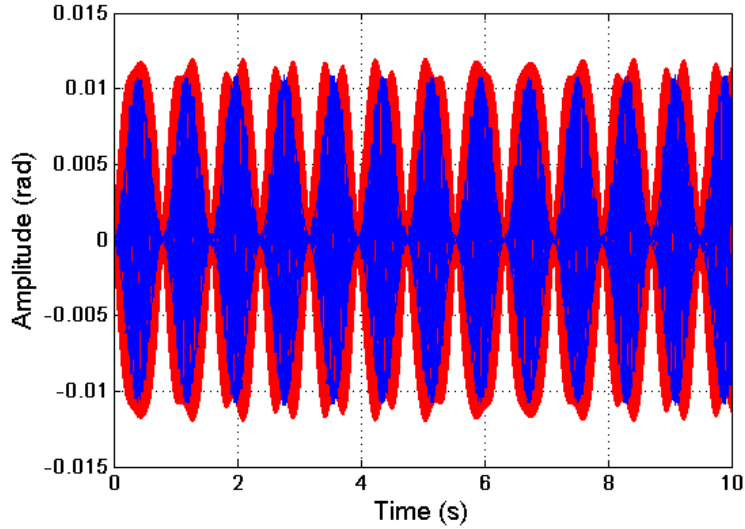


Figure 7.17: *In red, the displacement transmitted by the fuselage to the blades. Clearly corresponds to expression (7.43). In blue, blades' flap.*

As it can be seen in Figure 7.18, the presence of the lag degree of freedom increases the amplitudes of roll and pitch rotations as predicted from existing theory.

7.2.7 Tail Rotor

The tail rotor's function is to balance the main rotor torque and to provide yaw control. This is achieved through the action of the tail rotor thrust on a longitudinal arm perpendicular the main rotor shaft. The tail rotor has no cyclic feather control, just collective to control the thrust magnitude. The tail rotor shaft angle is fixed by the geometry of the tail rotor installation and the helicopter yaw angle, instead of being determined by the conditions to force equilibrium of the rotor [140].

When there is no cyclic feather control, the tail rotor usually has flap-feather coupling via a δ_3 angle set up. On the other hand, the blade is assumed to be freely articulated with zero hinge offset [144].

It is known that the δ_3 mechanical implementation increases the flap frequency, it acts like a spring on a flap hinge. In order to check this in the model here presented, the following data are taken from [144]. The δ_3 angle is equal to 45° for the cases in here.

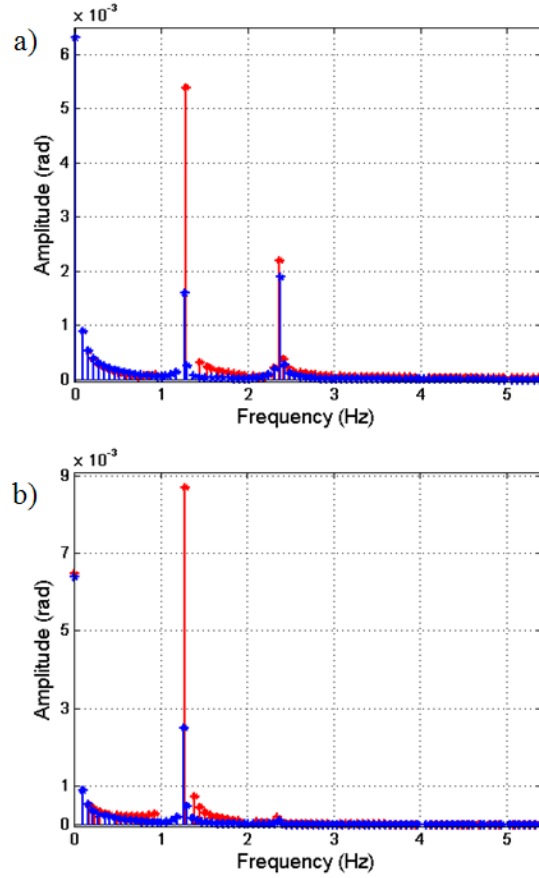


Figure 7.18: *a) Fuselage's roll vibrations spectrum. Blue, represents roll vibrations without lag hinge, and red represents roll vibrations with lag hinge included in the model. b) Fuselage's pitch spectrum. Blue, represents pitch motion without lag hinge, and red represents pitch with lag hinge included in the model.*

There is not any additional δ_3 feature modelled in this helicopter (-45°), because the programming allows to simulate both. In [144] the collective feather, coning angle, a_1 and b_1 flap angles for several advance ratios are shown and their values will be used in the following tests. Three different cases are considered: first, a collective feather of 0.24 rad, $a_1 = 0.017$ rad, $b_1 = -0.008$ rad and a coning angle equal to 0.078 rad is simulated, being the advance ratio 0.1. Second, a collective feather is equal to 0.21 rad, $a_1 = 0.043$ rad, $b_1 = -0.017$ rad and coning angle is equal to 0.087 rad for an advance ratio of 0.2. Third, the collective feather is equal to 0.26 rad, $a_1 = 0.087$ rad, $b_1 = -0.034$ rad and the coning angle is equal to 0.122 rad for an advance ratio of 0.3. In here, the helicopter is studied from the dynamical point of view, therefore the aerodynamic forces are not

included. The helicopter under study in these conditions will not advance forward, as this is not required in order to validate the flap-feather coupling in the model. The three simulations are carried out for 50 s and the previous numerical values of a_1 , b_1 , collective feather and coning angle are assigned to each simulation, respectively. Figure 7.19 shows the obtained flap frequencies for the first blade on the tail rotor, the flap initial angle is set to zero on each simulation. As it can be seen, the frequencies increase as a function of the advance ratio on each case. For the second blade on the tail rotor, similar tests were carried out obtaining similar flap frequency increase with the advance ratio.

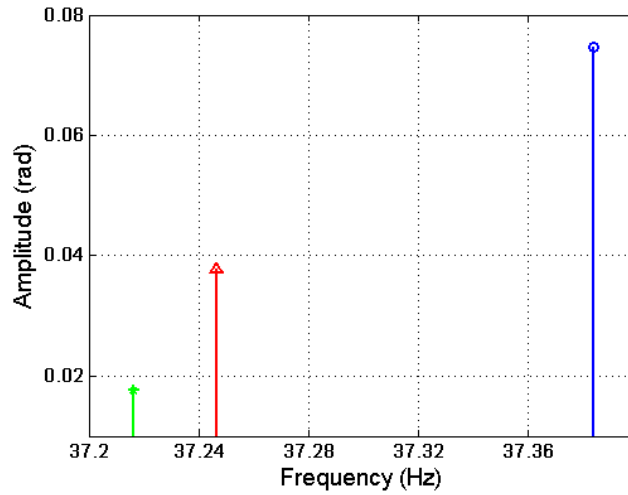


Figure 7.19: Flap frequencies for blade one on the tail rotor. In green '*', case one. In red '△', second case and in blue 'o', results for the third case.

Futhermore, the maximum disc tilt angle, β_{max} is given by [144]:

$$\beta_{max} = \sqrt{a_1^2 + b_1^2} \quad (7.46)$$

In the simulations carried out for the three above indicated cases, the values of β_{max} can be obtained and compared to those obtained in [144] (see Table 7.7).

Various simulations are carried out for the previous cases and the flap motion of blade one is studied on each case. The behaviour of blade two is similar. The simulation time is 50 s in all the cases.

Case	Theoretical Maximun disc tilt (degrees)	VehicleSim Maximun disc tilt (degrees)
1	1.00	1.07
2	3.00	2.64
3	5.00	5.35

Table 7.7: Disc tilt values for the three study cases with $\tan \delta_3 = 1$. The first column shows the number of case studied and the second column corresponds to Newman's values in degrees [144].

If the case one is simulated and the flap time history is shown (see Figure 7.20), the maximum flap amplitude is approximately 0.095 rad. This result can be validated using expression (7.46) and taking into account that the coning angle is 0.078 rad as well as the values shown in Table 7.7. β_{max} can be calculated, and it is equal to 0.0187 rad or (1.07 degrees). This value agrees with case 1 in Table 7.7. As a result, the maximum flap amplitude from the simulation should be 0.0967 rad i.e., (theoretical value). The simulated maximum flap amplitude is approximately 0.095 rad as Figure 7.20 shows. Which is a very acceptable value to be within the expected value range according to the theory within a very reasonable discrepancy limit.

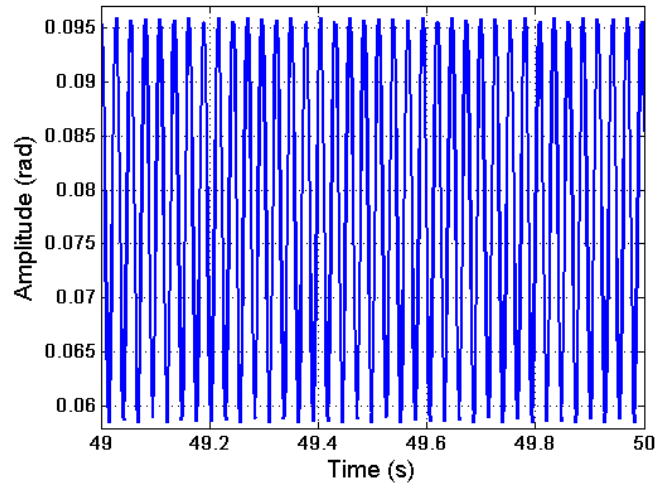


Figure 7.20: First tail rotor blade flap motion. It is worked out with $a_0 = 0.078$ rad, $a_1 = 0.017$ rad and $b_1 = -0.008$ rad. Only time between 49 - 50 seconds is shown in order to clearly see the flap behaviour.

Similarly, the second case is analyzed, the coning angle is 0.087 rad and the β_{max} is equal to 0.046 rad or (2.64 degrees). Table 7.7 shows a maximum disc tilt of 3.00 degrees or (0.052 rad). As a consequence, the theoretical maximum flap amplitude should be 0.133 rad. The simulated flap sets out a maximum amplitude of approximately 0.13 rad as Figure 7.21 describes. Theoretical and simulated results agree, within a very reasonable discrepancy limit.

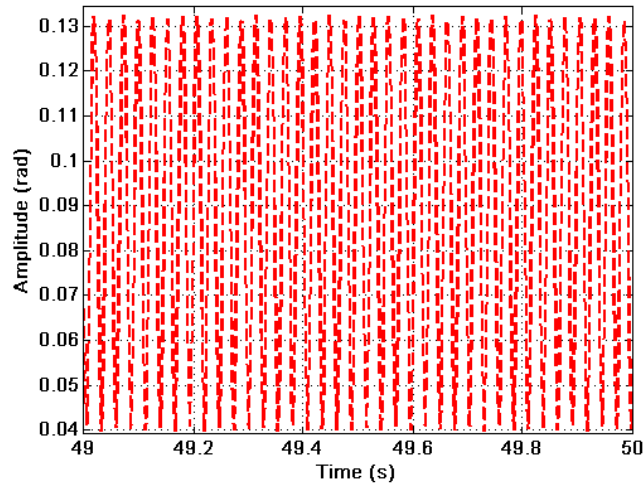


Figure 7.21: *First tail rotor blade flap with $a_0 = 0.087$ rad, $a_1 = 0.043$ rad and $b_1 = -0.017$ rad. Only time between 49 - 50 seconds is shown as in the previous figure.*

Finally, the third case is studied, the coning angle is 0.122 rad and the β_{max} is 0.093 rad or (5.35 degrees). Table 7.7 shows 5.00 degrees or (0.087 rad) for the for maximum disc tilt. The maximum flap amplitude should be 0.215 rad. In this case, the simulated flap motion shows a maximum amplitude of approximately 0.2 rad as Figure 7.21 shows.

It is known that a rotation about a hinge with flap angle β must produce a feather change of $-\beta \tan\delta_3$. The feedback gain for this arrangement is therefore $k_p = \tan\delta_3$. Note that positive coupling ($\delta_3 \geq 0$) represents negative feedback, decreasing the blade feather [140]. The simulated feather should reduce its magnitude. The feather angles from the previous simulations can also be analyzed and the influence of the positive coupling can also be observed, the results are shown in Table 7.8. As it can be seen, the feather angle decreases its value for each case, as a consequence of the positive coupling. This trend follows the expected behaviour.

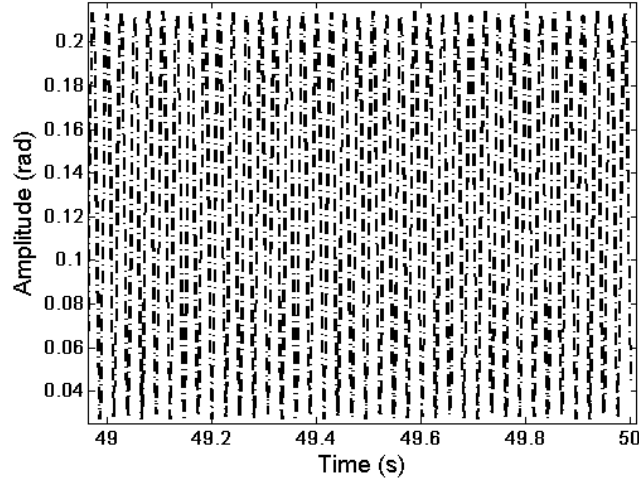


Figure 7.22: *First tail rotor blade flap angle history.* $a_0 = 0.122$ rad, $a_1 = 0.087$ rad and $b_1 = -0.034$ rad. Note the time span 49 - 50 seconds.

7.3 Stability and Control

7.3.1 Rotors' Angular Speeds

The main rotor is usually the greatest vibration source in the helicopter system and the dynamic characteristics of the rotor and fuselage must be kept within a tight tolerance frequency band. So the rotor blade natural frequencies are, in the main, dependent on the main rotor speed. As a result, the modelling of the helicopter must be done in such a way that the rotor speed is precisely controlled.

Case	Collective feather (rad)	Feedback gain for collective feather (rad)
1	0.24	0.18
2	0.21	0.17
3	0.26	0.23

Table 7.8: *Tail rotor collective feather.* First column shows the number of cases, the second shows the numerical value of the collective feather. The third column shows the feedback gain for the collective feather.

The control moments must be developed by the rotors and they depend of the equilibrium conditions on the helicopter. The balance of forces and moments determine the action of the rotor with respect to the fuselage [144]. The tail rotor propulsive force is included in the overall airframe drag and is balanced by the main rotor [140].

The control of the engine is normally performed by means of a fuel valve, therefore the governor must sense a change in the rotor speed brought about by a change in torque demand and adjust the fuel valve accordingly. This behaviour continues until engine torque and rotor torque demands are balanced [144].

The tail rotor gearing is chosen to be 5.25 according to [142]. In this model, this is implemented by two PID controllers; (as described in Chapter 5). The PID controller input, the reference value for the main rotor angular speed, is 44.4 rad/s and in the case of the tail rotor is $5.25 \cdot 44.4$ rad/s. The PID outputs are the rotational speeds of the main and tail rotors respectively. A simulation is carried out under the following conditions, the feather angles (cyclic and collective) are zero as well as the collective feather angle on the tail rotor. The flap and lag degrees of freedom do not have initial condition i.e., $\beta_0 = 0$ rad and $\xi_0 = 0$ rad. The tail rotor initial flap angle is also zero. Figure 7.23 shows the obtained angular speeds for both rotors as well as the corresponding control signal.

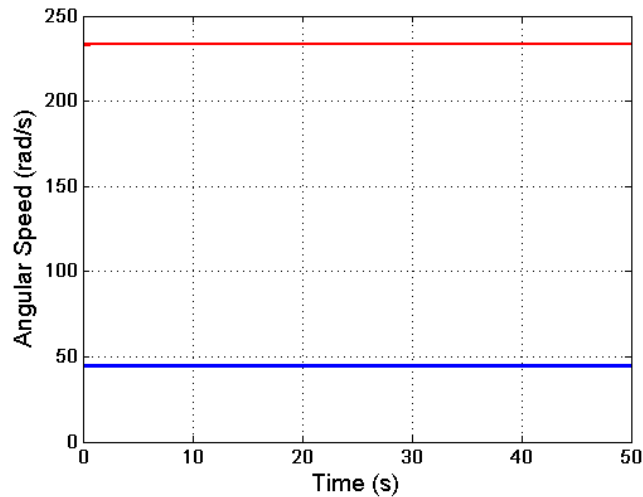


Figure 7.23: Angular speeds on both rotors. In blue, main rotor speed. In red, tail rotor speed. The control signals are shown on both cases, and clearly the speeds successfully follow the respective reference speeds.

On the other hand, figure 7.24 shows a detail of figure 7.23. As it can be seen, the main and tail rotors angular speeds reach their reference values in less than 10^{-3} s. These existing delays are in both cases just as a response of the PID controllers' action. Clearly there is a small engine delay; and these controllers implementations in VehicleSim are a good solution for the model here presented.

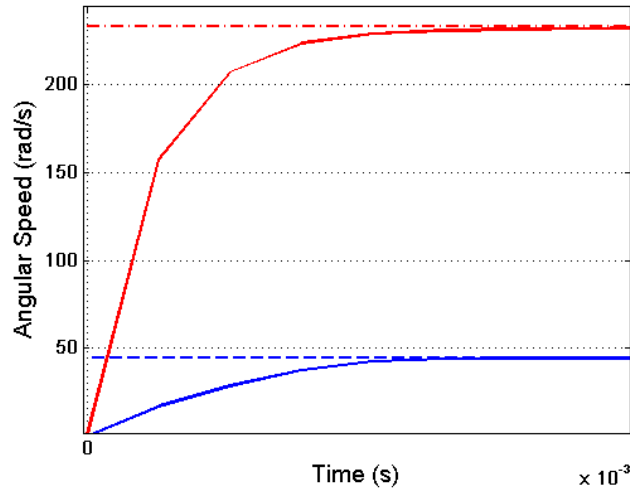


Figure 7.24: *Solid blue line represents angular speeds on the main rotor, dotted blue line is the control signal on the main rotor. Solid red line represents angular speeds on the tail rotor, dotted red line is the control signal on the tail rotor.*

7.3.2 Position and Rotation Control

The stability on the system is crucial in order to simulate the appearing vibrations. The stability of a helicopter can be considered as a special case of stability conception that is applied to any mechanical system. A helicopter is said to be statically stable if there is an initial tendency for it to return to its initial condition when it is displaced from that condition. It is statically unstable if it tends to diverge from trim after being perturbed [150].

The ability to completely control the position and height of the helicopter in space requires control of the forces and displacements about all three axes. The main rotor provides the longitudinal and lateral propulsive forces which means that there will exit a coupling between the longitudinal forces and the pitching moments, and between lateral

forces and rolling moments. This removes the independence from two of the six degrees of freedom. In other words, the ability to maintain longitudinal force equilibrium and to rotate in pitch to attain a desired attitude at will is sacrificed [144].

Thus, when the torques' action is applied to the main and tail rotors, the position and rotation equilibrium on the helicopter must be reached and the steady-state can be reached using simple controllers. This process is a fundamental step in the modelling of the helicopter here presented.

Position Control

In no-wind hover conditions, the tail rotor provides all the required antitorque compensation [151]. The helicopter has six degrees of freedom (three translations and three rotations). In order to achieve the position control various controllers are needed: the first on the longitudinal, the second on the lateral and finally on the vertical axis (directions). The effects of these position controllers are shown in Figure 7.25.

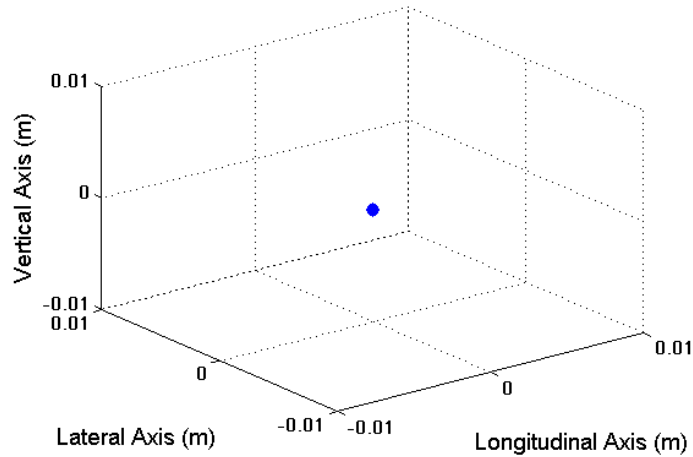


Figure 7.25: *Fuselage equilibrium position around the point $(0,0,0)$ in absence of external forces (vacuum after the action of the main and tail rotors torques).*

As it can be seen in Figure 7.25, the blue point represents the fuselage position during a simulation of 50 s, when the main and tail rotors torques are applied on the system. As a result, the fuselage position remains controlled in the original position i.e., the point $(0,0,0)$, being this equilibrium point in absence of external forces.

Rotation Control

When the main rotor blades rotate, the fuselage will rotate in the opposite direction if unopposed. An antitorque system is necessary to counteract this rotational force, the tail rotor system produces this antitorque action [151]. In fact, this must be modelled in order to obtain the desired rotational control. Several controllers must be considered for roll, pitch and yaw rotations, respectively. The impact of these controllers on the fuselage are shown, see Figure 7.26.

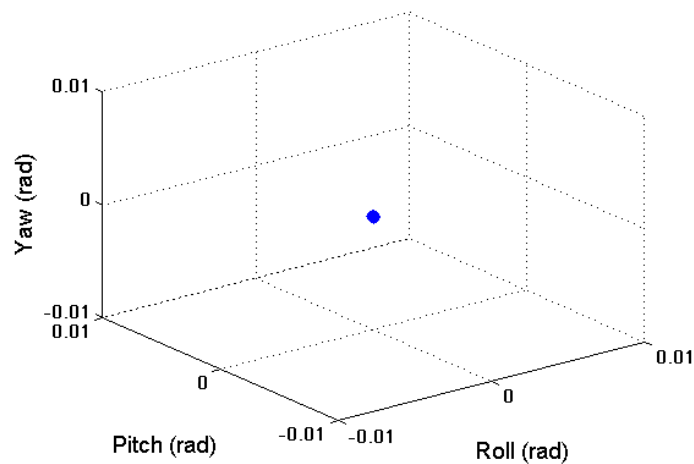


Figure 7.26: *Fuselage equilibrium around the point $(0,0,0)$ in vacuum after the action of the main and tail rotors torques.*

Figure 7.26 shows a blue point being the fuselage rotation during 50 s, when the main and tail rotors torques are applied on the system. Clearly, the fuselage remains constant in the original position i.e., the point $(0,0,0)$, it is the equilibrium point in absence of external forces.

7.4 Vibrations

In a rotorcraft system there are many sources of excitation that introduce forced vibrations. Such sources include the main and tail rotors, the transmission shafts, the engine, etc. The primary forced vibration source is the main rotor with the hinged blade system. Blade oscillations relative to all the hinges are also a source of vibrations.

Vibrations from the blades of the main and tail rotors are transmitted through the hubs. All parts of the helicopter are subjected to forced vibrations, but the amplitude of these vibrations differs. The amplitude magnitude depends on the stiffness of the structure, the closeness of the source of the exciting forces, their magnitude and points of application, and on the degree of closeness to resonance [92].

In [141], some reasons on why the control of vibrations is important are provided:

- Improvement of crew efficiency, and hence operational safety
- Improvement of passengers' comfort
- Improvement and reliability of the onboard avionic and mechanical equipment
- Reduction of airframe structural components fatigue

It is vital to control the vibration appearance throughout the design, development and in-service stages of a helicopter building project.

Helicopter vibrations can be classified into three categories: low, medium and high frequencies [151]:

a) Low frequency vibrations are the most common and originate at the main rotor in an out-of-track condition. These vibrations can be either as vertical or lateral. Vertical vibrations occur when one blade develops more lift than the rest at the same point of rotation in the rotor disc. These vibrations are felt through the airframe as a vertical bounce.

Lateral vibrations are also caused by the main rotor system due to an imbalance in the main rotor from either a difference of weight between the blades (spanwise imbalance) or a misalignment of the blades (chordwise imbalance).

b) Medium frequency vibrations are also inherent in all helicopter systems. An increase in normal medium frequency vibrations can be caused by a change in the aircraft's ability or by a loose aircraft component vibrating sympathetically with the rotor system. A rattling in the aircraft structure is an indication of their existence.

c) High frequency vibrations are characterized by a frequency too high to be measured accurately and are felt as a "buzz". High frequency vibrations are always present and sometimes difficult to determine when they become abnormal. Sources of high frequency vibrations can be anything rotating or vibrating at a speed equal to or greater than that of the tail rotor. Common sources are the tail rotor, engine, drive shaft, and barbell shaft, but the tail rotor is most commonly the culprit. Common tail rotor problems are an out-of-track condition, out-of-balance condition, or worn tail rotor components [151].

The main rotor is not a simple vibrating system as it consists of several rotating bodies linked by hinges. Its continuous state of rotation and its vibration motion is superimposed on a uniform rotation. A rotor as a vibrating system has identifying features such as blades (rigid or flexible), blades rigidly attached or through one of a variety of hinge systems, (whether in air or in vacuum) and general state of motion. Besides, an equivalent to the rotating force can be generated by other non-uniformities, and they can produce a difference in centrifugal force, as a consequence the blades rotate and an unbalance force appears. This is the most frequent cause of unbalance in helicopter rotors. Furthermore, the centrifugal restoring constraint in the lag motion of an articulated rigid blade about a drag hinge is weaker than that of the flap motion. This constraint is proportional to the square root of the lag hinge offset distance instead of being only marginally dependent on it [147]. Main rotor vibrations are transmitted to the fuselage and as a consequence, the fuselage will show several vibrations modes. Depending on which mode is excited, the amplitude of the vibration will vary with the position in the fuselage [144].

In a well-balanced rotor, there are a number of secondary sources of vibrations which should also be taken into account, for example, the flap hinges offset causes rolling and pitching vibrations that are transmitted to the fuselage. The dynamics behind this behaviour will be studied in here.

In order to study the vibrations appearing on the fuselage when the main and tail rotors start to rotate from rest up to a nominal value 44.4 rad/s and $5.25 \cdot 44.4$ rad/s, the rotors angular speed are generated without immediately response. These can be carried out due to the PID controllers implemented in VehicleSim. The reference value of the rotors angular speed are (`angular.speed + acceleration*t`). Their numerical values are defined at the beginning of the VehicleSim Lisp code. The initial rotor angular

speeds are zero and they are increased with an angular acceleration of 1 rad/s^2 , this allows to reach the nominal angular speed in 44.4 s. Once the desired speed reference values are reached, the acceleration is set to zero and the angular speeds remain constant at the prescribed values as Figure 7.27 shows.

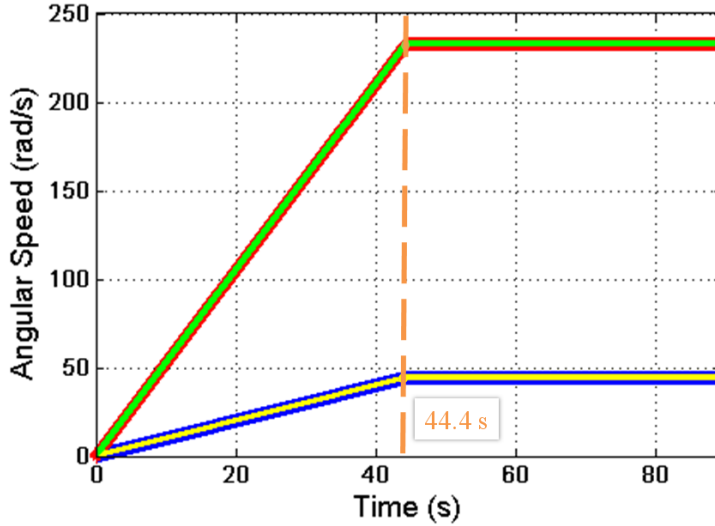


Figure 7.27: Rotor angular speeds. Yellow '-', the main rotor angular speed. Green '-', the tail rotor angular speed. The control signals needed to achieve them are shown on both cases. Blue '**', the reference signal for the main rotor speed. Red '**', the reference signal for the tail rotor speed.

7.4.1 Offset Flap Hinges' Vibrations

The following analysis is intended to highlight the main points needed in order to understand the vibrations at the flap hinge when there is certain offset distance in the rotor configuration. First of all, the flap hinge at the hub centre line is studied. Taking into account the elemental velocities (Figure 7.28), the normal velocity to the blade is given by $\Omega R \cos \beta$ and the vertical and radial components can be derived (see Figure 7.29).

The tangential speed is $R(d\beta/dt)$, and the radial speed is:

$$v_{rad} = -\frac{d\beta}{dt} R \sin \beta \quad (7.47)$$

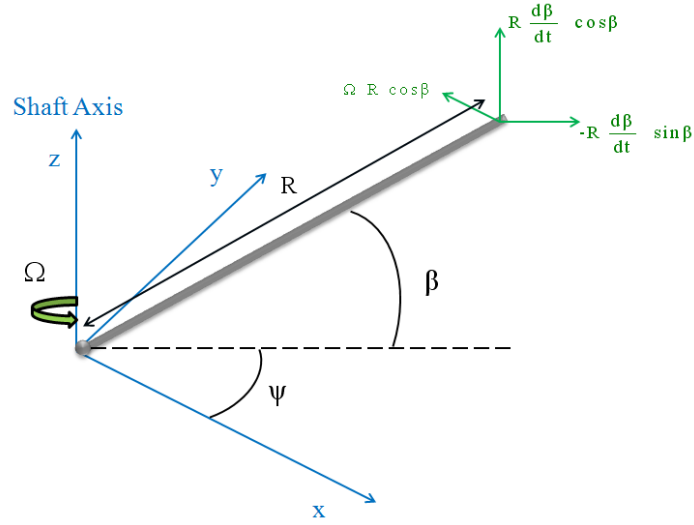


Figure 7.28: Blade flap element velocities, relative to the main rotor axes. This figure is done by the author and based on [150].

the vertical component of the velocity is given by:

$$v_{vert} = \frac{d\beta}{dt} R \cos\beta \quad (7.48)$$

In the calculation of the acceleration components on the element, the vertical component is treated separately.

Thus,

$$a_z = R \frac{d}{dt} \left(\frac{d\beta}{dt} \cos\beta \right) = R \frac{d^2\beta}{dt^2} \cos\beta + R \frac{d\beta}{dt} \frac{d}{dt} (\cos\beta) \quad (7.49)$$

Therefore,

$$a_z = R \frac{d^2\beta}{dt^2} \cos\beta - R \left(\frac{d\beta}{dt} \right)^2 \sin\beta \quad (7.50)$$

$a_z \cong R \ddot{\beta} \cos\beta$ since the second term is small and can be ignored.

Now, the accelerations are studied for a blade element when the hinge offset is taken into account and modelled in the system. The corresponding velocities are shown in Figure 7.30, (lag hinge is not considered).

Only the vertical acceleration a_z contributes to the hub moment:

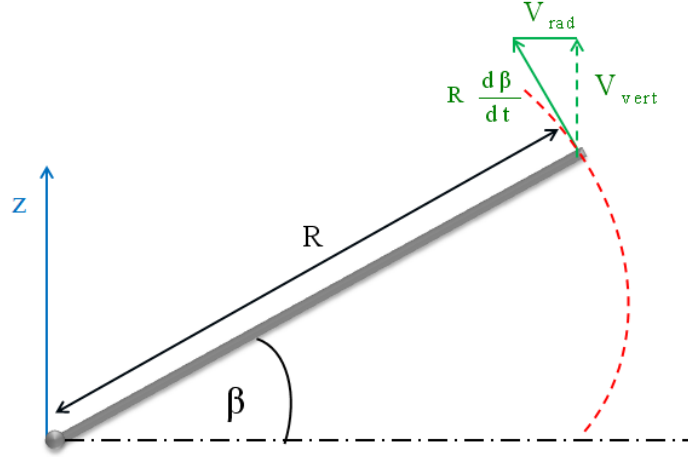


Figure 7.29: Vertical and radial velocities. This figure is drawn by the author and based on [150].

$$a_z = (R - eR) \frac{d}{dt} \left(\frac{d\beta}{dt} \cos\beta \right) = (R - eR) \left[\frac{d^2\beta}{dt^2} \cos\beta - \left(\frac{d\beta}{dt} \right)^2 \sin\beta \right] \quad (7.51)$$

The total vertical force appearing at the flap hinge is:

$$\Delta F = M_{MF} \left[\frac{d^2\beta}{dt^2} \cos\beta - \left(\frac{d\beta}{dt} \right)^2 \sin\beta \right] \quad (7.52)$$

where M_{MF} is the first moment of blade mass about the flap pin.

The centrifugal force is given by [150]:

$$\Delta C_F = \frac{M_{MF}}{\frac{1}{8}\rho V_T^2 R a C_0} \left[\frac{d^2\beta}{dt^2} \cos\beta - \left(\frac{d\beta}{dt} \right)^2 \sin\beta \right] = \chi \left[\frac{d^2\beta}{d\psi^2} - \left(\frac{d\beta}{d\psi} \right)^2 \beta \right] \quad (7.53)$$

being ρ the mass density on air, V_T the tip speed, R the overall blade radius, a the lift curve slope and finally, C_0 the blade chord at the theoretical hub root. χ is called the first moment of mass number.

Writing the flap angle β as:

$$\beta = a_0 - a_{1c} \cos\psi - b_{1s} \sin\psi \quad (7.54)$$

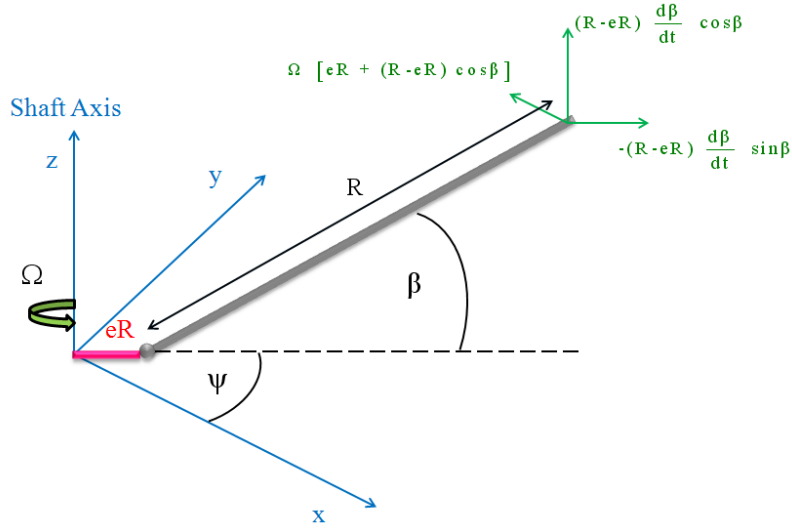


Figure 7.30: Speed components in a rotor with hinges' offset. This figure is plotted by the author and based on [150].

and obtaining its acceleration:

$$\frac{d^2\beta}{d\psi^2} = a_{1c}\cos\psi + b_{1s}\sin\psi \quad (7.55)$$

substituting this into equation (7.53), and assuming that $\beta (d\beta/d\psi)^2$ terms are negligible compared to the $d^2\beta/d\psi^2$ terms for small β ,

$$\Delta C_F = \chi (a_{1c}\cos\psi + b_{1s}\sin\psi) \quad (7.56)$$

The inertia forces have been obtained relative to the orbit equation (7.56), and the centrifugal forces act normal to the mechanical axis, see Figure 7.31.

The moment coefficient for the centrifugal force about the hub centre is $C_M = \gamma C_F$ where γ is the non-dimensional flap hinge offset eR/R [150].

The rolling moment due to the offset force (F) is given by $F\gamma R\sin\psi$ and the pitching moment is equal to $F\gamma R\cos\psi$ as Figure 7.32 shows. As a result, when the offset in the flap hinge is large, secondary vibrations will appear and transmitted to the fuselage. On the other hand, when the offset in the flap hinge is small, the hub centre will receive its effect [150].

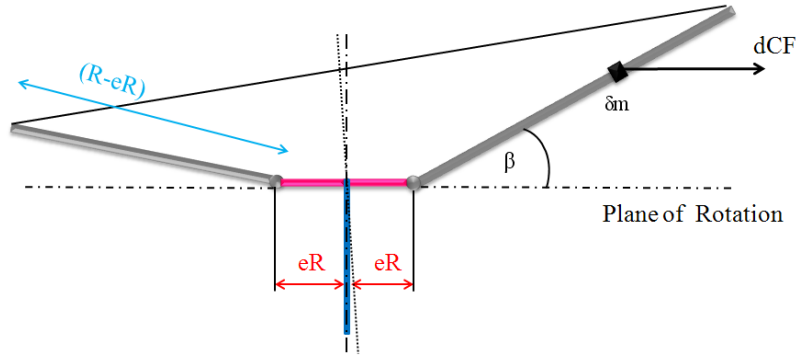


Figure 7.31: *Blade accelerations in an offset rotor. This figure is done by the author and based on [150].*

For the purpose of this study, two simulations will be carried out for two different offset values in order to check their influence on the fuselage vibrations appearance. The simulations are carried out for different initial flap angles on each blade; a vertical force appears as a consequence of the flap stiffness spring, unbalanced masses on the main rotor, vacuum, and no gravity are taken as simulation conditions. Also, the lag degree of freedom is not allowed in these cases, neither is the tail rotor angular rotation.

Six degrees of freedom are activated on the helicopter's fuselage. The mass of the blades on the main rotor are: $m_{bl1} = 31.06$ kg, $m_{bl2} = 31.26$ kg, $m_{bl3} = 29.96$ kg and $m_{bl4} = 31.16$ kg. The offset for the four blades is reduced to $eR = 0.01$ m. The initial flap angles are $\beta_1 = 0.0175$ rad, $\beta_2 = 0.075$ rad, $\beta_3 = 0.0675$ rad and $\beta_4 = 0.0875$ rad. The collective and cyclic feather angles are zero in the main rotor. The simulation time is 44.4 s, the initial angular speed on the main rotor is $\Omega = 0$ rad/s and the rotor has an angular acceleration of 1 rad/s². With this experimental set up, simulations are performed, and the corresponding vibrations appear on the fuselage, ready to be analyzed. These simulations conditions are just taken as example, being possible to produce fuselage vibrations with other several combinations of simulation conditions. In order to analyze the fuselage's vibrations, a Short Time Fourier Transform is applied (STFT). In mathematical terms, the STFT of a signal $X(t)$ can be defined as:

$$S_x(t, \omega) = \int_{-\infty}^{\infty} X(\tau) h(\tau - t) e^{-j\omega\tau} d\tau \quad (7.57)$$

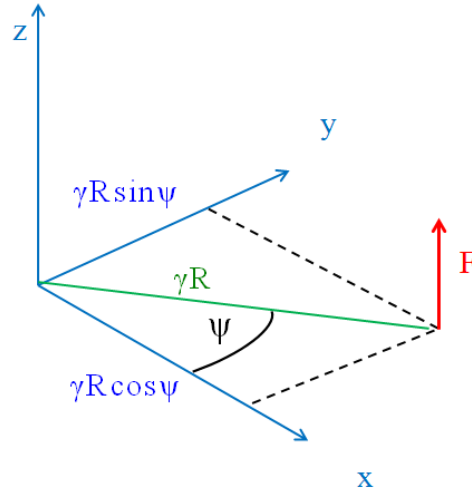


Figure 7.32: Conversion of offset hinge force to pitching and rolling moments. This figure is plotted by the author and based on [150].

$X(t)$ is the corresponding signal under study, and $h(t)$ is a finite support window function. The properties of the window function $h(t)$ have a significant effect on the STFT result and should be carefully chosen.

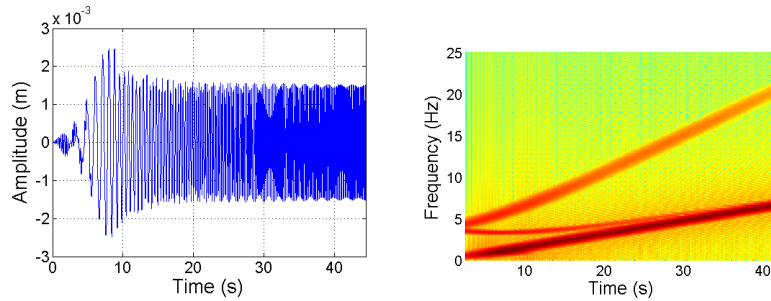


Figure 7.33: Left, fuselage oscillations on the X axis for $eR = 0.01$ m. Right, spectrogram of the vibrations shows various frequencies varying between 0 - 7 Hz, 4.5 - 21 Hz and 3.5 Hz, respectively.

Figure 7.33 shows the vibration and the spectrogram of frequencies on the fuselage's X axis. As it can be seen, there is a predominant frequency originated in the main rotor. Their values are between zero and 7 Hz, approximately. A second frequency between 4.5 Hz to 21 Hz is observed; it is caused by the different initial flap angles on each blade. Finally, a third frequency is detected around 3.5 Hz, it is generated by the inertial force and the centrifugal force on the blades. After 30 s or when the main rotor angular speed

7.4. VIBRATIONS

is around 20 rad/s its value takes the main rotor frequency. i.e., 7 Hz. The offset force is small and the angular speed is greater than 20 rad/s, its frequency is the main rotor frequency.

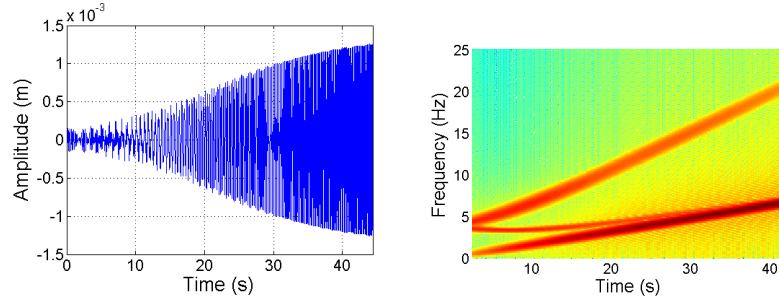


Figure 7.34: *Left, fuselage oscillations on the Y axis for $eR = 0.01$ m. Right, spectrogram of the vibrations shows various frequencies varying between 0 - 7 Hz, 4.5 - 21 Hz and 3.5 Hz, respectively.*

A similar analysis can be done for the fuselage's oscillations on the Y axis. The fuselage's vibration and the corresponding spectrogram are shown in Figure 7.34. Two predominant frequencies are identified as main rotor frequencies, their values are between zero and 7 Hz, approximately. A second frequency appears between 4.5 Hz to 21 Hz; it is caused by the different initial flap angles on each blade. Finally, a third frequency is detected around 3.5 Hz and after 30 s its value equals the main rotor frequency. The origin of this frequency is similar to the X axis case.

Now, a second simulation is carried out, with an offset $eR = 0.982$ m. The rest of parameters and conditions remain the same as in the previous case.

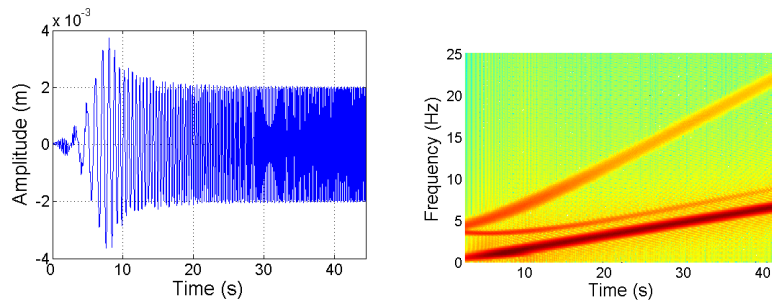


Figure 7.35: *Left, fuselage oscillations on the X axis for $eR = 0.982$ m. Right, spectrogram of the vibrations shows various frequencies varying between 0 - 7 Hz, 4.5 - 22.5 Hz and 3.5 - 9 Hz, respectively.*

The main purpose of this second simulation for a higher offset value is to detect secondary vibrations around the X and Y axis on the fuselage as a consequence of the offset force. The results of the simulation are shown in Figure 7.35, this is the vibrations and the frequencies spectrogram for the fuselage around the X axis. The spectrogram shows three predominant frequencies which come from the main rotor, (their values are between zero and 7 Hz, approximately). A second frequency between 4.5 Hz to 22.5 Hz is also observed, it is generated by the different initial flap angles. A third frequency is detected and values are between 3.5 Hz to 9 Hz, approximately. This is caused by the high offset on the flap hinge, being in this case, a value different to the main rotor frequency.

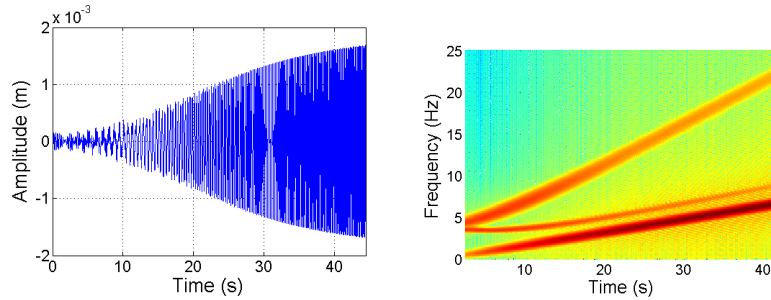


Figure 7.36: *Left, fuselage oscillations on the Y axis for $eR = 0.982$ m. Right, spectrogram of the vibrations shows various frequencies varying between 0 - 7 Hz, 4.5 - 21 Hz and 3.5 - 9 Hz, respectively.*

When a higher value of offset in the flap hinge is introduced, the vibrations that appear on the fuselage Y axis can be studied as well. The corresponding vibration and the spectrogram are shown in Figure 7.36. Two predominant frequencies are clearly identified: vibrations on the fuselage due to the main rotor have values between zero and 7 Hz. A second frequency between 4.5 Hz to 21 Hz is also present, it is caused by the different initial flap angles. Finally, a third frequency is observed between 3.5 Hz and 9 Hz, approximately. This is caused by the offset forces and its effects on the fuselage.

Figure 7.37 shows a comparison of the previous cases. On sections a) and c) the spectrograms for $eR = 0.01$ m and b) and d) for $eR = 0.982$ m. As it can be seen, when the offset on the flap hinge is high there are new spectral components when the main rotor angular speed is 44.4 rad/s (black circles mark). On the other hand, if the offset on the flap hinge is small these spectral components take similar values as to the main rotor, (blue circles) clearly, the flap hinge offset force generates a moment that induces

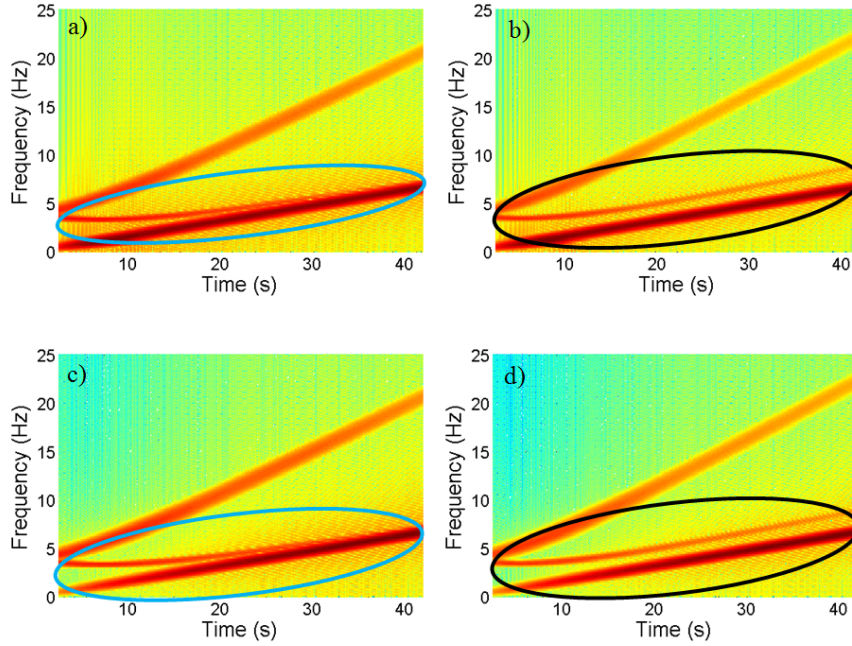


Figure 7.37: *a) and c) show the spectrograms for $eR = 0.01$ m cases and b) and d) show the spectrogram for $eR = 0.982$ m cases.*

vibrations on the fuselage's X and Y axis.

7.4.2 Lag Hinge Vibrations

In this section, the influence of main rotor lag hinge vibrations on the fuselage is studied and analyzed. Assume a force F applied to blade of length r_F in parallel to the rotor disc. The blade will move due to this force.

The equation of motion in this case is of the form:

$$I_D \frac{d^2 \xi}{dt^2} = r_F F \quad (7.58)$$

I_D is the blade second moment of mass about the lag hinge. The resultant force R at the root normal to the blade axis is the sum of the inertia forces along the blade and the impressed force F . The inertia force is then:

$$\int_0^R \delta m r \frac{d^2 \xi}{dt^2} = M_{mD} \frac{d^2 \xi}{dt^2} \quad (7.59)$$

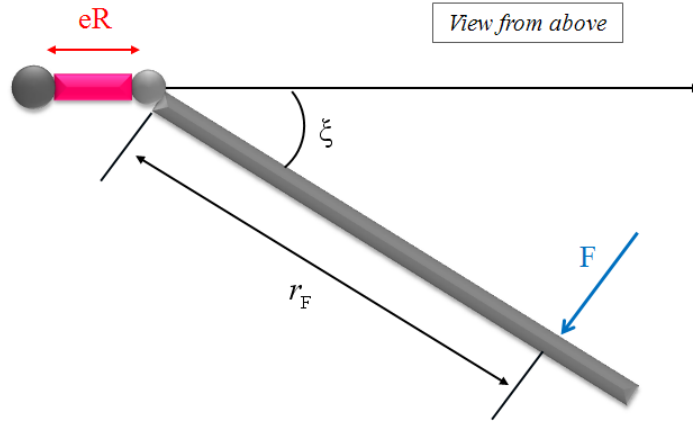


Figure 7.38: Sketch of the force applied on the blade with a lag hinge. This figure is drawn by the author and based on [150].

M_{mD} is the first mass moment about lag hinge.

$$R = F - M_{mD} \frac{d^2 \xi}{dt^2} \quad (7.60)$$

$$\frac{R}{F} = 1 - \frac{r_F M_{mD}}{I_D} \quad (7.61)$$

Note that $(R/F) = 0$ when $(r_F M_{mD}/I_D) = 1$. On the other hand, $M_{mD} = r_{c.g} m_b$ and $I_D = r_G^2 m_b$ i.e.,

$$r_F r_{c.g} m_b = r_G^2 m_b \quad (7.62)$$

$r_{c.g}$ is the radius of centre of gravity of the blade, m_b is the mass of the blade and r_G is the radius of gyration of the blade.

$$r_F = \frac{r_G^2}{r_{c.g}} \quad (7.63)$$

The radius of gyration about a given axis can be computed in terms of the mass moment of inertia around that axis, and the total mass; $r_G^2 = I/m_b$. The ratio $r_G^2/r_{c.g}$ is known as the "centre of percussion", and is the point where an applied dynamic load will cause movement without root end shear [150]. The dynamic load is introduced in the simulation by unbalance on the blade's centres of mass. On the other hand, when the main rotor reaches certain angular speed, the ratio $r_G^2/r_{c.m}$ is equal to 1 (i.e., $(R/F) = 0$) as well as the dynamic load as the resultant force R is zero.

If the centre of mass of each blade is located at different points, this configuration will introduce a dynamic load on the main rotor as well as vibrations on the fuselage. The flap degree of freedom in this case is not modelled in order to study only lag hinge originated vibrations.

The six degrees of freedom are allowed on the helicopter's fuselage and the mass of the blades on the main rotor and the tail are equally balanced. The centre of mass of the four blades on the main rotor are unbalanced as $y_{bl1} = 2.9846$ m, $y_{bl2} = 2.7846$ m, $y_{bl3} = 2.8846$ m and $y_{bl4} = 2.6846$ m. Collective and cyclic feather angles are zero in the main rotor. The tail rotor angular rotation is deactivated. The simulation time is 44.4 s, the initial angular speed is zero and an acceleration of 1 rad/s^2 is introduced in the simulation. This configuration is enough to generate vibrations on the fuselage. Several other combinations could be chosen. This particular one is provided as means of illustration and validation of the model.

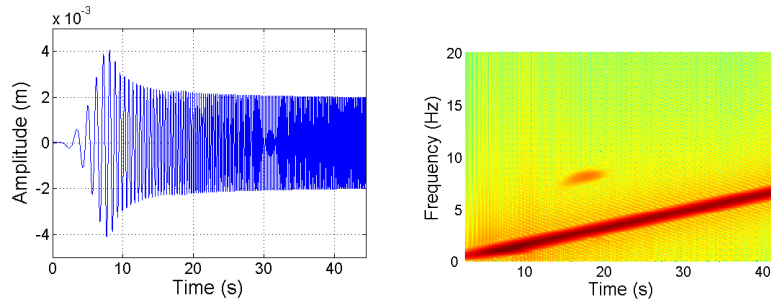


Figure 7.39: *Left, fuselage oscillations on the X axis for $y_{bl1} = 2.9846$ m, $y_{bl2} = 2.7846$ m, $y_{bl3} = 2.8846$ m, $y_{bl4} = 2.6846$ m. Right, spectrogram of the vibrations shows various frequencies varying between 0 - 7 Hz, 7 - 9 Hz, respectively.*

From the spectrogram of frequencies shown in Figure 7.39, the signal on the fuselage's X axis is a predominant frequency which comes from the main rotor, its values are between 0 and 7 Hz, approximately. As it can be seen, a second frequency is detected around 7 Hz and 9 Hz, being its time interval 5 s, after this time, the signal disappears. This frequency appears because during this time interval, the ratio $(R/F) \neq 0$ and so the applied dynamic load generates a force at the blade's root axis and it is transmitted to the fuselage in the form of vibration.

Similar analysis is carried out for vibrations appearing on the fuselage on the Y direction. In Figure 7.40, a predominant frequency is observed between 0 and 7 Hz, it is originated

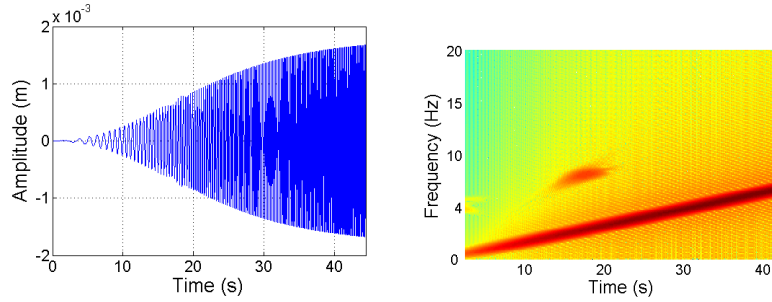


Figure 7.40: Left, fuselage oscillations on the Y axis for $y_{bl1} = 2.9846$ m, $y_{bl2} = 2.7846$ m, $y_{bl3} = 2.8846$ m, $y_{bl4} = 2.6846$ m. Right, spectrogram of the vibrations shows various frequencies varying between 0 - 7 Hz, 7 - 9 Hz, respectively.

at the main rotor. Furthermore, a second frequency is shown around 7 Hz and 9 Hz, being its time interval 7 s, after this time the signal disappears. Its origin is similar to the X axis case.

A second simulation is carried out with the same conditions and parameters as in the previous simulations, but the unbalanced centre of mass is $y_{bl1} = 3.9846$ m, $y_{bl2} = 1.7846$ m, $y_{bl3} = 3.8846$ m, $y_{bl4} = 1.6846$ m for the blade one, two, three and four on the main rotor, respectively.

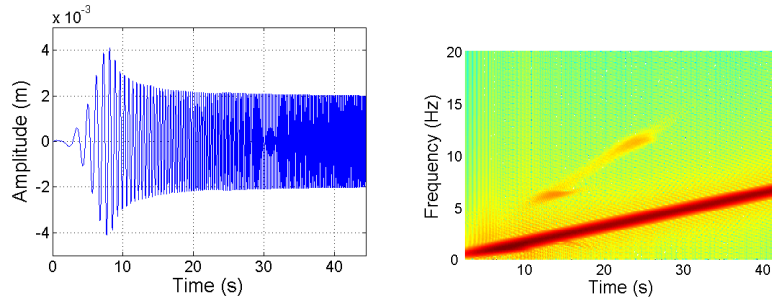


Figure 7.41: Left, fuselage oscillations on the X axis for $y_{bl1} = 3.9846$ m, $y_{bl2} = 1.7846$ m, $y_{bl3} = 3.8846$ m, $y_{bl4} = 1.6846$ m. Right, spectrogram of the vibrations shows various frequencies varying between 0 - 7 Hz and 6 - 12 Hz.

From the spectrogram of frequencies in Figure 7.41, the fuselage's oscillations around the X axis show a predominant frequency which is originated at the main rotor, its values are between 0 and 7 Hz, approximately. A second frequency between 6 Hz and 12 Hz is also observed, its interval of time is 10 to 26 s. In comparison to the previous simulation, it is clear that if the unbalance of centre of masses is increased, the frequency

of vibrations appearing on the fuselage also increases. This vibration appears during certain period of time after that, the ratio R/F is restored and the vibration disappears.

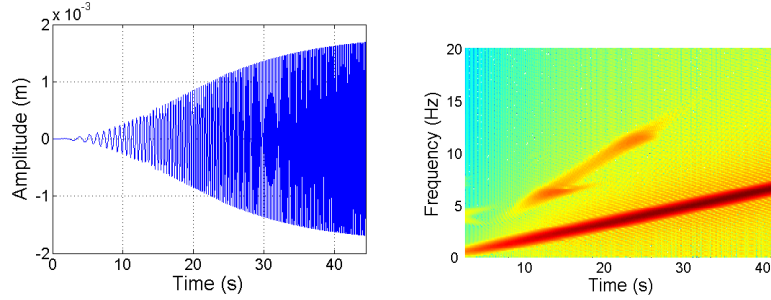


Figure 7.42: Left, fuselage oscillations on the Y axis for $y_{bl1} = 3.9846$ m, $y_{bl2} = 1.7846$ m, $y_{bl3} = 3.8846$ m, $y_{bl4} = 1.6846$ m. Right, spectrogram of the vibrations shows various frequencies varying between 0 - 7 Hz and 5 - 12 Hz.

The vibration appearing around the fuselage's Y axis can be studied in similar manner. From figure 7.42 it can be seen a predominant frequency between 0 and 7 Hz approximately, it is originated at the main rotor. Furthermore, a second frequency appears around 5 - 12 Hz, during the time interval of 10 - 26 s, after this time, the signal disappears. Its origin is of similar nature at those on the X axis case.

Figure 7.43 shows a comparison of these cases, a) and c) show the spectrograms for the first simulation when the unbalance of centre of mass is given by $y_{bl1} = 2.9846$ m, $y_{bl2} = 2.7846$ m, $y_{bl3} = 2.8846$ m, $y_{bl4} = 2.6846$ m. The tail rotor blades are also unbalanced as: $z_{bltl1} = 0.5672$ m and $z_{bltl2} = 0.5772$ m. b) and d) show the spectrograms for the simulation when the unbalance of centre of masses is $y_{bl1} = 3.9846$ m, $y_{bl2} = 1.7846$ m, $y_{bl3} = 3.8846$ m, $y_{bl4} = 1.6846$ m. The tail rotor blades are unbalanced as well: $z_{bltl1} = 0.5672$ m and $z_{bltl2} = 0.5772$ m. When the main rotor is accelerated from 0 rad/s to 44.4 rad/s there is an applied dynamic load causing a moment, showing its effect between 10 rad/s to 21 rad/s, as it is indicated in blue arrows (Figure 7.43). In this interval of angular speeds, the ratio $r_F = (r_G^2/r_{c.m.}) \neq 1$ and so $(R/F) \neq 0$. If the angular speed is greater than 21 rad/s, the ratio $r_F = (r_G^2/r_{c.m.}) = 1$ and as a consequence, $(R/F) = 0$ and the vibration disappears. On the other hand, if the unbalance of masses is increased, the frequencies also rise. In addition to this, the vibrations persist for a longer time than in the previous case (blue arrows). The impact of the unbalance of masses on the fuselage is clear to be observed, as Figure 7.43 shows.

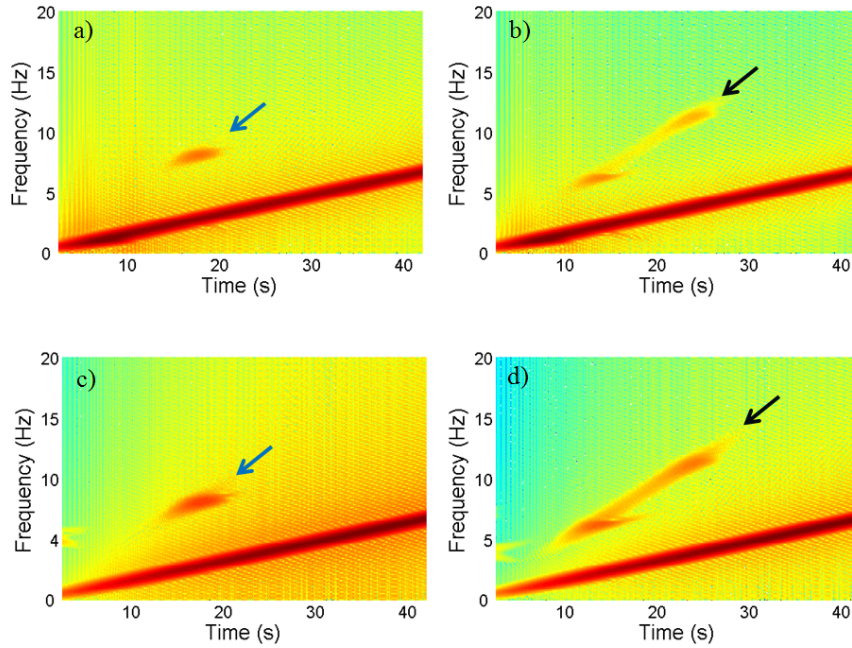


Figure 7.43: a) and c) show the spectrograms for the first simulation when the centre of mass unbalance is given by $y_{bl1} = 2.9846$ m, $y_{bl2} = 2.7846$ m, $y_{bl3} = 2.8846$ m, $y_{bl4} = 2.6846$ m. b) and d) show the spectrograms for the second simulation when the unbalance is given by $y_{bl1} = 3.9846$ m, $y_{bl2} = 1.7846$ m, $y_{bl3} = 3.8846$ m, $y_{bl4} = 1.6846$ m.

7.4.3 Rotors Induced Fuselage's Vibrations

In this section, the vibrations when the flap and lag modes are coupled will be studied when the main and tail rotor have a constant angular speed. In this case, the vibrations are generated by unbalance of masses in both rotors; the mass of the blades on the main rotor are $m_{bl1} = 31.06$ kg, $m_{bl2} = 31.26$ kg, $m_{bl3} = 29.96$ kg and $m_{bl4} = 31.16$ kg and on the tail rotor they are; $m_{blt1} = 6.212$ kg and $m_{blt2} = 6.222$ kg. The collective and cyclic feather angles are zero in the main rotor. The flap on the tail rotor is given by $a_0 = 0.01$ rad, $a_1 = 0.01$ rad and $b_1 = 0.01$ rad and the collective angle is 0.01 rad. The simulation time is 44.4 s, and the angular speed is constant at 44.4 rad/s and the acceleration is zero.

From the spectrogram of frequencies shown in Figure 7.44, the oscillation on the fuselage's X axis shows two predominant frequencies which are originated at the main rotor

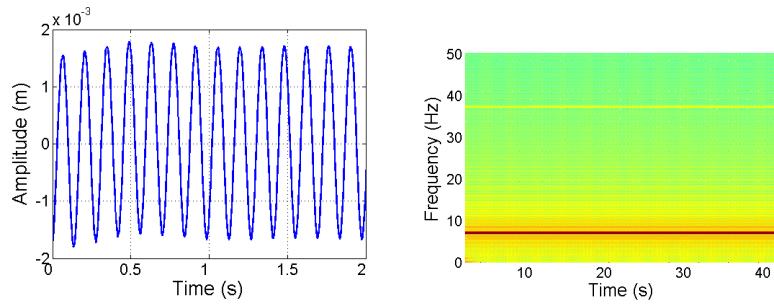


Figure 7.44: *Left, fuselage vibrations on the X axis for $m_{bl1} = 31.06$ kg, $m_{bl2} = 31.26$ kg, $m_{bl3} = 29.96$ kg and $m_{bl4} = 31.16$ kg and $m_{bltl1} = 6.212$ kg and $m_{bltl2} = 6.222$ kg. Right, spectrogram of the vibrations shows various frequencies at around 7 Hz and 37 Hz.*

(its value is equal 7 Hz, approximately) and at the tail rotor, in this case, the value is around of 37 Hz.

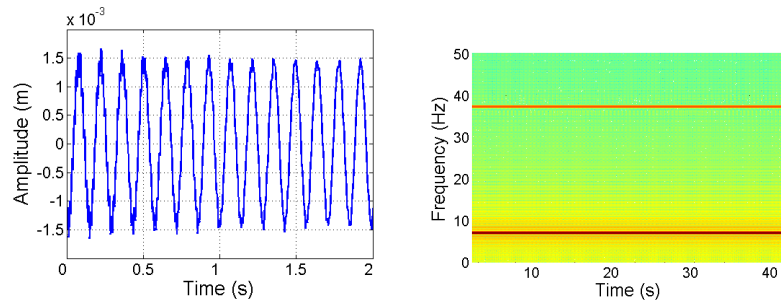


Figure 7.45: *Left, fuselage vibrations on the Y axis for $m_{bl1} = 31.06$ kg, $m_{bl2} = 31.26$ kg, $m_{bl3} = 29.96$ kg and $m_{bl4} = 31.16$ kg and $m_{bltl1} = 6.212$ kg and $m_{bltl2} = 6.222$ kg. Right, spectrogram of the vibrations shows various frequencies varying around 7 Hz and 37 Hz.*

Similar analysis can be carried out for the spectrogram of frequencies shown in around the Y axis on the fuselage (see Figure 7.45). Two predominant frequencies are presented and the origin are the main and tail rotors', similarly to the X axis case before.

7.5 Chapter Summary

The aim of this chapter is to demonstrate that the dynamical model built in VehicleSim behaviour coincides with that predicted by the theory. VehicleSim can be regarded as typical symbolic mechanical multibody modelling software, which writes ready-to-run simulation code. In fact, the linear and nonlinear equations for flap, lag and coupled flap-lag motions as well as feather motion have been obtained and validated.

In the present study, the effects of various values of blade offset, springs stiffness and damping coefficients fitted on the blades' hinges were studied for the flap and lag cases, in order to present a dynamic model of blade's motion. In these cases, the obtained results have proven to be correct by theory validation. As is the case with many nonlinear systems, the study of complex phenomenon on the dynamic structures is investigated via the eigenvalues of linearised models that are associated to the equilibrium of the nonlinear system. VehicleSim is used to generate the time histories of the nonlinear equations of motion and it also derives the linearised state-space models. The nonlinear equations are stored into two files with extensions .erd and .bin, the linearised equations of motion are stored as a Matlab file and the root locus was obtained to study the stability of the flap, lag as well as the fuselage.

The coupled vertical movement between the fuselage and the flap degree of freedom was studied. Several modes of oscillations were analyzed via eigenvalues and eigenvectors analysis. The influence of the mass ratio $mass_{blade}/mass_{fuselage}$ on the coupled modes has been demonstrated. The influence of the fuselage on the flap motion was also analyzed and studied as a consequence of the gyroscopic effect on the fuselage.

It is worth recalling that two studies showed a coupling between the fuselage and the flap degree of freedom. A third study was performed in order to analyze the influence of the lag degree of freedom on the fuselage. The simulations carried out in this chapter using the VehicleSim model showed good agreement with the theoretical findings existing in the literature.

The tail rotor and the effect of the delta three angles have also been studied for various cases. It was shown how the flap frequencies increased as a function of the advance ratio as a consequence of the delta three angle coupling. Furthermore, maximum flap amplitude and feather angle decrease was shown as a result of the existing positive

coupling.

The control of the six degrees of freedom of the helicopter has been implemented in the model by using PID controllers. This procedure was a priority task (in order to maintain the equilibrium on the system). The control action was shown for the translational and the rotational degrees of freedom, providing the system with the required equilibrium around the initial position. Additionally, the ratio between the angular speed on the main and tail rotors was modelled with immediate response, this ratio was achieved when both rotor were accelerated, being possible to simulate a delay on the rotors as a consequence of the engine response. On the other hand, the vibrations originated at the rotors were simulated and their effects on the fuselage were studied. Three different cases were analyzed and presented and in all of them, a clear impact of these vibrations into the fuselage was shown.

In conclusion, a comprehensive dynamical study for a helicopter with Sikorsky configuration was presented. The simulations were designed for different cases in order to validate the helicopter model obtained. The tests carried out proved the correct implementation of the model and its readiness to be used in future works for further modelling or control systems implementation purposes.

Chapter 8

Sikorsky Model in Presence of External Perturbations

The purpose of this chapter is to study the aerodynamic environment together with gravity on the helicopter as well as to study the effect the main rotor inclination has on the helicopter when aerodynamic forces are considered. As mentioned in previous chapters, vibrations play a relevant role in helicopter's performance. The effects are individually analyzed by assuming that the helicopter's nominal configuration is as described in Chapter 6. The analysis is carried out purely through simulations. The equations of motion are obtained for the cases of flap, lift, lag and drag forces. An aerodynamic analysis is carried out for a six degrees of freedom fuselage, a three degrees of freedom (flap, lag and feather) main rotor blades and flap-feather on the tail rotor coupling. Blade elements are modelled on the main and tail rotors to simulate the flight conditions of hover, climb, descent and forward flight. Each one of these flight conditions is simulated and the results are shown. After that, different trajectories are represented in forward flight, as well as combinations of several flight conditions so that the model can describe trajectories in a satisfactory manner. In addition to this, the drift effect is also considered and analyzed. The vibrations as a consequence of the varying rotating main rotor speed are carefully studied, they are analyzed in absence of aerodynamic forces. Finally, the impact of vibrations in hover flight is studied on the fuselage.

8.1 Earth/Ground Modelling

The first external force that is considered is the gravity. In order to restore the initial equilibrium under the action of this force, the ground is simulated on the fuselage (as it was described in Chapter 6). The state's time history is obtained by nonlinear simulation in VehicleSim and it is also used to visualise the result by using Matlab. The helicopter's position can be represented in a spatial representation easily and the main simulation results can be shown in only one graph. A simulation is carried out in VehicleSim when main and tail rotors are rotating with their corresponding angular speeds 44.4 rad/s and 233.1 rad/s respectively, the time simulation is 50 s. In order to prove that the ground action is well implemented in this model, Figure 8.1 is shown. As it can be seen, the helicopter remains on the vertical position along the Z axis at $Z = 0$ m. Without the ground action implemented on the fuselage, Figure 8.1 should have shown a vertical displacement along the Z axis (free fall).

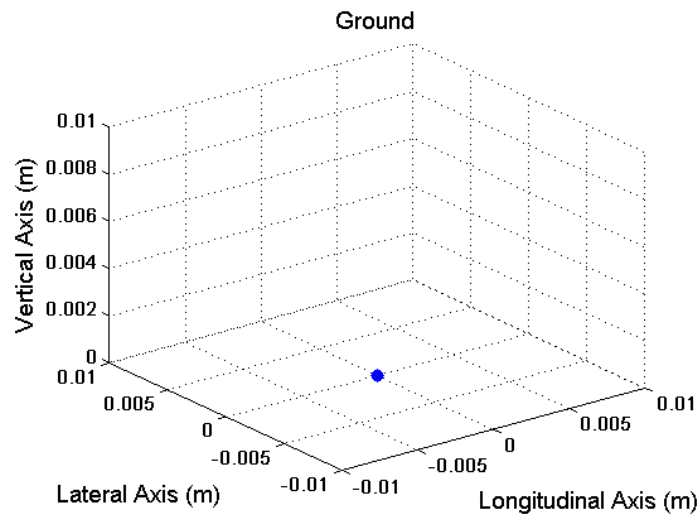


Figure 8.1: 3-D representation of the helicopter's position under the influence of ground force. Blue point represents the helicopter's position.

8.2 Aerodynamic Load and Flight

In this section, simulations are carried out taking into account the following conditions: an articulated main rotor has its blades attached to the hub with flap and lag hinges. The

flap hinge is usually offset from the centre of rotation because of mechanical constraints and to improve the helicopter handling qualities. The lag hinge must be offset in order for the shaft to transmit torque to the rotor. The purpose of the flap and lag hinges is to reduce the root blade loads. With a lag hinge, a mechanical lag damper to avoid a mechanical instability called ground resonance is needed [140]. As a consequence, the springs on the flap and lag hinges included in the dynamical model are not needed as the restoring moments are provided by the aerodynamic forces, the lag damper remains.

8.2.1 Aerodynamic Load Equations

The nonlinear equations of motion for the aerodynamic model can be obtained from VehicleSim. In order to validate these, they will be compared to those predicted by theoretical studies. The results for the case of uncoupled flap and lag degrees of freedom are presented in here. It is convenient to bear in mind that the case under study is for rigid blades, being flexibility and torsion two effects not considered in this work. The aerodynamic equations are obtained for one blade in hover flight conditions and the main rotor angular speed is given by restriction in order to obtain simpler equations. The corresponding aerodynamic forces are applied to the point $x_a = 0.0675$ m being this the coordinate of the blade's centre of pressure i.e., 3/4 chord [98]. The distance along the Y axis on the blades is $y_a = 3.24$ m.

Flap Equation with Aerodynamical Load Validation

Flap is the first degree of freedom on the main rotor blade under the influence of the aerodynamic forces to be studied. A restoring moment is provided by the lift force and this induces flap. As a result, a vertical force appears on the helicopter, a flap offset is also considered. Taking all these into account the equations of motion are obtained after a simulation is run.

As it was mentioned in Chapter 7, one of the most comprehensive surveys on rotor dynamics is proposed by [141], where the flap motion was represented by a second order differential equation of the form:

$$B\ddot{\beta} + \Omega^2 (B\cos\beta + M_b e x_g R^2) \sin\beta = M_A \quad (8.1)$$

where B is the moment of the inertia around the flap axis and M_A is the aerodynamic moment and M_b is the blade mass. In here, the position vector of the blade's c.g (centre of gravity) is $r_g = x_g R$. In our system, the blade's centre of gravity is considered to lie on the longitudinal axis, so it can be written as $r_g = y_g$. The equations are obtained with the term eR instead of eR^2 , as it was explained in Chapter 7.

With the model provided including the aerodynamical load, a simulation is carried out in VehicleSim. The software provides the nonlinear equation of motion corresponding to the dynamic and aerodynamic loads and the rotor's provided geometry. Equation (8.2) is the aerodynamic equation for a blade with flap degree of freedom and it can be validated by comparing it to equation (8.1).

$$\begin{aligned} & \ddot{\beta} (I_{blx} + m_{bl} \cdot y_{bl}^2) + \Omega^2 \cdot (((I_{blz} - I_{bly}) + m_{bl} \cdot y_{bl}^2) \cdot \cos\beta + (m_{bl} \cdot eR \cdot y_{bl})) \cdot \sin\beta \\ & = dy_a \cdot \frac{1}{2} \cdot \Omega^2 \cdot \rho \cdot chord \cdot (-(-2 \cdot \pi \cdot x_a \cdot (y_a^2 + eR^2) \cdot \sin(2 \cdot \pi \cdot q_{bl}) - 2 \cdot \pi \cdot (\cos(2 \cdot \pi \cdot q_{bl}) \cdot (y_a^3 + eR^3 \cdot \cos(2 \cdot \pi \cdot q_{bl})) + eR^3 \cdot \sin(2 \cdot \pi \cdot q_{bl})^2) + eR \cdot (y_a \cdot (-4 \cdot \pi \cdot x_a \cdot \sin(2 \cdot \pi \cdot q_{bl}) + eR \cdot (4 \cdot \pi - 4 \cdot \pi \cdot \cos(2 \cdot \pi \cdot q_{bl})^2) + y_a \cdot (2 \cdot \pi - \cos(2 \cdot \pi \cdot q_{bl}) \cdot (4 \cdot \pi + 2 \cdot \pi \cdot \cos(2 \cdot \pi \cdot q_{bl})) - 2 \cdot \pi \cdot \sin(2 \cdot \pi \cdot q_{bl})^2)) + eR \cdot (2 \cdot \pi \cdot eR - y_a \cdot (2 \cdot \pi \cdot \cos(2 \cdot \pi \cdot q_{bl}) + 4 \cdot \pi \cdot \sin(2 \cdot \pi \cdot q_{bl})^2)))))) \cdot \text{atan}(v_{ih}/\Omega \cdot (y_a + eR)) \end{aligned} \quad (8.2)$$

$q_{bl} = (nblades - blade_number_1)/nblades$, ρ is the air density, $chord$ is the chord of the blade, dy_a is the length differential interval, and v_{ih} is the hover induced velocity.

If a comparison between equations (8.1) and (8.2) is performed (although (8.2) is a more extensive equation), similarities between both can be found:

- $B\ddot{\beta} \cong (I_{blx} + m_{bl} \cdot y_{bl}^2) \ddot{\beta}$
- $\Omega^2 (B\cos\beta + M_b e x_g R^2) \sin\beta \cong \Omega^2 \cdot (((I_{blz} - I_{bly}) + m_{bl} \cdot y_{bl}^2) \cdot \cos\beta + (m_{bl} \cdot eR \cdot y_{bl})) \cdot \sin\beta$
- M_A is equal to the terms on the right hand side in equations (8.2)

Taking into account the previous considerations about the centre of gravity, after some simplifications, both equations (8.1) and (8.2) are shown to be equal.

Lag Equation with Aerodynamical Load Validation

The nonlinear lag aerodynamic equation can be obtained in a similar way using VehicleSim. It is compared to those available in the literature. In order to validate the equations obtained by VehicleSim, the following accepted expression for pure lag motion is considered [141]:

$$C\ddot{\xi} + M_b e x_g \Omega^2 R^2 \sin\xi = N \quad (8.3)$$

C is the moment of the inertia about the lag axis, N is the aerodynamic lag moment and M_b is the blade mass.

Equation (8.4) is the aerodynamic equation for a blade with lag, in order to validate it, it is compared to expression (8.3).

$$\begin{aligned} \ddot{\xi}(I_{blz} + m_{bl} \cdot y_{bl}^2) + \Omega^2 \cdot eR \cdot m_{bl} \cdot y_{bl} \cdot \sin\xi = & dy_a \cdot \frac{1}{2} \cdot \Omega^2 \cdot \rho \cdot chord \cdot (-x_a \cdot \sin(2 \cdot \pi \cdot \\ & q_{bl}) \cdot (eR \cdot (2 \cdot y_a \cdot (\delta_0) + eR \cdot (\delta_0)) + y_a \cdot (y_a \cdot (\delta_0) - atan(v_{ih}/\Omega \cdot (y_a + eR)) \cdot (y_a \cdot (\delta_1 \\ & + \delta_2 \cdot (-atan(v_{ih}/\Omega \cdot (y_a + eR)))) + eR \cdot (2 \cdot \delta_1 + \delta_2 \cdot (-2 \cdot atan(v_{ih}/\Omega \cdot (y_a + eR)))) \\ &)) + eR \cdot (eR \cdot (y_a \cdot (2 \cdot \delta_0 - 2 \cdot (\delta_0) \cdot \sin(2 \cdot \pi \cdot q_{bl})^2 + 2 \cdot atan(v_{ih}/\Omega \cdot (y_a + eR)) \cdot (\delta_1 \\ & \cdot \sin(2 \cdot \pi \cdot q_{bl})^2 + \delta_2 \cdot atan(v_{ih}/\Omega \cdot (y_a + eR)))) + x_a \cdot \sin(2 \cdot \pi \cdot q_{bl}) \cdot atan(v_{ih}/\Omega \cdot (y_a \\ & + eR)) \cdot (\delta_1 + \delta_2 \cdot (-atan(v_{ih}/\Omega \cdot (y_a + eR)))) + eR \cdot (\delta_0 - \sin(2 \cdot \pi \cdot q_{bl})^2 \cdot (\delta_0))) + y_a \\ & \cdot (-eR \cdot (atan(v_{ih}/\Omega \cdot (y_a + eR)) \cdot (2 \cdot \delta_1 + \delta_2 \cdot (2 \cdot \sin(2 \cdot \pi \cdot q_{bl})^2 \cdot atan(v_{ih}/\Omega \cdot (y_a + \\ & eR)))))) + y_a \cdot (\delta_0 - atan(v_{ih}/\Omega \cdot (y_a + eR)) \cdot (\delta_1 \cdot \cos(2 \cdot \pi \cdot q_{bl})^2 + \delta_2 \cdot (-\cos(2 \cdot \pi \cdot \\ & q_{bl})^2 \cdot atan(v_{ih}/\Omega \cdot (y_a + eR)))) - \sin(2 \cdot \pi \cdot q_{bl})^2 \cdot (\delta_0))) - \cos(2 \cdot \pi \cdot q_{bl}) \cdot (y_a \cdot (eR^2 \\ & \cdot (2 \cdot (\delta_0) \cdot \cos(2 \cdot \pi \cdot q_{bl}) + \delta_2 \cdot (atan(v_{ih}/\Omega \cdot (y_a + eR))^2)) + y_a \cdot (y_a \cdot (\delta_0 - atan(v_{ih} \\ & /\Omega \cdot (y_a + eR)) \cdot (\delta_1 + \delta_2 \cdot (-atan(v_{ih}/\Omega \cdot (y_a + eR)))))) + eR \cdot (2 \cdot \delta_0 + atan(v_{ih}/\Omega \cdot \\ & (y_a + eR)) \cdot (-2 \cdot \delta_1 - \delta_2 \cdot (-2 \cdot atan(v_{ih}/\Omega \cdot (y_a + eR)))))) + eR \cdot (y_a \cdot eR \cdot (\delta_0 - \\ & atan(v_{ih}/\Omega \cdot (y_a + eR)) \cdot (\delta_1 \cdot (1 + 2 \cdot \cos(2 \cdot \pi \cdot q_{bl})) + \delta_2 \cdot (-2 \cdot \cos(2 \cdot \pi \cdot q_{bl}) \cdot \\ & atan(v_{ih}/\Omega \cdot (y_a + eR)))) + \cos(2 \cdot \pi \cdot q_{bl}) \cdot (eR^2 \cdot (\delta_0) + y_a^2 \cdot (\delta_0 - atan(v_{ih}/\Omega \cdot \\ & (y_a + eR)) \cdot (\delta_1 + \delta_2 \cdot (-atan(v_{ih}/\Omega \cdot (y_a + eR))))))))) \end{aligned} \quad (8.4)$$

$q_{bl} = (nblades - blade_number_1)/nblades$, ρ is the air density, $chord$ is the blade's chord, dy_a is the length differential interval, v_{ih} is the induced velocity in hover and δ_0 , δ_1 and δ_2 are the corresponding drag coefficients values.

A term by term comparison between equation (8.3) (theory prediction) and equation (8.4) is carried out:

- $C\ddot{\xi} \cong (I_{blz} + m_{bl} \cdot y_{bl}^2)\ddot{\xi}$
- $M_{bexg}\Omega^2 R^2 \sin\xi = m_{bl} \cdot eR \cdot \Omega^2 \cdot y_{bl} \cdot \sin\xi$
- N is equal to the terms on the right hand side of in equation (8.4)

Taking into account the previous considerations for the c.g and the moment of the inertia around the lag axis, it is shown that these two expressions are equivalent. Equation (8.4) has therefore been validated.

8.2.2 Air Density

For any flight conditions the air density depends on height, this can be simulated for any flight conditions in VehicleSim. Figure 8.2 shows the results of a simulation in climb flight condition. The simulation was carried out with an initial height of 250 m. From this height, the helicopter ascends for 200 s in order to obtain various air density values for the helicopter's height and to validate these with data appearing in [98].

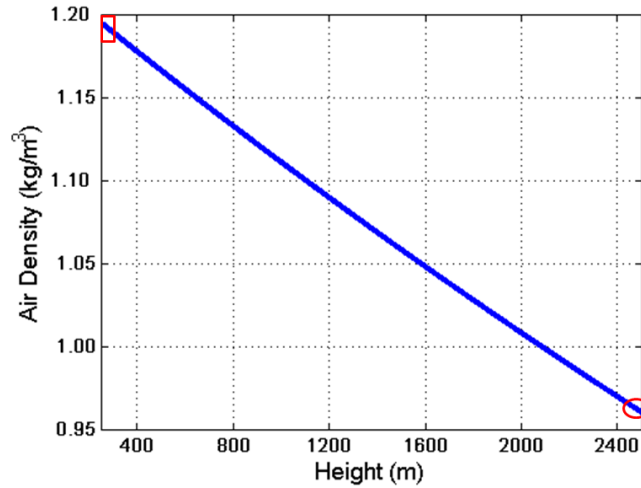


Figure 8.2: Variation of air density versus height calculated in VehicleSim. Red '□', represents the starting height. Red '○', final height.

In addition to this, Table 8.1 shows the air density ratio ρ/ρ_o where ρ is the corresponding air density as a function of the height and ρ_o is 1.225 kg/m^3 (air density at sea level). As it can be seen, the calculated air density values do match those in [98].

Height (m)	Air Density Ratio (ρ/ρ_o)	VehicleSim Air Density Ratio (ρ/ρ_o)
304	0.9771	0.9706
609	0.9428	0.9420
914	0.9151	0.9143
1219	0.8881	0.8881
1524	0.8617	0.8620
1828	0.8359	0.8367
2133	0.8106	0.8122
2428	0.7860	0.7893

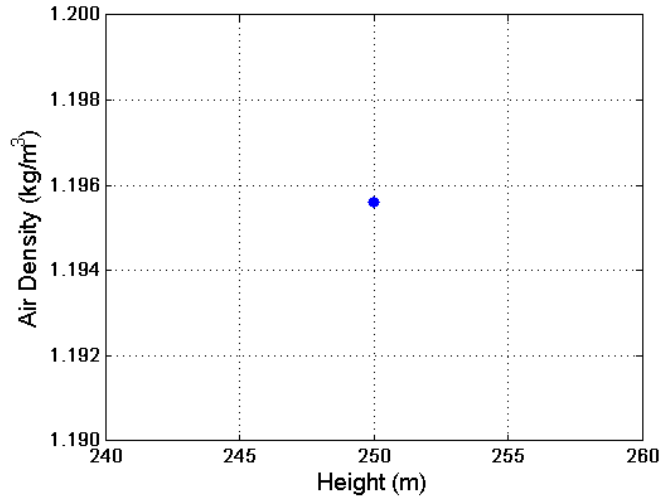
Table 8.1: *Real values for height and air density ratio versus VehicleSim obtained values [98].*

8.2.3 Hover Flight

Helicopter flight usually involves four types of aerodynamic conditions: hover, climb, descent and forward flight as well as take-off and landing. The two last conditions are not considered in the model proposed in this thesis. The first condition to be simulated in hover, for this purpose the thrust coefficient and main rotor solidity are calculated and after this, the collective feather angle is obtained by using the relationship between the thrust coefficient in hover and the solidity versus the collective feather as Figure 8.4 shows [145]. This figure shows experimental measurements for a helicopter in hover flight, it shows a standard example in the literature where the parameters are similar to the model considered in this work.

On the other hand, air density can be obtained from VehicleSim simulation in order to check its behaviour under this flight condition. The predicted behaviour should be to obtain a constant air density during the simulation due to the helicopter's height remains constant. Figure 8.3 shows the air density under hover flight condition obtained from VehicleSim simulation.

In order to select the main rotor collective feather in hover flight, Figure 8.4 is taken into account. As a consequence, if the collective feather angle is chosen approximately 10 degrees or (0.175 rad) and a simulation is carried out in VehicleSim during 50 s and

Figure 8.3: *Air density in hover flight.*

the helicopter's height is 250 m, VehicleSim provides the parameter $C_T/\sigma = 0.099$. So, the main rotor feather angle as well as C_T/σ match the expected ratio according to Figure 8.4. The induced velocity in hover is given by $v_{i0} = \sqrt{T/2\rho\pi R^2}$.

On the other hand, the thrust coefficient and the solidity are also calculated for the tail rotor. This allows to obtain the tail rotor collective feather angle in hover by using the information provided in Figure 8.5 [71]. The collective angle is given for $\theta_{0.75}$ i.e., collective angle calculated at 75% of the radius of rotor. Nevertheless, the blades on the tail rotor are rigid and without twist, so the feather angle is constant along the blade length and this graph can be only used as an estimation to obtain the tail rotor collective feather.

Once the main rotor feather angles is chosen, the tail rotor collective feather is selected as approximately 10 degrees or (0.175 rad) in order to calculate C_{Ttl}/σ_{tl} , a simulation is carried out for 50 seconds at $h = 250$ m and value obtained is $C_{Ttl}/\sigma_{tl} = 0.045$. Given that, the tail rotor feather angle and C_{Ttl}/σ_{tl} keep the expected ratio according to Figure 8.5. These values for the tail collective feather together with main rotor collective angle allow to simulate hover flight conditions. The yaw does not change, the helicopter keeps the initial orientation around Z axis. Finally, hover conditions are simulated at a height of 250 m. From $h = 0$ m to $h = 250$ m a climb flight takes place.

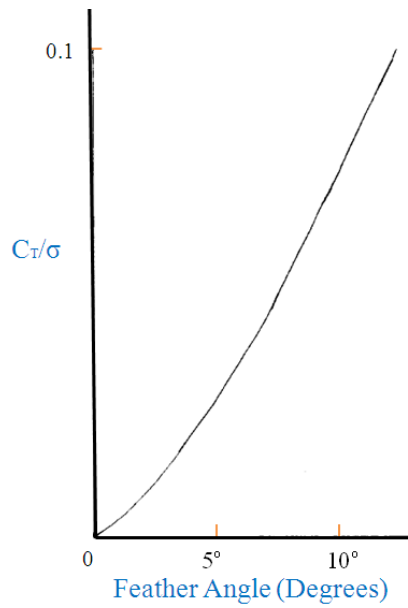


Figure 8.4: Main rotor hover characteristics: thrust coefficient divided by solidity versus feather collective angle. This graph is plotted by the author and based on [145].

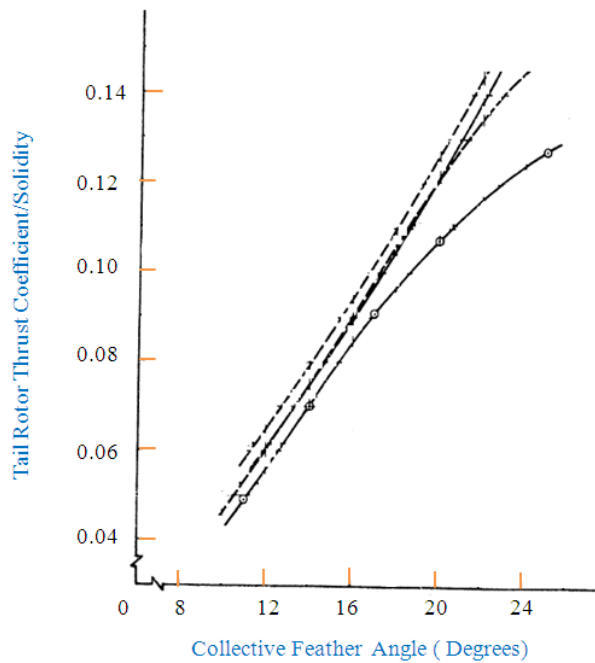


Figure 8.5: Tail rotor hover characteristics, thrust coefficient divided by solidity versus collective angle. This graph is plotted by the author and based on [71].

With these selected main and tail rotor collectives angles, a hover flight simulation is carried out in VehicleSim for 50 s. The spatial representation of this can be represented with Matlab as it was mentioned before in order to show the helicopter's position under these flight conditions. The expected behaviour should be a constant position at 250 m height during the simulation time. This behaviour can be seen in Figure 8.6.

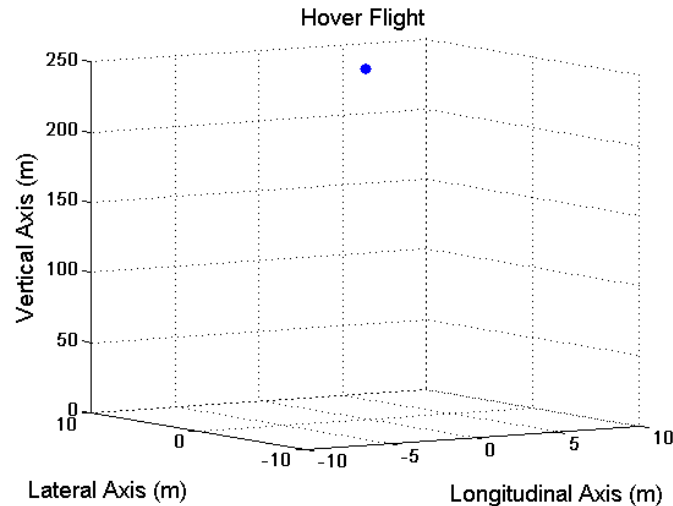


Figure 8.6: 3-D representation of hover flight conditions. Blue point represents the helicopter's position. Vertical axis value is 250 m. Longitudinal and lateral axes, their corresponding values are around the equilibrium point in each axis i.e., zero.

On the other hand, Figure 8.7 shows the flap amplitude of the four blades on the main rotor in hover flight. By using a FFT (Fast Fourier Transform) Matlab algorithm, the main rotor flap frequencies are calculated for the four blades. These are approximately 7.6 Hz or (47.7 rad/s). This is 1.07 the main rotor frequency. As it can be seen in Figure 8.7, the flap amplitudes decrease, the flap amplitude is damped due the aerodynamics existing around the rotor.

In order to analyze the flap behaviour for the main rotor blades, the simulation is carried out under the same flight conditions, nevertheless in this case the time is 100 s. Figure 8.8 shows the flap amplitude for the main rotor four blades in the last two seconds in order to allow a better view of the behaviour. As it can be seen, the flap keeps an almost constant amplitude, small variation can be observed as a consequence of the effect of the aerodynamic load and the main rotor angular speed under this flight conditions. The simulation can be carried out over this time and the system remains

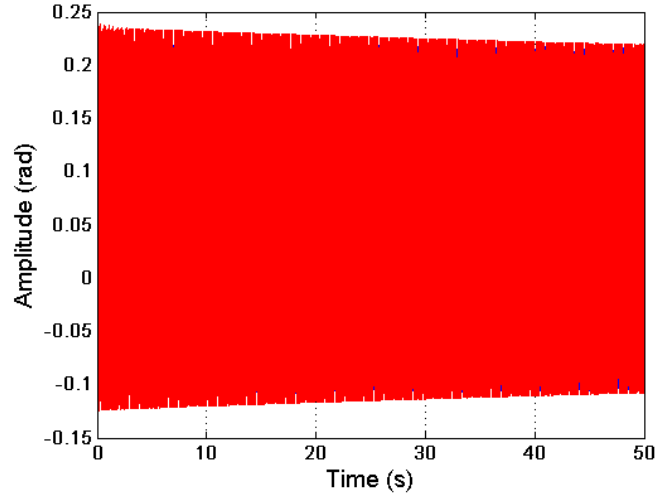


Figure 8.7: *Flap amplitude for the four main rotor blades in hover flight (blue (blade 1), green (blade 2), yellow (blade 3) and red (blade 4)).*

stable, but in order to simulate the hover flight with accuracy the controllers should be calibrated again. Figure 8.9 shows the tail rotor blades' flap amplitudes and details of this are represented in Figure 8.10. The flap frequencies are approximately 37.1 Hz or (approximately 233 rad/s), for both tail rotor blades, the simulation was carried for 50 s. These are approximately equal to the tail rotor rotational speed. The flap amplitude for the two tail rotor blades show behaviour a more stable behaviour due to the action of the flap and feather tail rotor controllers.

8.2.4 Climb Flight

In this section, climb flight is simulated under the following conditions: the climb velocity and induced climb velocity are chosen according to the model proposed by [98] (see Figure 8.11). The climb velocity is chosen to be: $v_c = 0.9 \cdot v_h$ (red circle in Figure 8.11), so the induced velocity is $v_{ic} = 0.65 \cdot v_h$. This climb velocity is enough to carry out a climb simulation in VehicleSim.

In addition to this, the main rotor collective feather is selected as $\theta = 0.09$ rad, this implies an angle of attack $\alpha = 0.014$ rad and an inflow angle $\phi = 0.076$ rad. These angles are calculated at a main rotor radius approximately (75 %). This configuration is chosen because both angle of attack and inflow angle are positive when a climbing

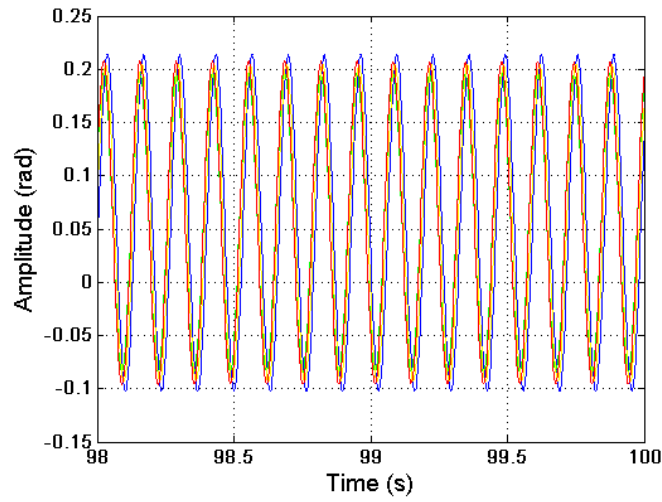


Figure 8.8: *Main rotor blades' flap amplitudes in hover flight for the last two seconds of the time interval (0 - 100) s (blue (blade 1), green (blade 2), yellow (blade 3) and red (blade 4)).*

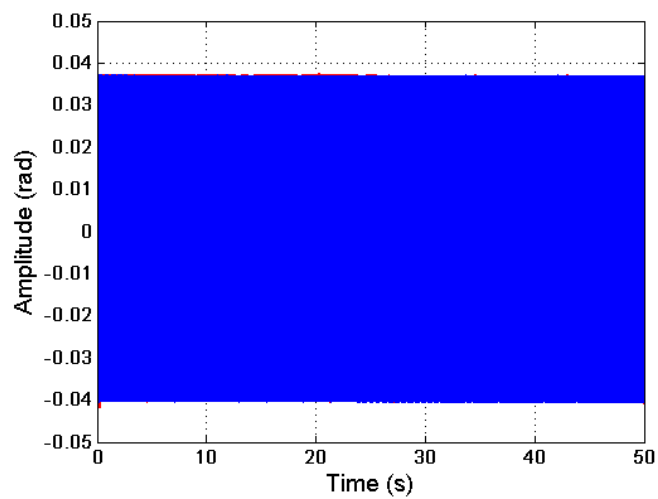


Figure 8.9: *Tail rotor blades' flap amplitudes in hover flight (dotted red line (blade 1), solid blue line (blade 2)).*

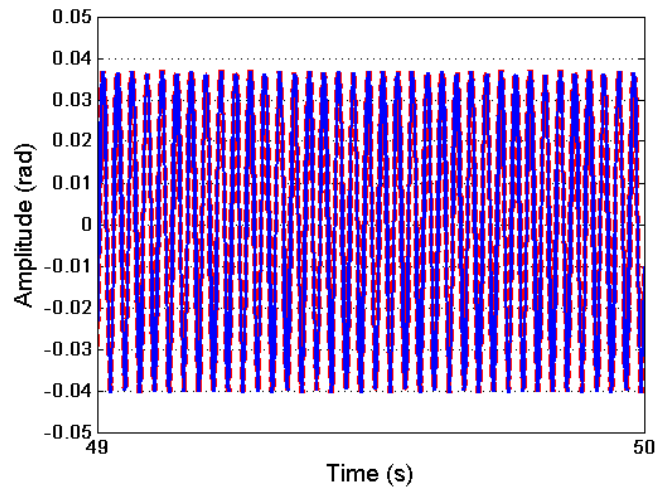


Figure 8.10: Zoom of figure 8.9. Tail rotor blades' flap amplitudes in hover flight (dotted red line (blade 1), solid blue line (blade 2)).

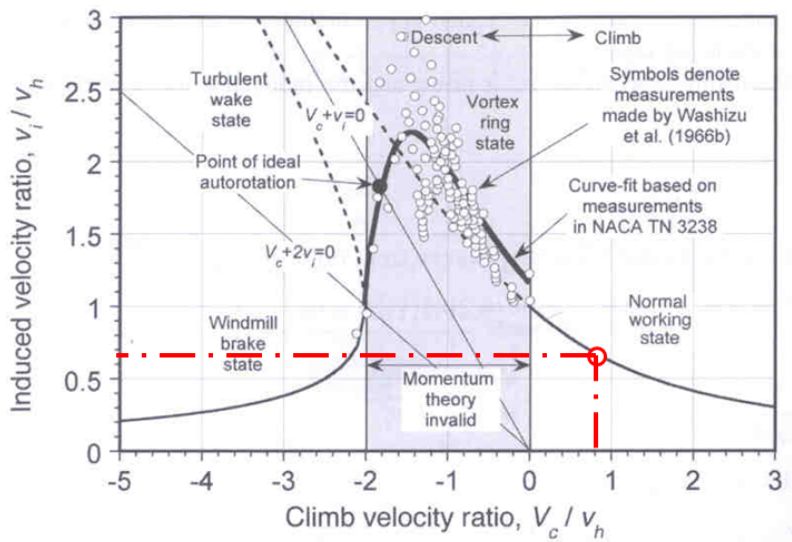


Figure 8.11: Induced velocity ratio as a function of climb velocity ratio based on momentum theory (complete induced velocity curve). Reproduced with permission from Cambridge University Press [98].

8.2. AERODYNAMIC LOAD AND FLIGHT

simulation is carried out in VehicleSim. Other combinations can be done, but this just was carried out as an example. Furthermore, the increased collective feather in climb flight can be estimated by using the expression: $\Delta\theta = (3/2)((v_c + v_{ic} - v_h)/(\Omega R))$ [140], where $\Delta\theta = 0.034$ rad or (approximately 2 degrees).

The tail rotor collective feather angle can be estimated, taking into account the values proposed in [74]. In here, the author shows that the tail rotor collective feather at a radius approximately (75 %) in hover flight is 12.70 degrees or (0.22 rad) and in forward flight conditions ($\mu = 0.132$) the collective feather angle is 11.06 degrees or (0.19 rad), being these the maximum values. As a consequence of this, the tail rotor blades' collective angle is taken as 11.45 degrees or (0.20 rad).

In order to simulate the climb flight a simulation is carried out in VehicleSim using the previous considerations. The simulation time is 50 s and the initial helicopter's height is 250 m. Figure 8.12 shows the helicopter's position under climb conditions. As it can be seen, the helicopter climbs from 250 m to 744 m, it covers 494 m in 50 s, its climb speed is 9.88 m/s. According to [144] a typical value for maximum climb speed is 5 – 10 m/s, so the simulated climb speed agrees with the theoretical values.

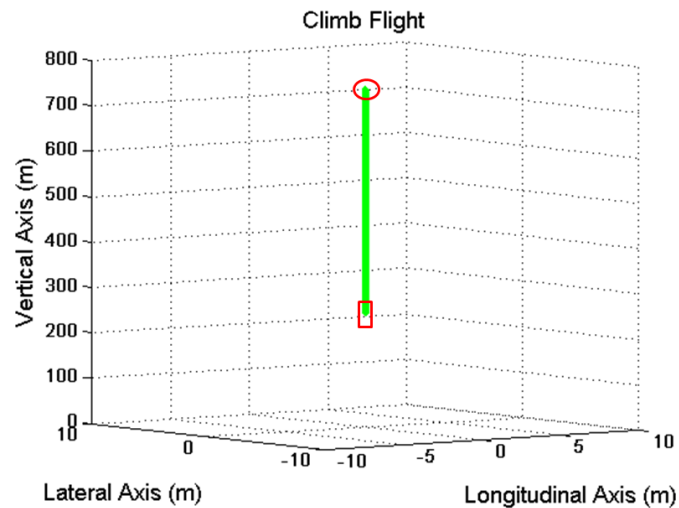


Figure 8.12: *Climb flight simulation. Green line shows the helicopter displacement from $h_i = 250$ m to $h_f = 744$ m. Red '□', represents the initial position. Red '○', final position.*

The air density should change according to helicopter's height, Figure 8.13 shows the expected air density during the climb flight.

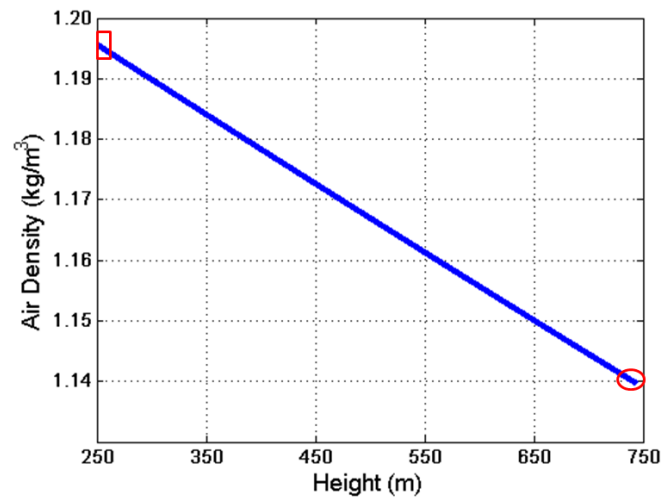


Figure 8.13: Variation of air density in climb flight. Red '□', represents the starting height. Red '○', final height.

Figure 8.14 shows the main rotor blades' flap amplitudes during climb flight. The frequencies are approximately 7.6 Hz or (47.7 rad/s). This is 1.07 of the main rotor angular speed. The flap amplitudes are damped as a consequence of the main rotor aerodynamic load.

In order to validate the four blades' flap behaviour, a second simulation under similar climb flight condition is carried out, in this case, the simulation time is 100 s. Figure 8.15 shows the behaviour for the last two seconds. The flap reaches an almost constant amplitude. As it can be seen, flap dynamics around 100 s are a slightly different in comparison with the hover flight i.e., the blades 3 and 4 show different flap amplitudes respect to the flap on the blades 1 and 2, due to the aerodynamic load. In here, the flap amplitude shows a behaviour different, because the lift coefficients are given as: $2\pi(\theta - \arctan((V_c + v_{ic})/\Omega y))$ and $2\pi(\theta - \arctan(v_{ih}/\Omega y))$ for climb and hover flight, respectively. As it can be seen, the induced velocities are presented in both equations. Nevertheless, the first lift coefficient contains an additional term, the climb velocity. As a consequence of this, the flap amplitudes show different behaviour under the corresponding aerodynamic load.

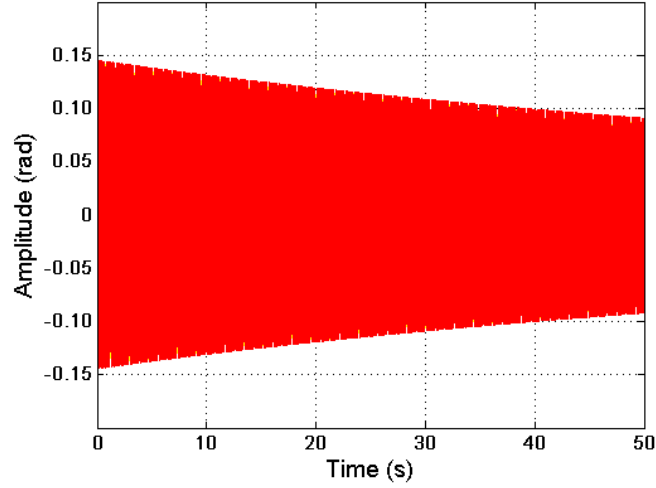


Figure 8.14: *Main rotor blades' flap amplitudes during climb flight (blue (blade 1), green (blade 2), yellow (blade 3) and red (blade 4)).*

The simulation is done over this time interval and the system remains stable, in order to simulate the climb flight with accuracy the controllers should be calibrated again.

Tail rotor flap dynamics are shown in Figure 8.16. Additionally, Figure 8.17 shows the flap amplitude for the tail rotor two blades in the last second in order to see the behaviour clearly. The blades' flap frequency is 37.1 Hz or (233.1 rad/s). This is approximately equal to the tail rotor frequency. In this case, the tail rotor flap amplitude for both blades shows a light increase as a consequence of the flap definition on the tail rotor when the aerodynamic loads are acting. The flap coefficients have a direct influence of the air density i.e., $a_0 = \Gamma (\theta_0 - (4/3) \lambda) / (8 + \Gamma \tan \delta_3)$, $a_1 = (q/\Omega) (((16/\Gamma) - K) / (1 + K^2))$ and $b_1 = -(q(1 + K(16/\Gamma))) / (\Omega(1 + K^2))$ where $\Gamma = (c\rho a R^4) / I_f$. As a result, the tail rotor blades' flap amplitudes increase their values when the height increases.

8.2.5 Descent Flight

Descent flight is also simulated in VehicleSim under the following conditions: the descent velocity and induced descent velocity are selected according to the information in [98] (see Figure 8.18). As a consequence, the descent velocity is chosen as: $-2.2 \cdot v_h$ (red circle in Figure 8.18) and the induced velocity is $0.6 \cdot v_h$ (see Figure 8.18). These velocities will be chosen as the values to be used in VehicleSim to simulate a descent flight.

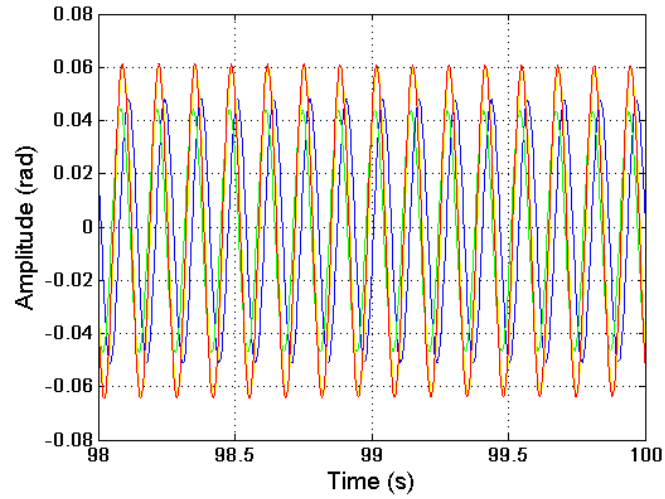


Figure 8.15: Flap amplitudes (blue (blade 1), green (blade 2), yellow (blade 3) and red (blade 4)). Climb flight for the last two seconds of the time interval (0 - 100) s.

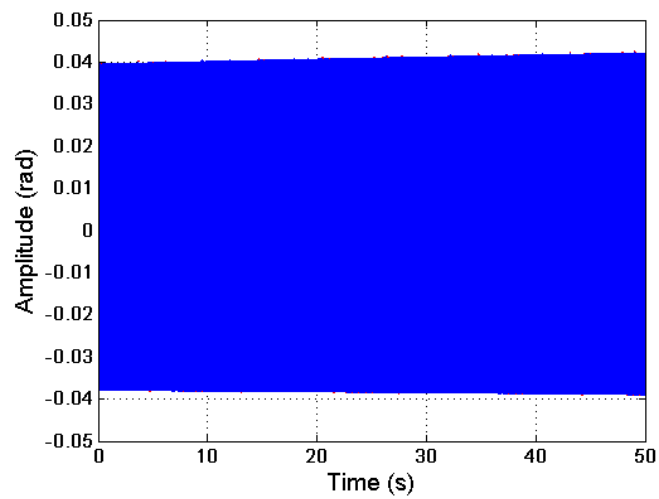


Figure 8.16: Tail rotor blades' flap amplitudes during climb flight (dotted red line (blade 1), solid blue line (blade 2)).

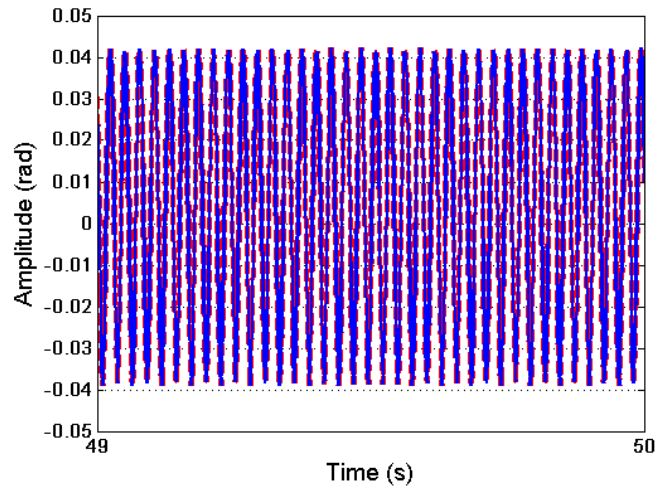


Figure 8.17: Zoom of figure 8.16. Tail rotor blades' flap amplitudes during climb flight (dotted red line (blade 1), solid blue line (blade 2)).

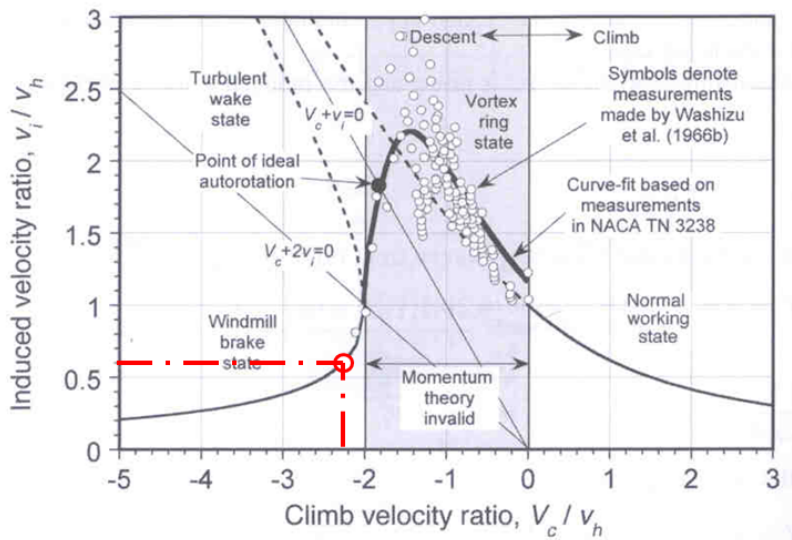


Figure 8.18: Induced velocity variation as a function of descent velocity based on momentum theory (complete induced velocity curve). Reproduced with permission from Cambridge University Press [98].

It is known that in vertical descent flight the climb velocity is negative whilst the induced velocity remains positive as the main rotor maintains lift [145]. The main rotor blades' collective feather angle is chosen as $\theta = -0.090$ rad, this provides an angle of attack $\alpha = -0.012$ rad and an inflow angle of $\phi = 0.078$ rad. These angles values correspond to a main rotor radius of about 75 % when the descent flight simulation is carried out in VehicleSim these values are negative. Other configurations are possible and this one in here is just an example. The estimation for the tail rotor blades' collective angle is taken from [74], being this estimation 11.45 degrees or (0.20 rad) for the tail rotor blades' feather angle.

In order to validate the descent flight, a simulation is carried out in VehicleSim. In this case, the simulation time is 8 s, the initial helicopter's height is 250 m and the final height is 78 m. It is expected to obtain a descent trajectory in which the helicopter covers 172 m, its descent speed is 21.5 m/s (see Figure 8.19).

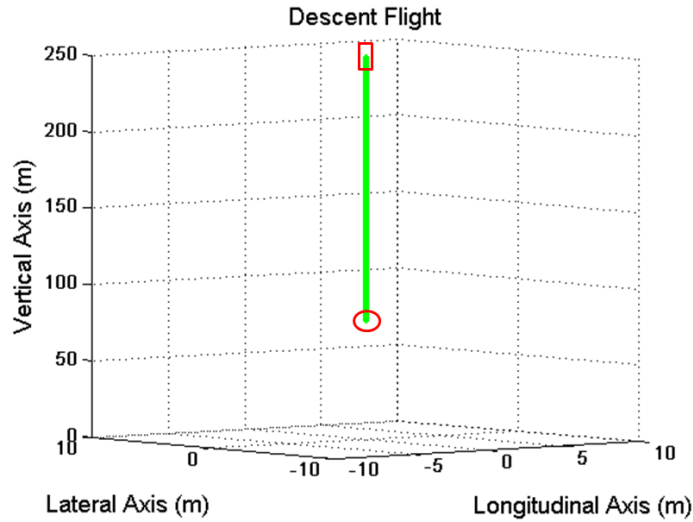


Figure 8.19: Representation in three dimensions in descent flight. Green line shows the helicopter's position. Red '□', represents the initial position. Red '○', final position.

The air density is also obtained, it is expected the air density to increase its value as Figure 8.20 shows. (In Figure 8.20, the horizontal axis should be interpreted correctly i.e., from higher height to lesser height).

Figure 8.21 shows the main rotor flap for the four blades in descent flight. The frequencies are approximately 7.6 Hz or (47.7 rad/s). The flap motions reach smaller

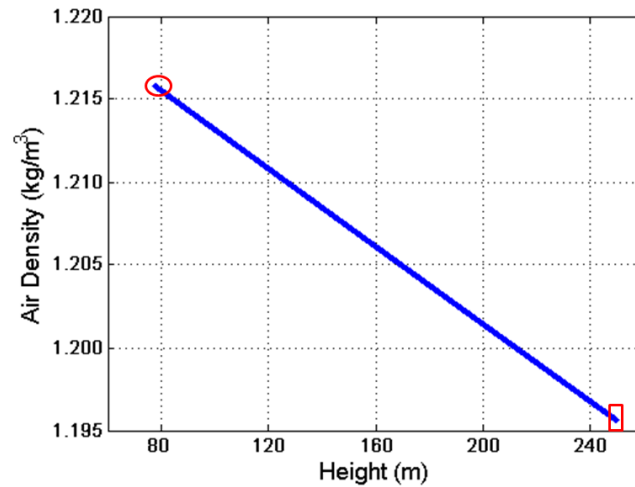


Figure 8.20: Variation of air density in descent flight. Red '□', represents the starting height. Red '○', final height.

amplitudes as a consequence of main rotor aerodynamic loads in this axial flight.

The flap on the tail rotor are also represented, see figures 8.22 and 8.23. These flap frequencies are approximately 37.1 Hz equal to the tail rotor frequency. In this case, it should be expected that the tail rotor flap frequency decreases its value due to air density increases it. This behaviour can be seen in Figure 8.22.

8.2.6 Forward Flight

The most general case of rectilinear helicopter flight assumes that the rotor axis is tilted from the vertical via certain angle and it is moving at constant speed along an inclined path where the lift is the vertical component (rate of climb) and the thrust is the horizontal component (see Figure 8.24) [146].

Forward Flight with Constant Climb Rate

In this section, forward flight with constant climb rate is achieved by using the fuselage's pitch PID controller. The controller input is 0.088 rad [142], as the reference and the controller's action provides the desired fuselage's pitch.

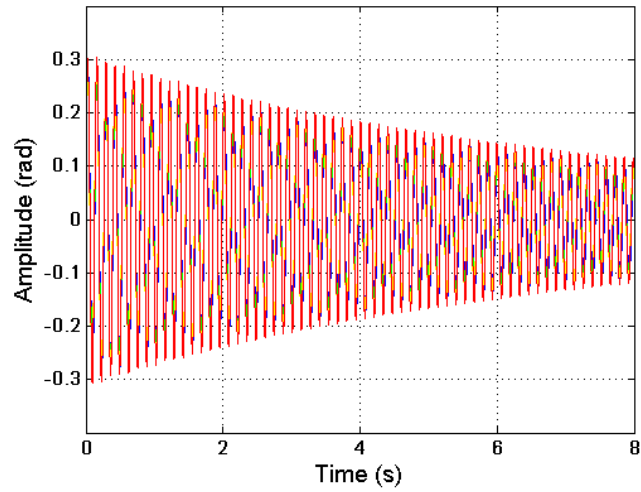


Figure 8.21: Main rotor blades' flap amplitudes in descent flight (blue (blade 1), green (blade 2), yellow (blade 3) and red (blade 4)).

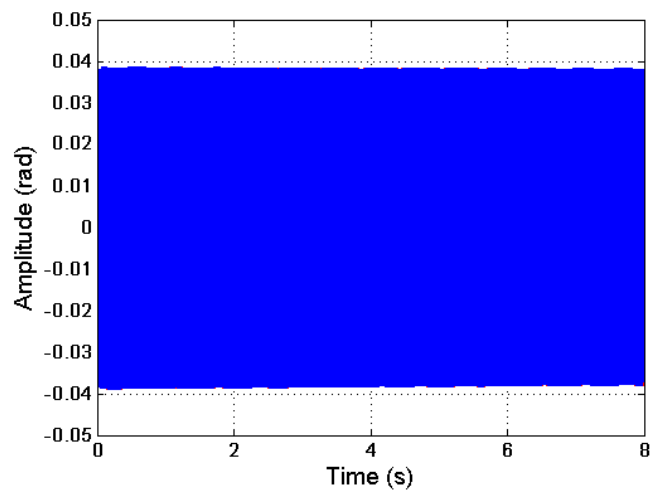


Figure 8.22: Tail rotor blades' flap amplitudes in descent flight (dotted red line (blade 1), solid blue line (blade 2)).

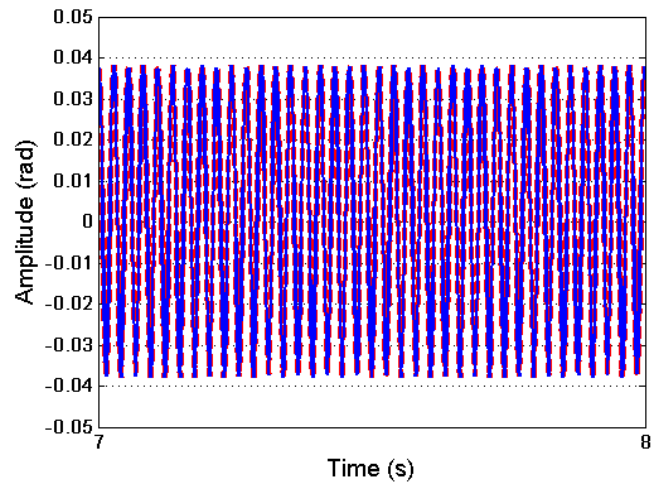


Figure 8.23: Zoom of figure 8.22. Tail rotor blades' flap amplitudes in descent flight (dotted red line (blade 1), solid blue line (blade 2)).

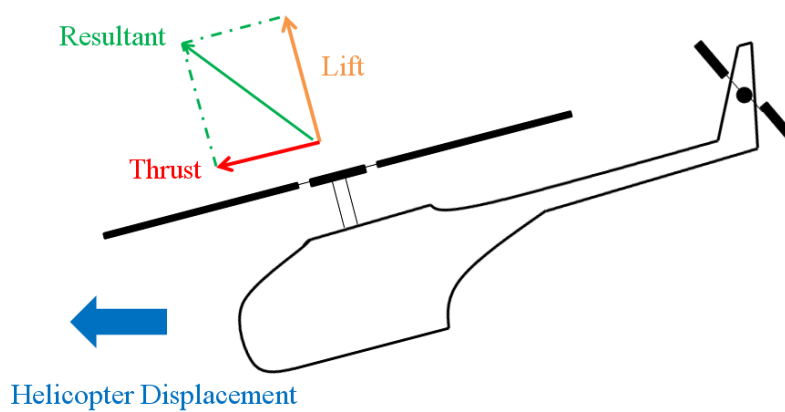


Figure 8.24: Forward flight.

In forward flight the following conditions are considered in order to carry out the simulation:

- The forward flight speed is given by $V = \mu\Omega R$. In this work, the corresponding advance ratio is $\mu = 0.1$, because the estimated tail rotor contribution is for low speed flight. The standard values for the advance ratio are taken to be in the range from 0.1 to 0.35 – 0.40 [140].
- The induced forward velocity is given by the relationship between the forward flight velocity and the hover velocity (v/v_h) as well as the induced forward velocity and hover velocity (v_i/v_h) as Figure 8.25 shows. This allows to obtain the induced forward velocity for $\mu = 0.1$ as $v_{i\,fw} = 0.4 \cdot v_h$. According to Figure 8.25, $v_h = v_{i0}$ [145].

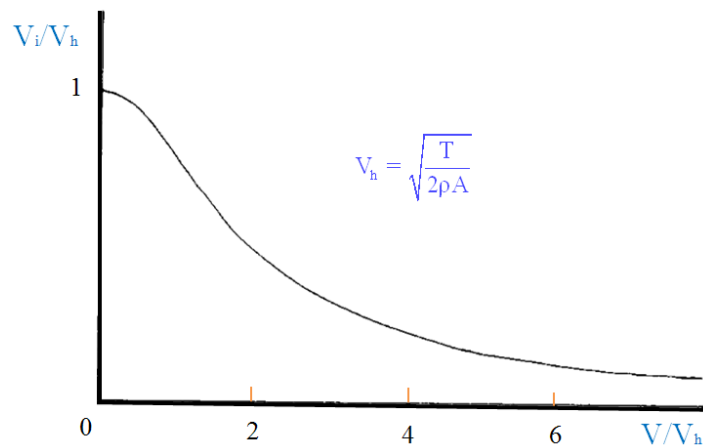


Figure 8.25: Variation of induced velocity with forward speed. This graph is plotted by the author and based on [145].

In order to choose the main rotor collective feather angle in forward flight, Figure 8.26 is used. If the main rotor collective feather angle is chosen to be about 8.5 degrees or (0.148 rad) and a forward flight simulation is carried out for 50 s at an initial height of 250 m and the fuselage’s tilt is 0.088 rad (approximately 5 degrees) according to [142], VehicleSim calculations show that the value of the ratio C_T/σ is 0.1.

The tail collective feather angle is obtained by using the advance ratio (see Figure 8.27) [141]. The advance ratio for this case was $\mu = 0.1$, therefore, the tail feather angle θ_{0t} is 5 degrees or (0.087 rad).

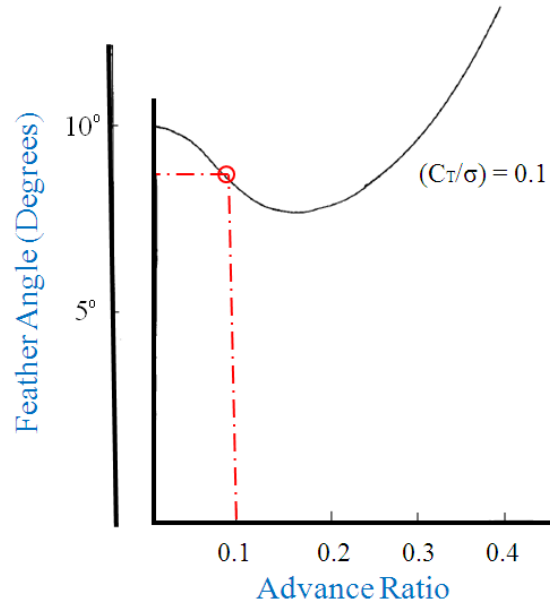


Figure 8.26: Calculated values of C_T/σ versus θ . This graph is drawn by the author and based on [145].

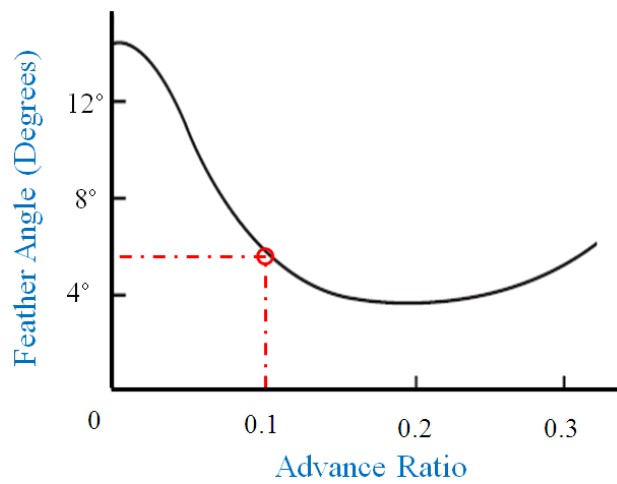


Figure 8.27: Tail rotor feather angle versus advance ratio in forward flight. This graph is plotted by the author and based on [141].

8.2. AERODYNAMIC LOAD AND FLIGHT

Once the main rotor collective feather angle was fixed as $\theta = 8.5$ degrees in order to simulate the forward flight the main rotor cyclic feather is found out by using the expressions: $\theta_{1S} = -a_1 - ((8/3)\mu((6C_T)/\sigma a) + 2\mu\lambda_{TPP}(1 - (3/2)\mu^2))/(1 - \mu^2 + 9/4\mu^4)$ and $\theta_{1C} = b_1 + ((4/3)\mu a_0)/(1 + (1/2)\mu^2)$. If a simulation is carried out for 50 s, VehicleSim provides the cyclic feather values, being these $\theta_{1S} = -0.078$ rad and $\theta_{1C} = 0.048$ rad, respectively. Taking into account these, the forward flight condition with rate climb can be simulated in VehicleSim. The simulated forward flight is represented, in Figure 8.28 by plotting in a 3D graph the corresponding vehicle's X , Y and Z coordinates for a 50 seconds simulation. It can be seen that the trajectory shown in Figure 8.28 coincides with an expected behaviour of forward flight with a fixed climb rate in which the vehicle travels 994 m at 20 m/s. In addition to this, the helicopter vertical displacement is approximately 110 m at 2.2 m/s.

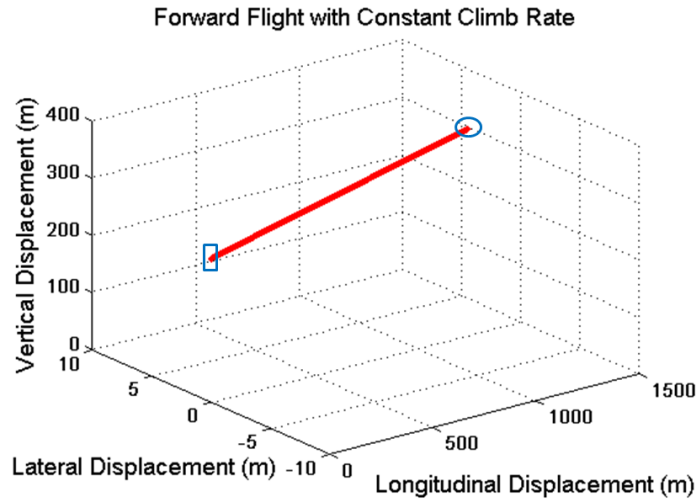


Figure 8.28: Vehicle's position for 50 seconds simulation in which the distance travelled is 994 m with a speed of $v_{fw} = 20$ m/s and climb rate of 110 m with a speed of 2.2 m/s. Blue '□', represents the initial position. Blue '○', final position.

The air density was also modelled as Figure 8.29 shows. As expected, in forward flight with constant climb rate the air density decreases (see Figure 8.29).

The main rotor blades, during forward flight and constant climb rate, do maintain a constant amplitude due to the aerodynamic load. This is shown in Figure 8.30. Additionally, Figure 8.31 shows the flap amplitude for the main rotor four blades in the last two seconds in order to allow a better view of the behaviour. The flap frequencies

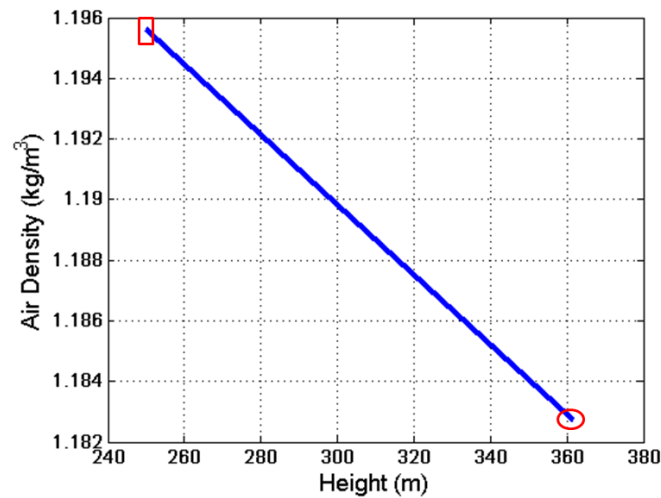


Figure 8.29: *VehicleSim* calculation of air density in forward flight with constant climb rate. Red '□', represents the starting height. Red '○', final height.

do match the rotor's angular speed as expected.

The tail rotor blades' flap are also seen (Figure 8.32). The flap frequencies in this case are near the tail rotor's frequency. In here, there is a climb component, so it should be expected that the tail rotor blades' flap amplitudes increase as it can be seen in Figure 8.32. In addition to this, Figure 8.33 shows the flap amplitude for the tail rotor two blades in the last second in order to see the behaviour clearly.

Forward Flight with Varying Tilt Angle

In here, forward flight is performed with a variable fuselage's pitch i.e., the PID controller input is zero and the controller's gains are changed in order to obtain the desired behaviour. The flight conditions are simulated with the same values as before but in this case, the tilt will be changed along a 4 seconds simulation. This is shown as an example, it can be extended in time with an appropriate controller calibration process.

Figure 8.35 shows the main rotor blades' flap amplitudes, their frequencies are near the main rotor's frequency.

The tail rotor blades' flap amplitudes are also obtained, see figures 8.36 and 8.37. In here, the helicopter's height is constant. As a consequence of this, the flap amplitudes

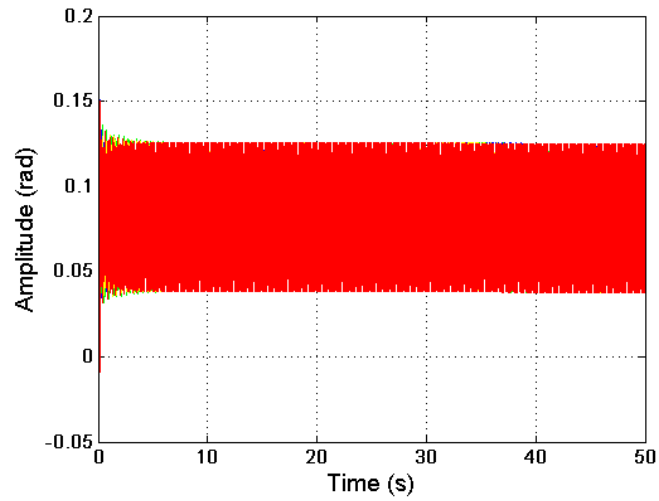


Figure 8.30: *Main rotor blades' flap amplitudes in forward flight with constant climb rate (blue (blade 1), green line (blade 2), yellow line (blade 3) and red line (blade 4)).*

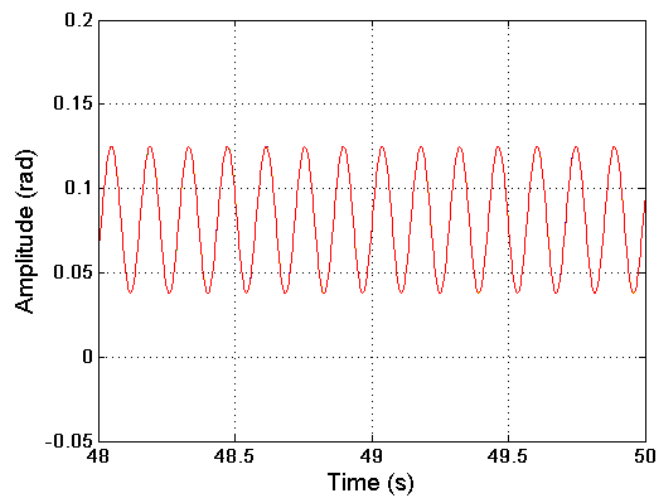


Figure 8.31: *Zoom of figure 8.30. Flap amplitudes in forward flight with constant climb rate (blue (blade 1), green line (blade 2), yellow line (blade 3) and red line (blade 4)).*

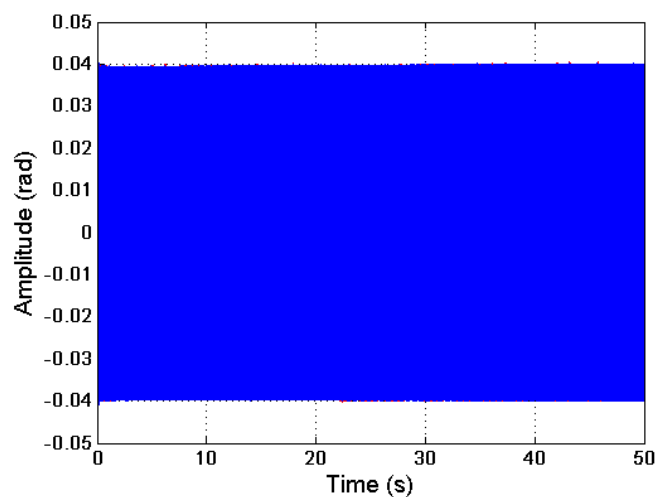


Figure 8.32: Tail rotor blades' flap amplitudes in forward flight with constant climb rate (dotted red line (blade 1), solid blue line (blade 2)).

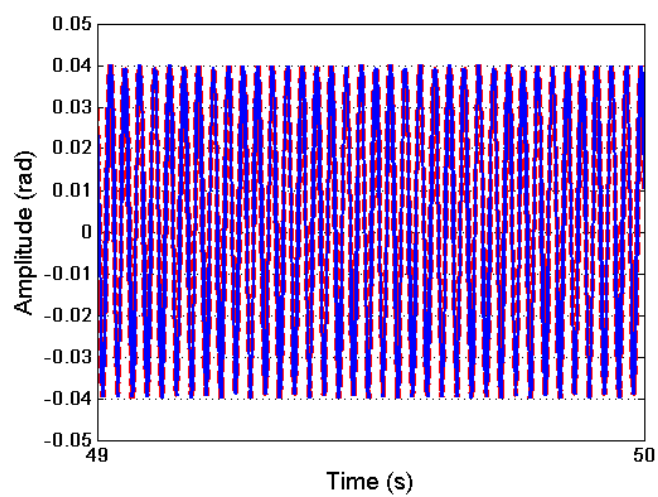


Figure 8.33: Zoom of figure 8.32. Tail rotor blades' flap amplitudes in forward flight with constant climb rate (dotted red line (blade 1), solid blue line (blade 2)).

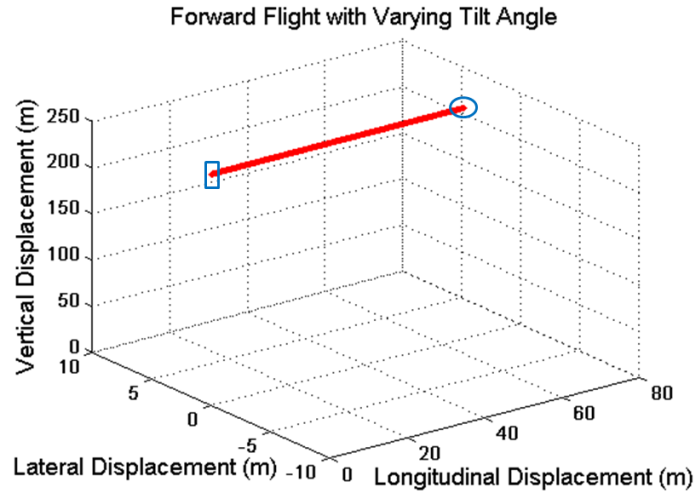


Figure 8.34: *Forward flight with varying tilt angle simulation. Red line shows the helicopter's position. Blue '□', represents the initial position. Blue '○', final position.*

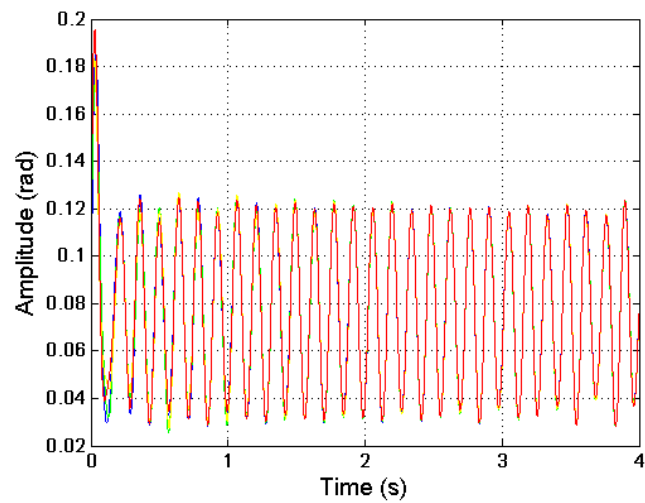


Figure 8.35: *Main rotor blades' flap amplitudes in forward flight with varying tilt angle (blue (blade 1), green (blade 2), yellow (blade 3) and red (blade 4)).*

remain constant according to the expected behaviour.

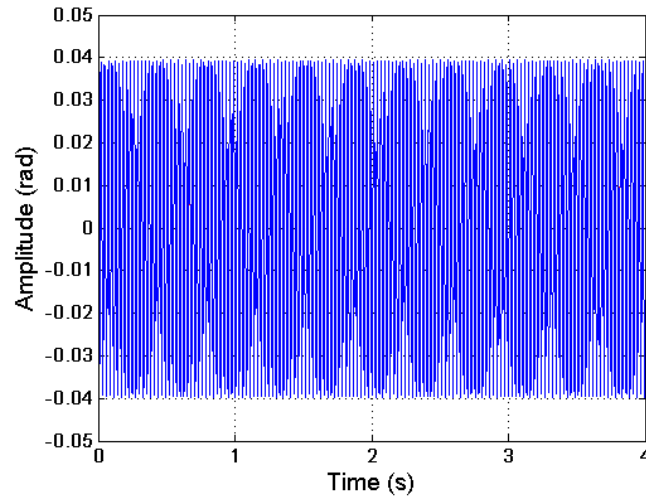


Figure 8.36: Tail rotor blades' flap amplitudes in forward flight with varying tilt angle (dotted red line (blade 1), solid blue line (blade 2)).

8.2.7 Trajectory Flight

Forward flight with constant climb rate can be also simulated for different orientations in space i.e., the rates of yaw ($\dot{\gamma}$) are changed using the fuselage's yaw controller defined in Chapter 6. Figure 8.38 shows three different trajectories under the action of this controller for $\dot{\gamma} = 0.1$ rad/s, $\dot{\gamma} = -0.1$ rad/s and $\dot{\gamma} = -0.2$ rad/s, respectively.

Several combinations of various flight conditions are considered in order to simulate a helicopter trajectory as Figure 8.39 shows. The trajectory starts with hover flight at a height of $h = 250$ m for 4 s, then a climb flight from $h = 250$ m up to $h = 279$ m for 2 s is performed. After this, forward flight with a constant rate climb is performed for 30 s, its initial height is $h = 279$ m and its final height is 336 m. Then, hover flight is simulated for 4 s at a constant height $h = 336$ m. Finally, a descent flight manoeuvre from $h = 336$ m down to $h = 254$ m is simulated for 4 s.

This trajectory simulation was just an example on the achievable manoeuvring that can be performed by the model here presented.

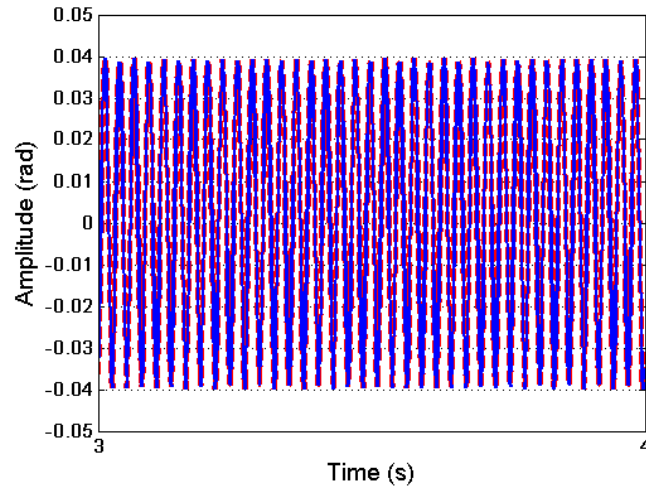


Figure 8.37: Zoom of figure 8.36. Tail rotor blades' flap amplitudes in forward flight with varying tilt angle (dotted red line (blade 1), solid blue line (blade 2)).

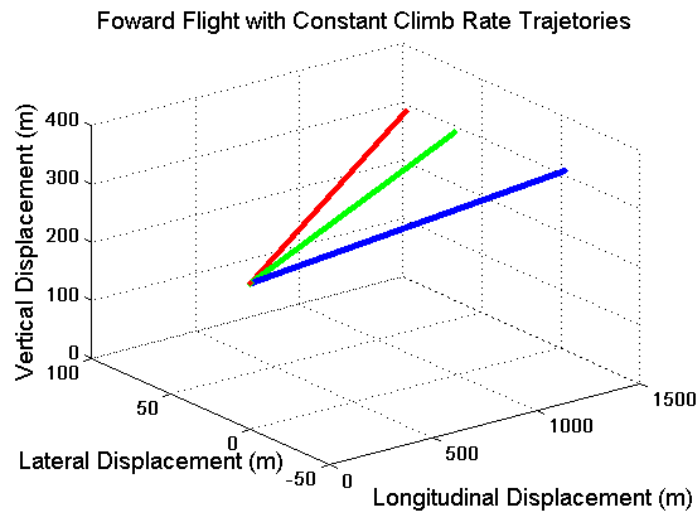
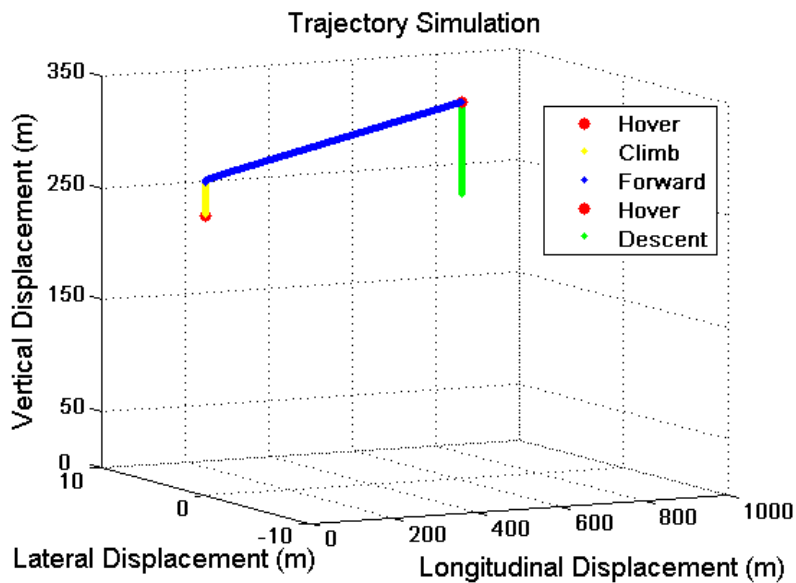


Figure 8.38: Several trajectories in forward flight with constant climb rate and different rates of yaw ($ryaw$). Red line, represents $ryaw = 0.1$ rad/s. Green line, $ryaw = -0.1$ rad/s. Blue line, $ryaw = -0.2$ rad/s.

Figure 8.39: *Helicopter trajectory.*

8.3 Main Rotor Induced Drift

As it was mentioned in Chapter 5, the tail rotor system is designed to provide an antitorque effect. Also, it produces thrust in the horizontal plane, causing the helicopter to drift right (or left) whilst in hover as Figure 8.40 shows.

This drift effect can be reduced if an additional force is considered in the opposite direction, which is the case when the main rotor shaft is tilted, as a consequence, a main thrust vector component provides this.

In Chapter 6, the main rotor and its inclination were modelled. In this section, the effect of this on the drift effect when the helicopter is in hover flight is studied. Two different angles of rotor tilt were considered: 0.0175 rad (1 degree) and 0.175 rad (10 degrees). When the lateral controller is cancelled, the drift effect induces a lateral displacement on Y axis. The fuselage is rotated around the X axis (roll) 0.175 rad (10 degrees), other roll angles can be chosen but in order to obtain a clear behaviour under these simulation conditions, it is shown as an example. Two hover simulations with these conditions as well as the hover conditions explained in the corresponding section are carried out for 12 s. The fuselage lateral displacement are represented in Figure 8.41 and details of this are shown in Figure 8.42 under the action of previous conditions.

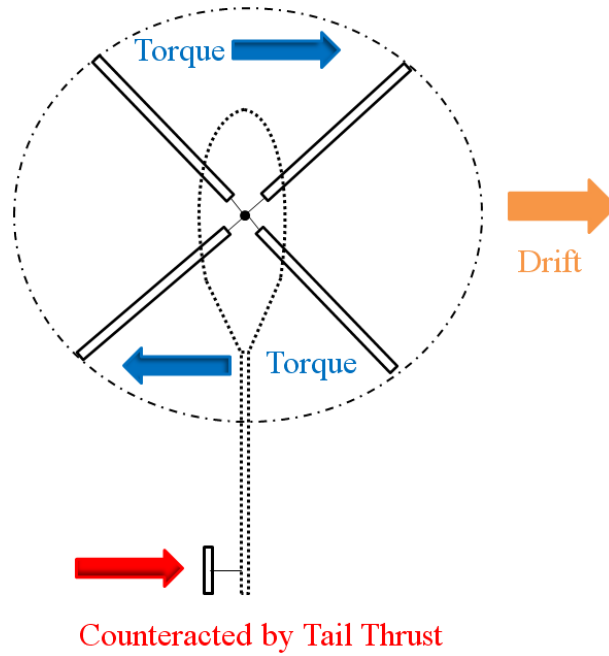


Figure 8.40: Schematic equilibrium of forces in a helicopter under the action of the main rotor torque and the tail rotor thrust and the resultant drift.

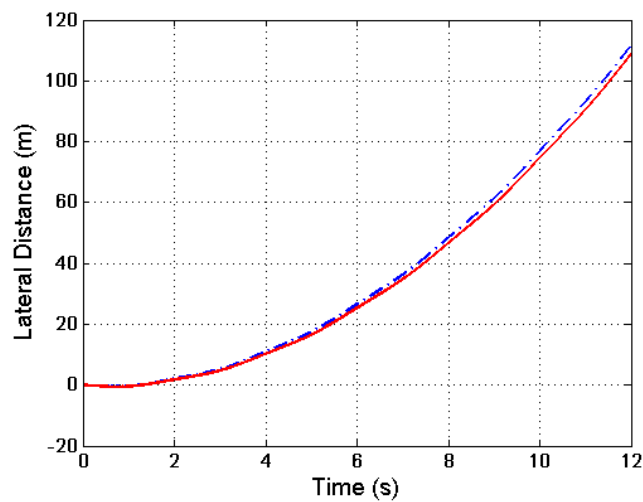


Figure 8.41: Helicopter's lateral displacements when the lateral controllers' action are cancelled and only the main rotor induced drift is acting.

As it can be seen in Figure 8.42, when the main rotor tilt angle is 0.175 rad the lateral distance travelled by the helicopter due to the induced drift is reduced by approximately 3 m in comparison to the same case simulation when the main rotor tilt is now 0.0175 rad on the first case, the fuselage's displacement is 108 m and on the second one is 112 m. The main rotor tilt does not reduce totally the drift effect because the aerodynamic loads are not considered on the fuselage and only on the blades in hover, this is not enough to fully compensate for the drift. Anyway, it has been shown how the main rotor tilt has an effect on the helicopter lateral drift.

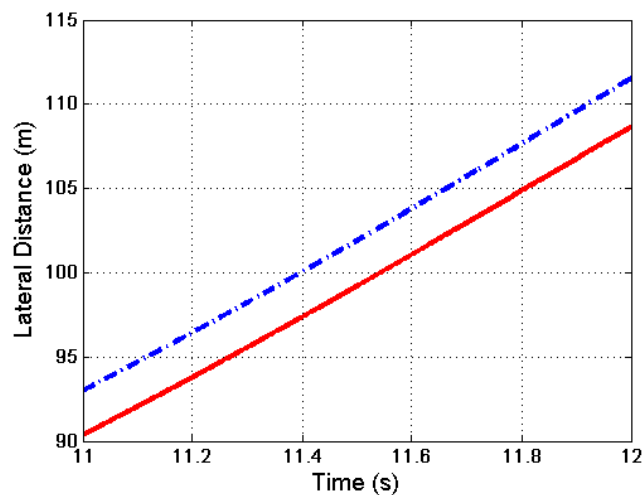


Figure 8.42: Zoom of figure 8.41. Red line represents the distance travelled by the fuselage when main rotor tilt is 0.175 rad and blue line represents the distance travelled by the fuselage when main rotor tilt is 0.0175 rad.

8.4 Vibrations

The purpose of this section is to study helicopter vibrations when different external perturbations affect the vehicle.

In aircraft's design, vibrations have remained one of the major problems affecting helicopter development for years. In fact, the maximum speed and manoeuvring capabilities for most of the modern helicopters are limited by excessive vibration. The major source of vibration in a helicopter is the main rotor, whereas in fixed-wing aircraft, the vibrations are originated by the engines or are caused by atmospheric turbulences in between

other reasons [150].

Vibrations affect helicopter handling qualities, contribute to the fatigue of structural components, reduce the reliability of on-board electronic equipment, and influence the precision of on board equipment such as cameras, measure devices, etc. Also, vibrations affect ride comfort, add to the fatigue of pilots, crew and increases maintenance time and cost. High vibration levels experienced by a helicopter could in many cases pose a limitation to the vehicle's forward speed and manoeuvring capabilities [95], [155], and in extreme conditions, vibrations can represent a serious threat to vehicle's safety.

Helicopter vibration is a problem which involves complex interactions between the inertial, structural and aerodynamic loads.

In general, vibrations appearing due to the main rotor's presence, tend to be equal to the main rotor rotating frequency or multiple of that frequency. The main rotor's frequency is a function of the angular speed at which it rotates. This is in general, the frequency of vibrations induced in the fuselage due to the main rotor's action [152].

The helicopter vibrations reduction has traditionally been a difficult task to achieve. First, vibrations should be analysed and studied in order to identify their main frequencies and the corresponding harmonics. This information can then be used to design a vibration reduction system on the helicopter if that is required, and also for diagnostic purposes as the harmonics are associated to distortion on the system [95].

8.4.1 Vibration Analysis with Main Rotor Varying Angular Velocity

The rotation of the helicopter rotor has a certain frequency. Any periodic vibration affecting the blades' motion within the rotor plane may have a characteristic frequency that can be related to the rotor.

The mass of the blades on the main rotor are: $m_{bl1} = 31.06$ kg, $m_{bl2} = 31.26$ kg, $m_{bl3} = 29.96$ kg and $m_{bl4} = 31.16$ kg. The main rotor angular speed, is 44.4 rad/s. The action of any external forces is neglected, for example: gravity. So, the system can be considered in the vacuum. As a consequence, unbalance of mass is considered on the main rotor blades in order to simulate the source of vibrations in the helicopter with

the requiring amplitude to be detected in the spectrum under the action of a varying rotating speed.

Varying Angular Velocity

When referring to the helicopter's fuselage, the induced vibrations frequency may be heterodyned by the rotor's frequency and the frequencies experienced in the fuselage may then be the frequencies of the sidebands.

It is known that when two signals of frequencies $\pm f_1$ and $\pm f_2$, are multiplied, the result is that the frequencies of each must be added. This results in four frequencies, $\pm(f_1 + f_2)$ and $\pm(f_1 - f_2)$, one of them is the sum of the input frequencies and the other is the difference between them. These are called sidebands. Sidebands are found extensively in avionics, where the deliberate use of the process is called heterodyning [143].

In order to reproduce this behaviour in the helicopter model, the main rotor's angular speed is implemented in VehicleSim as varying by using a PD controller in order to simulate the engine behaviour. The time dependant angular velocity is defined as [93]:

$$\Omega(t) = \Omega_1 + \Omega_2 \cos(\Omega_3 t) \quad (8.5)$$

where Ω_1 , Ω_2 and Ω_3 are angular speeds in rad/s. Equation (8.5) can be written as:

$$\Omega(t) = 2\pi f_1 + 2\pi f_2 \cos(2\pi f_3 t) \quad (8.6)$$

where f_1 , f_2 and f_3 are the corresponding frequencies expressed in Hz.

The main rotor's linear equation of motion obtained in VehicleSim is (see equation (8.7)):

$$\begin{aligned} & \dot{\Omega} [I_{rtz} + I_{blz} \cos^2 \theta + I_{blx} \sin^2 \theta + m_{bl} (y_{bl}^2 + eR(eR + 2y_{bl})) - k_d] \\ & = k_d \left((2\pi)^2 f_1 f_2 \sin(2\pi f_3 t) \right) - k_p (2\pi (f_1 + f_2 \cos(2\pi f_3 t)) - \Omega) \\ & - (2I_{blx} - 2I_{blz}) \Omega \dot{\theta} \cos \theta \sin \theta \end{aligned} \quad (8.7)$$

where k_p and k_d are the proportional and derivative controller gains. θ is the feather angle. I_{rtz} is the main rotor moment of inertial around the Z axis. I_{blx} and I_{blz} are the blades moments of inertia around the X and Z axes, and y_{bl} is the centre of mass of the blade along the Y axis. Equation (8.7) is shown for a blade with flap, lag and

feather, being the result analogous for the other blades. As it can be seen, equation (8.7) shows the contribution of the varying angular speed on the main rotor. The vibration spectrum in a helicopter can be described as a series of sinusoidal signals superimposed on a background of random noise. The main source of these sinusoidal signals is attributable to the harmonics appearing at the main rotor. The main rotor frequency of a helicopter is relatively low (typically 3 – 8 Hz) and inaccuracies in the rotor track, balance or blade pitch will result in vibrations at this frequency [154].

Several combinations of frequencies can be considered in order to study the vibrations appearing on the fuselage. In this work, $f_1 = 7$ Hz (according to the standard main rotor angular speed for this helicopter model 44.4 rad/s). On the other hand, the frequency f_3 will take the values: $f_3 = f_1$ and $f_3 = f_1/2$, these cases are of special interest because the fuselage is sensitive to vibrations from the main rotor at frequencies equal or multiple of this frequency [140].

On the other hand, f_2 will be changed in order to regulate the amplitude of the varying main rotor angular speed, see figures 8.43 and 8.44. So an additional perturbation will be taken into account in order to study its effect on the system. As a consequence of this, $f_2 = 0.16$ Hz or (1 rad/s), and $f_2 = 0.40$ Hz or (2.5 rad/s), these values are chosen as small varying rotating speed (1 rad/s) and high varying rotating speed (2.5 rad/s), other could also be considered but these are given as examples allowing to illustrate the behaviour under study.

Figure 8.43 shows the varying main rotor angular speeds when $f_3 = f_1/2 = 3.5$ Hz, $f_2 = 0.16$ Hz and $f_2 = 0.40$ Hz, the curves are obtained for cyclic feather angle of 0.1 rad or (5.72 degrees). All the simulations are carried out with these cyclic values. In addition to this, an interval of time of 1 second is shown in order to see the behaviour clearly, although the simulation was carried out for 44 seconds. In Figure 8.44 also shows, the varying main rotor angular speeds for the values: $f_3 = f_1 = 7$ Hz, $f_2 = 0.16$ Hz and $f_2 = 0.40$ Hz.

Typically, the main rotor frequency is detected on the fuselage as the main source of vibrations [129]. The varying angular speed should generate additional spectral components on the fuselage, as equation (8.7) suggests. The combination of frequencies (heterodyning) should be detected on the fuselage in the form of appearing vibrations [143]. On the other hand, harmonics should also appear when additional distortions

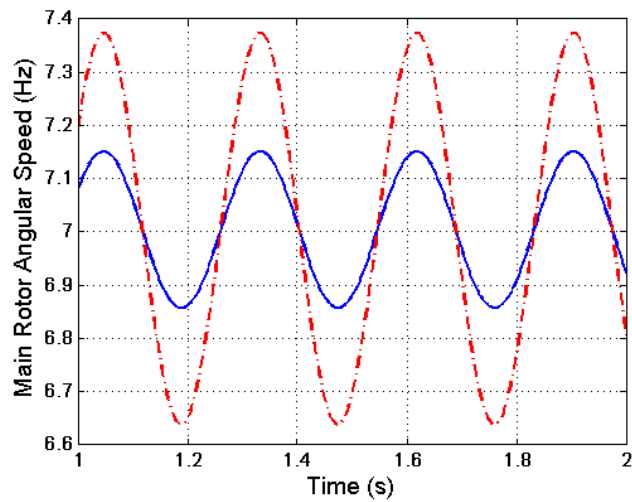


Figure 8.43: *Varying main rotor angular speed versus time. Solid blue line represents: $f_1 = 7$ Hz, $f_2 = 0.16$ Hz and $f_3 = f_1/2 = 3.5$ Hz. Dotted red line, $f_1 = 7$ Hz, $f_2 = 0.40$ Hz and $f_3 = f_1/2 = 3.5$ Hz.*

are considered i.e., the varying rotating speed raises its amplitude (see continuous and discontinuous lines in figures 8.43 and 8.44).

Vibrations Analysis

Helicopter vibration analysis is a difficult task due to the complexity of its structure, but reasonable accuracy is achievable with modern techniques.

There is a further consequence of the use of a rotating frame of reference that affects vibration frequencies created in the rotor and transmitted to the fuselage. The frequencies generated in the rotor may contain the rotational frequency of the rotor and the external perturbation frequency; both added and subtracted [143].

This work is carried out by estimating the vibration under the excitation conditions described previously i.e., varying main rotor angular speed and the corresponding frequencies $f_2 = 0.16$ Hz or $f_2 = 0.40$ Hz, $f_3 = f_1$ or $f_3 = f_1/2$. $f_1 = 7$ Hz and the cyclic feather angle is 0.1 rad. In order to carry out the proposed analysis it is necessary to follow the next steps: a) detection of vibrations on the fuselage as a consequence of the main rotor's varying speed and b) harmonic separation on the basis of the spectrogram

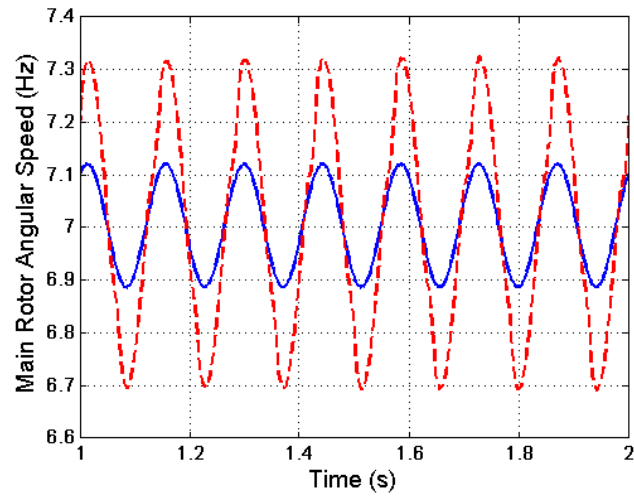


Figure 8.44: Varying main rotor angular speed versus time. Solid blue line represents: $f_1 = 7$ Hz, $f_2 = 0.16$ Hz and $f_3 = f_1$. Dotted red line, $f_1 = 7$ Hz, $f_2 = 0.40$ Hz and $f_3 = f_1$.

for identification of the detected vibration signals.

a) Heterodyning

If the main rotor angular speed is varying and the main rotor has unbalance of masses, as mentioned before, the fuselage may sense these in the form of appearing vibrations. In order to analyse the pure frequencies from the main rotor, the tail rotor angular speed degree of freedom is deactivated as VehicleSim allows to do so. The vibrations detected on the fuselage will then be originated at the main rotor only and the impact of these will be now studied in both the roll and pitch axes.

According to [143], if the main rotor angular speed varies and it is composed by two signals of different frequencies, the frequencies of each one must be added. A first simulation is carried out with a combination of frequencies: $f_3 = f_1/2 = 3.5$ Hz and $f_2 = 0.16$ Hz or (1 rad/s), in this case f_3 is half of f_1 (see Figure 8.43). The results of this simulation are shown in the spectrogram resulting of analyzing via STFT the fuselage's rotation around the X axis (roll) (Figure 8.45). As it can be seen, there are three main frequencies: 3.5 Hz = $f_1 - f_3$, 7 Hz = f_1 and 10.5 Hz = $f_1 + f_3$. This clearly shows a heterodyning behaviour as expected.

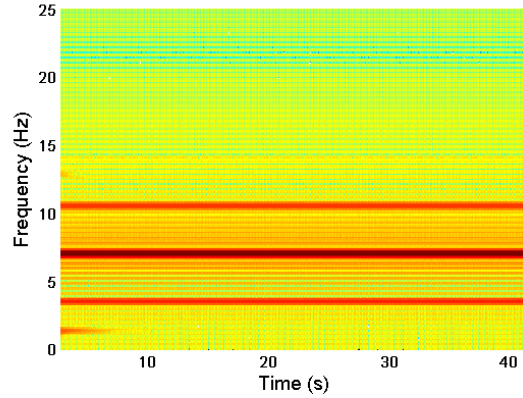


Figure 8.45: *Fuselage X position spectrogram when the varying main rotor speed is given by the frequencies: $f_1 = 7$ Hz, $f_2 = 0.16$ Hz and $f_3 = f_1/2 = 3.5$ Hz.*

If now the spectrogram is obtained for the fuselage's rotation around the Y axis (pitch) the heterodyning behaviour is also shown, see Figure 8.46.

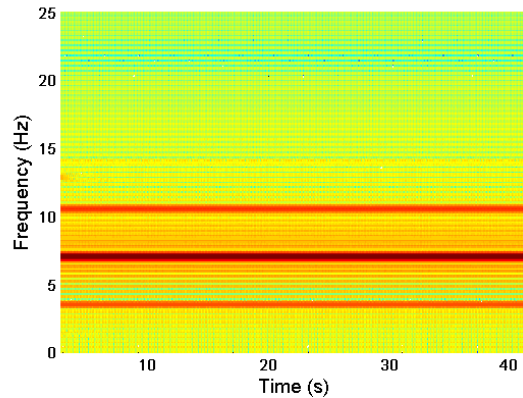


Figure 8.46: *Fuselage Y position spectrogram when the varying main rotor speed is given by the frequencies: $f_1 = 7$ Hz, $f_2 = 0.16$ Hz and $f_3 = f_1/2 = 3.5$ Hz.*

A second combination of frequencies can be carried out in order to show as the heterodyning behaviour is obtained under these new conditions. In this case, $f_3 = f_1 = 7$ Hz and $f_2 = 0.16$ Hz or (1 rad/s), here f_3 is equal to f_1 . The spectrogram of the fuselage's rotation around the X axis is shown in Figure 8.47. As it can be seen, there are two main frequencies: 7 Hz = f_1 and 14 Hz = $f_1 + f_3$, heterodyning behaviour is verified on the fuselage as a consequence of the varying angular speed. The spectrogram for the

fuselage rotation around the Y axis is represented in Figure 8.48: two main frequencies are clearly identified, their values are 7 Hz and 14 Hz, this coincides with the expected behaviour.

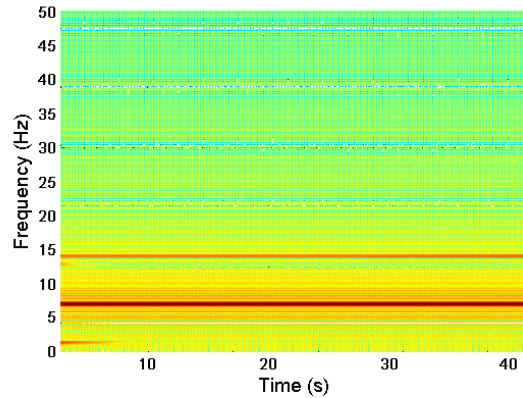


Figure 8.47: *Fuselage X position spectrogram when the varying main rotor speed is given by the frequencies: $f_1 = 7$ Hz, $f_2 = 0.16$ Hz and $f_3 = f_1 = 7$ Hz.*

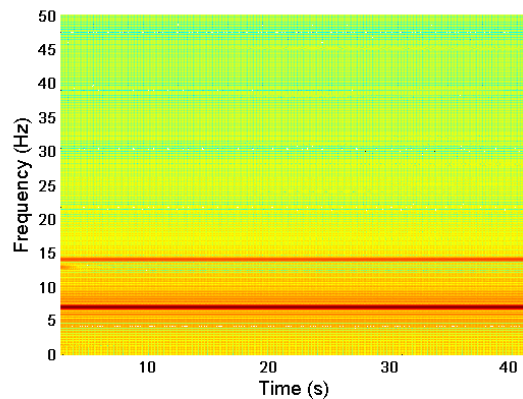


Figure 8.48: *Fuselage Y position spectrogram when the varying main rotor speed is given by the frequencies: $f_1 = 7$ Hz, $f_2 = 0.16$ Hz and $f_3 = f_1 = 7$ Hz.*

The rotor angular speed with these simulations, it has been shown that results in vibrations that affect the fuselage roll and pitch, and their sidebands are as expected.

b) Heterodyning and Increase in Varying Rotation Speed

The identification of existing sidebands is a strong indicator of failures in mechanical systems. The presence of harmonic or modulation series is then used as indicators of distortion or damage of one or more parts of a mechanical system. Mathematically,

a harmonic series is characterized by a fundamental frequency and defined as a set of spectral components of frequencies representing the harmonic order [153]. The next study will allow to test the presence and/or absence of harmonics as a consequence of the increase in the varying main rotor angular speed, being it a useful tool to detect anomalous behaviour. The harmonics may be generated as a consequence of an increase of f_2 in each case, which generates vibration excitations. f_2 is increased from 0.16 Hz or (1 rad/s) to 0.40 Hz or (2.5 rad/s).

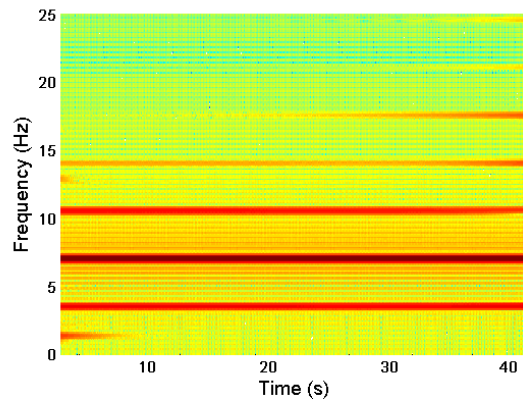


Figure 8.49: *Fuselage X rotation spectrogram when the varying main rotor speed is given by the frequencies: $f_1 = 7$ Hz, $f_2 = 0.40$ Hz and $f_3 = f_1/2 = 3.5$ Hz.*

Take $f_3 = f_1/2 = 3.5$ Hz and $f_2 = 0.40$ Hz or (2.5 rad/s), the varying main rotor angular speed changes as Figure 8.43 shows. The corresponding fuselage spectrogram of rotation around the X axis is represented in Figure 8.49.

A comparison can be performed between figures 8.45 and 8.49, as it can be seen, the frequencies 3.5 Hz, 7 Hz and 10.5 Hz are presented in the spectrogram in Figure 8.45, and harmonics appear in Figure 8.49 with frequencies 14 Hz = $f_1 + 2f_3$, 17.5 Hz = $f_1 + 3f_3$ as a consequence of the increase in f_2 .

Similar study can be carried out on the fuselage's pitch axis, being the behaviour analogous to the fuselage's roll axis, see Figure 8.50.

A final simulation is carried out with a combination of frequencies: $f_3 = f_1 = 7$ Hz and $f_2 = 0.40$ Hz or (2.5 rad/s). The spectrogram of the fuselage's rotation around the roll axis is represented in Figure 8.51. A comparison can be done between Figure 8.47 and Figure 8.51, the frequencies 7 Hz and 14 Hz appear in the spectrogram of Figure

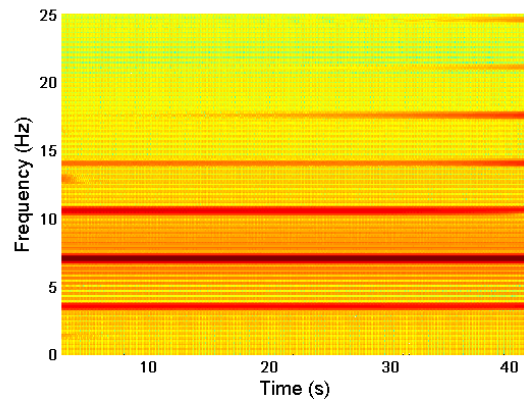


Figure 8.50: *Fuselage Y rotation spectrogram when the varying main rotor speed is given by the frequencies: $f_1 = 7$ Hz, $f_2 = 0.40$ Hz and $f_3 = f_1/2 = 3.5$ Hz.*

8.47, and harmonics appear with frequencies 21 Hz = $f_1 + 2f_3$, 28 Hz = $f_1 + 3f_3$, 42 Hz = $f_1 + 5f_3$ appear in the results shown in Figure 8.51.

Similarly, a spectrogram is obtained for the fuselage pitch axis rotation. As it can be seen in Figure 8.52, the spectrogram shows similar sequences of harmonics as the fuselage was showing in the case of X axis for this combination of frequencies.

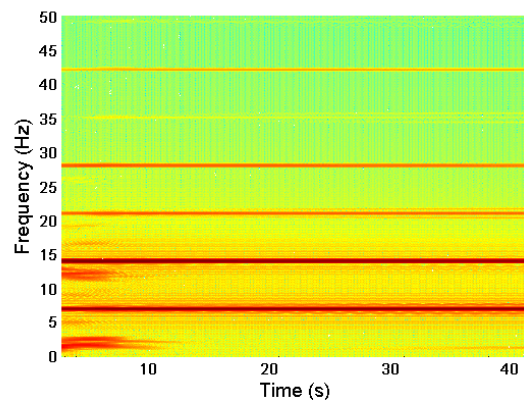


Figure 8.51: *Fuselage X rotation spectrogram when the varying main rotor speed is given by the frequencies: $f_1 = 7$ Hz, $f_2 = 0.40$ Hz and $f_3 = f_1 = 7$ Hz.*

The reason of this analysis is to study the effects on the fuselage's rotation (X and Y axes) spectrograms that the increase of f_2 has. The changes introduced in the rotor angular speed have an impact in the fuselage in the form of vibrations and subsequent harmonics that appear as expected from theoretical predictions.

The main vibrations sources on a helicopter are mechanical and aerodynamical excitations. These results allow to establish analogies between a rotor the varying angular speed and the simulated behaviour.

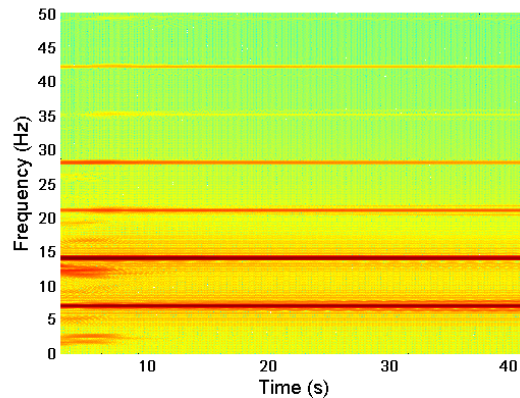


Figure 8.52: *Fuselage Y rotation spectrogram when the varying main rotor speed is given by the frequencies: $f_1 = 7$ Hz, $f_2 = 0.40$ Hz and $f_3 = f_1 = 7$ Hz.*

8.4.2 Vibrations in Hover

Helicopter vibrations have been treated in the previous section as well as in Chapter 7. In those cases the influence of the aerodynamic load was not considered. In this section, the vibrations appearing on the fuselage's axes X and Y during hover flight are studied. It is known that vibrations are generally low in hover [140]. In this case, there are some significant differences with respect to the vibrations analysed previously. As well there is some difference with respect to the helicopter model described in previous chapter i.e., the flap and lag degrees of freedom do not have springs fitted on them, although the lag maintains a damper. In addition to this, it does not exist an unbalance of masses on the main and tail rotors.

A hover flight simulation is carried out for 50 s, the height is $h = 250$ m and the main rotor's collective feather angle is 0.175 rad and tail rotor's collective feather angle is also 0.175 rad. Figure 8.53 left, shows the fuselage's oscillations (vibrations) around the X axis during hover flight. Figure 8.53 right, shows a spectrogram obtained for this simulation.

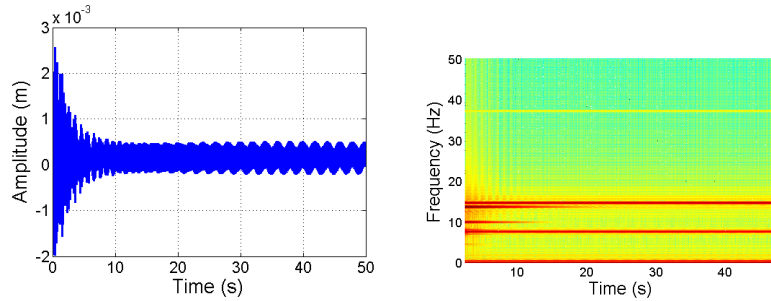


Figure 8.53: *Left, hover flight vibrations around the fuselage's X axis. Right, spectrogram of the simulation.*

As it can be seen, Figure 8.53 shows various predominant frequencies which come from the main rotor loads (their values are approximately 7.6 Hz), this frequency is the flap frequency as it was mentioned in section 8.2.3. There is also a second predominant frequency (its value is approximately 15.2 Hz) this is twice, the flap frequency and a third predominant frequency is found at around 37.1 Hz, this frequency is the flap frequency on the tail rotor, as it explained in section 8.2.3.

The vibration around the Y axis is shown in Figure 8.54.

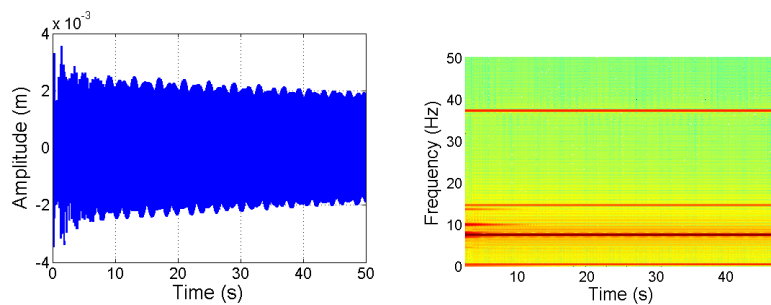


Figure 8.54: *Left, hover flight vibrations around the fuselage's Y axis. Right, spectrogram of the simulation.*

Similar analysis is carried out for the oscillations appearing on the fuselage's Y axis. The three predominant frequencies of these vibrations are shown in the spectrogram in Figure 8.54 right. These are approximately 7.6 Hz which origin caused by the main rotor flap, the second frequency is approximately 15.2 Hz, its value is twice the main rotor flap frequency and the third frequency is around 37.1 Hz, it is associated to the

tail rotor flap motion.

As it can be seen, the aerodynamic loads are sources of vibrations on the helicopter's fuselage. The spectrograms in hover flight obtained under the influence of aerodynamic loads agree with the theoretical prediction: a) there is an important source of helicopter vibration, the aerodynamics forces [140], b) the aerodynamic loads on a helicopter rotor blade vary considerably as it moves around the rotor disc. These loads arise from the aerodynamic forces on the rotor blades, together with the inertial forces produced by the flap and lag motions of the blade [141].

8.5 Chapter Summary

The aim of this chapter was to show that external forces such as gravity, aerodynamic loads and varying angular speed on the main rotor can be simulated in VehicleSim and their effects can be analysed and studied.

The first external force to be added into the model is the gravity, its influence on the rotorcraft has been shown and the ground action has been modelled on the fuselage. The equilibrium positions for the blades on the main and tail rotors have been also simulated under the action of gravity.

The nonlinear aerodynamic equations for flap and lag motion as well as lift and drag forces were modelled and full details of their validation have been provided.

On the other hand, hover, climb, descent and forward flight conditions have been simulated and the parameters used in each case have been carefully described as well as the flight conditions. Several trajectories in forward flight have been simulated in order to show that the modelled helicopter can fly with different orientation in the space. Besides, combinations of different flight conditions have been done. In this way, it has been shown as the helicopter model here presented is capable of performing trajectories.

In addition to this, a model in which the main rotor angular speed is not constant and changes by means of a PD controller has been presented. This allows to obtain different combinations of frequencies between the main rotor standard frequency and external varying frequencies, this combination of frequencies is important in order to study and analyze the vibrations appearing in the fuselage as a consequence of these perturbations.

Various tests in absence of external perturbations were carried out in order to study pure vibrations on the fuselage's roll and pitch axes under the action of this varying rotating speed.

Fuselage's vibrations spectrograms have been obtained and analyzed by using a Short Time Fourier Transform process. Heterodyning conditions were found in the spectrograms for the various cases analyzed, i.e., when the frequency f_3 changes its value as $f_3 = f_1$ and $f_3 = f_1/2$, the obtained results match those predicted by theoretical approaches. On the other hand, sequences of harmonics on the spectrograms were observed when the main rotor varying angular speed increases the frequency f_2 . These results are still on a preliminary phase and the author expects that they will allow to develop further analogies with experimental results in future work. Spectrograms analysis on the fuselage roll and pitch axes reflected appearing vibrations as a consequence of the varying nature of the main rotor angular speed, these results have been shown to satisfy theoretical predictions.

Finally, the vibrations in hover around the X and Y were also obtained. It has been shown that the presence of aerodynamic load increases the vibrations on the fuselage as dictated by the theoretical prediction.

Part IV

Conclusions

Chapter 9

Conclusions and Future Work

9.1 Conclusions

9.1.1 Main Findings

The motivation of this work came from the need to provide a comprehensive helicopter model, that is not too computationally demanding to implement and could be used for control applications, stability analysis, etc. In particular, a detailed helicopter simulation model using VehicleSim has been developed. It has been shown that the very preliminary results obtained in Autosim by Tomas-Rodriguez [124], [125], can be expanded by the multibody modelling code VehicleSim in order to build up a high fidelity helicopter model on Sikorsky configuration that accounts for both dynamics and aerodynamics. The approach developed in here provides a robust model of a helicopter, VehicleSim gives this in the sense of modelling uncertainties because it is usual on the modelling process to perform linearisations that fail to capture some of fundamental nonlinear dynamics and couplings. In addition to this, automated equations obtained using this software provide an accurate representation of the complex system's dynamics. VehicleSim commands have been used to describe the components of the helicopter multibody system in a parent-child relationship according to their physical constraints and joints. Furthermore, VehicleSim code has been used to generate a C simulation program, capable of computing general motions corresponding to specific initial conditions

and external forcing inputs.

9.1.2 Contribution to the Knowledge

Both linear and nonlinear equations for the main rotor flap and lag degrees of freedom and flap-lag coupling as well as feather (all this in vacuum conditions) have been provided and all of them have been validated with the existing theory. Two appendices are included in order to validate with analytical mechanical equations the flap and lag expressions obtained from VehicleSim. The effects of various values of blade offset and springs stiffness fitted on the blades' hinges were analyzed for the flap and lag cases, and the obtained results proved to be correct by theory validation. Main rotor flap and lag degrees of freedom have been validated using a frequency domain approach in absence of external forces. Fuselage and main rotor interaction has been studied and validated using modal analysis. In fact, the stability of the system has been studied using the root locus methodology. This was carried out as the full nonlinear equations of motion of the helicopter model were obtained in C, time histories generated and the linearised state-space model was also obtained in symbolic form as a Matlab m-file. A typical local stability study in VehicleSim requires the importation of quasi-steady time histories from the nonlinear simulation to the symbolic linearised equations of motion. In addition to this, the shape modes have been analyzed using modal analysis, and the results showed the existence of a coupling between the fuselage vertical displacement and the main rotor blade flap mode. The influence of the mass ratio, $mass_{blade}/mass_{fuselage}$, on the coupled modes was demonstrated, and the influence of the lag degree of freedom on the fuselage was also analyzed. The fuselage influence on the flap was studied as a consequence of the gyroscopic movement on the fuselage. The results showed good agreement with the theoretical findings existing in the literature.

Dynamic vibrations (mainly from the main rotor) appearing on the fuselage have been as well studied, being an unbalance of mass the main source of vibrations. Vibrations originated at the main rotor were simulated and their effects on the fuselage were studied; first, the offset of the flap hinge and its effect on the fuselage were considered. Secondly, the lag hinge vibrations due to the applied dynamic load. Furthermore, an unbalance of mass on both rotors was taken into account and analyzed, being the frequencies of the obtained vibrations in agreement to the expected results. Fuselage vibration

9.1. CONCLUSIONS

spectrograms were obtained and analyzed by using a Short Time Fourier Transform process.

The tail rotor was modelled as well as the flap and feather degrees of freedom on this rotor. The coupling flap-feather (via delta three angle) has been modelled and validated with theoretical results. In fact, for various cases, it was shown how the flap frequencies increased as a function of the advance ratio as a consequence of this coupling.

Both main and tail rotors angular speeds have been implemented by using PID controllers. This allows to simulate the torques on both rotors. Furthermore, the helicopter's six degrees of freedom were controlled around the equilibrium position i.e., the point $(0, 0, 0)$. The action of the external forces on the system adds extra complexity in the modelling process. Gravity was the first external force added to the system in absence of aerodynamic forces. The ground was simulated on the fuselage, this showed that the fuselage remains around the equilibrium point $(0, 0, 0)$ when this is adequately modelled.

A helicopter aerodynamic model has also been built using blade element theory on the main and tail rotors. Nonlinear aerodynamic have been modelled and they have been validated with specialist literature. Hover, climb, descent and forward flight have been simulated. The orientation in space has been shown as well as the corresponding forward trajectories when the aerodynamic model is acting. Different flight conditions can be combined and simulated to allow the model to follow certain trajectories.

Rotor tilt was considered and modelled on the main rotor as real helicopters do. The effect that tilt has on the system was studied on hover flight conditions. The results showed that the tilt on the main rotor has a contribution on the drift effect: under the simulation conditions taken into account in this work, the tilt on the main rotor slightly reduces the drift effect.

Vibrations when an external perturbation is acting on the main rotor such as varying angular speed have been studied according to the expression $\Omega(t) = 2\pi f_1 + 2\pi f_2 \cos(2\pi f_3 t)$ where f_1 is the main rotor frequency and f_2 and f_3 are the corresponding external frequencies expressed in Hz. In fact, a model in which the main rotor angular speed is not constant and changes by means of a PD controller has been induced in the model. This allows to obtain different combinations of frequencies between the main rotor standard frequency and the external varying frequencies, the combination of frequencies are

important in order to study and analyze the vibrations appearing in the fuselage as a consequence of these perturbations. Various tests in absence of external perturbations were carried out in order to study pure vibrations on the fuselage's roll and pitch axes under the action of only the main rotor varying angular speed.

Heterodyning conditions were found in the spectrograms for the various cases considered i.e., when frequency f_3 changes its value as $f_3 = f_1$ and $f_3 = f_1/2$, the obtained results match those predicted by theoretical approaches. On the other hand, sequences of harmonics on the spectrograms were observed when the main rotor varying angular speed increases the frequency f_2 . Finally, aerodynamic vibrations in hover flight have been simulated and analyzed, showing that the aerodynamic forces have the expected behaviour if the vibrations are compared to the vibrations obtained in absence of the external forces i.e., the noise is increased and the spectral components are larger.

On the other hand, an UAV helicopter dynamical model has also been modelled. This model has been developed under the umbrella of an academic collaboration with ULL (La Laguna University, Spain). Previous theoretical knowledge was used to model as well as to implement this helicopter model. Moreover, this model was used to analyze the vibrations appearing on the fuselage as a consequence of mass imbalance on the main rotor, the vibrations obtained were analysed using a FFT (Fast Fourier Transform) Matlab algorithm and these results agreed with experimental values proposed by various authors. Once the model was built in VehicleSim and validated, La Laguna University developed a robust control methodology for an onboard vision system.

During the timeframe in which this work has been carried out, journal articles have been published as well as conference contributions have been made:

1) Marichal, G. N., Tomas-Rodriguez, M., Hernandez, A., Castillo-Rivera, S., Campoy, P. *Vibration Reduction for Vision Systems on Board UAV Using a Neuro-Fuzzy Controller*. June 2013. Journal of Control and Vibrations. 25, pp. 1-12. SAGE Journals, 2013. ISSN 1077-5463.

2) Marichal-Plasencia, G. N., Tomas-Rodriguez, M., Castillo-Rivera, S., Hernandez-Lopez, A. *Modelling and Analysis of Vibrations in a UAV Helicopter with a Vision System*. 2012. International Journal of Advanced Robotic Systems. Vol. 9, 220. ISSN:1729-8806.

- 3) Castillo-Rivera, S., Tomas-Rodriguez, M., Marichal-Plasencia, G. N. *Helicopter Main Rotor Vibration Analysis with Varying Rotating Speed*. XXXV Conference of Automation. Valencia 3-5 September 2014. Spain. pp. 34-41. ISBN-13: 978-84-697-5089-6.
- 4) Castillo-Rivera, S., Tomas-Rodriguez, M., Marichal-Plasencia, G. N., Hernandez-Lopez, A. *Estudio de la Interaccion del Fuselaje y el Movimiento de Aleteo de las Palas del Rotor Principal en un Helicoptero*. XXXIV Conference of Automation. Terrassa 4-6 September 2013. Spain. pp. 514-521. ISBN 978-84-616-5063-7.
- 5) Marichal-Plasencia, G. N., Tomas-Rodriguez, M., Campoy, P., Hernandez-Lopez, A., Castillo-Rivera, S. *Reduccion de las Vibraciones de un Sistema de Vision a Bordo de un Helicoptero Mediante un Controlador Inteligente*. XXXIII Conference of Automation. Vigo 5-7 September 2012. Spain. pp. 179-186. ISBN 978-84-8158-5834.
- 6) Marichal-Plasencia, G. N., Tomas-Rodriguez, M., Campoy, P., Castillo-Rivera, S., Hernandez-Lopez, A. *Generacion de Vibraciones a Partir de la Simulacion de un Helicoptero para el Estudio de Sus Efectos Sobre el Sistema de Vision*. XXXII Conference of Automation. Sevilla 7-9 September 2011. Spain. ISBN 978-84-694-6454-0.

9.1.3 Scope of the Investigation

The presented work has several limitations as the blades are rigid in both rotors.

The fuselage's aerodynamic effects have not been taken into account. The aerodynamic modelling was focused only on both rotors using blade element theory.

The ground effect is not simulated as neither it is the landing and take off manoeuvre on the ground. In addition to this, hover, climb, descent and forward flight are simulated with an initial height of $h = 250$ m as well as different trajectories. On the contrary, other heights could be selected when the controllers' gains are calibrated for the corresponding reference.

In conclusion, a full dynamical helicopter model was presented as well as an aerodynamic model. The complexity involved in the modelling process helicopter has been explained and evidenced. The need for automated methods in the analysis of such systems has been demonstrated. This work opens the door for future helicopter studies as this model provides the basis for not too complicated approach to these type of vehicles,

with the guarantee of being a validated model, in which nonlinearities and couplings (often simplified in the current existing models) are captured and maintained, increasing in this way the fidelity of the future research carried out on this work.

9.2 Future Work

Several tasks could be completed as future work and in fact, some of them are being explored at present.

9.2.1 Helicopter Model Improvements

In this work, the blades were assumed to be rigid bodies and they have been modelled as such. In the improved helicopter model, an implementation of flexible blades would be possible using VehicleSim. In order to carry this out, the blades could be divided into, for example, twenty blade elements. Each blade element would have a degree of freedom respect to the previous one. In addition to this, the flexibility between each of them could be modelled with a spring on each blade element. Their values would be selected using optimization methods that the author is currently studying. The optimization could be carried out by comparison with blade flexibility parameters according to the helicopter model used in this work.

One interesting result would be to characterize the fuselage's flexibility. A finite-element fuselage's model can be used to obtain mode shapes of the flexible structure. This will allow to study the coupled main rotor and fuselage. As a consequence of this, new mode shapes will appear and the corresponding studies could be analyzed.

9.2.2 Aerodynamic Modelling

On the other hand, aerodynamic forces could be included directly acting on the fuselage, as well as at the blades, which is the current taken approach.

Another area of future investigation would be use of CFD approaches to complete the picture of an advanced aerodynamical model. As CFD approaches can be implemented in VehicleSim as an external source to model features such as rotor wake, interaction

problems between the blades under determined aerodynamic conditions, tip vortex, etc.

The ground effect could be also modelled in order to simulate the landing and take off manoeuvre on the ground. Furthermore, the hover, climb, descent and forward flight could be modelled for different initial heights and several trajectories. The controllers' gains in these cases, need to be calibrated for the corresponding cases.

9.2.3 Trajectory Optimization

The trajectory optimization could be also studied in order to calculate the optimal control inputs and the resulting response of a rotorcraft, which minimize a cost function (or maximize) while satisfying given constraints such as requirements for a determinate manoeuvre.

So, an analysis should be done to determine with precision which is the maximum theoretical helicopter's performance. As a result, this must inevitably lead to conservative design choices or restrictions on the rotorcraft operation.

9.2.4 Control Implementation

The helicopter models presented in here can now be used to design and to test robust control systems for helicopter control.

Robust controllers could be synthesized could be by the H-infinity loop shaping approach. The simulation results should show that the robust controller stabilizes the system and rejects the disturbances considered on the helicopter as aerodynamic loads. Formulation and comparative studies between the classical controller PID and the robust H-infinity loop shaping controller could be provided with simulations results in presence of the noise disturbance in the closed loop control of the helicopter's different degrees of freedom.

9.2.5 Future Contribution to the Knowledge

This work allows to establish analogies between the varying rotating speed of the rotor and experimental behaviour such as dynamic, aerodynamic loads, etc. Experimental

9.2. FUTURE WORK

spectrograms could be studied and analogies could be established with the results proposed in this thesis.

Finally, at present, the author is writing up the contents on the modelling aspects of this thesis and expects to submit an international journal article in the next months.

Part V

Appendices

Appendix A

Nonlinear Flap Equation using Lagrange's Method

In this appendix, the calculations for validating the nonlinear flap equation provided as (7.9) are derived.

The Lagrangian function is the difference between the kinetic energy of a system and its potential energy:

$$L = T - V \quad (\text{A.1})$$

In the case of the flap degree of freedom (β) the Lagrange's equation can be written as:

$$\frac{d}{dt} \left(\frac{\partial L}{\partial \dot{\beta}} \right) - \frac{\partial L}{\partial \beta} = F_y \frac{\partial y}{\partial \beta} \quad (\text{A.2})$$

where β is the generalized coordinate for the flap mode and the right hand side term in the above equation represents the generalized force.

The kinetic energy of an extended mass confined to three dimensions is given by:

$$T = \frac{1}{2} m_{bl} (\dot{x}^2 + \dot{y}^2 + \dot{z}^2) + \frac{1}{2} I_{blx} \dot{\beta}^2 \quad (\text{A.3})$$

In this case, the mass under consideration is the blade's mass. The potential energy corresponding to the flap spring is:

$$V = \frac{1}{2}k_{fj}\beta^2 \quad (\text{A.4})$$

where k_{fj} denotes the spring stiffness.

The corresponding space coordinates and their derivatives are:

$$x = 0 \quad , \quad \dot{x} = 0 \quad (\text{A.5})$$

$$y = y_{bl}\cos\beta \quad , \quad \dot{y} = -y_{bl}\dot{\beta}\sin\beta \quad (\text{A.6})$$

$$z = y_{bl}\sin\beta \quad , \quad \dot{z} = y_{bl}\dot{\beta}\cos\beta \quad (\text{A.7})$$

Now, the Lagrangian function is written as:

$$\begin{aligned} L = \frac{1}{2}m_{bl}(\dot{x}^2 + \dot{y}^2 + \dot{z}^2) + \frac{1}{2}I_{blx}\omega_x^2 - \frac{1}{2}k_{fj}\beta^2 = \frac{1}{2}m_{bl}\left(y_{bl}^2\dot{\beta}^2\sin^2\beta + y_{bl}^2\dot{\beta}^2\cos^2\beta\right) \\ + \frac{1}{2}I_{blx}\dot{\beta}^2 - \frac{1}{2}k_{fj}\beta^2 \end{aligned} \quad (\text{A.8})$$

In order to obtain the Lagrange's equations, first, the derivative of the Lagrange function with respect to the generalized coordinate needs to be calculated.

$$\frac{\partial L}{\partial \beta} = m_{bl}y_{bl}^2\dot{\beta}\sin^2\beta + m_{bl}y_{bl}^2\dot{\beta}\cos^2\beta + I_{blx}\dot{\beta} \quad (\text{A.9})$$

Next, the derivative of the above equation with respect to time is obtained:

$$\frac{d}{dt}\left(\frac{\partial L}{\partial \dot{\beta}}\right) = m_{bl}y_{bl}^2\ddot{\beta}\sin^2\beta + m_{bl}y_{bl}^2\ddot{\beta}\cos^2\beta + I_{blx}\ddot{\beta} \quad (\text{A.10})$$

And finally, the derivative of the Lagrangian function with respect to β is also calculated.

$$\frac{\partial L}{\partial \beta} = -k_{fj}\beta \quad (\text{A.11})$$

On the other hand, the first Euler's equation of motion for a rigid body is considered as:

$$I_{blx}\dot{\omega}_x + (I_{blz} - I_{bly})\omega_y\omega_z = \tau_x \quad (\text{A.12})$$

The angular speeds are:

$$\dot{\omega}_x = 0 \quad ; \quad \omega_y = \Omega\cos\beta \quad ; \quad \omega_z = \Omega \quad (\text{A.13})$$

Then, equation (A.12) can be written as:

$$(I_{blz} - I_{bly})\Omega^2 \cos\beta = \tau_x = fy_{bl} \quad (\text{A.14})$$

where f is the component of the force F_y that generates this moment on the blade.

Therefore, the force along the Y axis is equal to:

$$F_y = m_{bl}y_{bl}\Omega^2 \cos\beta + m_{bl}eR\Omega^2 + (I_{blz} - I_{bly})\Omega^2 \cos\beta / y_{bl} \quad (\text{A.15})$$

the first and second terms on the right hand side do consider the centre of mass and the blade's offset under the action of a centrifugal force. The third term is inherited from equation (A.14).

Additionally to this:

$$\frac{\partial y}{\partial \beta} = -y_{bl} \sin\beta \quad (\text{A.16})$$

y is the corresponding space coordinate (see equation (A.2))

Finally, equation (A.2) can be written as:

$$\begin{aligned} I_{blx}\ddot{\beta} + m_{bl}y_{bl}^2\ddot{\beta} + k_{fj}\beta &= -m_{bl}y_{bl}^2\Omega^2 \cos\beta \sin\beta - m_{bl}y_{bl}eR\Omega^2 \sin\beta \\ &- (I_{blz} - I_{bly})\Omega^2 \cos\beta \sin\beta \end{aligned} \quad (\text{A.17})$$

which as it can be seen, coincides with the expression obtained in VehicleSim for the nonlinear flap equation of motion in section 7.1.1.

Appendix B

Nonlinear Lag Equation using Lagrange's Method

The Lagrangian function is given by:

$$L = T - V \quad (\text{B.1})$$

In the case of the lag degree of freedom (ξ) the Lagrange's equation is:

$$\frac{d}{dt} \left(\frac{\partial L}{\partial \dot{\xi}} \right) - \frac{\partial L}{\partial \xi} + \frac{\partial F}{\partial \xi} = F_y \frac{\partial y}{\partial \xi} \quad (\text{B.2})$$

where ξ is the generalized coordinate for the lag and the right hand side term in the above equation represents the generalized force.

The kinetic energy of an extended mass confined to three dimensions is given by:

$$T = \frac{1}{2} m_{bl} (\dot{x}^2 + \dot{y}^2 + \dot{z}^2) + \frac{1}{2} I_{blz} \dot{\xi}^2 \quad (\text{B.3})$$

In this case, the mass under consideration is the blade's mass. The elastic potential energy corresponding to the lag spring is:

$$V = \frac{1}{2} k_{lj} \xi^2 \quad (\text{B.4})$$

where k_{lj} denotes the spring stiffness.

The damper force is included as a generalized force:

$$F = \frac{1}{2}d_{lj}\dot{\xi}^2 \quad (\text{B.5})$$

where d_{lj} is the damping constant.

The corresponding space coordinates and their derivatives are:

$$x = y_{bl}\sin\xi \quad , \quad \dot{x} = y_{bl}\dot{\xi}\cos\xi \quad (\text{B.6})$$

$$y = y_{bl}\cos\xi \quad , \quad \dot{y} = -y_{bl}\dot{\xi}\sin\xi \quad (\text{B.7})$$

$$z = 0 \quad , \quad \dot{z} = 0 \quad (\text{B.8})$$

Now, the Lagrangian function is written as:

$$L = \frac{1}{2}m_{bl}(\dot{x}^2 + \dot{y}^2 + \dot{z}^2) + \frac{1}{2}I_{blz}\omega_z^2 - \frac{1}{2}k_{lj}\xi^2 = \frac{1}{2}m_{bl}\left(y_{bl}^2\dot{\xi}^2\sin^2\xi + y_{bl}^2\dot{\xi}^2\cos^2\xi\right) + \frac{1}{2}I_{blz}\dot{\xi}^2 - \frac{1}{2}k_{lj}\xi^2 \quad (\text{B.9})$$

In order to obtain the Lagrange's equations, first the derivative of the Lagrange function with respect to the generalized coordinate needs to be calculated.

$$\frac{\partial L}{\partial \dot{\xi}} = m_{bl}y_{bl}^2\dot{\xi}\sin^2\xi + m_{bl}y_{bl}^2\dot{\xi}\cos^2\xi + I_{blz}\dot{\xi} \quad (\text{B.10})$$

Next, the derivative of the above equation with respect to time is obtained:

$$\frac{d}{dt}\left(\frac{\partial L}{\partial \dot{\xi}}\right) = m_{bl}y_{bl}^2\ddot{\xi}\sin^2\xi + m_{bl}y_{bl}^2\ddot{\xi}\cos^2\xi + I_{blz}\ddot{\xi} \quad (\text{B.11})$$

And finally, the derivative of the Lagrangian function with respect to ξ is also calculated.

$$\frac{\partial L}{\partial \xi} = -k_{lj}\xi \quad (\text{B.12})$$

The derivative for the damping generalized force is worked out:

$$\frac{\partial F}{\partial \dot{\xi}} = d_{lj}\dot{\xi} \quad (\text{B.13})$$

On the other hand, the third Euler's equation of motion for a rigid body is considered.

$$I_{blz}\dot{\omega}_z + (I_{bly} - I_{blx})\omega_x\omega_y = \tau_z \quad (\text{B.14})$$

The angular speeds are:

$$\dot{\omega}_z = 0 ; \omega_x = 0 ; \omega_y = 0 \quad (\text{B.15})$$

Now equation (B.14) can be written as:

$$\tau_z = 0 \quad (\text{B.16})$$

Therefore, the force along the Y axis is equal to:

$$F_y = m_{bl}eR\Omega^2 \quad (\text{B.17})$$

the term on the right hand side in equation (B.17) is given by considering the offset for the blade under the action of a centrifugal force.

Additionally to this:

$$\frac{\partial y}{\partial \xi} = -y_{bl}\sin\xi \quad (\text{B.18})$$

Finally, equation (B.2) can be written as:

$$I_{blz}\ddot{\xi} + m_{bl}y_{bl}^2\ddot{\xi} = -m_{bl}eR\Omega^2y_{bl}\sin\xi - k_{lj}\xi - d_{lj}\dot{\xi} \quad (\text{B.19})$$

wich as it can be seen coincides with expression for the nonlinear lag equation obtained in VehicleSim in section 7.1.2.

Bibliography

- [1] Leishman, J. G. *A History of Helicopter Flight*. 2000. Cambridge University Press
- [2] Roget, B. *Individual Blade Control for Vibration Reduction of a Helicopter with Dissimilar Blades*. 2004. Thesis. University of Maryland, College Park, USA
- [3] Flight Standards Service. *Rotorcraft Flying Handbook*. 2000. U.S. Department of Transportation. Federal Aviation Administration
- [4] Brown, R. E., Houston, S. *CFD-Based Simulation and Experiment in Helicopter Aeromechanics*. September 2003. Imperial College London and University of Glasgow, Glasgow, 8-9
- [5] Narramore, J. C. *Computational Fluid Dynamics Development and Validation at Bell Helicopter*. 1995. Textron Bell Helicopter, Fort Worth, TX. In AGARD, Aerodynamics and Aeroacoustics of Rotorcraft 13. N96-13582 02-01
- [6] Johnson, W. *A History of Rotorcraft Comprehensive Analyses*. 2012. NASA/TP-2012-216012
- [7] Blankenship, B. L., Harvey, K. W. *A Digital Analysis for Helicopter Performance and Rotor Blade Bending Moments*. October 1962. Journal of the American Helicopter Society. Vol. 7, no. 4, pp. 55-69
- [8] Duhon, J. M., Harvey, K. W., Blankenship, B. L. *Computer Flight Testing of Rotorcraft*. October 1965. Journal of the American Helicopter Society. Vol. 10, no. 4, pp. 36-48
- [9] Gabel, R. *Current Loads Technology for Helicopter Rotors*. March 1973. AGARD CP 122

BIBLIOGRAPHY

- [10] Johnson, W. *CAMRAD/JA A Comprehensive Analytical Model of Rotorcraft Aerodynamics and Dynamics*. 1988. Johnson Aeronautics Version. Volume I: Theory Manual
- [11] Arcidiacono, P. J., Carlson, R. G. *Helicopter Rotor Loads Prediction*. March 1973. AGARD CP 122
- [12] Arcidiacono, P. J. *Prediction of Rotor Instability at High Forward Speeds*. February 1969. Volume I. Steady Flight Differential Equations of Motion for a Flexible Helicopter Blade with Chordwise Mass Unbalance. USAAVLABS TR 68-18A
- [13] Reichert, G. *Loads Prediction Methods for Hingeless Rotor Helicopters*. March 1973. AGARD CP 122
- [14] Kerr, A. W., Davis, J. M. *A System for Interdisciplinary Analysis. A Key to Improved Rotorcraft Design*. May 1979. American Helicopter Society 35th Annual Forum, Washington, D.C
- [15] Kerr, A. W., Stephens, W. B. *The Development of a System for Interdisciplinary Analysis of Rotorcraft Flight Characteristics*. May 1982. AGARD CP 334
- [16] Corrigan, J. J., Schillings, J. J., Yin, S. K., Hsieh, P. Y. *Developments in Dynamics Methodology at Bell Helicopter Textron*. June 1988. American Helicopter Society 44th Annual Forum, Washington, D.C
- [17] Yen, J. G., Corrigan, J. J., Schillings, J. J., Hsieh, P. Y. *Comprehensive Analysis Methodology at Bell Helicopter: COPTER*. January 1994. American Helicopter Society Aeromechanics Specialists Conference, San Francisco, CA
- [18] Corrigan, J. J., Bennett, R. L., Hsieh P. Y. *COPTER 2000: The QTR and Beyond*. May 2001. American Helicopter Society 57th Annual Forum, Washington, D.C
- [19] Sangha, K. B. *Bearingless Rotors and Higher Harmonic Control Modeling Using RACAP*. June 1988. American Helicopter Society 44th Annual Forum, Washington, D.C
- [20] Sangha, K. B., Weisenburger, R. K., Straub, F. K. *Rotor/Airframe Aeroelastic Analyses Using the Transfer Matrix Approach*. April 1990. AIAA Paper 90-1119

BIBLIOGRAPHY

- [21] Landgrebe, A. J., Egolf, T. A. *Rotorcraft Wake Analysis for the Prediction of Induced Velocities*. January 1976. USAAMRDL TR 75-45
- [22] Lemnios, A. Z., Smith, A. F. *An Analytical Evaluation of the Controllable Twist Rotor Performance and Dynamic Behavior*. May 1972. USAAMRDL TR 72-16
- [23] Lemnios, A. Z. *Rotary Wing Design Methodology*. March 1973. AGARD CP 122
- [24] Burtsev, B. N. *Aeroelasticity of a Coaxial Helicopter Rotor*. September 1991. Seventeenth European Rotorcraft Forum, Berlin, Germany
- [25] Bourtsev, B. N., Selemenev, S. V., Vagis V. P. *Coaxial Helicopter Rotor Design and Aeromechanics*. September 1999. Twenty-Fifth European Rotorcraft Forum, Rome, Italy
- [26] Van der Wall, B. *Analytic Formulation of Unsteady Profile Aerodynamics and Its Application to Simulation of Rotors*. August 1992. ESA TT 1244
- [27] Du Val, R. W. *A Real-Time Blade Element Helicopter Simulation for Handling Qualities Analysis*. September 1989. Fifteenth European Rotorcraft Forum, Amsterdam, The Netherlands
- [28] Du Val, R. W. *A Low Cost High Fidelity Real-Time Rotorcraft Simulation for Control and Handling Qualities Analysis*. April 1998. HeliJapan. AHS International Meeting on Rotorcraft Technology and Disaster Relief, Gifu, Japan
- [29] Du Val, R. W. *A Real-Time Multi-Body Dynamics Architecture for Rotorcraft Simulation*. November 2001. American Helicopter Society and Royal Aeronautical Society International Conference on The Challenge of Realistic Rotorcraft Simulation, London, UK
- [30] Quackenbush, T. R., Bliss, D. B., Wachspress, D. A., Boschitsch, A. H., Chua, K. *Computation of Rotor Aerodynamic Loads in Forward Flight Using a Full-Span Free Wake Analysis*. December 1990. NASA CR 177611
- [31] Bir, G., Chopra, I., Nguyen, K. *Development of UMARC (University of Maryland Advanced Rotorcraft Code)*. May 1990. American Helicopter Society 46th Annual Forum, Washington, D.C

BIBLIOGRAPHY

- [32] Bir, G., Chopra, I. *Status of University of Maryland Advanced Rotorcraft Code*. January 1994. American Helicopter Society Aeromechanics Specialists Conference, San Francisco, CA
- [33] Juggins, P. T. W. *Application of the Westland CRFD Program to Total Helicopter Dynamics*. November 1989. American Helicopter Society National Specialists. Meeting on Rotorcraft Dynamics, Arlington, TX
- [34] Hansford, R. E. *Considerations in the Development of the Coupled Rotor Fuselage Model*. October 1994. Journal of the American Helicopter Society. Vol. 39, no. 4, pp. 70-81
- [35] Dietz, M., Maucher, C., Schimke, D. *Addressing Today Aeromechanic Questions by Industrial Answers. American Helicopter Society Specialists*. January 2010. Conference on Aeromechanics, San Francisco, CA
- [36] Benoit, B., Dequin, A. M., Kampa, K., von Grunhagen, W., Basset, P. M., Gimonet, B. *HOST, A General Helicopter Simulation Tool for Germany and France*. May 2000. American Helicopter Society 56th Annual Forum, Virginia Beach, VA
- [37] Bauchau, O. A., Bottasso, C. L., Dindar, M., Murty, H. S., Rusak, Z., Shephard, M. S. *Aeroelastic Stability of Rotor Blades Using a Parallel Adaptive Finite Element Solver*. October 1995. American Helicopter Society 2nd International Aeromechanics Specialists. Conference, Bridgeport, CT
- [38] Bauchau, O. A., Bottasso, C. L., Nikishkov, Y. G. *Modeling Rotorcraft Dynamics with Finite Element Multibody Procedures*. May-June 2001. Mathematical and Computer Modeling. Vol. 33, no. 10-11, pp. 1113-1137
- [39] Saberi, H., Khoshlahjeh, M., Ormiston, R. A., Rutkowski M. J. *Overview of RCAS and Application to Advanced Rotorcraft Problems*. January 2004. American Helicopter Society 4th Decennial Specialists. Conference on Aeromechanics, San Francisco, CA
- [40] Ghiringhelli, G. L., Masarati, P., Mantegazza, P., Nixon, M. W. *Multi-Body Analysis of the 1/5 Scale Wind Tunnel Model of the V-22 Tiltrotor*. May 1999. American Helicopter Society 55th Annual Forum, Montreal, Canada
- [41] Quaranta, G., Bindolino, G., Masarati, P., Mantegazza, P. *Toward a Computational Framework for Rotorcraft Multi-Physics Analysis: Adding Computational*

BIBLIOGRAPHY

- Aerodynamics to Multibody Rotor Models*. September 2004. Thirtieth European Rotorcraft Forum, Marseilles, France
- [42] Garrad, W., Low, E. *Eigenspace Design of Helicopter Flight Control Systems*. 1990. Technical report, Dept. of Aerospace Engineering and Mechanics, Univ. of Minnesota
- [43] Kienitz, K., Wu, Q. *Robust Stabilization of a Helicopter Model*. 1990. Proceedings of the 29th CDC, 1990, 2607-2612
- [44] Kaloust, J., Ham, C., Qu, Z. *Nonlinear Autopilot Control Design for a 2-DOF Helicopter Model*. 1997. Control Theory and Applications, IEE Proceedings, 144, 6, 612-616
- [45] Verdult, V., Lovera, M., Verhaegen, M. *Identification of Linear Parameter-Varying State-Space Models with Application to Helicopter Rotor Dynamics*. September 2004. International Journal of Control. Vol. 77, no. 13, pp. 1149-1159
- [46] Sreenat, N., Krishnaprasad, P. S. *Multibody Simulation in an Object Oriented Programming Environment*. 1988. Advance in Symbolic Computation. SIAM Publi, Philadelphia ed. R. Grossman
- [47] Vigano, L., Magnani, G. *Acausal Modelling of Helicopter Dynamics for Automatic Flight Control Applications*. September 2006. The Modelica Association. Proceeding of the 5th International Modelica Conference. September 4-5
- [48] Engelson, V., Larsson, H., Fritzson, P. *A Design, Simulation and Visualization Environment for Object-Oriented Mechanical and Multi-Domain Models in Modelica*. 1999. Conference: Information Visualization. Proceedings 1999 IEEE International Conference
- [49] Zupancic, B., Sodja, A. *Advanced Multi-Domain Modelling: Advantages and Dangers*. 2011. UKSim 13th International Conference on Modelling and Simulation. DOI 10.1109/UKSIM.2011.56
- [50] Robinson, C. S. *Modeling and Analysis of the Helicopter Ground Resonance Utilizing Symbolic Processing and Dynamic Simulation Software*. 1997. Thesis. Naval Postgraduate School. Monterey, California
- [51] Pan, L., Renliang, C. *A Mathematical Model for Helicopter Comprehensive Analysis*. Junio 2010. Chinese Journal of Aeronautics. Vol. 23, issue 3, pp. 320-326

- [52] Robinson, C. S., King, R. L., Wood, E. R. *Non-linear Simulation of Coupled Rotor-Fuselage Response Using Symbolically Derived Equations of Motion. Part 1: Derivation*. 2004. Proceedings of the Institution of Mechanical Engineering Engineers, Part G: Journal of Aerospace Engineering. 218:1 DOI: 10.1177/095441000421800101
- [53] Flowers, G. T., Tongue, B. H. *Nonlinear Rotorcraft Analysis Using Symbolic Manipulation*. April 1988. Ministry of Supply. Appl. Math. Modelling. Vol. 12, pp. 154-160
- [54] Avila, J. C., Brogliato, B., Dzul, A., Lozano, R. *Nonlinear Modelling and Control of Helicopters*. 2003. Automatica, 39, 1583-1596
- [55] Bauchau, O. A., Kang, N. K. *A Multibody Formulation for Helicopter Structural Dynamic Analysis*. April 1993. Journal of the American Helicopter Society. 38(2), pp. 3-14
- [56] Bauchau, O. A., Wang, J. *Stability Analysis of Complex Multibody Systems*. 2006. Journal of Computational and Nonlinear Dynamics. 1, no. 1, pp. 71-80
- [57] Bertogalli, V., Bisi, F., Lovera, M. *Modelling Helicopter Rotor Dynamics with ADAMS*. 1995. ADAMS User Conference, Ann Arbor, Michigan, USA
- [58] Bianchi, F. *Helicopter Tail Rotor Analysis: Experience in Agusta with ADAMS*. 2000. 15th European ADAMS User Conference
- [59] Brown, R. E. *Rotor Wake Modeling for Flight Dynamic Simulation of Helicopters*. 2000. AIAA Journal. Vol. 38, no. 1, pp. 57-63
- [60] Phillips, C., Brown, R. E. *The Effect of Helicopter Configuration on the Fluid Dynamics of Brownout*. September 2008. 34th European Rotorcraft Forum. Liverpool, England
- [61] Phillips, C., Kim, H. W., Brown, R. E. *The Flow Physics of Helicopter Brownout*. May 2010. American Helicopter Society. 66th Annual Forum, Phoenix, AZ, May 11-13
- [62] Phillips, C., Kim, H. W., Brown, R. E. *Helicopter Brownout - Can it be Modelled?*. June 2010. Royal Aeronautical Society Rotorcraft Group Conference. June 16-17, London

BIBLIOGRAPHY

- [63] <http://www.carsim.com>. Last access: 18 November 2014
- [64] Sayers, M. W. *Symbolic Computer Language for Multibody Systems*. Nov-Dec 1991. J. Guidance. Vol. 14, no. 6, pp. 1153-1163
- [65] Majhi, J. R., Ganguli, R. *Helicopter Blade Flapping with and without Small Angle Assumption in the Presence of Dynamic Stall*. 2009. Applied Mathematical Modelling. doi:10.1016/j.apm.2010.02.010
- [66] Pavel, M. D. *An Investigation of the Lead-Lag Instability of the Micon 1500/600 Wind Turbine*. November 1999. Flight Mechanics and Propulsion Group. Delft University of Technology. Faculty of Aerospace Engineering. Memorandum M-878. ST-LR-1006
- [67] Ormiston, R. A., Bousman W. G. *An Theoretical and Experimental Investigation of Flap-Lag Stability of Hingeless Helicopter Rotor Blades*. 1972. Army Air Mobility Research and Development Laboratory AD-750 359. Moffett Field, California
- [68] Al-jawi, A. A. N., Mohamad, A. S. *The Characteristic of a Linear Rotorcraft Model*. November 1995. The Fourth Saudi Engineering Conference. Vol. IV
- [69] Du Val, R. W. *Inertial Dynamics of a General Purpose Rotor Model*. March 1979. NASA. Technical Memorandum 78557
- [70] Hohenemser, K. H. *Hingeless Rotorcraft Flight Dynamics*. 1974. Advisory Group for Aerospace Research and Development AD-A007 953. Paris, France
- [71] Wiesner, W., Kohler, G. *Tail Rotor Design Guide*. January 1974. Army Air Mobility Research and Development Laboratory AD-775 391
- [72] Amer, K. B., Gessow, A. *Charts for Estimating Tail-Rotor Contribution to Helicopter Directional Stability and Control in Low-Speed Flight*. October 1953. Langley Aeronautical Laboratory. National Advisory Committee for Aeronautics. Report 1216
- [73] Pereira, J. M., Vieira, R., de Andrade, D. *The Influence of the Positive Pitch-Flap Coupling (Negative Delta-Three) on the Flapping Response of an Articulated Tail Rotor*. 2010. Proceedings of the 9th Brazilian Conference on Dynamics Control and their Applications Serra Negra, SP. ISSN 2178-3667

BIBLIOGRAPHY

- [74] Stanislawski, J. *Simulations Investigation of Tail Rotor Behavior in Directional Maneuver of Helicopter*. Transactions of the Institute of Aviation. No. 193
- [75] Guo-cai, H., Jin-wu, X., Xiao-gu, Z. *Dynamic Stability Analysis for Helicopter Rotor/Fuselage Coupled Nonlinear Systems*. February 2003. Chinese Journal of Aeronautics. Vol. 16, issue 1, pp. 22-28
- [76] Keller, J. D. *An Investigation of Helicopter Dynamic Coupling Using an Analytical Model*. NASA-CR-197420. Report Princeton University
- [77] Manimala, B., Walker, D., Padfield, G. *Rotorcraft Simulation Modelling and Validation for Control Law Design and Load Prediction*. September 2005. 31st European Rotorcraft Forum, 13-15 September, Florence, Italy
- [78] Zbrozek, J. K. *The Simple Harmonic Motion of a Helicopter Rotor with Hinged Blades*. 1949. Ministry of Supply. Aeronautical Research Council Reports and Memoranda. R & M. No. 2812
- [79] Steward, W. *Higher Harmonics of Flapping on the Helicopter Rotor*. 1952. Ministry of Aviation. Aeronautical Research Council Current Papers. Report 2459
- [80] Lowis, O. J. *The Stability of Rotor Blade Flapping Motion at High Tip Speed ratios*. 1963. Ministry of Technology. Aeronautical Research Council Reports and Memoranda. R & M. No. 3544
- [81] Wilde, E., Bramwell, A. R. S., Summerscales, R. *The Flapping Behaviour of a Helicopter Rotor at High Tip-Speed Ratios*. 1966. Ministry of Aviation. Aeronautical Research Council Current Papers. CP. No. 877
- [82] Ornistom, R. A. *Rotor Dynamic Considerations for Large Wind Power Generator Systems*. U.S. Army Air Mobility R&D Laboratory Moffet Field, California
- [83] Stafford, R. O., Giurgiutiu, V. *Semi-analytic Methods for Rotating Timoshenko Beams*. 1975. Int. J. Mech. Sci. Vol. 17, no. 11-12, pp. 719-727
- [84] Giurgiutiu, V., Stafford, R. O. *Semi-analytic Methods for Frequencies and Mode Shapes of Rotor Blades*. 1977. Vertica. Vol. 1, pp. 291-306
- [85] Vyas, N. S., Rao, J. S. *Equations of Motion of a Blade Rotating with Variable Angular Velocity*. 1992. Journal of Sound and Vibration. 156(2), pp. 327-336

BIBLIOGRAPHY

- [86] Chen, R. T. N. *Flap-Lag Equations of Motion of Rigid, Articulated Rotor Blades with Three Hinge Sequences*. 1987. NASA Technical Memorandum 100023
- [87] Gessow, A., Amer, K. B. *An Introduction to the Physical Aspects of Helicopter Stability*. September 1949. Langley Aeronautical Laboratory. National Advisory Committee for Aeronautics. Report 993
- [88] Reeder, J. P., Gustafson, F. B. *On The Flying Qualities of Helicopters*. November 1948. Langley Aeronautical Laboratory. National Advisory Committee for Aeronautics. Report 1799
- [89] Curtiss, H. C. *Sensitivity of Hingeless Rotor Blade Flap Lag Stability in Hover to Analytical Modelling Assumptions*. January 1975. Princeton University. Department of Aerospace and Mechanical Sciences, AMS Report No. 1236
- [90] Ormiston, R. A., Hodges, D. H. *Linear Flap-Lag Dynamics of Hingeless Helicopter Rotor Blades in Hover*. 1972. Journal of the American Helicopter Society. Vol. 17, no. 2, pp. 2-14
- [91] Antequera, N., Santos, M., de la Cruz, J. M. *A Helicopter Control Based on Eigenstructure Assignment*. 2006. IEEE. 1-4244-0681-1/06
- [92] Bazov, D. I. *Helicopter Aerodynamics*. 1969. Nasa Technical Translation. NASA TT F-676
- [93] Chen, Y., Yao, M., Zhang, W. *Nonlinear Vibrations of the Blade with Varying Rotating Speed*. 2011. IEEE. 978-1-4244-9439-2/11
- [94] Santos, I. F., Saracho, C. M., Smith, J. T., Eiland, J. *Contribution to Experimental Validation of Linear and Non-Linear Dynamics Models for Representing Rotor-Blade Parametric Coupled Vibrations*. 2004. Journal of Sound and Vibration. 271 (2004) 883-904
- [95] Keysan, O., Ertan, H. B. *Higher Order Rotor Slot Harmonics for Rotor Speed Position Estimation*. 2010. 12th International Conference on Optimization of Electrical and Electronic Equipment, OPTIM. 978-1-4244-7040-4
- [96] http://dsp.vscht.cz/konference_matlab/matlab07/prispevky/tuma_j/tuma_j.pdf.
Last access: 18 November 2014

BIBLIOGRAPHY

- [97] Schulz, G. *Active Multivariable Vibration Isolation for a Helicopter*. 1979. Automatica. Vol. 15, pp. 461-466
- [98] Leishman, J. G. *Principles of Helicopter Aerodynamics*. 2007. Cambridge University Press
- [99] Castles Jr, W., New, N. C. *A Blade-Element Analysis for Lifting Rotors that is Applicable for Large Inflow and Blade Angles and Any Reasonable Blade Geometry*. July 1952. Langley Aeronautical Laboratory. National Advisory Committee for Aeronautics. TN 2656
- [100] Myers Jr, G. C. *Flight Measurements of Helicopter Blade Motion with a Comparison Between Theoretical and Experimental Results*. April 1947. Langley Aeronautical Laboratory. National Advisory Committee for Aeronautics. TN 1266
- [101] Majhi, J. R., Ganguli, R. *Modeling Helicopter Rotor Blade Flapping Motion Considering Nonlinear Aerodynamics*. 2008. CMES. Vol. 27, no. 1, pp. 25-36
- [102] Vilchis, J. C. A., Brogliato, B., Dzulc, A., Lozano, R. *Nonlinear Modelling and Control of Helicopters*. 2003. Automatica 39, pp. 1583-1596
- [103] Dingeldein, R. C., Schaefer, R. F. *Full-Scale Investigation of Aerodynamic Characteristics of a Typical Single-Rotor Helicopter in Forward Flight*. February 1947. Langley Aeronautical Laboratory. National Advisory Committee for Aeronautics. Report 905
- [104] Mikhailov, S. A., Nikolaev, E. I., Shilova, N. A. *Stability of 3D-Motion of Helicopter Rotor Blade*. European Conference for Aerospace Sciences. (EUCASS)
- [105] Salazar, T. *Mathematical Model and Simulation for a Helicopter with Tail Rotor*. Advances in Computational Intelligence, Man-Machine Systems and Cybernetics. ISBN: 978-960-474-257-8
- [106] Siva, C., Murugan, M. S., Ganguli, R. *Effect of Uncertainty on Helicopter Performance Predictions*. 2009. Proceedings of the Institution of Mechanical Engineers, Part G: Journal of Aerospace Engineering. DOI: 10.1243/09544100JAERO638
- [107] Griffiths, D. A., Leishman, J. G. *A Study of Dual-Rotor Interference and Ground Effect Using a Free-Vortex Model*. June 2002. American Helicopter Society International. 58th Annual Forum and Technology Display. Montreal, Canada

BIBLIOGRAPHY

- [108] Leishman, J. G., Bhagwat, M. J., Bagai, A. *Free-Vortex Filament Methods for the Analysis of Helicopter Rotor Wakes*. September-October 2002. Journal of Aircraft. Vol. 39, no. 5, pp. 759-775
- [109] Bhagwat, M. J., Leishman, J. G. *On the Aerodynamic Stability of Helicopter Rotor Wakes*. May 2000. American Helicopter Society. 56th Annual Forum. Virginia Beach, VA
- [110] Ahlin, G. A., Brown, R. E. *Predicting the Onset of the Vortex Ring State under Accelerated Flight Conditions*. June 2005. American Helicopter Society. 61st Annual National Forum, Grapevine, Texas
- [111] Caradonna, F. X. *The Application of CFD to Rotary Wing Flow Problems*. November 1990. Advisory Group for Aerospace Research & Development. AGARD Report. No. 781
- [112] Caradonna, F. X. *The BVI Prediction Problem and the Role of CFD*. June 1999. Proceedings of CEAS Forum on Aeroacoustics of Rotors and Propellers. 20000619031
- [113] Velez, C. M., Agudelo, A., Alvarez, J. *Modeling, Simulation and Rapid Prototyping of an Unmanned Mini-Helicopter*. August 2006. AIAA Modeling and Simulation Technologies Conference and Exhibit, AIAA 2006-6737, 21-24 August, Keystone, Colorado
- [114] Johnson, E. N., DeBitetto, P. A. *Modeling and Simulation for Small Autonomous Helicopter Development*. 1997. American Institute of Aeronautics and Astronautics
- [115] Cai, G., Feng, L., Chen, B. M., Lee, T. H. *Systematic Design Methodology and Construction of UAV Helicopters*. 2008. Mechatronics. Vol. 18, issue 10, pp. 545-558
- [116] Dunbabin, M., Brosnan, S., Roberts, J., Coke, P. *Vibration Isolation for Autonomous Helicopter Flight*. April 2004. International Conference on Robotics & Automation. 0-7803-8232-3/04, IEEE. New Orleans
- [117] Affanni, A. *Design and Dynamic Characterization of a Gyroscopic System for Aerobatic UAV Helicopters*. January 2012. Measurement. Vol. 46, issue 1, pp. 775-783

BIBLIOGRAPHY

- [118] Kim, S. K., Tilbury, D. M. *Mathematical Modeling and Experimental Identification of an Unmanned Helicopter Robot with Flybar Dynamics*. 2004. Journal of Robotic Systems. 21(3), pp. 95-116
- [119] Cunha, R., Silvestre, C. *Dynamic Modeling and Stability Analysis of Model-Scale Helicopters with Bell-Hiller Stabilizing Bar*. 2003. AIAA Guidance and Control Conference, Texas, USA
- [120] Lau, T. K., Liu, Y., Lin, K. *A New Method of Modeling the Actuation Dynamics of a Miniature Hingeless Helicopter Using Gyroscopic Moments*. May 2010. IEEE International Conference on Robotics and Automation, Anchorage Convention District May 3-8, Anchorage, Alaska, USA
- [121] <http://www.carsim.com/products/supporting/vehiclesim/index.php>. Last access: 18 November 2014
- [122] Sharp, R. S., Evangelou, S., Limebeer, D. J. N. *Advances in the Modeling of Motorcycle Dynamics*. 2004. Multibody System Dynamics 12(3), pp. 251-283
- [123] Sharp, R. S., Evangelou, S., Limebeer, D. J. N. *Multibody Aspects of Motorcycle Modeling with Special Reference to Autosim Advances in Computational Multibody Systems*. 2005. J. G. Ambrosio (Ed.), Springer-Verlag, Dordrecht, The Netherlands. 45-68
- [124] Tomas-Rodriguez, M., Sharp, R. S. *Automated Modeling of Rotorcraft Dynamics with Special Reference to Autosim*. 2007. Automation Science and Engineering, CASE 2007. IEEE International Conference, 2007. pp. 974-979
- [125] Tomas-Rodriguez, M. *Multibody Modeling of Rotorcraft Dynamics*. MPhil Thesis. 2008. Aeronautical Engineering Department. Imperial College. London, UK
- [126] Evangelou, S., Limebeer, D. J. N., Tomas-Rodriguez, M. *Influence of Road Camber on Motorcycle Stability*. 2008. Transactions of the ASME, Journal of Applied Mechanics. Vol. 75
- [127] Evangelou, S., Tomas-Rodriguez, M. *Modelling, Simulation and Control of Two-Wheeled Vehicles*. 2014. Wiley & Sons. Chapter. "Dynamic Modes and Steering Compensation". ISBN: 978-1-119-95018-9

- [128] Marichal-Plasencia, G. N., Tomas-Rodriguez, M., Castillo-Rivera, S., Hernandez-Lopez, A. *Modelling Analysis of Vibrations in a UAV Helicopter with a Vision System*. 2012. International Journal of Advanced Robotic Systems. Vol. 9, 220. 2012. ISSN:1729-8806
- [129] Marichal, G. N., Tomas-Rodriguez, M., Hernandez, A., Castillo-Rivera, S., Campoy, P. *Vibration Reduction for Vision System on Board UAV Using a Neuro-Fuzzy Controller*. June 2013. Journal of Control and Vibrations. 25, pp. 1-12. SAGE Journals, 2013. ISSN 1077-5463
- [130] Moreno-Ramirez, C., Garcia-Fernandez, P., de-Juan, A., Tomas-Rodriguez, M. *New Advances in Mechanisms, Transmissions and Applications Mechanisms and Machine Science*. January 2014. Vol. 17, Springer Verlag. Chapter "Interconnected Suspension System on Sport Motorcycles". ISBN: 978-94-007-7484-1
- [131] Estelles-Martinez, S., Tomas-Rodriguez, M. *Seguimiento de Trayectorias Tridimensionales de un Quadrotor Mediante Control PVA*. January-March 2014. Revista Iberoamericana de Automatica e Informatica Industrial RIAI. Vol. 11, issue 1, pp. 54-67
- [132] Mechanical Simulation Corporation. *VehicleSim Solver Programs Reference Manual*. 1996-2008. Mechanical Simulation. <http://www.carsim.com>. Last access: 18 November 2014
- [133] Mechanical Simulation Corporation. *VehicleSim Browser Reference Manual for BikeSim, CarSim, and TruckSim*. 1996-2008. Mechanical Simulation. <http://www.carsim.com>. Last access: 18 November 2014
- [134] Mechanical Simulation Corporation. *VehicleSim Lisp Reference Manual Version 1.0*. 1997-2008. Mechanical Simulation. <http://www.carsim.com>. Last access: 18 November 2014
- [135] Mechanical Simulation Corporation. *VehicleSim Lisp Introductory Guide Version 1.0*. 1997-2008. Mechanical Simulation. <http://www.carsim.com>. Last access: 18 November 2014
- [136] Mancini, A., Caponetti, F., Monteriu, A., Frontoni, E., Zingaretti, P., Longhi, S. *Safe Flying for an UAV Helicopter*. July 2007. Proceedings of the 15th Mediterranean Conference on Control & Automation, July 27-29, Athens, Greece

BIBLIOGRAPHY

- [137] Allen, L. *Making the Leap from AutoCad to Autodesk Inventor*. 10 Easy Steps form CADENCE Magazine Columnist
- [138] Daftuar, R. K. *Users Guide to Autodesk Inventor 5.3*. Purdue University School of Electrical Engineering Team 461 Westside Boiler Invasion
- [139] Kyosho Corporation. *Radio Controlled Engine Powered Helicopter Caliber 3*. 2006. Instruction Manual. No. 21236/21237
- [140] Johnson, W. *Helicopter Theory*. 1980. Princeton, NJ: Princeton Univ. Press
- [141] Bramwell, A. R. S., Done, G., Balmford, D. *Bramwell's Helicopter Dynamics*. 2001. Butterworth-Heinemann
- [142] Padfield, G. D. *Helicopter Flight Dynamics: The Theory and Application of Flying Qualities and Simulation Modelling*. 2007. Blackwell Publishing
- [143] Watkinson, J. *The Art of the Helicopter*. 2004. Elsevier Butterworth-Heinemann
- [144] Newman, S. *The Foundations of Helicopter Flight*. 1994. Edward Arnold
- [145] Seddon, J. *Basic Helicopter Aerodynamics*. 1990. Blackwell Scientific Publications (BSP) Professional Books
- [146] Stepniewski, W. Z. *Introduction to Helicopter Aerodynamics*. 1958. Rotorcraft Publishing Committee. Morton, Pa
- [147] Shapiro, J. *Principles of Helicopter Engineering*. 1955. Temple Press Limited
- [148] AGARD Lecture Series. *Helicopter Aerodynamics and Dynamics*. 1973. Technical Editing and Reproduction Ltd. No. 63
- [149] Cook, M. V. *Flight Dynamics Principles*. 1997. Butterworth-Heinemann
- [150] Payne, P. R. *Helicopter Dynamics and Aerodynamics*. 1959. Sir Isaac Pitman & Sons, LTD
- [151] Naval Air Training Command. *Introduction to Helicopter Aerodynamics Workbook*. 2000. NAS Corpus Christi, Texas. CNATRA P-401 (REV 09-00)
- [152] Ferrer, R., Kryszinski, T., Aubourg, P., Bellizi, S. *New Methods for Rotor Tracking and Balance Tuning and Defect Detection Applied to Eurocopter Products American Helicopter Society*. May 2001. 57th Annual Forum, May 9-11, Washington, DC,

BIBLIOGRAPHY

- [153] Gerber, T., Martin, N., Mailhe, C. *Identification of Harmonics and Sidebands in a Finite Set of Spectral Components*. 2013. The Tenth International Conference on Condition Monitoring and Machinery Failure Prevention Technologies (CM & MFPT), Cracovie, Poland
- [154] Halfpenny, A., Walton, T. *New Techniques for Vibration Qualification of Vibrating Equipment on Aircraft*. 2010. Aircraft Airworthiness & Sustainment
- [155] Nguyen, K. *High Harmonic Control Analysis for Vibration Reduction of Helicopter Rotor Systems*. 1994. NASA Technical Memorandum 103855